



12-2017

Determining ^{235}U Enrichment Using a Dual-Energy Approach for Delayed Neutron Measurements

Angela Lynn Lousteau

University of Tennessee, Knoxville, aloustea@vols.utk.edu

Follow this and additional works at: https://trace.tennessee.edu/utk_graddiss

 Part of the [Nuclear Engineering Commons](#)

Recommended Citation

Lousteau, Angela Lynn, "Determining ^{235}U Enrichment Using a Dual-Energy Approach for Delayed Neutron Measurements. " PhD diss., University of Tennessee, 2017.
https://trace.tennessee.edu/utk_graddiss/4748

This Dissertation is brought to you for free and open access by the Graduate School at TRACE: Tennessee Research and Creative Exchange. It has been accepted for inclusion in Doctoral Dissertations by an authorized administrator of TRACE: Tennessee Research and Creative Exchange. For more information, please contact trace@utk.edu.

To the Graduate Council:

I am submitting herewith a dissertation written by Angela Lynn Lousteau entitled "Determining 235U Enrichment Using a Dual-Energy Approach for Delayed Neutron Measurements." I have examined the final electronic copy of this dissertation for form and content and recommend that it be accepted in partial fulfillment of the requirements for the degree of Doctor of Philosophy, with a major in Nuclear Engineering.

Jason P. Hayward, Major Professor

We have read this dissertation and recommend its acceptance:

Ron Pevey, Steven Skutnik, Charles Britton

Accepted for the Council:

Dixie L. Thompson

Vice Provost and Dean of the Graduate School

(Original signatures are on file with official student records.)

**Determining ^{235}U Enrichment Using a Dual-Energy
Approach for Delayed Neutron Measurements**

A Dissertation Presented for the

Doctor of Philosophy

Degree

The University of Tennessee, Knoxville

Angela Lynn Lousteau

December 2017

Copyright © 2017 by Angela Lousteau
All rights reserved.

ACKNOWLEDGEMENTS

First, I'd like to thank my major advisor, Dr. Jason Hayward. Your guidance made it possible for me to successfully complete this journey. I appreciate your availability and willingness to answer all my questions and the structure and organization you helped me achieve. I also sincerely thank Dr. Ron Pevey, Dr. Steve Skutnik, and Dr. Chuck Britton for not only agreeing to participate on my committee but also for providing meaningful feedback pushing me to improve my work. I'd like to thank Bob McElroy and Stephen Croft for your mentorship throughout this process. Both of you voluntarily provided excellent guidance and pushed me to become a better and more knowledgeable researcher. I truly believe I am a better researcher because of your mentorship. I can only hope to one day be as brilliant as you both are today.

I'd like to thank my supervisor at ORNL, Chris Pickett, for supporting me throughout this endeavor. I appreciate your willingness to work with me as I balanced my work, school, and home life. I also thank Alan Icenhour for stopping by my office that one day to recommend that I return to school for a Ph.D. Thank you for the motivation. Thank you to Jason Crye, who convinced me that Alan's idea was a good one. I blamed you on the bad days when I wanted to quit, but you continued to encourage me, and for that I am grateful. I also appreciate all the time Nathan Rowe spent helping me debug my MatLab scripts and for all the support getting setup on our server. Thank you also to Greg Nutter whom I equate to the wizard of Oz...always there in the background making things work!

Lastly, I thank my family for always believing in me. Thank you for your words of encouragement, especially when the days were long and I was having a hard time finding the motivation to continue. Thank you, Matt, for all the support over these last years. Not only have you encouraged me throughout this entire journey, but you carried the burden of supporting our family as well. Thank you for all the time you spent entertaining our three beautiful children so that I could chug along.

ABSTRACT

Bulk uranium items are often measured using active neutron interrogation systems to take advantage of the relatively high penetrability of neutrons, providing the ability to quickly and accurately measure uranium masses in large, dense configurations. Active techniques employ an external neutron source to induce fission in the uranium and subsequently measure emitted prompt fission or delayed neutrons. Unfortunately, the emitted neutrons from ^{235}U [uranium-235] and ^{238}U [uranium-238] are, for all practical purposes, indistinguishable; therefore, commonly used systems such as the Active Well Coincidence Counter, the ^{252}Cf [californium-252] Shuffler, and other systems based on measurement of prompt or delayed fission neutrons require many representative calibration standards and/or well-known isotopic information to interpret the results (i.e., extract an isotopic mass from the effective fissionable mass), thus limiting these techniques for safeguards applications. The primary objective of this research was to develop and demonstrate a dual-energy neutron interrogation technique using a ^{252}Cf Shuffler measurement chamber for determination of uranium enrichment, thus eliminating the need for a (traditionally separate) gamma isotopic measurement.

This new technique exploits the change in fission rates as a function of interrogating neutron energy to independently determine the ^{235}U and ^{238}U content in the measurement item. Dual neutron interrogation energies were achieved by adding a deuterium- tritium (D-T) neutron generator into the measurement chamber of the Oak Ridge National Laboratory ^{252}Cf Shuffler. Results from traditional ^{252}Cf measurements and the new D-T measurements were then used to develop a relationship between uranium enrichment and the ratio of the two delayed neutron count rates. Parameter studies were performed to optimize the measurements for each source using a combination of modeling/simulation and experimental measurements. This dissertation presents the detailed development of this novel dual-energy neutron interrogation technique. The results are promising and

with engineering refinements could be deployed for routine assay of certain types of materials.

TABLE OF CONTENTS

1	INTRODUCTION	1
1.1	Motivation.....	1
1.2	Dissertation Overview	5
1.3	Research Goals, Benefits, and Potential Applications.....	8
1.4	Original Contributions	10
2	BACKGROUND	11
2.1	Overview of Safeguards-related NDA Methods for ²³⁵ U Mass Determination	11
2.1.1	Passive Neutron Techniques.....	12
2.1.2	Active Neutron Techniques	17
2.1.3	Passive Gamma-based Techniques	27
2.1.4	Active Gamma Techniques.....	30
2.2	Overview of Safeguards-related NDA Methods for Uranium Enrichment Determination	32
2.2.1	Common Enrichment Methods for Uranium	32
2.2.2	Limitations	35
2.3	²⁵² Cf Shuffler	36

2.3.1	Hardware.....	37
2.3.2	Shuffling Mechanics	39
2.3.3	Complications	40
2.3.4	Interrogation Source Characteristics.....	42
2.4	Delayed Neutron Concepts	44
2.4.1	Keepin 6-group Delayed Neutron Model	45
2.4.2	Calculating Delayed Neutron Emission Rates and Expected Count Rates...	46
2.5	Effective Mass	51
2.6	Prior Work	53
2.6.1	Advanced Enrichment Techniques Using Delayed Neutrons.....	53
2.6.2	Multi-Energy Approach using Delayed Neutrons	54
2.6.3	Sensitivity studies	57
2.6.4	MCNP6 Delayed Neutron Capabilities.....	57
2.6.5	Source Replacement.....	58
3	MODEL AND SIMULATION.....	60
3.1	MCNP6 Model of the ORNL ²⁵² Cf Shuffler.....	60
3.2	Validation of MCNP6 Model.....	63
3.2.1	²⁵² Cf Efficiency Profiles	64

3.2.2	Die-away Time.....	68
3.3	Determining Fission Rates from MCNP6.....	71
4	MEASUREMENT DESIGN	73
4.1	Implementation of a Secondary Neutron Source	73
4.1.1	Potential Secondary Neutron Sources.....	73
4.1.2	Selection of Secondary Neutron Source	78
4.2	Optimal Positioning of the Secondary Source	81
4.3	Selection of Spectrum Tailoring Materials	86
4.4	²⁵² Cf Shuffler Characterization.....	88
4.4.1	High Voltage Plateau	88
4.4.2	²⁵² Cf Efficiency.....	89
4.4.3	Delayed Neutron Efficiency	90
4.4.4	Dead-time Measurements	92
4.5	Measurement Setup.....	93
4.5.1	²⁵² Cf Measurement Setup.....	93
4.5.2	D-T Measurement Setup.....	94
4.6	Optimization of Measurement Times	95
4.6.1	²⁵² Cf-based Measurements.....	95

4.6.2	D-T-based Measurements	96
4.7	Measurement Method and Scenarios	97
5	RESULTS AND ANALYSIS.....	100
5.1	Expected Delayed Neutron Rates and DEANI Results	100
5.1.1	Simulated Induced Fission Rates	100
5.1.2	Estimated Delayed Neutron Rates	101
5.2	Measurement Data using DEANI method	107
5.2.1	Traditional ²⁵² Cf Measurements	107
5.2.2	D-T-based Measurements	109
5.2.3	Delayed Neutron Ratios	114
5.3	Experimental Verification of the DEANI Measurement Technique	117
5.4	Potential Replacements of the ²⁵² Cf Source.....	122
5.5	Die-away Measurements.....	126
5.6	Sensitivity to Energy-Dependent Delayed Neutron Group Constants.....	129
5.7	Influence of 8-Group Structure on Analytical Results	140
5.8	MCNP6 Delayed Neutron Data	143
5.9	Gamma Results	144
5.9.1	WinU235.....	145

5.9.2	MGAU	146
6	CONCLUSIONS.....	147
6.1	Discussion of Results and Research Outcomes	147
6.1.1	DEANI Methodology.....	147
6.1.2	Potential ²⁵² Cf Source Replacement	154
6.1.3	Sensitivity to Energy-Dependent Delayed Neutron Group Data.....	154
6.1.4	Sensitivity Analysis for the 8- Group Delayed Neutron Data	155
6.2	Future Work	156
6.3	Summary	158
	LIST OF REFERENCES	160
	APPENDICES	176
	Appendix A: Example Data Files	177
	Appendix B: Source Information.....	227
	Appendix C: Uncertainty Analyses and Equations.....	230
	VITA.....	233

LIST OF TABLES

Table 1. Significant Quantities for Nuclear Materials as Defined by the IAEA [2].....	1
Table 2. Neutron Bank Properties in the ²⁵² Cf Shuffler.....	38
Table 3. Delayed Neutron Parameters for Keepin 6-Group Model [27]	46
Table 4. Summary of Simulated and Measured Die-away Time Constants	70
Table 5. Characteristics of ²⁵² Cf and AmLi Sources [7].....	76
Table 6. Ratios of Induced Fission Rates.....	79
Table 7. Fission Rates per Source Particle for Various D-T Locations.....	84
Table 8. Reported Delayed Neutron Spectra	91
Table 9. Dead-time Measurement Results	93
Table 10. ²⁵² Cf-based Shuffler Measurement Parameters	98
Table 11. Calculated Induced Fission Rates for Various CRMs	102
Table 12. Fixed Parameters for Determining Delayed Neutron Counts.....	103
Table 13. Calculated Delayed Neutron Counts by Isotope.....	104
Table 14. The Expected Total Delayed Neutron Count Rates Over 34 Shuffles	105
Table 15. ²⁵² Cf-induced Delayed Neutron Rates	108
Table 16. D-T-induced Delayed Neutron Rates	112

Table 17. Delayed Neutron Ratios for CRM Items	114
Table 18. Estimated Enrichments Using Leave-One-Out Method	118
Table 19. Summary of Verification Measurement Results.....	121
Table 20. Total Delayed Neutron Yields	130
Table 21. Energy-dependent Delayed Neutron Group Constants for ^{235}U	131
Table 22. Energy-dependent Delayed Neutron Group Constants for ^{238}U	132
Table 23. Summary of Delayed Neutron Datasets Considered	132
Table 24. Combinations of Delayed Neutron Datasets Considered for Sensitivity Analysis	133
Table 25. 8-group Delayed Neutron Constants.....	141
Table 26. WINU235 Settings.....	145
Table 27. WINU235 Measurement Results	146
Table 28. MGAU Measurement Results.....	146
Table A. 1 Excerpt from MCNP6 Output File.....	216
Table B. 1. Source Activities	227
Table B. 2. NBL CRM Source Specifications	227

LIST OF FIGURES

Figure 1. AmLi neutron spectrum and ^{252}Cf neutron spectrum (Watt fission spectrum) overlaid onto ^{235}U and ^{238}U total fission cross-section [9],[10],[11].	6
Figure 2. HHNM [16].	13
Figure 3. Antech fork detector [15].	13
Figure 4. Rossi-Alpha distribution describing the timing structure of the shift register [7].	15
Figure 5. Neutron coincidence gate structure applied to a generic pulse train.	16
Figure 6. AWCC and supporting electronics [14].	18
Figure 7. UNCL and supporting electronics [14].	18
Figure 8. Die-away for interrogating flux (pink) and interrogating flux with fissile item (blue) [25].	21
Figure 9. DDA Package Monitor at ORNL.	22
Figure 10. Active/Passive Neutron Assay system for waste measurements [25].	22
Figure 11. The Uranium Scrap Shuffler [29].	25
Figure 12. Shuffler for 55 gal drums [29].	25
Figure 13. Canberra SGS, which scans vertically along the height of the drum.	30
Figure 14. Canberra TGS, which scans vertically and horizontally across the drum.	30

Figure 15. Basic ^{252}Cf Shuffler measurement process [29].	39
Figure 16. The ^{252}Cf Shuffler at ORNL.	41
Figure 17. Comparison of ^{252}Cf neutron energy spectra using a Watt and Maxwellian distribution.	43
Figure 18. Delayed neutron yield rate for thermal fission of ^{235}U .	47
Figure 19. Group-dependent delayed neutron yields from ^{235}U and ^{238}U .	48
Figure 20. Relative delayed neutron emission rate per shuffler.	51
Figure 21. Cross-sectional front view of the ^{252}Cf Shuffler.	62
Figure 22. Cross-sectional top-down view of the ^{252}Cf Shuffler.	63
Figure 23. Measurement item sitting on a small rotator and stainless steel stand.	64
Figure 24. Efficiency profile in the x-direction across the measurement chamber.	66
Figure 25. Efficiency profile in the y-direction across the measurement chamber.	66
Figure 26. Vertical efficiency profile (z-direction) across the measurement cavity.	66
Figure 27. Efficiency map in the vicinity of the uranium measurement area.	67
Figure 28. F8 capture tally results for ^{252}Cf simulation for a fixed gate of $1\mu\text{s}$.	69
Figure 29. Measured die-away using ^{252}Cf for a fixed gate of $10\mu\text{s}$.	69
Figure 30. AmLi neutron energy spectra [9].	74
Figure 31. Comparison of AmBe and AmLi neutron energy spectra [9, 92].	75

Figure 32. Basic diagram of a neutron generator.....	77
Figure 33. Ratio of ^{252}Cf -induced delayed neutrons to that of potential secondary neutron sources.....	80
Figure 34. Cross-section (x,y) of the shuffler cavity showing the D-T generator positions evaluated.	82
Figure 35. Induced fission rates for nat. U and HEU at various D-T positions.....	83
Figure 36. Installed D-T generator.....	85
Figure 37. Neutron energy spectra for ^{252}Cf and D-T sources.....	87
Figure 38. Neutron energy spectra incident on the measurement item for ^{252}Cf and D-T sources.....	87
Figure 39. High Voltage Plateau for ^{252}Cf Shuffler.....	89
Figure 40. Delayed neutron energy spectra used to calculate efficiency in the shuffler. .	92
Figure 41. Shuffler counting window for the D-T measurements.	97
Figure 42. Expected delayed neutron rates from ^{252}Cf - and D-T- induced fissions.	106
Figure 43. Ratio of delayed neutron count rates for ^{252}Cf and D-T interrogation vs. ^{235}U enrichment.....	106
Figure 44. Comparison of measured and simulated delayed neutron rates from ^{252}Cf interrogation.....	108
Figure 45. Flux monitor counting window for D-T measurements.....	111

Figure 46. Comparison of measured and simulated delayed neutron rates from D-T interrogation.....	113
Figure 47. Comparison of measured and simulated ratios of delayed neutron rates.	115
Figure 48. Delayed neutron ratios with scaling.	116
Figure 49. Verification measurements plotted along measurement curve.....	122
Figure 50. Comparison of delayed neutron rates from various interrogating neutron sources.....	123
Figure 51. Delayed Neutron Ratios for interrogation by various alternatives to ^{252}Cf and D-T.....	125
Figure 52. Simulated fission event-triggered capture distribution for ^{252}Cf and D-T in the shuffler.	127
Figure 53. Fission event-triggered capture distribution showing buildup.	127
Figure 54. Comparison of fission event- and neutron event- triggered capture distributions.....	128
Figure 55. Analytically determined delayed neutron ratios using various combinations of delayed neutron group constants.....	134
Figure 56. Energy-dependent delayed neutron data (reduced).	135
Figure 57. Delayed neutron rates from ^{252}Cf interrogation using various delayed neutron constants.....	136
Figure 58. Delayed neutron rates from DT interrogation using various delayed neutron constants.....	137

Figure 59. Measured and calculated ratios using estimated D-T emission rate.....	139
Figure 60. Bi-variate plot of calculated and measured delayed neutron ratios.....	139
Figure 61. Expected delayed neutron rates using 8-group delayed neutron parameters.	142
Figure 62. Calculated ratios using 6-group and 8-group parameters.....	142
Figure B. 1. Diagram of the CRM containers.....	228

1 INTRODUCTION

This chapter describes the motivation and application for the development of the Dual Energy Approach for Neutron Interrogation (DEANI) method. A brief overview of this dissertation work including major research goals is presented. The original contributions to the safeguards-related nondestructive assay (NDA) field are also outlined in this chapter.

1.1 Motivation

Article III of the Treaty on Nonproliferation of Nuclear Weapons (NPT) states that all non-nuclear weapons states consent to the application of safeguards as agreed upon by the International Atomic Energy Agency (IAEA) [1]. In this legal framework, safeguards is the set of verification measures and activities required to confirm compliance with all responsibilities set forth in the safeguards agreement between the State and the IAEA. The objective for these nuclear safeguards measures is “the timely detection of diversion of significant quantities (SQ) of nuclear materials ... and deterrence of such diversion by the risk of early detection” [2]. SQs of nuclear materials (i.e., special fissionable material, ^{239}Pu , enriched ^{233}U or ^{235}U , and source materials), as defined by the IAEA, are provided in Table 1. The purpose of the IAEA safeguards system is to ensure that member states are correctly and completely reporting all nuclear activities as specified in their safeguards agreement mandated by information circular (INFCIRC) 153 [3],[4].

Table 1. Significant Quantities for Nuclear Materials as Defined by the IAEA [2]

Direct Use		Indirect Use	
Material	SQ	Material	SQ
Pu (containing $< 80\%$ ^{238}Pu)	8 kg Pu	U ($^{235}\text{U} < 20\%$)	75 kg ^{235}U , or 10 t nat. U, or 20 t depleted U
^{233}U	8 kg ^{233}U		
HEU ($^{235}\text{U} \geq 20\%$)	25 kg ^{235}U	Th	20 t Th

Further, the State is responsible for implementing a measurement system to determine the *quantity* of nuclear materials “received, produced, shipped, lost, or otherwise removed from inventory, and the quantities on inventory” and the measurement uncertainties that accompany those measurements [4]. This implementation of nuclear material accounting practices supports the quantification and reporting of nuclear materials [5]. The verification of these declarations is often achieved through IAEA inspection activities, authorized in Article XII of the NPT, which aim to verify quantities of nuclear materials and/or confirm various attributes (e.g., enrichment) of the material. The ability of the IAEA to effectively detect discrepancies (with high confidence and in a timely manner) serves to deter illicit activities, and/or quickly discover any attempt to divert the safeguarded materials.

Safeguards measures are now routinely applied to many stages across the nuclear fuel cycle: mining and milling, conversion, enrichment, fuel fabrication plants, nuclear reactors, spent fuel reprocessing facilities, and spent fuel storage locations. This work focuses on uranium applications. For uranium enrichment facilities, the safeguards concerns include diversion of uranium, production of highly enriched uranium (HEU), and production of excess low enriched uranium (LEU). While some inspection effort may be placed on the cascade/ process area or the feed area, the bulk of the inspection effort is placed on the large uranium hexafluoride (UF_6) cylinders. For fuel fabrication facilities, the UF_6 product (from the enrichment facility) is converted to oxide, followed by fuel pellets, pins, and even assemblies. The primary safeguards concern in these facilities is diversion of uranium. Inspection activities in these facilities must deal with materials in multiple forms (e.g., powders, pellets, fuel pins, and fuel assemblies), various process streams (e.g., bulk, waste, scrap, and product) and in potentially large quantities. In all cases, the State must be able to accurately measure the quantity of special fissionable material (also called special nuclear material (SNM)) among other things for reporting purposes, and the IAEA must be able to verify those values. The overall safeguards

strategy applied is a combination of technical and other approaches. Physical measurements are typically applied at key measurement points in and between material balance areas. The accuracy required depends on the material attractiveness and flow rates and is often guided by international target values.

In both of these types of process facilities, the mass and enrichment of uranium can be accurately determined by carefully weighing the materials and performing destructive assay (DA) analysis (to verify chemical form, concentration, and enrichment). Unfortunately, these DA techniques are too expensive, time-consuming, and taxing on both the inspectors and the facility operators to be a practical solution [3]; therefore, other NDA techniques are often employed. While NDA techniques are cost effective and provide relatively fast results, they are generally more difficult than, and not as accurate as, DA methods. The primary goal of this research is to improve one such NDA technique for bulk uranium applications, specifically delayed neutron counting using a ^{252}Cf Shuffler. In particular for heterogeneous matrices and shielded bulk material, enrichment measurement by high-resolution gamma spectrometry can be compromised. Since enrichment is needed to interpret active neutron assays, an independent method for estimating enrichment is needed.

As described above, the quantification of ^{235}U mass and determination of enrichment throughout the nuclear fuel cycle is necessary to ensure compliance with all State obligations and to support IAEA verification activities. While the key goal of safeguards measurements in a uranium processing facility is determination of the ^{235}U mass specifically, all neutron interrogation techniques currently in use (e.g., neutron coincidence counting, delayed neutron counting, and differential die-away (DDA) analysis) have *some* sensitivity to the presence of ^{238}U , which historically is ignored. The neutron assays are therefore not strictly reporting the ^{235}U content but rather some combination of ^{235}U and ^{238}U , typically referred to as an effective mass. Extracting the actual ^{235}U mass is only achieved by applying representative calibrations and prior

knowledge regarding the isotopic composition of the item. In situations where the isotopic concentrations are not well known, large errors are possible. For example, items containing large amounts of depleted uranium (in place of or shielding HEU) may erroneously appear to be larger quantities of ^{235}U [6], which provides a credible diversion scenario that must be addressed through improved (more accurate) measurements. Verifying the enrichment and the mass of material in cylinders and/or larger bulk samples using NDA techniques is especially difficult and is the focus of many research and development (R&D) ventures.

The isotopic information needed to convert these measured responses to fissile mass has historically been obtained using passive gamma-ray spectrometry. Self-attenuation of the low-energy, uranium gamma-rays complicate the measurements such that these techniques only evaluate the enrichment in the thin layer at the surface of the item. Thus, the measured enrichment may not reflect the enrichment of an inhomogeneous item where the infinite thickness layer may only be a few millimeters. In addition, passive gamma methods are limited by attenuation in container walls and/or other dense materials present in the item matrix. For relatively small, homogenous samples with little self- and sample container-attenuation, the fissile content can be accurately determined using gamma-ray measurement techniques; however, for more complex measurement items, this limited sampling of the item can result in poor enrichment determination and bias in the active neutron interrogation measurement results. The need for matrix and lump corrections also complicate the measurement and may severely hinder the ability to accurately determine the uranium enrichment using these gamma techniques.

Given that the isotopic measurement may not reflect the enrichment of the interior of a sample, a more penetrating enrichment measurement technique is desired. Active gamma techniques are more penetrating and do play a significant role in specialized applications; however, they often require extremely large photon fluxes to obtain statistically significant measurement signals. To address these limitations and challenges, the ability

to use energetic neutrons to determine uranium enrichment in support of sufficiently accurate determination of ^{235}U mass has been studied herein. The primary goal of this work was to determine and demonstrate whether or not two neutron sources with different average neutron energies can be used to independently determine the uranium enrichment, and thus the ^{235}U and ^{238}U content, without the need for prior isotopic information and while minimizing calibration standard requirements.

1.2 Dissertation Overview

Active neutron interrogation methods for assaying uranium-bearing items rely on external sources inducing fission in the fissile material within the sample (then subsequently measuring prompt and/or fission neutrons). These interrogation sources (often AmLi or ^{252}Cf) emit neutrons with a distribution of energies; therefore, the incident energy of a given neutron is not exactly known. Based on average energies and attempts to tailor the neutron spectrum for these interrogating sources, it has become common practice to ignore the induced fissions and subsequent neutron emissions from ^{238}U . However, this practice is flawed as it is impossible to completely prevent fission in other isotopes present in the item. Figure 1 shows the neutron energy distributions for both AmLi neutrons and ^{252}Cf neutrons. The total fission cross-sections for ^{235}U and ^{238}U are also plotted.

AmLi sources, commonly used in IAEA systems, have an average energy of approximately 0.5 MeV [7],[8]. In this energy region, the ^{235}U fission cross-section is 3-4 orders of magnitude larger than that of ^{238}U . However, AmLi spectra have a high-energy tail or structure in the 2 MeV range, as evident in the plot. The relative intensity of the $\text{O}(\alpha,\text{n})$ contribution depends on the microstructure of the AmO_2 and LiHO powder mixture used to make the sources. In this energy range the difference in the fission cross-sections is considerably smaller. Still, most of the fissions induced occur in ^{235}U .

For sources with higher average neutron energies, like ^{252}Cf , the neutron contribution from ^{238}U fission is larger. As shown in the plot, the cross-section for ^{238}U rises dramatically between 0.5 and 1.5 MeV. At 2.14 MeV, the average neutron energy for ^{252}Cf fission neutrons, the ^{238}U cross-section is much larger and is no longer negligible [7]. Since the interrogating neutrons in both these cases clearly have *some* probability of inducing fission in ^{238}U , it is likely that a measured neutron signal will include contributions from ^{238}U making it difficult to quantify the fissile content of an item directly without appropriate reference materials.

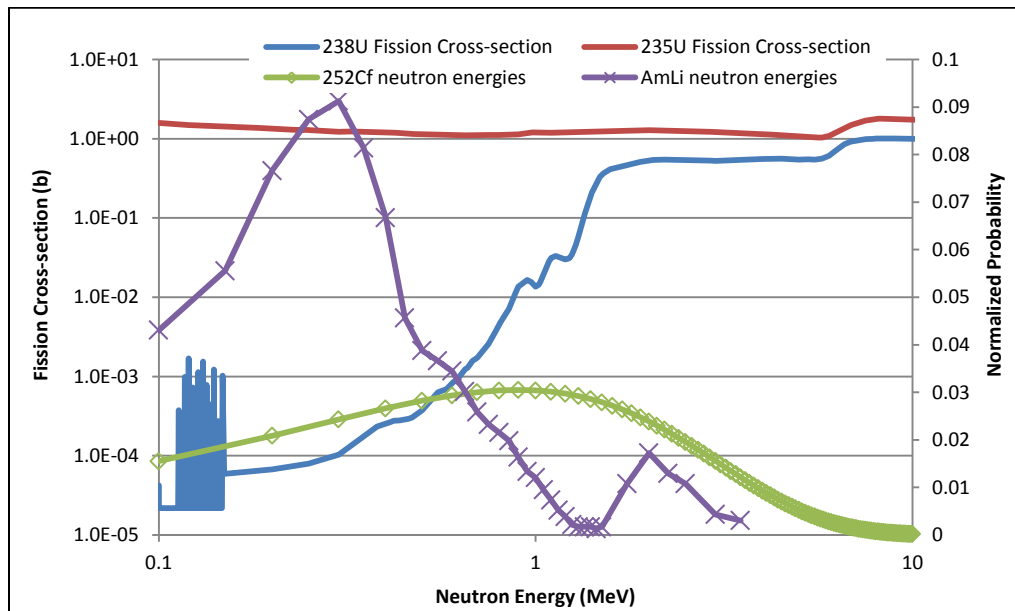


Figure 1. AmLi neutron spectrum and ^{252}Cf neutron spectrum (Watt fission spectrum) overlaid onto ^{235}U and ^{238}U total fission cross-section [9],[10],[11].

In some ideal measurement scenarios, all items to be assayed have the same enrichment, and a calibration using standards representative of that enrichment is available. In this case, the calibration curve accounts for the ^{238}U effectively, and accurate results for the

fissile content may be obtained. When it is necessary to measure items of varying enrichment, alternative methods must be used to avoid biased measurement results. Currently, there are only two ways to address contributions from ^{238}U .

The first option is to tailor the spectrum to lower the fission neutron energies before they reach the item and induce fission in the ^{238}U . The main disadvantage of this technique is that it lowers the flux of penetrating neutrons inducing fission in the ^{235}U ultimately decreasing the precision of the measurement. To compensate for the loss of neutrons, a stronger neutron source must be used, resulting in a bigger and more expensive system due to the increased cost of materials needed to adequately shield the larger source.

The second option is to produce multiple calibration curves that adequately represent the unknown or target measurement item. Some analysis software, such as the ^{252}Cf item analysis software used with the ^{252}Cf shuffler, can interpolate between established calibration curves to provide results specific to the item enrichment. Unfortunately, this requires many calibration standards that may not be available for safeguards activities. Additionally, precision is lost due to the interpolation of the data [12].

The focus of this research was to develop the DEANI method to perform deeply penetrating (beyond a few infinite thicknesses for 186 keV gamma-rays) enrichment measurements to support the quantification of ^{235}U and ^{238}U within a measurement item while reducing the need for prior isotopic information and minimizing complicated calibrations. Because the fission cross sections of ^{235}U and ^{238}U have very different energy dependencies, the induced fission rates in the material can be influenced by the incident neutron energy. Through the addition of a second interrogation source (of a differing energy), the different isotopes in the sample can be preferentially interrogated leading to a measureable difference in the neutron signal. A relationship between the measured delayed neutron data and uranium enrichment of the item was established and used to differentiate the isotopes, thus determining the enrichment of the sample.

Specifically, the DEANI method is a two-part method; each measurement uses a different interrogation source to induce fission in the measurement item. The resulting delayed neutrons are measured. The ratio of these delayed neutron count rates is then calculated and used to determine the enrichment of the sample. The work outlined here describes the measurement design process, simulations, and measurements used to develop and verify the DEANI method.

The development and demonstration of this dual-energy approach has been achieved using a modified ^{252}Cf Shuffler at Oak Ridge National Laboratory (ORNL) and delayed neutron rates as the observable of the approach. The shuffler was chosen as the primary development tool because of its outstanding statistical precision and accuracy (when suitably calibrated) in determining ^{235}U mass, its ability to more readily accommodate the addition of a secondary neutron source, and its availability for R&D work.

Additionally, the primary measurement items used in this study were New Brunswick Laboratory (NBL) certified reference materials (CRMs) consisting of approximately 230 g of U_3O_8 inside welded aluminum cans. While these items do not constitute extremely difficult measurement scenarios, they are well known and were available to aid in the development of the technique. As with the active neutron techniques, the dual-energy method should work for other material types, amounts, and packaging, including inhomogeneous items. This is discussed later in the dissertation.

1.3 Research Goals, Benefits, and Potential Applications

The ultimate goal of this work was to determine whether or not the ^{235}U enrichment of bulk uranium items can be accurately determined using the dual-energy approach briefly discussed above, to establish the scientific basis of the method and define its performance capability. Development of this method required design and physical integration of the secondary neutron source, careful examination and optimization of measurement parameters for each interrogation source, and careful selection and evaluation of

appropriate nuclear data sets (i.e., delayed neutron group data). These tasks were accomplished through a combination of simulation-based calculations and experimental measurements. Monte Carlo N-Particle (MCNP) simulations were used to extract fission rates for analytical calculation of the delayed neutron rates, determine optimal system parameters, perform sensitivity analyses, and to demonstrate expected performance; the application of this technique was studied experimentally using the ORNL ^{252}Cf Shuffler. Post-processing analysis scripts were written to interpret both measurement and simulation data.

Central to the successful demonstration of this technique was the optimization of the measurement system for both neutron sources. The physical measurement characteristics (e.g., choice of secondary source, source location/positioning, shielding or required spectrum tailoring materials) for the secondary measurements were carefully considered. A variety of potential neutron sources including deuterium-deuterium (D-D) and deuterium-tritium (D-T) neutron generators were evaluated to determine the best secondary neutron source for this approach. The D-D generator was also evaluated as a replacement for the ^{252}Cf in the shuffler. The measurement parameters (e.g., timing structure, number of shuffles, etc.) were also optimized for each source. The appropriate nuclear data sets were selected, and as a result of this study the sensitivity to these nuclear data sets was quantified. Additionally, an examination of a proposed 8-group delayed neutron precursor model was conducted to determine its effect on the expected results.

This methodology has the potential to increase the effectiveness of both domestic and international safeguards by improving the accuracy of neutron measurements targeting direct quantification of fissile content, especially for large, dense items that cannot be accurately measured with gamma isotopic measurements. Existing and newly proposed NDA systems may also benefit from such a deeply penetrating measurement technique. For example, integration into the proposed UF_6 cylinder portal, designed to

systematically monitor UF₆ cylinders using ³He tubes in the walls of the portal may be possible [13]. This dual energy approach may also be a beneficial addition to current passive UF₆ cylinder measurement systems, such as the passive neutron enrichment meter (PNEM), which currently require isotopic information to interpret the results. It also has the potential for standoff quantification of fissile mass within arrays of waste containers as may be encountered inside waste storage vaults.

1.4 Original Contributions

Original contributions from the development of the DEANI method include:

- A new technique for estimating ²³⁵U enrichment through dual-energy interrogation and measurement of delayed neutrons has been developed and successfully demonstrated.
- Experimental measurements based on a D-T generator inside a ²⁵²Cf Shuffler are reported for the first time. This included adaptation and optimization of a ²⁵²Cf Shuffler for operation with a neutron generator (including measurement parameters and physical adaptation of the counter)
- A report of the impact of thermal-, fast-, and high-energy delayed neutron group constants and nubar values on estimated delayed neutron rates have been reported
- The generation of post-processing scripts to support data analysis of the DEANI method, which may form the basis for future integrated analysis software packages
- A study of the potential replacement of the ²⁵²Cf source with a D-D generator
- A comparison of 6-group delayed neutron model and 8-group delayed neutron model for delayed neutron measurements in a ²⁵²Cf Shuffler was reported
- An evaluation of Monte Carlo N- Particle 6 (MCNP6) delayed neutron capabilities with respect to the ²⁵²Cf Shuffler

2 BACKGROUND

This chapter is intended to provide abundant background information related to safeguards measurement techniques and currently used systems (focusing on both passive and active, neutron and gamma methods) primarily focused on the measurement of uranium. It is meant to provide an overview of the current technologies used and on current related works. The ^{252}Cf Shuffler is thoroughly discussed in this chapter as are the fundamentals of delayed neutron counting.

2.1 Overview of Safeguards-related NDA Methods for ^{235}U Mass Determination

There are many NDA measurement techniques used to characterize nuclear materials throughout the nuclear fuel cycle. Some techniques and instruments are capable of quantitatively measuring the fissile mass while others only qualitatively measure some attribute of the material (e.g., enrichment). The following subsections briefly summarize common quantitative measurement techniques and current technologies used by the IAEA, State authorities, and/or facility operators to account for nuclear materials. These subsections are divided into passive and active neutron and gamma methods. Passive methods measure particles emitted from spontaneous decay of atoms whereas active methods measure emissions from induced reactions by an external source.

Passive methods have two distinct advantages with regards to safeguards measurement: they require no external radiation sources and they are suitable for unattended monitoring applications. The key drawback for passive measurements is shielding in the forms of self-attenuation and/or self-shielding of the signal, attenuation from the matrix surrounding the materials, and/or intentionally engineered shielding. Active methods, on the other hand, require the use of an external radiation source but are far more penetrating than passive methods. The measurement application generally directs the type of measurement needed.

2.1.1 Passive Neutron Techniques

Passive neutron techniques rely on spontaneous fission of the nuclear materials to generate a neutron signal. These techniques are ideal for Pu measurements where the spontaneous fission yields are large (e.g., $1.02\text{E}3$ n/s/g for ^{240}Pu); however, they are generally not practical for uranium applications where the spontaneous fission yields are extremely low (e.g., $2.99\text{E-}4$ n/s/g for ^{235}U) and the observable signatures are small. Therefore, passive neutron techniques are only briefly discussed.

2.1.1.1 Gross Neutron Counting

The simplest form of neutron measurement is gross, also called totals or singles, counting. In gross neutron counting, every detected neutron counts as a single event and is added together to produce a summed neutron signal, the total neutron rate. Because there is little to no energy or time-correlation information for the detected neutrons, the source of neutrons (e.g., from fission or (α,n)) cannot be characterized adequately. Therefore, gross neutron counting is generally used to survey items or areas for the presence of fissile nuclear material. The IAEA currently uses the Handheld Neutron Monitor (HHNM) shown in Figure 2, which employs three ^3He tubes along with other components, to search for and locate neutron sources based on an alarm threshold set during a background measurement [14]. The use of ^3He for neutron detection is well documented and will not be covered here [7].

Another ^3He tube based gross counting system, the Portable Neutron Uranium Hold-up Monitor (PNUH), is used by the IAEA to measure the amount of uranium hold-up inside the process equipment at various enrichment facilities [14]. This system is designed to measure the dominant $F(\alpha,n)$ neutrons from materials such as UO_2F_2 , and through extremely careful calibration and analysis, convert the response to a mass value for uranium. This system requires extensive process knowledge and isotopic information to accurately analyze the measurement signal. Similarly, UF_6 cylinders with enrichments

above a few percent have a large $F(\alpha,n)$ signal (from the ^{234}U) that can be measured passively. This technique requires knowledge of the $^{234}\text{U}/^{235}\text{U}$ ratio.

Gross neutron counting, coupled with gamma spectrometry, is also the primary target for the fork detector and the unattended fuel flow monitor, both of which measure spent fuel. The fork detector, shown in Figure 3, combines gross neutron and gamma measurements using four fission chambers and two ion chambers, respectively [15]. The fork design allows the system to fit securely around the fuel assembly in a spent fuel pool. The ratio of neutron to gamma-ray signal is used to confirm the presence of the spent fuel.



Figure 2. HHNM [16].

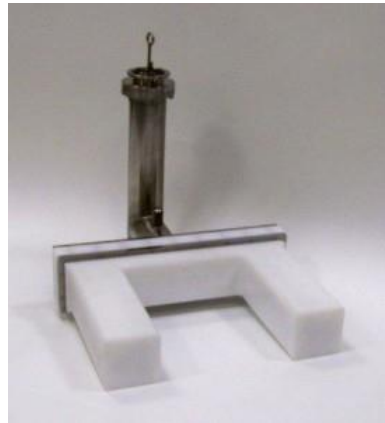


Figure 3. Antech fork detector [15].

While gross counting techniques are extremely useful for verifying the presence of nuclear materials or detecting relative changes in materials, very limited information regarding the nuclear material itself is obtained from the neutron signal alone (i.e., without supporting/complementary measurements and/or complicated calibration schemes). More complex neutron counting techniques must be employed to perform quantitative assays.

2.1.1.2 Coincidence and/or Multiplicity Counting

Coincidence counting methods can be performed in either passive or active modes. Passive modes, used primarily for Pu applications are discussed here. During a fission event anywhere from 0 to 8 neutrons may be released simultaneously. This value (number of neutrons emitted during fission) is referred to as the multiplicity. The average multiplicity value, $\bar{\nu}$, is characteristic of the fissioning isotope. Coincidence counting is a time-correlated neutron measurement technique that takes advantage of the multiplicity distribution of neutrons emitted during a fission event. In practice, the coincidence rate, or number of times a pair of neutrons is detected within a predetermined time gate, is measured. Since this coincidence rate can be related back to number of fissions occurring, the effective mass (discussed in section 2.5) of the sample can be estimated.

Measuring the coincidence rate is not a trivial process. Even though all fission neutrons from a single event are assumed to be emitted simultaneously, they are not generally detected at the exact same time. Instead these neutrons bounce around in the surrounding moderator, thermalizing and thus increasing the detection efficiency of the counter. The additional time needed for this slowing-down process means that the neutrons from a single event may be detected as different times. To account for this slowing down time and correlate the fission neutrons, advanced pulse-processing electronics (i.e., a shift register) are used. The shift register separates the incoming neutron pulse train into correlated (from a specific fission event) and uncorrelated (random or background) events [17]. A Rossi-alpha distribution, shown in Figure 4, is used to describe the time-correlation process [18]. The exponential die-away is evident in the distribution.

In short, a neutron pulse comes in and “triggers” the shift register. After a short time delay called the pre-delay, P, a counting interval, G, of a predetermined gate-width (time interval) begins. This first gate is called the reals plus accidentals gate, or R + A gate, where reals are another term for coincidences or doubles. During this time, the shift register keeps track of how many pairs of neutrons it detects. After the R + A gate closes

there is a long delay (much longer than the die-away time of the detector) ensuring that all neutrons associated with the initial trigger have decayed or leaked out of the system. After the long delay, a second gate, also G, begins. This accidentals gate, or simply A gate, captures accidental coincidences (pairs not related to the initial trigger event).

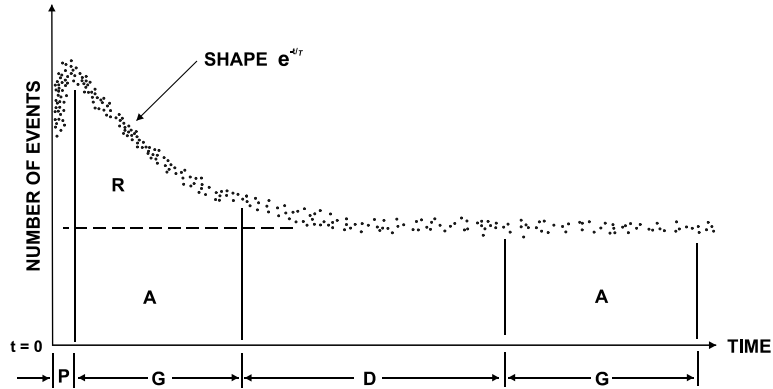


Figure 4. Rossi-Alpha distribution describing the timing structure of the shift register [7].

The shift register stores all incoming pulses in a buffer to reduce the dead-time of the counter. The timing structure is applied to each neutron that is detected. An example pulse train and depiction of how each neutron is treated is shown in Figure 5. The analysis of this data, which is more complex than simply subtracting $R + A - A$, is thoroughly discussed in literature [7].

Calibration curves are obtained by plotting the measured coincidence rate as a function of mass for a number of well-known standards. It is important that the standards used to generate this curve be representative of the unknown items (i.e., enrichment, matrix composition, density, and geometry) because of the nonlinear response due to multiplication and self-absorption. In the case of passive measurements, the measured response can then be used to produce an effective ^{240}Pu mass. It is important to note that

while the coincidence rate is related to the nuclear material content in the sample, precise knowledge of the item isotopics is needed to back into the fissile mass from the effective mass.

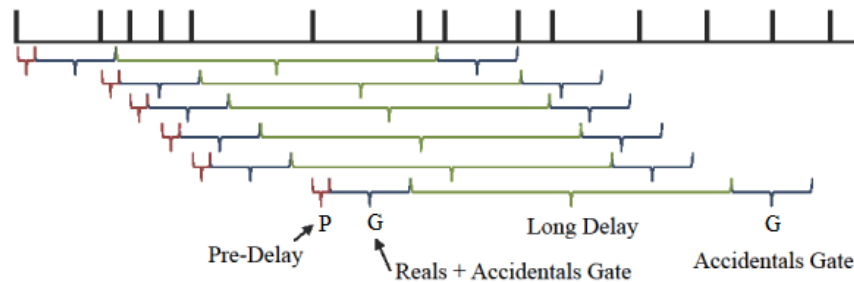


Figure 5. Neutron coincidence gate structure applied to a generic pulse train.

Coincidence counters come in an array of shapes and sizes depending on the particular application. Most coincidence counters used in safeguards applications are considered portable instruments which aid in inspection type inspections. Los Alamos National Laboratory designed the High Level Neutron Coincidence Counter (HLNCC) (the first generation portable neutron coincidence counter) to measure large PuO₂ items. The modular design of the HLNCC provides flexibility of the measurement cavity to accommodate various item geometries within the measurement well. The system contains 18 ³He tubes in a high-density polyethylene (HDPE) matrix and has an efficiency of approximately 17.5% [7]. The Inventory Sample Coincidence Counter (ISCC) is a similar well-type counter, albeit used to measure relatively small samples. The ISCC is extremely portable (with respect to safeguards equipment) and has an efficiency of nearly 35% making it ideal for inspection type activities [7]. Many other adaptations of these

passive coincidence counters exist and, other than their size and application, work in a similar manner.

The PNEM is another passive NDA system that combines both totals and coincidence counting to determine the enrichment and mass of ^{235}U in UF_6 storage cylinders. This system relies on the totals rate to estimate the uranium mass and the ratio of the doubles to singles to determine the ^{235}U enrichment. The PNEM system can also be combined with the Cd-ratio technique to provide additional details for feed and tail cylinders [19, 20].

Multiplicity counting is a similar technique but is aimed at measuring the singles, doubles, and triples rate (three neutrons within the gate). The advantage of multiplicity counting in Pu applications is that you can solve for all three unknowns (i.e., $^{240}\text{Pu}_{\text{eff}}$ mass, multiplication, and (α, n) rate). The advantage of multiplicity counting in U applications is the ability to determine the self-multiplication thereby reducing the bias caused by irregular geometries and densities. Unfortunately, these measurements are very difficult and require a counter with very efficiency, short die-away times, and short dead-times.

2.1.2 Active Neutron Techniques

Because uranium does not have a strong spontaneous fission signature, active neutron techniques are often used. In active neutron methods, the measurement item is interrogated by an external neutron source in order to induce fission in the item. That interrogation source varies by application.

2.1.2.1 Active Coincidence and/or Multiplicity Counting

Coincidence and multiplicity counting can also be implemented in active mode. While the principles of coincidence and multiplicity counting are the same as discussed in the previous section, active techniques utilize an external neutron source (often called the

interrogating source) to induce the fission events in fissile materials (usually ^{235}U). AmLi and ^{252}Cf are the most common interrogation sources used today. The significant difference in active coincidence counting is the presence of a high neutron background from the interrogating source.

The most common active neutron coincidence counters employed by the IAEA are the Active Well Coincidence Counter (AWCC), the Uranium Neutron Coincidence Collar (UNCL), and the Advanced Experimental Fuel Counter (AEFC). The AWCC and the UNCL are shown in Figure 6 and Figure 7, respectively.



Figure 6. AWCC and supporting electronics [14]. Figure 7. UNCL and supporting electronics [14].

The AWCC is the workhorse for neutron-based safeguards applications involving the measurement of bulk uranium items with a diameter up to 20 cm and a height up to 35 cm. The traditional system contains 42 ^3He tubes in an HPDE matrix. Two 10^4 n/s

$^{241}\text{AmLi}$ sources located at the top and bottom of the counting chamber emit (α,n) neutrons that penetrate the sample and induce fission in the uranium. The fission neutrons, which again are emitted in groups or multiplicities between 0 and 8, are released simultaneously. Detection and analysis of these time-correlated neutrons, coupled with isotopic information, allows the ^{235}U mass to be determined.

AWCCs have a number of advantages including operational flexibility (i.e., the ability to run in passive or active mode and the ability to operate in thermal or fast mode); a relatively high detection efficiency of ~26%; sustainability (^3He tubes have proven to be rugged and have a long life); and a transportable design. In thermal mode, the sensitivity of the AWCC can be as good as 1 g ^{235}U [7]. The source-to-sample coupling of the AWCC limits the measurement accuracy for irregular or non-predictable sample geometries; the size of the measurement cavity restricts the measurement of larger items such as waste drums, fuel assemblies, or UF_6 cylinders; and AmLi sources are becoming increasingly difficult to obtain (no longer commercially available). The precision and sensitivity are also limited because of the high background generated in the system by the AmLi sources.

The UNCL is primarily used for verification of ^{235}U mass in LEU fuel assemblies. The detector contains 18 ^3He tubes divided amongst four HDPE slabs that fit snugly around a fuel assembly. The UNCL also utilizes an AmLi source located in the “door” of the collar [21]. The coincidence rates, coupled with the active length of the pins/assemblies, are used to calculate the ^{235}U mass of the assembly, assuming the UNCL has been carefully calibrated using representative standards. Complications arise for certain types of fuel, particularly BWR fuel where burnable poisons are present. Adaptations for the UNCL have been developed to reduce the error associated with burnable poisons [22].

The AEFC can operate in either passive or active mode (where it employs an AmLi neutron source) and is used to characterize spent fuel under water. This system contains

^3He tubes in two rows (inner and outer). The inner row measures the coincident rate while the outer row measures the fission rate of the item [14].

Variants of these active coincidence counting measurement systems are also in use, however, all require calibration standards representative of the measurement item (e.g., same material type, enrichment, etc.) and isotopic information to back out the fissile mass. Additional drawbacks of active coincidence techniques include an increased signal-to-noise ratio caused by the presence of the interrogation source(s). This increase in background neutrons leads to a decrease in measurement precision and increases the minimum detection limit. Additionally, self-induced fission within the sample, called multiplication, can also significantly affect the measurement results.

2.1.2.2 Differential Die-away

DDA is a technique that exploits the difference in the die-away times between thermal interrogating neutron flux established in the measurement cavity and the flux generated by prompt fission neutrons within a fast neutron detection system to determine whether or not fissile material is present [23]. In most cases, the interrogating neutron flux is produced by a D-T neutron generator although some studies have suggested that ^{252}Cf may serve as an alternative interrogation source [24]. When no fissile material is present, these fast interrogation neutrons die-away quickly and the temporal decay can be represented as a simple, single exponential. When fissile material is present, the induced fission neutrons appear as a secondary fast neutron source in the system, thereby introducing a second exponential term in the die-away equation. Figure 8 [25] shows the difference in the die-away data for the interrogating flux and for the interrogating flux plus fission flux. Around channel 200, the fission neutrons begin contributing to the signal and there is a clear difference between the die-away curves.

Since DDA is generally used as a screening tool for the presence of fissile materials (sensitive to ~ 1 mg U or Pu in a 10-minute assay), it is generally used in applications

such as go/no-go clearances, package monitoring, and waste assay; however, optimization and modification of the DDA technique to improve the quantitative capability is an ongoing topic of research. Previous studies have shown that the ratio of fission neutron response to that of the interrogating source is dependent upon the ^{235}U content. This ratio can therefore be used to generate a calibration curve allowing the mass of ^{235}U to be determined under specified conditions [26]. Further, the position of the fissile material inside large containers can be estimated based on the ratio of the amplitude of each exponential term in the die-away equation. A package monitor and waste assay system are shown in Figure 9 and Figure 10, respectively.

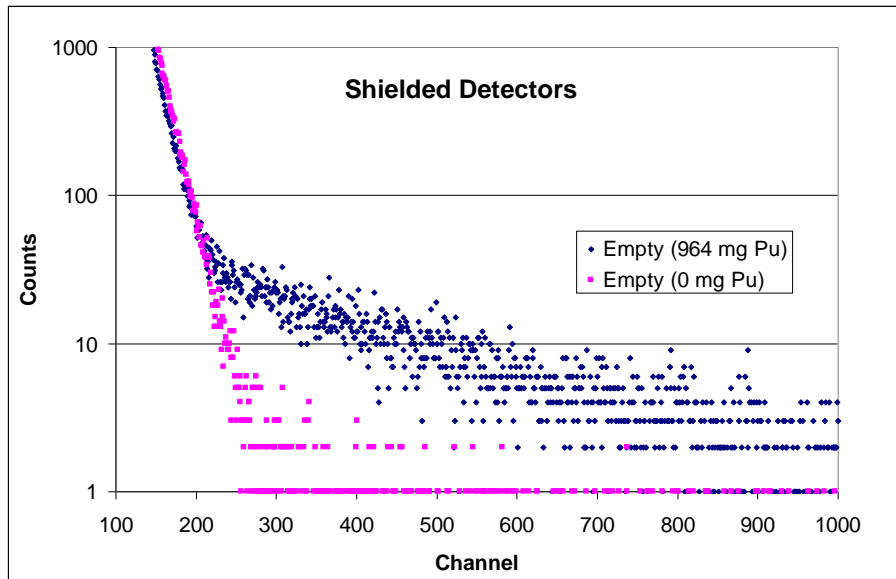


Figure 8. Die-away for interrogating flux (pink) and interrogating flux with fissile item (blue) [25].

A major benefit of a DDA system is the speed at which large numbers of items can be scanned; milligram quantities of ^{235}U equivalent can be detected on the order of a minute. The drawbacks are that lower energy neutrons result in larger self-absorption effects and

do not deeply penetrate large, dense items. This results in large matrix effects and complicates measurements.



Figure 9. DDA Package Monitor at ORNL.

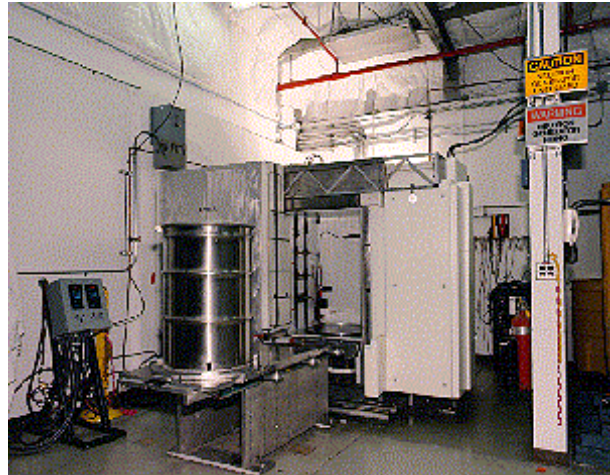


Figure 10. Active/Passive Neutron Assay system for waste measurements [25].

2.1.2.3 Delayed Neutron Counting

Delayed neutron counting is a technique that takes advantage of the time delay between prompt neutron emission (from fission) and neutron emission from de-exciting fission product daughters. Recall, when a nucleus fissions it generally results in the production of large fission products, neutrons, gammas, and/or other subatomic particles. These particles are often described as “prompt”, to signify that they are emitted “instantaneously” at the time of scission (on the order of picoseconds). These prompt neutrons are the target of DDA and active coincidence and multiplicity counting techniques.

Fission products are often neutron-rich and typically decay by beta emission resulting in a highly-excited daughter product that may subsequently de-excite by neutron emission. These neutrons are referred to as “ β -delayed” or simply “delayed” neutrons because they are emitted a relatively long time after the initial fission event. The fission products that lead to delayed neutron emission are called delayed neutron precursors while their daughters are called delayed neutron emitters. The time at which the delayed neutron appears is strongly dependent on the half-life of the precursor since the daughter product de-excites almost instantly. Therefore, the probability of delayed neutron emission and the related time constants are linked to the precursor, not the emitter.

Delayed neutrons make up a very small fraction of the total neutrons emitted from a fission event (0.65 % in ^{235}U and 1.48 % in ^{238}U) [27]; however, these delayed neutrons (with average energies between 300-600 keV) play a huge role in reactor kinetics and make it possible to control nuclear reactors [28]. For measurement applications, they provide a relatively large neutron signal in a very low background environment under most measurement conditions supporting high-precision assays of nuclear materials.

To use delayed neutrons as a signature, a strong interrogation source is used to irradiate and induce fission in the measurement sample. After some prescribed irradiation time, the source is removed and delayed neutrons are subsequently counted. The use of a carefully chosen time structure allows for discrimination between source neutrons and fission neutrons. Because the source is removed during the measurement of delayed neutrons, the background is extremely low and the signal-to-noise ratio is large resulting in very precise measurements. Any additional sources of neutrons present in the measurement cavity reduce precision. These sources may include spontaneous fission, photo-fission induced by prompt gammas, or other nuclear reaction resulting in delayed neutron emitters. The spontaneous fission interference is responsible for the poorer precision in plutonium applications (compared to uranium applications). To distinguish delayed

neutrons from these sources of “background”, long background measurements and again careful timing characteristics must be used.

Delayed neutron counting is traditionally applied to the measurement of items containing a single fissile isotope, such as ^{235}U (since ^{234}U , ^{236}U , and ^{238}U are not fissile and ^{235}U is the primary target for assay of HEU components and fuel). Samples containing more than one fissile isotope (such as mixed-oxide) can be measured passively then actively where the passive signal is taken as the background for the measurement.

If the isotopics are well-known and representative calibrations are available, the mass can be determined very accurately since delayed neutron count rates are proportional to the effective mass of the fissile isotope. The ^{252}Cf Shuffler, discussed in depth in section 2.3, is one delayed neutron system used to measure the fissile content in a variety of items. Figure 11 and Figure 12 show two types of shufflers used to measure uranium items. Shufflers are most beneficial for uranium applications where spontaneous fission rates are low and fill the measurement gap for large, dense or bulky items where gamma-ray measurements are ineffective due to attenuation in the material or matrix.

While delayed neutrons measurements are less sensitive for plutonium applications because of the intrinsically high background from spontaneous fission, most systems (including the ^{252}Cf Shuffler) are flexible enough to also operate as a passive neutron counter. The primary limitations for delayed neutron counters are the need for a strong, high flux neutron source, the large footprint of the system, the cost of ^3He , and the sensitivity to background neutrons. Since delayed neutrons are the topic of this research, concepts and theory specific to delayed neutron counting are further discussed in section 2.4.

For all quantitative neutron measurements, isotopic information and/or extensive calibrations are required to extract the fissile mass. Both coincidence counting and delayed neutron counting are capable of providing a quantitative result, while DDA is

most often used as a screening tool to determine whether or not fissile materials are present. The primary goal of this research is to determine whether or not the isotopes can be determined well enough through the implementation of this dual-energy approach such that secondary isotopic measurements are not warranted.



Figure 11. The Uranium Scrap Shuffler [29].



Figure 12. Shuffler for 55 gal drums [29].

2.1.2.4 Neutron Activation Analysis

Neutron activation analysis (NAA) is one of the most common active techniques used for characterization of mg quantity materials. NAA is a useful technique that provides timely, highly sensitivity measurements. The identification of fissile materials, namely ^{235}U and ^{239}Pu , through the measurement of photon-induced and neutron-induced delayed gamma-rays was introduced by Hollas et. al. and Beddingfield and Cecil, respectively [30, 31]. Both Hollas and Beddingfield concluded that the intensity ratios of fission product gamma-rays could be used as a signature for identifying isotopes present in the

given measurement item. Since, many investigations on various fission product ratios have been completed [32-36].

NAA is often performed by pneumatically transferring prepared samples into a nuclear reactor where it is subject to a high neutron flux. D-T generators have also been used as the interrogating flux for NAA measurements but are plagued by a relatively low flux, lower cross-sections of threshold reactions, and interference of other induced gamma-rays [37]. D-T generators have also been used to evaluate the ability to characterize radioactive waste drums; however, these types of samples often have high gamma backgrounds requiring heavy collimation and shielding. Thus, a larger interrogation flux is required to obtain a measurable gamma signal with good precision.

The resulting delayed gammas are often measured. Delayed gammas can be measured in a similar manner to that of the shuffler and are somewhat easier to measure (when using a pulsed source) than prompt fission photons because of their relatively long half-life. Nicol et.al. used a D-T generator to induce fission in 225L waste drums to characterize the ^{235}U and ^{239}Pu content [33]. Between neutron pulses, the delayed gammas from various fission products were measured. While this technique proved useful for low and medium activity drums, the high gamma background (primarily from ^{137}Cs contamination) coupled with the reduced measurement signal from the required collimation ultimately limits the application for bulk uranium items in many safeguards applications. A larger incident neutron flux would induce more fissions in the drum thereby increasing the production of the delayed gammas and may help reduce the measurement uncertainty; however, such a large neutron flux is seldom available for most safeguards applications. Studies on the measurement of higher energy gamma-rays are also being proposed and are ongoing areas of active research [38]. Plastic scintillator based systems have also been used to screen cargo for SNM [39].

While mass quantification of ^{235}U is a more challenging task, it can be done given the following two conditions are met: the fission rate per source neutron is well known (achieved using Monte Carlo simulations) and the attenuation of the delayed gammas can be accounted for through gamma transmission measurements. Current delayed gamma research aiming to quantify ^{235}U mass includes evaluation of differences and ratios between various fission product yields coupled with Monte-Carlo simulation techniques and/or delayed neutron measurements [40].

In theory, delayed gammas possess a higher intensity and longer half-lives than their delayed neutron counterparts. Advantages of NAA techniques using delayed gamma-rays include higher penetrability in comparison to passive gamma techniques, shorter detector die-away times relative to neutron counters, higher detector efficiencies with smaller footprints, and the potential to glean more information from the measurement (e.g., energy/ isotopic information). Delayed gamma methods excel for low background (minimal fission product contamination) and for small samples where dense, unknown matrices do not complicate the measurements.

Delayed gamma techniques also share some of the same disadvantages as their delayed neutron counterpart including increased background due to the presence of the interrogating source and an increased active background due to other nuclear reactions occurring in the sample or detection materials themselves (e.g., $^{16}\text{O}(n,p)$). In fact, gamma-ray measurements are susceptible to increased background rates from residual activation. Fission in both ^{235}U and ^{238}U also complicate the direct measurement of the fissile content, which is the primary motivation for this study.

2.1.3 Passive Gamma-based Techniques

Many gamma spectrometry methods are used to verify and/or confirm the presence of a type of materials (e.g., the Spent Fuel Attribute Tester (SFAT) which confirms the presence of spent fuel based on the fission product and activation product signatures) or

verify a specific material attribute (e.g., the U/Pu Inspector, which uses a peak ratio method in the Multi-Group Analysis for Uranium (MGAU) software to determine ^{235}U enrichment) [14]. In many cases, these measurements are complementary to other quantitative techniques (e.g., they are used to provide isotopic details for analysis of quantification measurements). There are some gamma-based methods, however, that can provide a quantitative value for the fissile content within a given item.

For example, the combined procedure for uranium concentration and enrichment assay (CMPU) determines the concentration of uranium through absorption edge spectrometry and ^{235}U enrichment through basic gamma spectrometry. Similarly, the Hybrid K-edge Densitometer (HKED) is a system that combines K-edge transmission with x-ray fluorescence to determine the U and Pu concentrations in aqueous reprocessing streams [41]. Also coupled with isotopic information, this technique can provide the desired isotopic masses required for safeguards applications.

The In-Situ Object Counting System (ISOCS) is a widely used technique that generates mathematically-calculated efficiency values without the need for radioactive sources. This is possible because the detector has undergone extensive factory characterization whereby an MCNP model is developed to accurately reproduce (within 5%) a set of measurements collected at the factory. The MCNP model is then used to generate a large lookup table of efficiencies versus position by energy for a point source. Users build a virtual model of a measured sample and detector, which includes physical parameters such as the inner and outer container dimensions, chemical composition, and density of the materials, that is used by the software to generate an efficiency curve. This curve can then be used for the quantitative measurement of the object. The system employs the use of a gamma-ray detector (primarily High-Purity Germanium (HPGe)) characterized specifically for use with ISOCS along with the supporting electronics and software. ISOCS is especially useful when representative calibration sources and standards are not

available for empirical efficiency calibration or when sample items do not meet standards assumptions [42].

The Segmented Gamma Scanner (SGS), shown in Figure 13, is a system extensively used for the quantitative measurement of HEU in a low-density matrix inside 200 L drums. The basis of this method is the acquisition of high resolution gamma-ray spectra using a collimated HPGe detector. The drum is measured in segments along the vertical axis of the drum as it is rotated to smooth out inhomogeneities in each segment. A second scan with a transmission source exposed is used to derive matrix-content attenuation correction factors for the gamma lines of interest [43]. The SGS can measure down to 0.1 g ^{235}U up to 1 kg with average accuracy of $\pm 20\%$ for 0.3 g/cc density drums [44]. The Tomographic Gamma Scanner (TGS), shown in Figure 14, is a similar system that provides an item-specific, attenuation-corrected, quantitative image of a drum containing SNM or transuranic waste using the same image reconstruction technology initially developed in the medical field. The TGS is capable of measuring between 0.4 g and 1 kg of ^{235}U with average accuracy of $\pm 20\%$ for 1 g/cc density drums [45].

SNM in waste and scrap product is particularly difficult to assay due to the wide range of isotopes present in the complex inhomogeneous matrix contained in a drum or can. While both the SGS and TGS are used to measure nuclear materials for waste disposition purposes, they have been underutilized for safeguards applications primarily due to complicated calibrations, high empirical uncertainties associated with unknown shielding of low-energy gamma-rays characteristic of ^{235}U , and outdated algorithms and technology. The self-attenuation and attenuation in the surrounding matrix limits the application of passive gamma-based techniques especially for larger, denser materials or measurement items often found in waste or scrap materials.



Figure 13. Canberra SGS, which scans vertically along the height of the drum.



Figure 14. Canberra TGS, which scans vertically and horizontally across the drum.

2.1.4 Active Gamma Techniques

Again, active techniques are of special interest for uranium applications where passive neutron emission is low and passive gammas are low-energy and easily attenuated. Active gamma techniques rely on photon-induced fission (generally via electron accelerators) and measurement of the subsequent high-energy gamma-ray emissions from the resulting short-lived fission products. These gamma-rays (prompt or delayed) are the target measurement signal. Resulting delayed neutrons (discussed in Section 2.1.2.3) may also be measured.

Specific applications for active gamma measurements include detection of SNM in cargo, characterization of nuclear fuels and byproducts, arms control and treaty verification, and standoff detection. These applications are often focused on detecting and characterizing measurement items making them a suitable alternative to active neutron counting for homeland security applications. Active gamma techniques are also useful when measuring spent fuel (or other materials) in thick concrete containers that would thermalize a neutron interrogation flux prior to reaching the target material. These techniques excel when measuring low-density items where the gamma-rays are highly

penetrating and shielding is limited; however, they suffer from reduced signal intensity with higher density matrices.

The limiting factor for most active gamma techniques regarding safeguards applications specifically is the large photon flux required to generate a statistically significant signal. This is often achieved using an electron accelerator to create Bremsstrahlung, which produces a high intensity flux requiring massive amounts of shielding. This results in a prohibitively expensive system for safeguards applications. In addition, only a small fraction of the photon spectrum is at useful energies. Other factors that limit active gamma techniques, with respect to safeguards applications, include complications from gamma pile-up and photo-fission resonances, neutron damage to HPGe crystals, large detector dead-times, and gamma self-shielding. There is also a larger ambient gamma background in comparison to a neutron measurement. The presence of resonances and large dead-times minimize the potential for prompt gamma measurements, whereas delayed gammas may be measured between pulses.

An alternate active gamma technique, called nuclear resonance fluorescence, has also been investigated as a way to characterize SNM. This method employs Bremsstrahlung from an electron accelerator to excite nuclei at specific energy states such that those nuclei de-excite through the emission of high energy gamma-rays. Traditional gamma spectrometry techniques can then be applied to detect, identify, and even quantify SNM in a measured item [46].

Both neutron and photon interrogation (using an electron linear accelerator) have been used to induce fission and generate a delayed neutron signal. The measurement application often determines the type of interrogation source needed; Neutrons are used for most safeguards-related NDA measurements while photon interrogation is used for fissile material detection and to some extent identification [47]. Neutron-induced fission was briefly discussed in Section 2.1.2. The advantages of neutron-induced fission include

repeatability through the use of a pulsed source (i.e., a neutron generator), higher gamma-ray yields (about a factor of 2 in comparison to photon-induced fission), and the availability of published data for many neutron interrogation applications (neutron induced fission has been more heavily studied) [48]. Although there is less research discussed in literature regarding the use of photo-fission sources, they may be used to induce fission in SNM and have an advantage in that the die-away time after irradiation is quite small compared to that of a neutron source. This allows the very short-lived but higher yielding precursors to be measured [30].

2.2 Overview of Safeguards-related NDA Methods for Uranium Enrichment Determination

Determination of uranium enrichment by NDA techniques is a critical element in the assay of nuclear materials. Uranium enrichment measurements are one of the most common measurements performed in support of nuclear safeguards and provide qualitative information about nuclear material that is often required to interpret other quantitative measurement system results. These confirmation measurements may be performed using various tools and techniques; the best technique is often dependent on the material composition, measurement geometry, sample geometry, matrix, and many other factors. Below is a summary of the most common systems and techniques used to determine the isotopic fractions of uranium-bearing items.

2.2.1 Common Enrichment Methods for Uranium

2.2.1.1 Enrichment Meter Principle

Many enrichment software algorithms, including WINU235 [49], rely on the basic enrichment meter principle. For an infinitely thick uranium sample, the 186 keV gamma flux at the surface of the sample reaches an equilibrium proportional to the ^{235}U enrichment of that sample (almost independent of the physical form). Since all 186 keV gammas measured are assumed to come from the sample, many aspects of the

measurement must be carefully controlled and/or well known (i.e., matrix uniformity; enrichment uniformity; container material and thickness; infinitely thick sample size; collimated/shielded detector; detector to source distance; counting electronic properties such as dead-time, stability, pile-up; and detector characteristics like size, efficiency, energy resolution) [50]. In addition, due to lack of accurate physical constants (nuclear data) and difficulty determining the absolute gamma detection efficiency, it is necessary to relate the sample measurements to at least two appropriate calibration standards. The applicability of given calibration standards can be extended to other materials types by carefully applying correction factors that normalize the gamma response with respect to differences in the matrix composition and container wall [51].

The enrichment meter principle can be applied using any detector system capable of recording gamma-ray spectra but is generally performed with a NaI detector due to its cost effectiveness. In fact, the On-Line Enrichment Monitor, a system used to measure the ^{235}U enrichment in process pipes using a temperature- and pressure- dependent adaptation of the enrichment meter technique [52].

2.2.1.2 Improved Enrichment Meter

The NaI Gamma Enrichment Measurements code (NaIGEM) is based on the enrichment meter principle; however, it is enhanced by an algorithm that fits computed response profiles to the measured data in the 186 keV gamma-ray region by the method of least-squares. Components of the spectral fit include the known gamma-rays from ^{235}U between 143 keV and 205 keV, Compton scattering (both in the detector and the low-angle scattering in the sample and container walls), iodine escape peaks, and thorium interferences. These response profiles account for spectrum shifts (gain changes), changes in the detector resolution, Compton scattering in the source and in the absorbing materials, and responses to account for other activities. The peak fitting method is an iterative process that must converge to account for changes in gain and resolution prior to calculating the uranium isotopics through comparison of the measured spectrum to the

single calibration spectrum required by this technique. This calibration measurement is permanent for a given detector/collimator type [53]. The HM-5, a device heavily used in international safeguards, employs the NaIGEM code [54].

2.2.1.3 Peak Ratio Techniques

Peak ratio techniques are indirect analysis methods that use ratios of simultaneously observed gamma lines from ^{235}U and ^{238}U in a given spectrum. Because of the dependence on the indirect measurement of various daughter products, the applicability of this technique is limited to aged uranium where secular equilibrium has been reached. Additional difficulties arise in determining the total relative detection efficiency over a wide energy range and in evaluating the unresolved complex triplet region containing gamma- and x- rays which require the use of a HPGe detector. However, peak ratio techniques have a tremendous advantage in many applications since they are significantly less dependent on sample parameters such as size, geometry, chemical composition, container properties, detector characteristics, measurement geometry, etc. [51].

The MGAU code (utilized by the U/Pu Inspector system widely used in the safeguards community) employs an algorithm that analyzes high resolution gamma spectra to determine the relative abundances of the uranium isotopes [55]. The primary advantage of this system is that it requires no efficiency calibration for matrix density, matrix type, or container making it ideal for routine or repetitive measurement applications. MGAU generally analyzes spectral information from two regions: the ^{235}U and ^{238}U gamma-rays in the 88-100keV range and also from the K-beta region to derive enrichment information and develop a local intrinsic efficiency curve, respectively. The local efficiency curve accounts for the detector efficiency as a function of energy, the attenuation caused by the sample container, and the self-absorption in the uranium material itself. In order to take advantage of the x-rays in the K-beta region, MGAU requires that the daughter isotopes be in equilibrium with the ^{235}U and ^{238}U parent isotopes. The optimum enrichment range

is between 3-20% ^{235}U ; however, acceptable measurement results are obtained for enrichments ranging from depleted up to 93% [56].

The Fixed-Energy, Response Function Analysis with Multiple Efficiencies (FRAM) software package is another isotopic analysis software package used to determine enrichment. It can be applied to bulk or item measurements. FRAM was originally developed to support Pu measurements, however, the algorithms were adapted to take advantage of $^{235}\text{U}/^{238}\text{U}$ ratios; thus providing the enrichment of the measurement item. Updates to FRAM now include analyses for ^{234}U , ^{236}U , and a correction that can be applied when a measurement item does not meet the secular equilibrium requirements [57]. Like MGAU, FRAM requires no calibration, no infinite thickness, and no container wall input. However, for U applications, it is still dependent on the lower energy gamma-rays from ^{235}U which present measurement challenges for large, dense items.

2.2.1.4 Passive Neutron Enrichment Measurement

As briefly mentioned in Section 2.1, the PNEM system is capable of roughly estimating the ^{235}U enrichment using the ratio of single to doubles for UF_6 cylinders. Since the U mass in these cylinders is relatively large, the passive singles rate is statistically significant and can be easily measured. This signal comes primarily from the $^{19}\text{F}(\alpha,n)$ reactions in ^{234}U . Since ^{234}U enrichment tracks with ^{235}U enrichment, the signal was used. Other neutron techniques to measure ^{235}U enrichment were not heavily pursued until recent years. Some of these efforts are outlined in Section 2.6.

2.2.2 Limitations

Gamma-rays are easily attenuated and even with corrections, there comes a point (dependent on the linear attenuation coefficients of the material and the matrix, the volume and shape of the material and container, the position and orientation of the item with respect to the detector, and the size, shape and efficiency of the detector) where the attenuation is too large and the accuracy of the assay is lost. For methods that rely on the

sample being infinitely thick, the technique is essentially blind to the rest of the material, and large errors can be obtained for inhomogeneous items. Peak ratio techniques are slightly better, but again are based on low energy gamma- and x-rays that are easily attenuated. As bulk uranium sample sizes increase or when there are potential shielding matrices encompassing the nuclear material, more penetrating techniques are necessary.

Gamma measurements are also inherently susceptible to background radiation primarily from cosmic-rays. Shielding can be applied to the gamma systems and the background can be accounted for; however, it must be done carefully to avoid measurement bias. While neutrons are also present in the background, they are so in smaller intensities. Passive neutron measurements (like the PNEM) also require knowledge of the $^{234}\text{U}/^{235}\text{U}$ ratio as a function of enrichment and ultimately are indirect measurement techniques that infer the isotopics as a result of the measurement of the ^{234}U .

2.3 ^{252}Cf Shuffler

This work was conducted using a ^{252}Cf Drum Shuffler [29] at ORNL. The ^{252}Cf Shuffler is an active neutron interrogation system used to quantify fissile material. It employs a ^{252}Cf neutron source to induce fissions in the item and measures the resulting delayed fission neutrons inside the counting chamber. Shufflers are generally used when the highest degree of precision is required for an assay or when gram quantities are too small to be measured by other means. While less frequently used in safeguards applications, they provide outstanding precision and accuracy for bulk uranium in comparison to AWCCs, due to the high background from the AmLi sources. Items such as spent fuel assemblies, low level waste drums, leached hulls, process materials, scrap, and waste have all been successfully measured in a ^{252}Cf Shuffler. [58]

Developed in the late 1970s, ^{252}Cf shufflers rely on the ^{252}Cf source to induce fissions in the fissile material and subsequently measure the delayed fission neutrons emitted from the sample. This delayed neutron count rate is then correlated to a ^{235}U mass, assuming

that the isotopic concentrations of the sample are known. The accuracy of shuffler measurements can be as good as 0.3% while the minimum detectable quantity is between 0.06 to 0.4 g ^{235}U [29].

A very important assumption made when developing the analysis routines for the ^{252}Cf Shuffler is that only one fissionable isotope is in the material being measured. While it is unlikely that only one fissionable isotope will be present, care has been taken to tailor the ^{252}Cf spectrum such that most neutrons are well below the induced fission threshold for ^{238}U (~ 1 MeV). While these lower energy neutrons favor inducing fission in the ^{235}U , there is still some probability of inducing fission in ^{238}U . This work will attempt to emphasize that contribution through the use of a secondary higher energy neutron source.

2.3.1 Hardware

The shuffler, shown in Figure 16, is composed of two main assemblies: the detection assembly (lower half) and the source housing/storage assembly (upper half). The detection assembly contains the large volume counting chamber surrounded by banks of ^3He detectors and HDPE. The cylindrical counting chamber is approximately 30 in across and 117 in tall. There are a total of eight neutron detector banks (six vertical banks around the counting chamber, one horizontal bank under the counting chamber, and one horizontal bank mounted at the top of the counting chamber) and 64 ^3He tubes. Since the interrogation flux incident on the fissile material can be perturbed by hydrogenous materials, the shuffler also uses two ^3He flux monitors: one bare and one wrapped in Cd. The ratio of these two signals provides a flux monitor correction that can be applied for strongly moderating items.

The ^3He tubes were manufactured by Reuter-Stokes and have a 0.1 in stainless steel wall construction. The tubes are grouped into banks, each embedded inside the HDPE moderator necessary to moderate neutrons and increases detector efficiency. A 1 mm thick layer of Cd covers the inner face of the neutron banks. The neutron bank properties

are summarized in Table 2. The bottom detector bank lies beneath a 2.5 in stainless steel plate (drum rotator) at the bottom of the counting chamber. A 1 mm Cd layer covers the top and bottom of the lower detector bank. The top detector bank is also covered with Cd and is supported by a 1/4 in steel plate at the top of the counting chamber.

Table 2. Neutron Bank Properties in the ^{252}Cf Shuffler

Bank	No. of ^3He tubes	Pressure (atm)	Tube Diameter (in)	Active Tube Length (in)	Tube Pitch (in)
Right Side	7	4	1	39	2.333
Right Rear	6	4	1	39	2.333
Right Door	7	4	1	39	2.333
Left Side	7	4	1	39	2.333
Left Rear	6	4	1	39	2.333
Left Door	7	4	1	39	2.333
Top	12	4	1	26	2.364
Bottom	12	4	1	26	2.364

A double-layer (1 mm steel in front of 1 mm Cd), cylindrical liner surrounds the counting chamber to both protect and prevent thermal neutrons from re-entering the counting chamber. This liner extends the height of the counting chamber and around the side and rear detectors. Outside (or behind) the detector banks, large HDPE blocks are used to 1) reduce the background in the counting chamber and 2) provide shielding from the ^{252}Cf source while it is in the counting chamber. The large amounts of polyethylene are needed to properly shield the ^{252}Cf source and account for the large size of the ^{252}Cf Shuffler.

A stainless steel reflector 10 in wide is located directly between the left and right rear detector banks and is used to soften the neutron spectrum and reflect more neutrons into the counting chamber, effectively increasing the irradiation flux inside the measurement chamber. The ^{252}Cf source guide tube is located towards the front of this reflector at the interface of the counting chamber. The source itself is attached to a Teleflex cable (driven up and down by a stepper motor) and resides in the storage location inside the top half of

the shuffler until needed. The entire upper half of the shuffler is the shielded storage housing for the ^{252}Cf source. The stepper motor and source guide tubes are attached to the outer wall of the storage housing.

2.3.2 Shuffling Mechanics

To take advantage of the low background environment in the shuffler, the interrogating source must be removed from the measurement chamber during the counting interval. This is achieved with the help of a stepper motor that drives the ^{252}Cf source into and out of the measurement chamber as shown in Figure 15.

As part of the measurement process, a long background measurement (with the source in the storage housing) is completed. The ^{252}Cf source is then driven into the counting chamber where it irradiates and induces fission in the item being measured. After a prescribed irradiation time, the source is rapidly withdrawn from the counting chamber. Once the source is stored, a counting interval begins and delayed neutrons are detected. Details regarding the counting sequence used in this work are provided in Chapter 4.

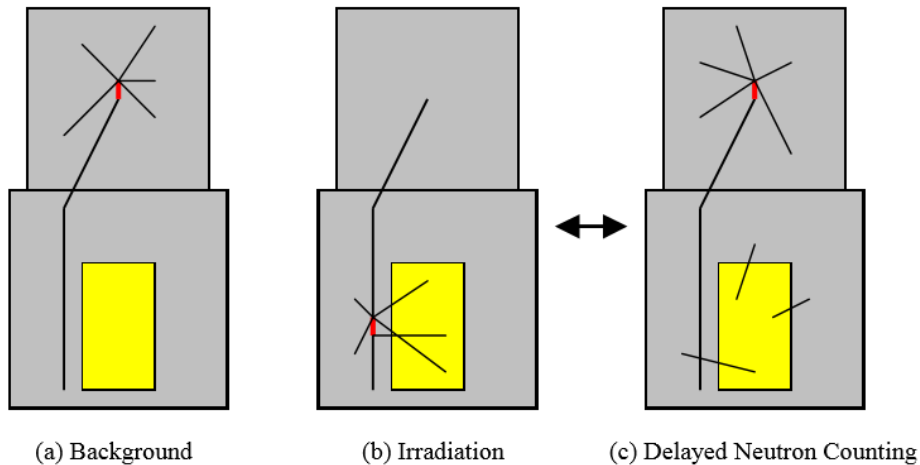


Figure 15. Basic ^{252}Cf Shuffler measurement process [29].

At the end of the counting cycle, the irradiation and counting process is repeated until the desirable measurement precision is achieved. The name ^{252}Cf Shuffler comes from the fact that the ^{252}Cf source is shuffled back and forth many times over the course of the measurement. Optimization of the timing intervals is performed to maximize accuracy and precision. A picture of the ORNL ^{252}Cf Drum Shuffler is provided in Figure 16.

2.3.3 Complications

Not every delayed neutron emitted is counted in the shuffler. This is partly due to the efficiency of the system; however, the nature of the measurement further reduces the countable fraction. Because the counting window does not begin until after the source is removed and shielded from the counting chamber, the very short-lived groups have already decayed. Additionally, the longer-lived groups are not detected because the counting window is simply too short (on the order of 5-15 seconds). Determining the countable fraction of delayed neutrons is covered in depth in Section 2.4.

The presence of other neutron sources also complicates the delayed neutron analysis since the detectors cannot differentiate between the sources of measured neutrons. These interfering sources include spontaneous fission and multiplication in the item itself, ^{252}Cf source neutrons that leak into the counting chamber, gamma-induced fission neutrons, and other delayed neutrons stemming from various nuclear reactions in the sample. Photo-fission and other nuclear reactions leading to neutron production are very small in ^{252}Cf Shuffler applications [58] and are generally neglected; however, this work makes use of a harder source spectrum (relative to Cf) such that this assumption warrants revisiting.

Lastly, the ability to extract the ^{235}U mass from the results relies on the availability of representative calibration standards and knowledge of the isotopic concentrations. For bulky, inhomogeneous items, the latter may be difficult to obtain through traditional gamma methods.



Figure 16. The ^{252}Cf Shuffler at ORNL.

2.3.4 Interrogation Source Characteristics

Since less than 1% of all fission neutrons are “delayed”, many fissions are needed to produce a measurable and statistically significant number of delayed neutrons. This means that a very strong interrogation source is needed to induce those fissions. ^{252}Cf is the most common spontaneous fission source and is used in many nuclear measurement applications. The ^{252}Cf source used in the shuffler is generally on the order of tens to hundreds of micrograms. ^{252}Cf has a high specific activity (2.34×10^{12} n/s/g), producing a neutron flux large enough to effectively irradiate samples inside the system. The average number of neutrons emitted per fission, $\bar{\nu}$, is 3.757 [7]. Because of its relatively short half-life (~ 2.65 y), the ^{252}Cf source must be replaced every 3-5 years for the shuffler to maintain good precision in relatively short count times.

The average neutron energy is 2.14 MeV and is most often described using the Watt fission spectrum described in Eq. 1, where E is neutron energy, a is 1.025 MeV and b is 2.926 MeV^{-1} for ^{252}Cf [29, 59].

$$N(E) = \exp\left(-\frac{E}{a}\right) \cdot \sinh(\sqrt{bE}) \quad \text{Eq. 1}$$

Occasionally a Maxwellian distribution, given in Eq. 2 is used to describe the neutron spectrum [7]. For ^{252}Cf , a is 1.43 MeV.

$$N(E) = \sqrt{E} \cdot \exp\left(-\frac{E}{a}\right) \quad \text{Eq. 2}$$

Figure 17 shows the difference in the two distributions. Note that the Watt spectrum was used for all simulation work pertaining to this dissertation.

Based on the Watt distribution, the average energy is over 2 Mev: however, the most probable energy is just 0.9 keV, just under the threshold for fission in ^{238}U . The advantages of using ^{252}Cf as the interrogating neutron source for uranium assay have been well-documented and include the constant, predictable intensity and yield of source

neutrons, the fact that minimal source maintenance is required, and the ability to scan measurement items which reduces the sensitivity to size and geometry.

The greatest drawbacks are the short half-life of the source and the inability to turn the source off. To eliminate frequent replacement of the source, larger than necessary sources are generally acquired so that the source has a longer useful lifetime. To remove and store the source from the counting chamber, a heavily shielded storage location is needed. This housing serves to reduce the dose from larger source and prevent neutrons from leaking into the counting chamber.

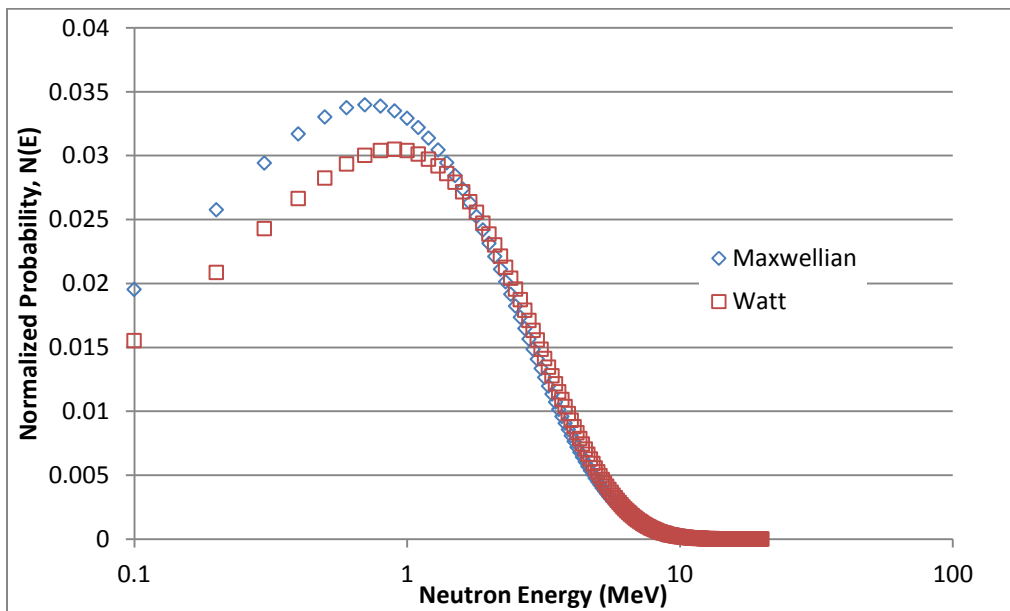


Figure 17. Comparison of ^{252}Cf neutron energy spectra using a Watt and Maxwellian distribution.

Proper decay corrections for ^{252}Cf must also be considered when using older systems (as is the case for the ORNL ^{252}Cf Shuffler). When using calibration sources such as ^{252}Cf , it is common for users to decay-correct the activity using properties of only ^{252}Cf , ignoring

the contribution from (and longer half-life of) ^{250}Cf . For sources more than ~ 10 years old, this leads to an underestimate of the neutron emission rate and can significantly affect calculations sensitive to the neutron yield. Eq. 3 shows the proper decay corrections used in this study:

$$S(t_2) = S(t_1)e^{(-\lambda_{252}(\delta t))} \left[\frac{1+R_1 e^{(\lambda_{eff}(\delta t))}}{1+R_1} \right], \quad \text{Eq. 3}$$

where $S(t_n)$ is the neutron rate at time, t_n , δt is the difference between t_2 and t_1 , λ_{252} is the decay constant for ^{252}Cf , λ_{250} is the decay constant for ^{250}Cf , λ_{eff} is the difference between λ_{252} and λ_{250} , and R_1 is the ratio of $S_{250}(t_1)$ and $S_{252}(t_1)$, which is 0.004742. This calculation is especially important since the ^{252}Cf source in the ORNL Shuffler is over 20 years old.

The DEANI method will implement a secondary source to influence the delayed neutron rates through interrogation with a different neutron energy spectrum. Background information of the sources considered in this study is provided in detail in Section 4.1.1.

2.4 Delayed Neutron Concepts

As briefly described in Section 2.1.2.3, delayed neutrons are emitted from the progeny (called the delayed neutron emitters) of β -decaying, neutron-rich fission products (called the delayed neutron precursors). Since their discovery in 1939, the characteristics of those delayed neutrons have been studied [60]. There are over 200 different precursors associated with ^{235}U fission, all with different half-lives and decay constants. Fortunately, a simplified group structure was developed and has been successfully used to describe these precursors. The following sub-sections describe the process by which delayed neutrons count rates are calculated and measured.

2.4.1 *Keepin 6-group Delayed Neutron Model*

G. Robert Keepin performed a comprehensive study of delayed neutrons which laid the foundation for delayed neutron work over the last 50 years. His major finding was that while there are many precursors that lead to delayed neutron emission, a 6-group representation could be used to summarize and describe them. Table 3 gives the thermal 6-group data for ^{235}U and the fast 6-group data for ^{238}U determined using both instantaneous- and long- irradiations outlined by Keepin in 1957 [61]. Note that delayed neutron yields are characteristic of the fissioning isotope and dependent on incident neutron energy as are the energy distributions of the delayed neutrons. The average delayed neutron energy is ~ 0.4 MeV, compared to the average prompt neutron energy of ~ 2 MeV [28].

The spectrum-averaged, total delayed neutron fractions for ^{235}U (thermal) and ^{238}U (fast) are 0.0158 ± 0.0005 and 0.0412 ± 0.0017 , respectively [27]. Other datasets exist, for example, Tuttle reported values of 0.01621 ± 0.0005 for ^{235}U and 0.0439 ± 0.0010 for ^{238}U [62]. Others have studied the use of single effective group structures through 8 or more group structures using both fixed and variable group time constant. Updated values (0.0162 and 0.0465) have also been proposed and were briefly evaluated with the accompanying 8-group structure for treating delayed neutron groups [63]. These results are discussed in Chapter 5.

Traditionally the thermal datasets are often used for ^{235}U . Since the cross-section for ^{238}U is largely negligible at thermal energies, the fast datasets are often used when considering ^{238}U . Note that the ^{235}U data listed in Table 3 and used throughout this work (unless otherwise noted) are for thermally-induced fission, while the ^{238}U data are described for fast-induced fission (from fission neutron). However, since there is no clear guidance on the boundaries between the thermal, fast, and high energy regions, it has been recommended to use fast fission data for both ^{235}U and ^{238}U [62]. This, along with the

introduction of the 14.1 MeV neutrons for the DEANI method, is the basis for the data constant sensitivity study discussed in Chapter 5.

Table 3. Delayed Neutron Parameters for Keepin 6-Group Model [27]

Delayed neutron parameters for ²³⁵ U (thermal)					
Group	Half-life (s)	% of DN	λ_j	B_{jv} (abs. yield)	
1	55.72 ± 1.28	3.3	0.01244 ± 0.0003	0.00052 ± 0.00005	
2	22.72 ± 0.71	21.9	0.03051 ± 0.001	0.00346 ± 0.00018	
3	6.22 ± 0.23	19.6	0.1114 ± 0.004	0.0031 ± 0.00036	
4	2.3 ± 0.09	39.5	0.3014 ± 0.011	0.00624 ± 0.00026	
5	0.61 ± 0.083	11.5	1.136 ± 0.15	0.00182 ± 0.00015	
6	0.23 ± 0.025	4.2	3.014 ± 0.29	0.00066 ± 0.00008	
Delayed neutron parameters for ²³⁸ U (fast)					
Group	Half-life (s)	% of DN	λ_j	B_{jv} (abs. yield)	
1	52.38 ± 1.29	1.3	0.0132 ± 0.0003	0.00054 ± 0.00005	
2	21.58 ± 0.39	13.7	0.0321 ± 0.0006	0.00564 ± 0.00025	
3	5 ± 0.19	16.2	0.139 ± 0.005	0.00667 ± 0.00087	
4	1.93 ± 0.07	38.8	0.358 ± 0.014	0.01599 ± 0.00081	
5	0.49 ± 0.023	22.5	1.41 ± 0.067	0.00927 ± 0.0006	
6	0.172 ± 0.009	7.5	4.02 ± 0.214	0.00309 ± 0.00024	

2.4.2 Calculating Delayed Neutron Emission Rates and Expected Count Rates

According to the convention adopted in this work, $\bar{\nu}$, is the average number of neutrons emitted during a fission event (including both prompt and delayed neutrons). The fraction of $\bar{\nu}$ that appear as delayed neutrons of the j^{th} group is β_j , with a corresponding decay constant, λ_j . Hence, the number of delayed neutrons per fission from group j is $\beta_j \bar{\nu}$, which is treated as a single quantity herein. The total number of delayed neutrons emitted per fission is the sum over all groups, $\Sigma (\beta_j \bar{\nu})$. The delayed neutron emission rate is then $\lambda_j \beta_j \bar{\nu} \exp(-\lambda_j t)$. This group-dependent emission rate from ²³⁵U is shown on a logarithmic scale in Figure 18.

This figure summarizes the decay of each group. Groups 1 and 2 are long-lived, while groups 5 and 6 are very short-lived. When the measurement item contains a single fissionable isotope, the total delayed neutron count can be adequately described by a single exponential (this is true for each group). When more than one fissionable isotope is present, the total delayed neutron count must be described by a linear combination dependent on each fissile or fissionable isotope present.

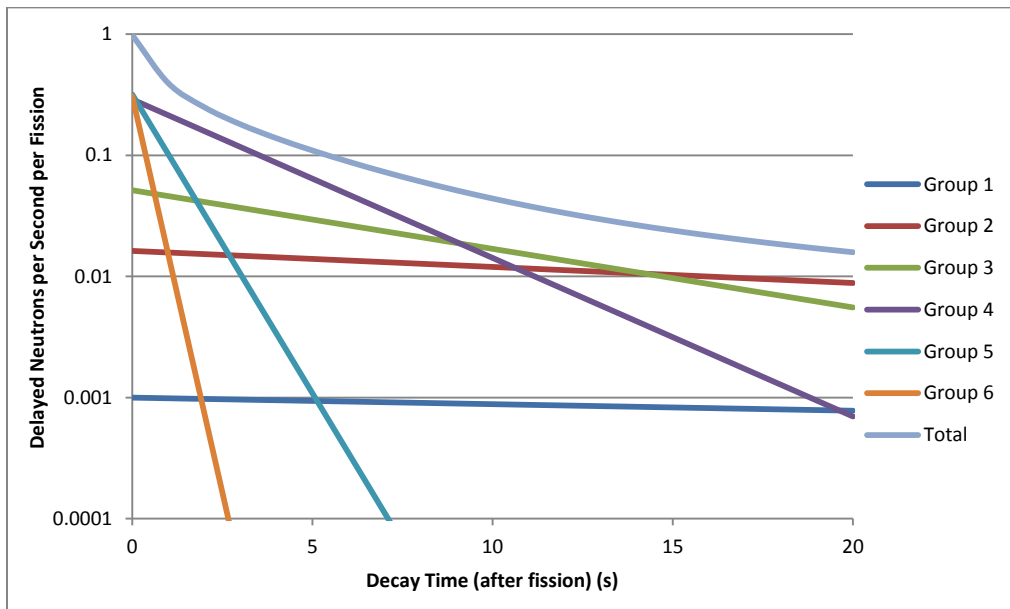


Figure 18. Delayed neutron yield rate for thermal fission of ^{235}U .

The delayed neutron yield per fission is dependent on the fissioning isotope and the incident energy of the interrogating neutron [64]. Figure 19 shows the difference in the delayed neutron yields per fission for ^{235}U and ^{238}U . The yields are larger for ^{238}U , underscoring the importance of understanding the contributions that come from the ^{238}U ; Even though the fission rate in ^{238}U may be small, those fissions produce more delayed

neutrons than the same number of fissions would produce in ^{235}U and should not be ignored. Keepin asserted that ^{238}U produces a larger neutron yields because the β -decay chains are longer. It is also important to note that most of the delayed neutrons come from groups 3 and 4. This is an important factor in optimizing delayed neutron measurement parameters.

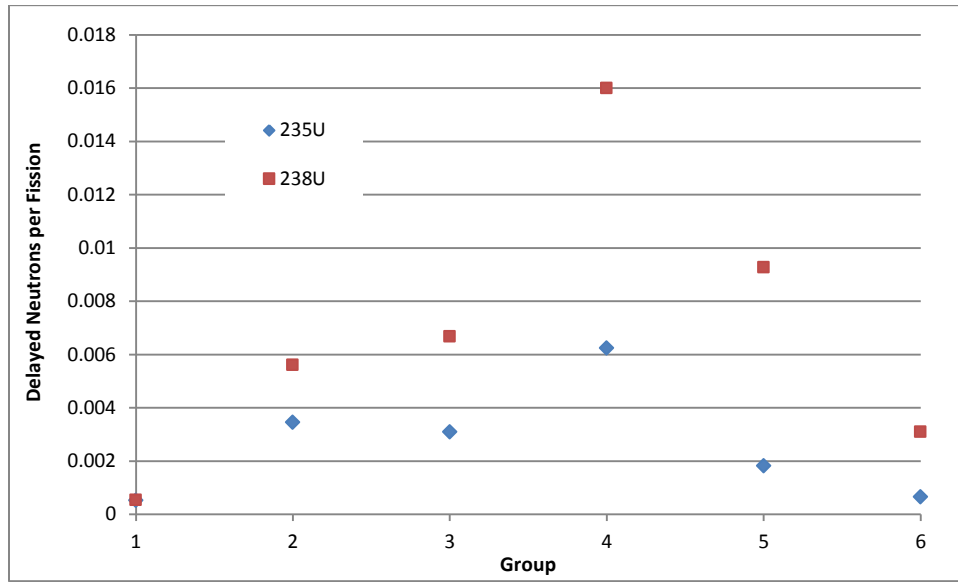


Figure 19. Group-dependent delayed neutron yields from ^{235}U and ^{238}U .

The fundamental delayed neutron production equations are derived in depth in previous work [58]. A summary of fundamental delayed neutron equations are provided here. The average neutron production rate from fission is described by Eq. 4:

$$f = \frac{\nu m N_A \sigma_f \phi}{A} = R_{IF} \bar{v} , \quad \text{Eq. 4}$$

where $\bar{\nu}$ is the average number of neutrons per fission (which includes delayed neutrons), m is the mass of the fissile nuclide, N_A is Avogadro's number, σ_f is the spectrum weighted fission cross-section, ϕ is the average irradiation flux, A is the atomic weight of the fissile material, and R_{IF} is the induced fission rate. The neutron production rate is dependent on the neutron flux and the cross-section, which is dependent on the interrogation energy.

When the sample is irradiated, the neutron precursor population, P , grows in and decays such that the rate of change of P for the j th group is given by Eq. 5:

$$\frac{dP_j}{dt} = R_{IF}\nu\beta_j - \lambda_j P_j, \quad \text{Eq. 5}$$

which is the production rate minus the decay rate of precursors in the j^{th} group. Equation 6 gives the precursor population for the j th group after the irradiation period, t_{irr} .

$$P_j(t_{irr}) = \left(\frac{R_{IF}\nu\beta_j}{\lambda_j}\right) [1 - \exp(-\lambda_j t_{irr})] \quad \text{Eq. 6}$$

For the ^{252}Cf Shuffler, there is a short delay while the ^{252}Cf source is removed from the counting chamber prior to the start of the delayed neutron counting interval. During this time, precursors are decaying. Once the counting interval begins, delayed neutrons are measured. The population at any time during the counting interval is described by Eq. 7:

$$P_j(t) = \left(\frac{R_{IF}\nu\beta_j}{\lambda_j}\right) [1 - \exp(-\lambda_j t_{irr})] [\exp(-\lambda_j t_{delay})] [\exp(-\lambda_j t)], \quad \text{Eq. 7}$$

where t_{delay} is the delay time between the irradiation window and the start of the counting window, and t is the time in the counting window.

To get the total delayed neutron counts for the j th group during the interval and again assuming a single fissioning isotope, the time integral of Eq. 8 is multiplied by the efficiency of the detector, ε (which is taken to be independent of the group j):

$$D_j = \varepsilon \left(\frac{R_{IFV} \beta_j}{\lambda_j} \right) [1 - \exp(-\lambda_j t_{irr})] [\exp(-\lambda_j t_{delay})] [1 - \exp(-\lambda_j t_{count})], \quad \text{Eq. 8}$$

where t_{count} is the length of the counting interval. This is the number of counts expected for a single shuffle. For a shuffler measurement with multiple cycles, the total counts can be obtained by summing D_j over all groups and multiplying by a cycle correction as shown in Eq. 9:

$$D = \sum_{j=1}^6 (D_j) \cdot \left\{ \frac{n - (n+1) \exp(-\lambda_j \tau) + \exp(-(n+1)\lambda_j \tau)}{(1 - \exp(-\lambda_j \tau))^2} \right\}, \quad \text{Eq. 9}$$

where n is the number of shuffles and τ is the total time for each cycle. Figure 20 shows an example of the relative delayed neutron emission rate per shuffler for 5 shuffles.

It is important to note that D is not the number of delayed neutrons that could have been counted. Because of the cyclical nature of the shuffler measurement and the selected measurement intervals, it is not possible to detect all of the delayed neutrons that are emitted. Most of the delayed neutrons from group 5 and 6 have already decayed before the counting interval begins. The delayed neutrons from groups 1 and 2 have a very long half-life and do not decay during the corresponding counting interval. In fact, it is estimated that nearly 30% of the signal in a given cycle comes from previous cycle irradiations [65].

The countable fraction, F_C , or number of delayed neutrons available for counting is given by Eq. 10 and can be maximized by optimizing the time intervals of the shuffler cycles. The denominator is the maximum number of delayed neutrons that *could* have been counted.

$$F_C = \frac{\sum_{j=1}^6 \left(\frac{\varepsilon f \beta_j}{\lambda_j} \right) [1 - \exp(-t_{irr} \lambda_j)] [\exp(-(n+1)t_{irr} \tau)]}{\varepsilon f t_{irr} \sum \beta_j} \quad \text{Eq. 10}$$

The work outlined in this dissertation exploits the dependence of R_{IF} , the induced fission rate, on the interrogation energy. Simulations of the shuffler measurements were performed to estimate the induced fission rates in the ^{235}U and the ^{238}U in the sample. These induced fission rates were used to calculate an expected delayed neutron count rate. Measurements in the ^{252}Cf Shuffler were completed to validate the simulations and prove the process. This is discussed in detail in the following chapters.

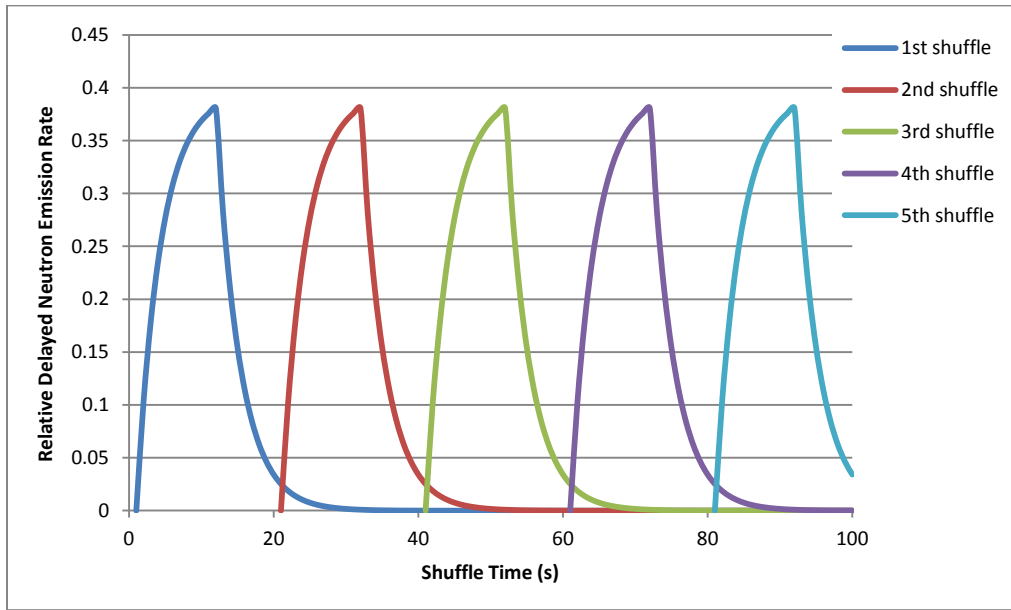


Figure 20. Relative delayed neutron emission rate per shuffler.

2.5 Effective Mass

Recall that delayed neutrons from both ^{235}U and ^{238}U contribute to the delayed neutron measurement signal even though thermally-induced fission from ^{235}U dominates. The assay thus reports an “effective” mass ($m_{235U_{eff}}$) similar to that conceptualized for coincidence counting [6]. For the purposes of this work however, the effective mass is

defined as the mass of ^{235}U that would produce the same delayed neutron count rate as some combination of ^{235}U and ^{238}U , as shown in Eq. 11.

$$m_{235U_{eff}} = m_{235U} + g * m_{238U} \quad \text{Eq. 11}$$

In this equation, g is a coefficient heavily dependent on the induced fission rate in ^{238}U along with other factors, including the system configuration and the delayed neutron parameters for ^{238}U . The value of g may be determined through calibrations of the system of through Monte Carlo simulation.

The coefficient, g , is taken as a constant for a given system. While g may be well predicted from basic nuclear data for simple and dilute items, self-shielding, multiplication, and matrix effects complicate the analysis for large, dense, or “lumpy” items. By changing the neutron interrogation energy, and thus, the induced fission rates, we effectively create a new system. For a fixed condition (e.g., cans of U_3O_8 in air):

$$m_{235U_{eff}}^{(1)} = m_{235U} + g^{(1)} * m_{238U} , \quad \text{Eq. 12}$$

$$m_{235U_{eff}}^{(2)} = m_{235U} + g^{(2)} * m_{238U} , \quad \text{Eq. 13}$$

where the superscripts 1 and 2 represent the systems with interrogation sources 1 and 2, respectively. Equations 12 and 13 provide two equations and two unknowns (m_{235U} and m_{238U}), since the values of $m_{235U_{eff}}$ are measured and the values of g will be determined through careful calibration of the systems. In order to utilize this system of equations, f must be measurably different for the two systems. For this dual-energy approach, this would allow the isotopic mass to be determined without the need for the isotopic fractions.

2.6 Prior Work

Minimal effort had been dedicated to improving delayed neutron counting techniques until recently. Most of these recent studies have focused on replacing interrogation sources or using newer hardware. Until a recent spent fuel measurement campaign was initiated by the Department of Energy, little work had been performed on using delayed neutrons to determine uranium enrichment. This section briefly discusses these efforts and others related to this dissertation.

2.6.1 Advanced Enrichment Techniques Using Delayed Neutrons

While various advanced enrichment/isotopic measurement techniques have been developed they are generally application specific and not widely applied to safeguards measurements of bulk materials. Recent work has been performed using a delayed neutron re-interrogation technique where delayed neutron population is forced into a near-steady-state equilibrium through continuous irradiation by a D-T neutron source [66]. Since the delayed neutron precursors reach equilibrium after some irradiation time, an intrinsic source of (delayed) neutrons is present. Once this equilibrium is achieved, the D-T source is turned off. The delayed neutrons in the system can then go on to re-interrogate the sample inducing more fissions in the fissile material. The measurement of the delayed neutron response is then believed to be dependent on the enrichment of the item. The enrichment can then be determined through careful analysis of the shape and kinetic behavior of the delayed neutron response curve. This particular study showed that uranium enrichment could be estimated, however, errors on the lower enrichment items were upwards of 48%. Improvements to this re-interrogation technique include using better fitting algorithms to determine the analysis coefficients, optimizing irradiation times based on production of precursors, and exploring options for the delayed neutron group data may improve the results of this proposed method. Follow-on work was conducted using a reactor beam to interrogate the measurement sample [67]. While the results were on par with the previous results, only mg quantities were measured.

Studies have also been performed on items containing mixtures of uranium and plutonium, specifically for spent fuel applications, since traditional delayed neutron counting techniques do not work well when more than one fissionable isotope is present. One study in particular evaluated the ability to differentiate between decay times for each fissile isotope in a given item. In this experimental work, the items were irradiated in a research reactor using a pneumatic transfer system. By counting the delayed neutrons within the first 30 s post-irradiation, the difference in the decay shapes for ^{235}U and ^{239}Pu could be exploited. After the initial 30 s, the decay curves became less distinguishable. The study examined ideal examples where ^{235}U and ^{239}Pu were the only fissionable isotopes in the sample and the results were promising. However, no accounts were provided for realistic cases where other fissionable isotopes were present (e.g., ^{238}U or ^{240}Pu) [68].

Combinations of delayed and prompt neutron counting have also been evaluated by Los Alamos National Laboratory (LANL) as a potential technique for spent fuel measurements. This combined technique leverages D-T neutrons to first induce fission in the sample and quickly measure the die away of prompt neutrons, then subsequently measure the delayed neutrons emitted from the sample [69]. Because the ^3He detectors cannot distinguish between prompt and delayed neutrons, careful timing structures must be applied to the measurement. The system also cannot determine from which isotope the neutrons were emitted; therefore, the measurement result is in the form of an “effective” mass, similar to the concept of $^{240}\text{Pu}_{\text{eff}}$ mass used in passive coincidence counting [6]. While this technique shows that delayed and prompt neutron measurements may be effectively integrated, the results are again dependent on knowledge of the isotopic concentrations in the item.

2.6.2 Multi-Energy Approach using Delayed Neutrons

Menlove, et.al. [70], investigated the potential for using a multi-spectra irradiation technique for measurement of fissionable materials in the early 1970s. In his work, he

proposed that mixtures of fertile and fissile materials could be effectively measured using the delayed neutron signal from a high-energy (D-T generator) irradiation flux and a moderated irradiation flux (D-T generator encapsulated by moderating materials). This study focused a great deal on the spectrum tailoring aspect of the technique. Tungsten, Pb, C, and CH₂ were all evaluated as potential moderators. The technique was focused on finding moderating scenarios that produced the largest ²³⁵U/²³⁸U fission ratios.

In his experiments, Menlove used a ³He-based slab detector and an irradiation time of 45 ms, significantly longer than the 10 μs pulses used in this dissertation. Additionally, only one irradiation was performed per assay, unlike the cyclical shuffler-type measurements performed here. Menlove asserted that through calibrations using like standards, the following relationship could be established.

$$D_{E_i} = \sum_{j=1}^n A_{i,j} m_j \quad \text{Eq.14}$$

In Eq. 14, D is the delayed neutron yield, E_i is the interrogating neutron energy, m_j is the mass of the j^{th} isotope, n is the number of fissionable isotopes, and $A_{i,j}$ are coefficients determined through calibration. Equations 15 and 16 show the equivalent set of equations for the method proposed in this dissertation.

$$D_{252_{cf}} = A_{252_{cf},235U} \cdot m_{235U} + A_{252_{cf},238U} \cdot m_{238U} \quad \text{Eq.15}$$

$$D_{DT} = A_{DT,235U} \cdot m_{235U} + A_{DT,238U} \cdot m_{238U} \quad \text{Eq.16}$$

Once the calibration coefficients are determined, the set of equations can be solved. The results from this work showed the potential of using a multi-energy approach. This methodology differs from the work in this dissertation primarily because it relies heavily on the determination of the calibration coefficients. By employing the ratio of the delayed neutron count rates the dependence on calibrations is minimized.

In 1985, a similar multi-energy technique was pursued to measure uranium and thorium in geological materials [71]. In this work, two identical mg quantity samples were irradiated in a research reactor. One sample was covered with a Cd and boron carbide-filter and one was bare to obtain different energy spectra. The time structure for these measurements included a 60 s irradiation, 20 s delay, and 60 s count time. The counter was made of 6 BF₃ tubes arranged in a polyethylene cylinder. The results from this study showed that a relationship between delayed neutrons and enrichment could be established, although measurement results using the Cd filters only confirmed the method for enrichments up to 10%.

In 2014, Dolan, et.al., acknowledged that multi-energy interrogation may be used to look for different isotopes of uranium via fast neutron detection [72]. In that study, an associated particle D-T generator and an AmLi source were used to preferentially induce fission in ²³⁸U and ²³⁵U, respectively. In this work, however, liquid scintillations (fast neutron detectors) were used to measure the time-tagged fission neutrons (in a time-of-flight manner) and estimate the total uranium mass. The AmLi source is then used in part two of the measurement where the fission gammas are used to trigger the time-of-flight of the AmLi-induced fission neutrons. A relationship between the photon-neutron measurements and the enrichment is then obtained. This method for determining the enrichment was only experimentally validated for LEU samples and reported a statistical uncertainty of approximately 4.4%.

While studies have been performed on the use of a D-T generator in a shuffler application, no experimental work has been performed. No experimental work has been performed to investigate the use of multiple neutron interrogation energies for delayed neutron counting and its ability to determine ²³⁵U enrichment.

Delayed neutron counting has been studied for the detection and identification of fissile isotopes, most exploiting the difference in temporal behavior of the delayed neutrons

from different isotopes [47, 73]. In 2016, Mayer, et.al., showed that an accelerator-based ($^{11}\text{B}(d,n\gamma)^{12}\text{C}$) source could be used to irradiate an item to infer the presence of SNM based on the temporal behavior of delayed neutron buildup and decay signatures. Using a EJ-309 liquid scintillator and a Li-doped glass and polyvinyl-toluene scintillator, with relatively low efficiency for delayed neutron detection (~1-2%), the ability to detect the delayed neutrons was confirmed. While the interrogation source used in this work was a dual particle source (emitting 5 MeV neutrons and 15.1 MeV photons), the measurement technique is comparable to that of dual- or multi-energy interrogation.

2.6.3 Sensitivity studies

Sensitivity studies related to delayed neutron parameters have been thoroughly examined from the perspective of reactor kinetics [74-76], which is expected due to their significant role in reactor operations. For delayed neutron assay of nuclear materials, there is little published work discussing the choice of delayed neutron parameters (e.g., Keepin values vs. Pikaikin values) used or which energy-dependent dataset to use (e.g., Keepin's thermal- energy parameters vs. Keepin's fast- or high-energy parameters).

The sensitivity of a delayed neutron assay to the group structure has also been studied as part of this dissertation. The literature provides suggested 8-group parameters and those have been studied for their role in reactor kinetic calculations [63, 77-80]. While use of this 8-group structure over the widely accepted 6-group structure is not expected to have a significant effect on assay results, sensitivity to the structure for material assay applications has not been widely addressed.

2.6.4 MCNP6 Delayed Neutron Capabilities

MCNP6 is said to have improved delayed particle production capabilities [81-83]. Benchmark and validation efforts have been made in regards to the delayed gamma capability [84]; however, little documentation on the benchmarking of delayed neutron capabilities exists. One study aimed to simulate reactor-based irradiations and

measurement of resulting delayed neutrons as a function of energy deposition and temporal behavior [85]. The crude model showed an over-production of delayed neutrons and a measurable difference in die-away times as count times increased towards 100 s.

2.6.5 Source Replacement

Early on, researchers at LANL studied the use of photo-neutron sources, such as ^{124}Sb , as an alternative interrogation source to ^{252}Cf for delayed neutron applications. These sources were not pursued for long because of the small neutron yields (in comparison to ^{252}Cf) and extremely shorter half-lives (limiting the lifetime of the source) [58].

As sites move to eliminate or at least reduce the number of radioactive sources they must maintain, alternative neutron sources for active neutron interrogation systems are being evaluated. One early study performed by LANL used the delayed neutron capabilities in Monte Carlo N- Particle Extended (MCNPX) to show that neutron generators could potentially replace ^{252}Cf in shufflers although quantitative results were not presented at the time [86].

A later theoretical (simulation-based) study on the potential for D-T neutron generator to replace the ^{252}Cf source in a shuffler was also performed [87]. The two biggest challenges with neutron source replacement are achieving the necessary neutron yields and matching the energy spectra of the source neutrons. Historically, neutron generators were not used as the interrogating source for delayed neutron counting, primarily because of the low neutron emission rate (10^6 n/s vs. 10^9 for ^{252}Cf). Thanks to recent developments in neutron generator design, they have been significantly improved and shown to produce higher fluxes in a more compact design, which is extremely important for delayed neutron applications.

Matching the energy spectrum of those sources to be replaced is important because of the strong energy dependence of neutron cross-sections and is a more difficult challenge. As described in section 2.3.3.2, D-T neutrons are emitted with energies around 14.1 MeV,

much higher than the average ^{252}Cf neutron energy of about 2 MeV. Therefore, more extreme spectrum tailoring methods must be used to reduce the D-T neutron energies. This same study examined many material combinations and showed that tungsten offered the most desirable spectrum tailoring properties. However, tungsten is impractical primarily due to cost, so combinations of iron and other high-z materials were chosen. Based on MCNPX simulations, it was shown that D-T neutron energies could be reduced such that fission in ^{238}U was minimized. Unfortunately, the size and spatial sensitivity increases with the use of presently available D-T generators since they are stationary and cannot scan the item as the ^{252}Cf mechanism allows. While the potential replacement of ^{252}Cf has been studied, the same need for isotopic information remains.

3 MODEL AND SIMULATION

In order to predict the induced fission rates for various items and for different interrogating energies, a high-fidelity model of the ORNL ^{252}Cf Shuffler was developed using MCNP6 [81]. These simulations provided the data needed for the preliminary proof of principle work, supported efforts to optimize the measurement technique, provided a mechanism by which sensitivity analyses were performed, and allowed for extrapolation of the newly developed technique to other materials not available to measure at ORNL. The development of this model also allowed a brief look at the delayed neutron capabilities of MCNP6, which is discussed in Chapter 5.

3.1 MCNP6 Model of the ORNL ^{252}Cf Shuffler

The geometry parameters used in the model were taken from the manufacturer drawings and from physical measurement of the system. The key features are outlined here.

- 1) Detector Banks: The model utilizes the *j LIKE n BUT* feature which supports the use of repeated structures. The new cell *j* inherits the parameters of the referenced cell *n* with the exception of those parameters following the word *BUT*. The shuffler model used this feature along with the cell transformation *TRCL card. The asterisk signifies that the angles used in the rotation matrix are in units of degrees. These cards for repeated structures were used for the ^3He tubes (active regions, inactive regions, cladding), the HDPE slabs around the detector banks, and the air gaps between the tubes and the moderator.
- 2) Al junction boxes were included on top of each detector bank
- 3) Cd liners were included around each detector bank
- 4) Outer HDPE shielding and the ^{252}Cf storage assembly were included
- 5) The stainless steel and Cd liner around the measurement cavity was included
- 6) The stainless steel drum rotator was included as the base of the measurement cavity

- 7) The stainless steel reflector with Cd liner was used to tailor the ^{252}Cf spectrum was included as was the source guide tube
- 8) The concrete support and well that houses the drum rotator motor were added
- 9) The source stand and small rotator were included in the model
- 10) A simplified model of the D-T generator was added. This included a stainless steel shell for the generator, a copper heat sink, and SF_6 gas
- 11) An additional Cd-covered flux monitor (used during the D-T measurements) was added to the model to account for neutron absorption
- 12) The measurement items were added and changes as necessary
- 13) ^{252}Cf source: The source definition (SDEF) card specified the use of the Watt spectrum using 1.025 and 2.926 as the coefficients. It was modeled as a point source in the source guide tube unless otherwise noted. The coordinates for the irradiation position were (0, 38.8, 35.8)
- 14) D-T source: The D-T source was modeled as a mono-energetic 14.1 MeV source at a position with coordinates (21.5, 22, 36)
- 15) The most current ENDF/B continuous-energy cross-section libraries were used

Figure 21 shows a cross-sectional front-view of the modeled shuffler. Recall, the shuffler details were provided in Section 2.3. The shuffler contains large amounts of HDPE (the tan/beige-colored cells), both in the detector banks and surrounding the shuffler for shielding purposes. The large block at the top of the shuffler is the ^{252}Cf housing and is necessary to shield personnel for the source. While the density of HDPE can vary between 0.92 and 0.965, 0.95 g/cc was used in the model. The entire instrument sits atop a concrete base (gray) allowing the lower detector bank and the drum rotator motor (represented in purple) to sit below in the well. The light purple cell in the well represents the drum motor and other electrical and mechanical effects, which were represented by a homogenous block of one-quarter density stainless steel (1.97 g/cc). In this diagram, the

top and bottom neutron banks are clearly visible. The red shading represents the active region of the ^3He tubes.

For reference, the vertical axis is referred to as the z-axis, the horizontal axis from left-to-right is the x-axis, and the horizontal axis from front-to-back is the y-axis. The center of reference for the model (0, 0, 0) is the bottom of the measurement chamber, centered left-to-right and front-to-back. An example MCNP6 input deck is provided in Appendix A.

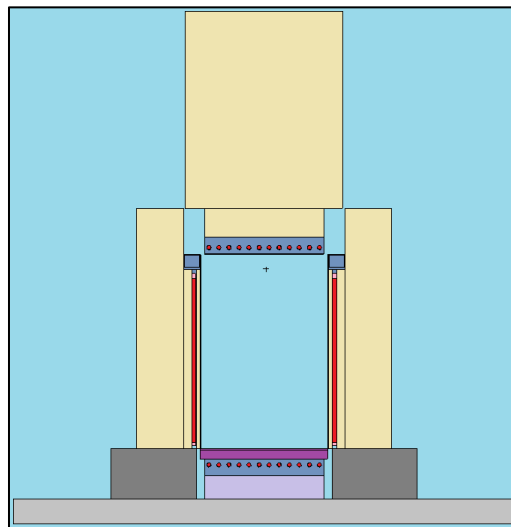


Figure 21. Cross-sectional front view of the ^{252}Cf Shuffler.

Figure 22 shows the top-down view of the shuffler. The six vertical neutron banks are clearly visible and surround a large measurement chamber. The cadmium and stainless steel liner surrounding the measurement chamber is also visible. The purple block at the back of the shuffler represents the stainless steel reflector that aids in tailoring the ^{252}Cf neutron energies and increasing the neutron flux in the cavity. Towards the front of the reflector is the small source guide tube where the ^{252}Cf source is shuffled back and forth

into the measurement chamber. The concentric circles in the measurement cavity represent a measurement item.

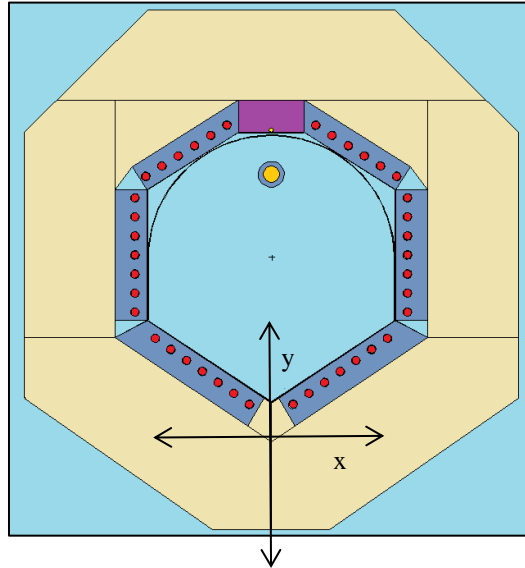


Figure 22. Cross-sectional top-down view of the ^{252}Cf Shuffler.

Figure 23 shows a close-up of the measurement item (an NBL CRM standard) and the stand and small rotator that support it. For the majority of the measurements, and unless otherwise stated, the uranium items were placed atop this rotator during measurement. The center of the uranium in the item was at (0, 38.8, 36). MATLAB [88] scripts were also written to extract the pertinent data from the MCNP6 output files.

3.2 Validation of MCNP6 Model

A number of passive measurements were performed in an attempt to validate the MCNP6 model of the ORNL shuffler. A comparison of the measured and simulated ^{252}Cf efficiency at many locations inside the shuffler was performed to provide confidence in the model. Additionally, the die-away time was compared. Both the efficiency mapping

and die-away measurements were performed using a JSR-15 Handheld Multiplicity Register (HHMR) [89] and the IAEA Neutron Coincidence Counting (INCC) software v5.12 [90]. Details regarding specific sources used in this work are provided in Appendix B.

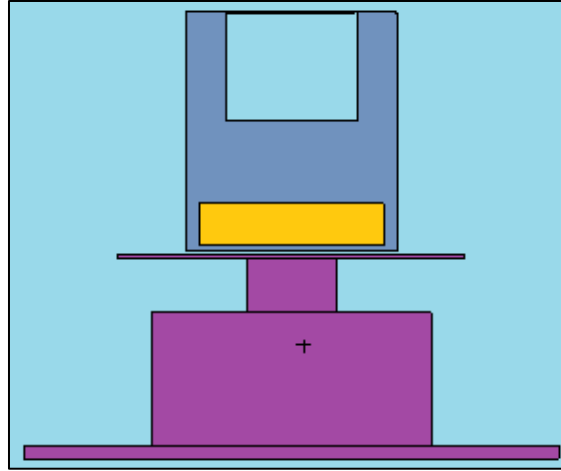


Figure 23. Measurement item sitting on a small rotator and stainless steel stand.

3.2.1 ^{252}Cf Efficiency Profiles

Since the ^{252}Cf efficiency is generally used to quote the efficiency of neutron detectors, it was used to validate the MCNP6 model of the shuffler. Simulations were performed to determine the ^{252}Cf efficiency with respect to position at over 120 locations inside the large measurement chamber. The efficiency was also measured at over 80 locations inside the counting chamber using a National Institute of Standards and Technology (NIST)-certified ^{252}Cf source (^{252}Cf -5685). The simulated and measured efficiencies were compared in both shape and scale to validate the MCNP6 model.

Figure 24 and Figure 25 show the horizontal x- and y- efficiency profiles. Recall that the x- profile maps the chamber from left-to-right. The y- profile maps the measurement chamber from front-to-back. The measured data are represented by the green triangles, while the simulated data are represented by the blue circles. The percent difference between the measured and simulated efficiencies is also plotted (red squares) to quantify the differences in the results using the secondary y-axis. The error bars on the measurement data are purely from counting statistics and do not include the uncertainty in the source emission rate (~1% at the 68% confidence level). The statistical error from MCNP6 simulations is negligible; thus, error bars are not visible.

Although there appears to be a ~ 4% bias between the measured and simulated results, the smooth, flat behavior of the ratio of efficiencies across the measurement cavity shows consistency of the bias between the simulations and measurements in the x-direction. The same is mostly true of the horizontal data in the y-direction; however, there is more agreement between the model and the measurements at the very front (near the doors) and the very back (near the source transfer tube), as indicated by the difference at those points. At the back of the shuffler (represented by the positive positions), the detector banks are separated by just over 20 cm to accommodate the source transfer tube and steel reflector. The lower efficiencies in this area can be attributed to this gap between neutron detector banks. At the front of the shuffler (represented by the negative positions), the detector banks are more closely positioned, thus resulting in a higher efficiency. This non-symmetric nature of the shuffler accounts for the difference in the shapes of the x- and y-efficiency profiles.

Figure 26 shows the vertical efficiency profile in the measurement chamber. The difference in the measured to simulated efficiency ranged from ~1% at the top of the assay chamber to ~5% at the top of the chamber, indicating a degree of difference between the model and the measurement.

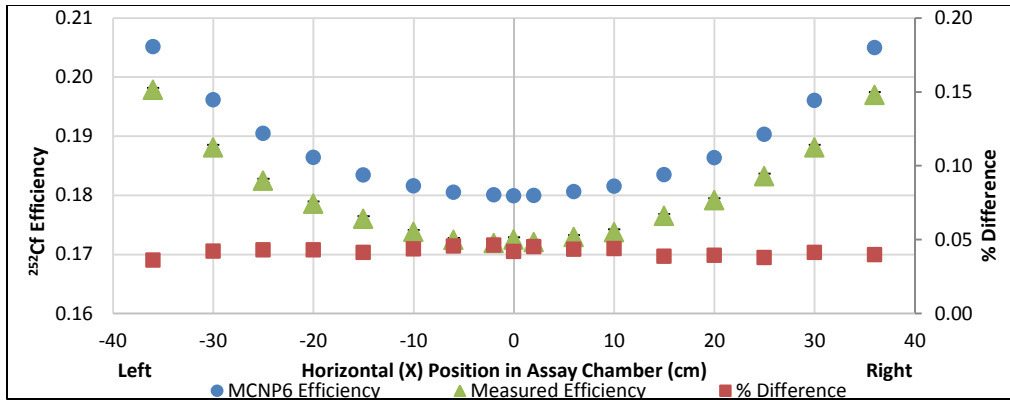


Figure 24. Efficiency profile in the x-direction across the measurement chamber.

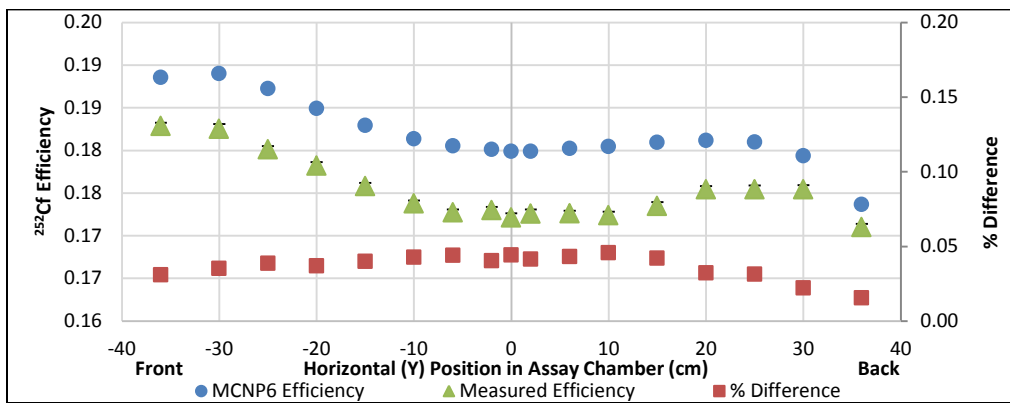


Figure 25. Efficiency profile in the y-direction across the measurement chamber.

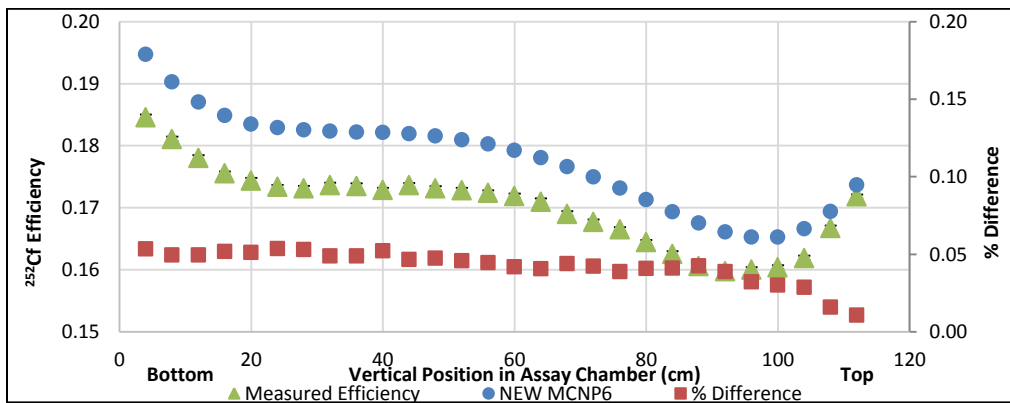


Figure 26. Vertical efficiency profile (z-direction) across the measurement cavity.

Asymmetry from top to bottom is likely attributable to the presence of the rotator below the cavity floor (steel tends to increase detection efficiency) and to the vertical tube bank junction boxes at the top of the cavity (effectively a dead space for detection efficiency). While great effort has been made to create a high-fidelity representation of the shuffler as built based on physical dimensions and materials, it is an extremely complicated geometry and perfect agreement of modeled and calculated performance is not expected. However, the general trends and relative behavior are reproduced which gives confidence that the model is fit for said purposes.

Since the DEANI methodology was primarily demonstrated using small U_3O_8 cans of uranium, additional efficiency measurements were performed in and around the smaller area where the majority of the measurements were performed. This data is plotted in Figure 27. Note that the horizontal axis does not reflect the measurement position, only the sequential measurement number. The key result is that the differences between the measured and simulated efficiencies are fairly constant across the entire measurement area at about 4%.

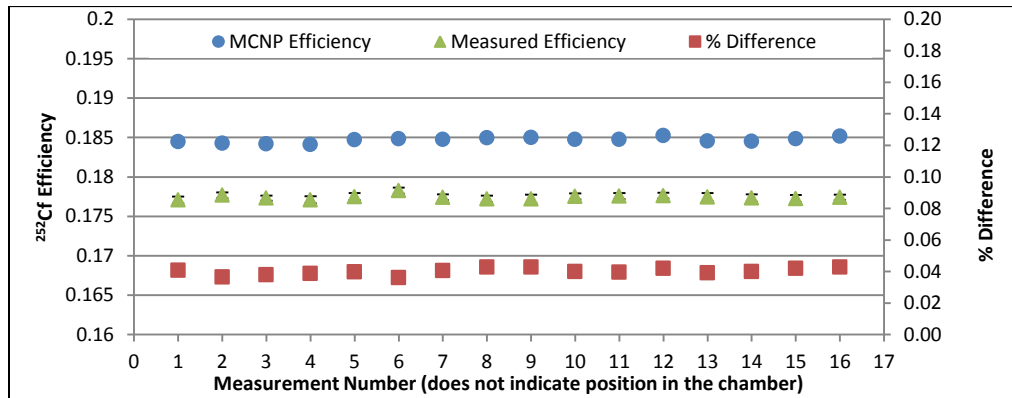


Figure 27. Efficiency map in the vicinity of the uranium measurement area.

3.2.2 Die-away Time

Measurements and simulations based on passive operation of the ORNL ^{252}Cf Shuffler were performed to determine the die-away time of the system. A comparison of the simulated and measured die-away times was used to further validate the MCNP6 model of the ^{252}Cf Shuffler. The measured and simulated doubles rates as a function of pre-delay using a ^{252}Cf source and simulated time capture distribution for ^{252}Cf were obtained. Additionally, the die-away structure was investigated to better understand the slowing down time, the thermalization time, and the migration or diffusion time of neutrons in the system. This is discussed in more detail in Chapter 5.

The simulated die-away curves were obtained two ways. The first was to directly simulate the coincidence rates using the F8 capture tally. The pre-delay and gate width were defined within the tally parameters. Both cases, fixed pre-delay and fixed gate, were evaluated for the ^{252}Cf -based simulation. The F8 capture tally was not applied to the D-T generator since there are no true (fission) coincidences from the generator. An alternate approach is use the traditional F4 tally with the time card entry. This tally is used to bin the neutrons by time of capture or detection and will be referred to as the fission event-triggered capture time distribution. This simulation was performed for both the ^{252}Cf source and the D-T generator neutrons although the D-T data is discussed in Section 5.4.

The ^{252}Cf source used for these measurements was ^{252}Cf -6081 which was placed at the center of the measurement chamber. Figure 28 and Figure 29 show the simulated (fixed gate) die-away data and the measured (fixed gate) die-away data, respectively. Notice the buildup (due to dead-time) is evident in the measured data for short pre-delays. The JSR-15 measured the signal-triggered coincidence rate (ie., every detection of a neutron opens a coincidence gate after the pre-delay and is corrected for chance (or accidental) coincidences. The difference in the shapes of these curves is also discussed in Chapter 5.

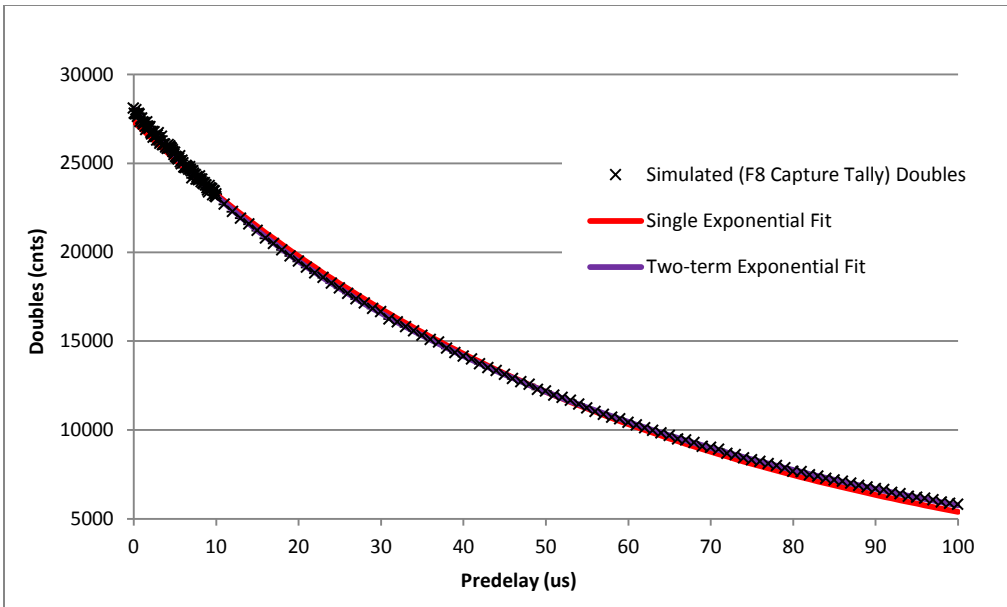


Figure 28. F8 capture tally results for ^{252}Cf simulation for a fixed gate of $1\ \mu\text{s}$.

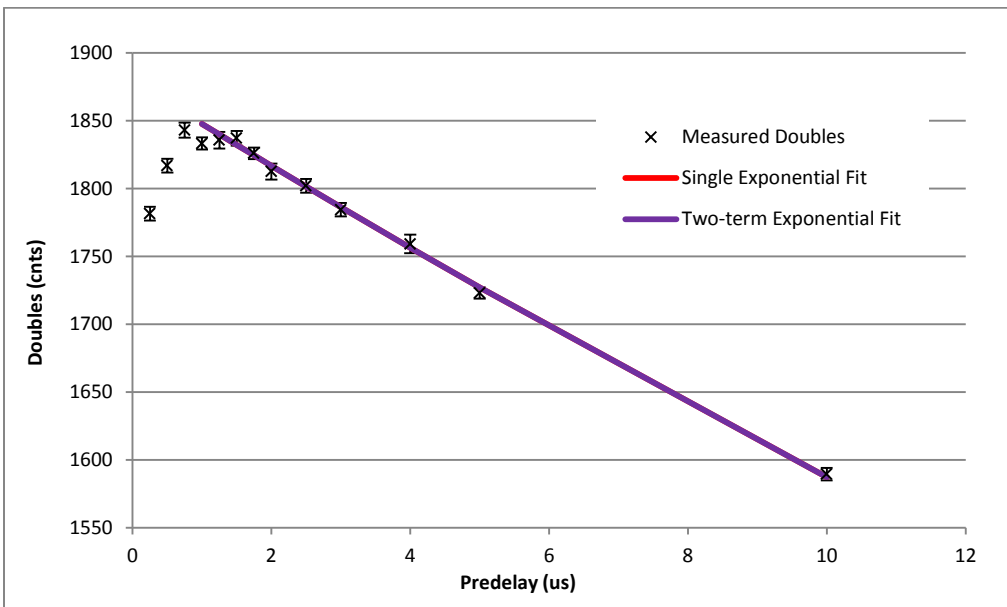


Figure 29. Measured die-away using ^{252}Cf for a fixed gate of $10\ \mu\text{s}$.

A chi-squared fit was used to fit the data with a single exponential and a two-term exponential. Those fits are also provided in the plots. The simulated data can be well represented by both the single and two-term exponential. The measured data cannot be directly compared to the simulated data due to limitations in the data collection electronics; INCC specifies a minimum gate width of 10 μs , and the simulations were performed with a fixed gate of 1 μs . Additionally, the measurements only go out to a pre-delay of 10 μs . For this short data-set, a single exponential adequately fits the data.

The die-away times were determined using a Chi-squared minimization. Note that the fit was applied from 1 - 10 μs for the measured data and 0 - 100 μs for the simulated data. A summary of the calculated die-away time constant for each scenario is given in Table 4. The time constants using the single exponential fit for the simulations match well to the measured data. The two-term fit results in a higher die-away time. This is possibly due to the limited parameter constraints applied to the fit and the time frame over which the fits were applied. For the purpose of code validation, the agreement between the die-away times for the single exponential fits suggests good agreement between the MCNP6 model and the physical dimensions of the ^{252}Cf Shuffler, particularly since the die-away time is heavily dependent on the geometry of the counter. Taking the pre-delay out to longer values for the measured data may improve the estimated die-away time for the measured data.

Table 4. Summary of Simulated and Measured Die-away Time Constants

Die-away	Single Exponential Fit	Two-term Exponential Fit
τ (Simulated) (μs)	61.56	67.51
τ (Measured) (μs)	59.24	--

Based on the extensive efficiency mapping and die-away comparisons performed, the MCNP6 model was deemed adequate to simulate ORNL ^{252}Cf Shuffler measurements and to determine the induced fission rates of various items within the shuffler.

3.3 Determining Fission Rates from MCNP6

Determining the expected induced fission rates in ^{235}U and ^{238}U to understand how they change with interrogating neutron energy is central to this work. Because the induced fission cross-section of ^{238}U increases drastically in the 1-2 MeV range, the fission rates (from higher energy neutron interrogation) are expected to increase significantly in ^{238}U . Since the induced fission cross-section for ^{235}U is relatively constant from 0.5 MeV and up, the expected fission rates are not expected to increase drastically. This is the basis for the discriminating power obtained from the dual-energy approach.

The MCNP6 model was used to calculate the induced fission rates for eight uranium standards of varying enrichment, each modeled according to its certificate (i.e., correct isotopics, density, and fill height) [51]. A summary of the key CRM parameters is provided in Appendix B. The interrogating sources were positioned to match the measurement design, and no vertical scanning was simulated.

The induced fission rates and uncertainties can then be calculated as:

$$R_{IF} = \frac{G_I}{(\bar{\nu}_I - 1)} * (S), \quad \text{Eq. 17}$$

$$\sigma_{R_{IF}} = R_{IF} \frac{\sigma_{\nu_I}}{\bar{\nu}_I - 1}, \quad \text{Eq. 18}$$

where R_{IF} is the induced fission rate per source particle, G_I is the weight gain by fission for isotope I (i.e., net neutron gain from fission, determined using MCNP6), $\bar{\nu}_I$ is the average number of neutrons emitted per fission for isotope I , and S is the neutron

emission rate (n/s) for the interrogating source. A snippet showing the values for G_I as provided in an example MCNP6 output file is provided in Appendix A.

4 MEASUREMENT DESIGN

The development of the DEANI method required careful consideration of measurement design parameters including evaluation and selection of an adequate secondary neutron source, optimization of the secondary source location, assessing the need for spectrum tailoring materials, characterizing the shuffler response, optimization of measurement times, and developing the measurement procedure. The development of the measurement technique was achieved through a combination of measurements and simulation. This chapter outlines the design outcomes and provides details related to the aforementioned measurement design parameters.

4.1 Implementation of a Secondary Neutron Source

4.1.1 Potential Secondary Neutron Sources

To take advantage of the dual-energy approach, a second neutron interrogation source with a distinct spectrum was required. The following sub-sections briefly describe the neutron sources considered for this work, namely AmLi, AmBe, and both D-D and D-T neutron generators. Recall that ^{252}Cf in a steel source block is the primary interrogation source for this shuffler-based method. Photon sources were not considered for this work because of cost, complexity, and shielding considerations.

4.1.1.1 $^{241}\text{AmLi}$

AmLi sources are commonly used in active uranium assay techniques because the relatively low average neutron energy of ~ 0.5 MeV reduces the impact of fissionable isotopes within the measurement item, namely ^{238}U . However, the neutron energy spectrum can vary for different AmLi sources due to the presence of impurities in the source materials, because of imperfect mixing, and/or due to the interfaces between the two elements [7],[8]. Although AmLi neutrons have low energies on average, there is a higher energy tail that results from the (α,n) reactions with oxygen. The oxygen

impurities appear due to the manufacturing process of the source (mixing AmO₂ with LiO₂ or LiHO). Figure 30 shows one commonly accepted AmLi spectrum [9].

AmLi sources are physically larger than other common sources (e.g., ²⁵²Cf or AmBe) and require a tungsten shield to reduce the dose from the strong 60-keV ²⁴¹Am gamma-rays. If not fabricated carefully, AmLi sources could also be contaminated with Pu. While AmLi sources are useful sources in active coincidence counting applications, the lower neutron yield (compared to ²⁵²Cf) limits its applications in delayed neutron counting where a large flux is needed. As a reference, the two large AmLi source used in the AWCC emit 10⁴ n/s where the small (in comparison) ²⁵²Cf source in the shuffler emits on the order of 10⁹ n/s. AmLis are also very expensive and no longer commercially made in the United States, therefore many studies on AmLi replacement are ongoing [91].

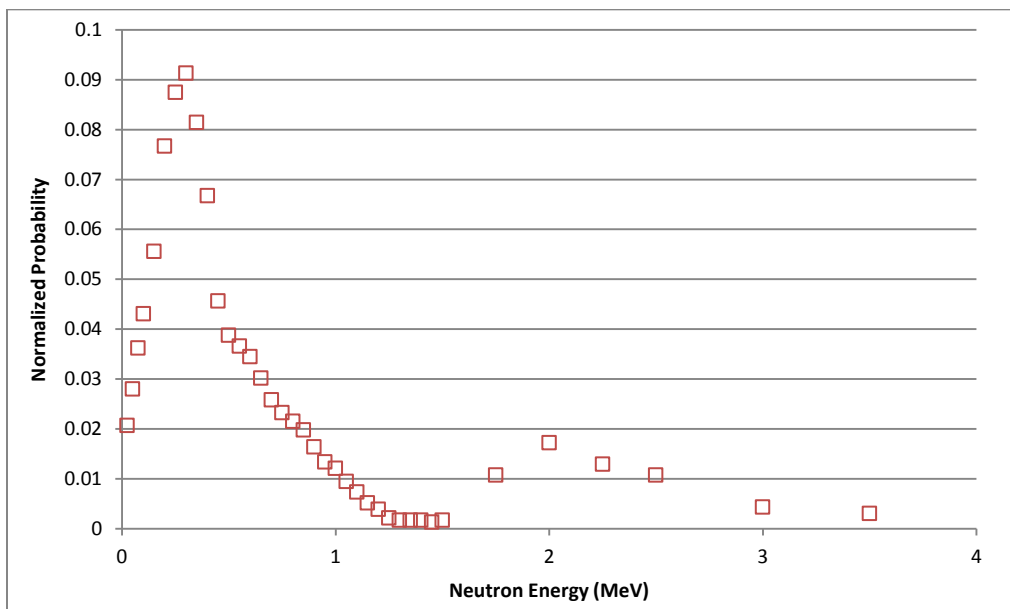


Figure 30. AmLi neutron energy spectra [9].

4.1.1.2 $^{241}\text{AmBe}$

AmBe sources are relatively inexpensive, fairly compact yet still significantly more bulky than the ^{252}Cf , and easily portable. The average neutron energy from these sources is ~ 5 MeV [7], which can readily induce fissions in fissionable isotopes like ^{238}U . Figure 31 shows the AmBe neutron energy spectra alongside that of AmLi. While the average neutron energy is ~ 5 MeV, the distribution spans upwards of 10 MeV. Recall Figure 1 (cross-section plot) where the fission cross-sections for ^{238}U and ^{235}U are very similar in this high-energy region. A comparison of important source characteristics for ^{252}Cf , AmLi, and AmBe is provided in Table 5.

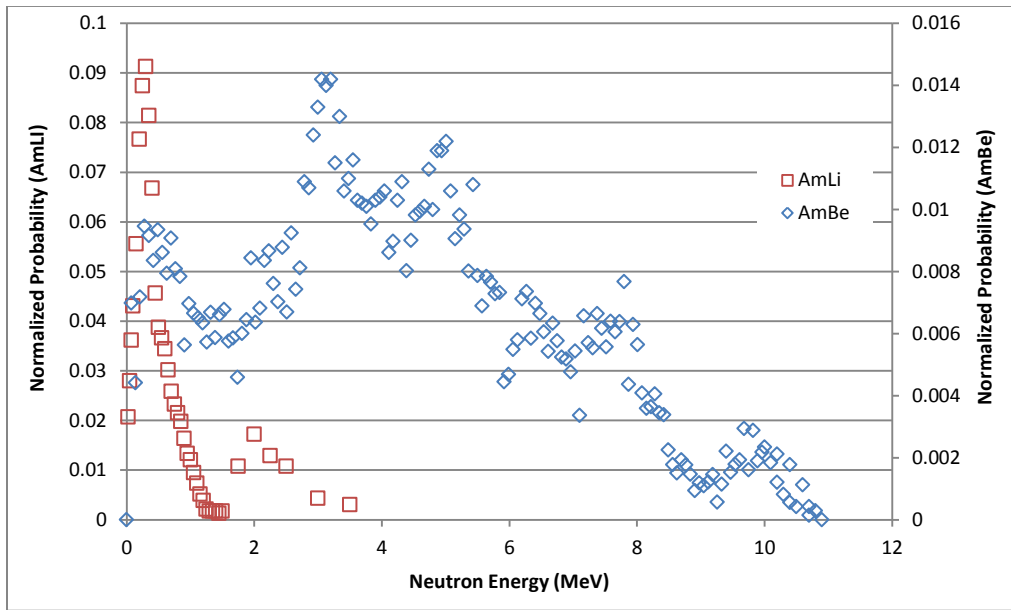


Figure 31. Comparison of AmBe and AmLi neutron energy spectra [9, 92].

4.1.1.3 Neutron Generators

Neutron generators provide a relatively high flux neutron source that can be used as an alternative to nuclear reactor beams, especially in safeguards applications where access to a reactor beam is not feasible. Neutron generators have many applications including use in medicine, neutron activation analysis, neutron radiography and imaging, homeland security applications such as cargo and package monitoring, and material analysis. Recent advances in neutron generator design, specifically the use of new ion sources and the move from vacuum pumps to vacuum-sealed neutron tubes, have improved the reliability and reduced the size of previous generators.

Table 5. Characteristics of ^{252}Cf and AmLi Sources [7]

Characteristics of common neutron sources	^{252}Cf	AmLi	AmBe
Total half-life (yr)	2.646	432	432
Spontaneous fission half-life (yr)	85.5	--	--
Neutron yield (n/s-g)	2.34E12		
Gamma-ray yield (γ /s-g)	1.3E13	--	--
Average neutron energy (MeV)	2.14	0.5 (max \approx 1.5)	5.0 (max \approx 11)
Neutron activity (n/s-Ci)	4.4E9	6.0E4	2-3E6
Avg. spontaneous fission neutron multiplicity	3.757	--	--

Simply described, neutron generators consist of a vacuum tight enclosure (neutron tube) that encompasses an ion source, ion optic elements, and a beam target. The ion source generates ions which are accelerated by an electric field down towards the beam target causing a fusion reaction that results in bursts of neutrons. A basic diagram of a neutron generator is provided in Figure 32.

There are many neutron generator designs using different combinations of ion sources and target materials. Ideal ion source qualities include a strong beam with little gas consumption, low gas pressure, low power requirements, high reliability, and long

lifetime. Ion currents predominantly made up of atomic ions (rather than molecular ions) are most desirable since they lead to higher neutron output. The most common ion source is the Penning ion source; however, newer generators are making use of an RF induction plasma which yields a higher neutron flux than the Penning source [93]. Ideal targets include metal hydrides where hydrogen is abundant. The ability to withstand high temperatures, long lifetimes, high neutron production, and stability are also traits of a good beam target [94]. Titanium and zirconium tend to be very good beam targets for D-T generators when saturated with ^3H , while gold tends to be a good beam target for D-D generators when saturated with ^2H . Mixed target generators are also useful in some applications as they can be self-replenishing. While this leads to longer lifetimes, they produce a lower neutron yield.

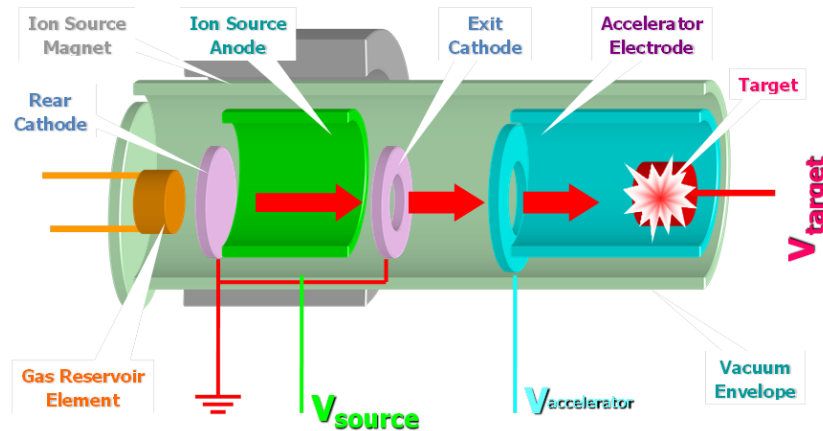


Figure 32. Basic diagram of a neutron generator.

Neutron generators typically operate in one of two modes: pulsed or continuous. Continuous operation is most useful when a steady stream of neutrons is needed. In pulse mode, neutrons are generated only during some predetermined time interval (usually on

the order of 10-100 μ s) [48]. This mode of operation is useful when bursts of neutrons are needed.

Two types of neutron generators were considered: D-D and D-T. D-D generators produce fast neutrons using relatively low voltage accelerators through the following reaction: ${}^2\text{H} + {}^2\text{H} \rightarrow {}^3\text{He} + {}^1_0\text{n} + 3.266 \text{ MeV}$. This exothermic reaction results in the emission of 2.4 MeV neutrons. Until recently, the neutron yield for D-D generators was on the order of 10^6 n/s, which limited its application where high fluxes were needed. Recent advances have increased the possible yield to 10^8 - 10^{10} n/s and increased their potential use, although compact designs are still unavailable.

D-T generators can also produce high energy neutrons using relatively low voltage accelerators through the following exothermic reaction: ${}^2\text{H} + {}^3\text{H} \rightarrow {}^4\text{He} + {}^1_0\text{n} + 17.586 \text{ MeV}$ emitting neutrons with energy of 14.1 MeV. The high yield of D-T neutrons (on the order of 10^8 - 10^{10} n/s) in a compact design makes it more appealing than D-D. Drawbacks for D-T generator use are primarily maintenance related and while ${}^3\text{H}$ has a 12.32 yr half-life, this generally exceeds the working life of the generator itself. Another consideration is that ${}^3\text{H}$ is generally accountable material requiring permits and special licensing and in some cases may be subject to export control limitations.

4.1.2 Selection of Secondary Neutron Source

The secondary neutron source was selected based on the ratio of induced fission rates from ${}^{252}\text{Cf}$ -interrogation to the induced fission rates from interrogation by the secondary source. These expected fission rates were calculated using the MCNP6 model discussed in Chapter 3. For these simulations, the SDEF card was modified to reflect the secondary source at position (20,20,36), which represents a position nearby and vertically aligned with the measurement items. The spectral data used for the AmLi and AmBe sources are provided in Appendix B.

Simulations were performed for each neutron source to obtain the fission rates in each of the eight CRM standards. The fission rates were used since the timing parameters had not been optimized for the addition of the second source. As discussed in Chapter 5, these parameters do affect the delayed neutron rates, especially in the case of the generators where the counting structure is on a much smaller time scale. Since the goal of this work is to determine the uranium enrichment of an item based on the *ratio* of ^{252}Cf -induced count rates to that of the secondary source, simulations for ^{252}Cf were also performed. Note that the ^{252}Cf source in these simulations was also located at (20,20,36) strictly for this comparison of these data points. The calculated ratios are provided in Table 6.

Table 6. Ratios of Induced Fission Rates

w%	$^{252}\text{Cf}/\text{DT}$	$^{252}\text{Cf}/\text{DD}$	$^{252}\text{Cf}/\text{AmLi}$	$^{252}\text{Cf}/\text{AmBe}$
0.31	0.195 ± 0.001	0.722 ± 0.004	8.454 ± 0.078	0.647 ± 0.003
0.72	0.200 ± 0.001	0.703 ± 0.004	6.778 ± 0.067	0.652 ± 0.003
1.94	0.212 ± 0.001	0.740 ± 0.005	4.317 ± 0.051	0.676 ± 0.005
2.95	0.221 ± 0.002	0.751 ± 0.006	3.219 ± 0.041	0.689 ± 0.006
4.46	0.219 ± 0.002	0.752 ± 0.009	2.354 ± 0.034	0.686 ± 0.008
20.11	0.333 ± 0.008	0.881 ± 0.020	1.107 ± 0.024	0.827 ± 0.019
52.49	0.487 ± 0.014	0.983 ± 0.027	0.862 ± 0.023	0.947 ± 0.026
93.17	0.606 ± 0.018	1.025 ± 0.030	0.756 ± 0.022	1.009 ± 0.029

These ratios are also plotted in Figure 33 as a function of uranium enrichment. Note that the $^{252}\text{Cf}/\text{AmLi}$ ratios are represented by the secondary y-axis. While most of the datasets exhibit a similar trend of increasing ratio with increasing enrichment, the $^{252}\text{Cf}/\text{AmLi}$ data does not. The difference can be attributed to the fact that the average AmLi neutron energy is ~ 0.5 MeV, well below the 1 MeV “threshold” for fission in ^{238}U . In the case where enrichment is low, the ^{252}Cf neutrons are much more likely to cause fission in the prevalent ^{238}U than the lower energy AmLi neutrons resulting in a large ratio value. As

the enrichment increases, there is less ^{238}U to fission and the AmLi neutrons begin to dominate fission in the now prevalent ^{235}U .

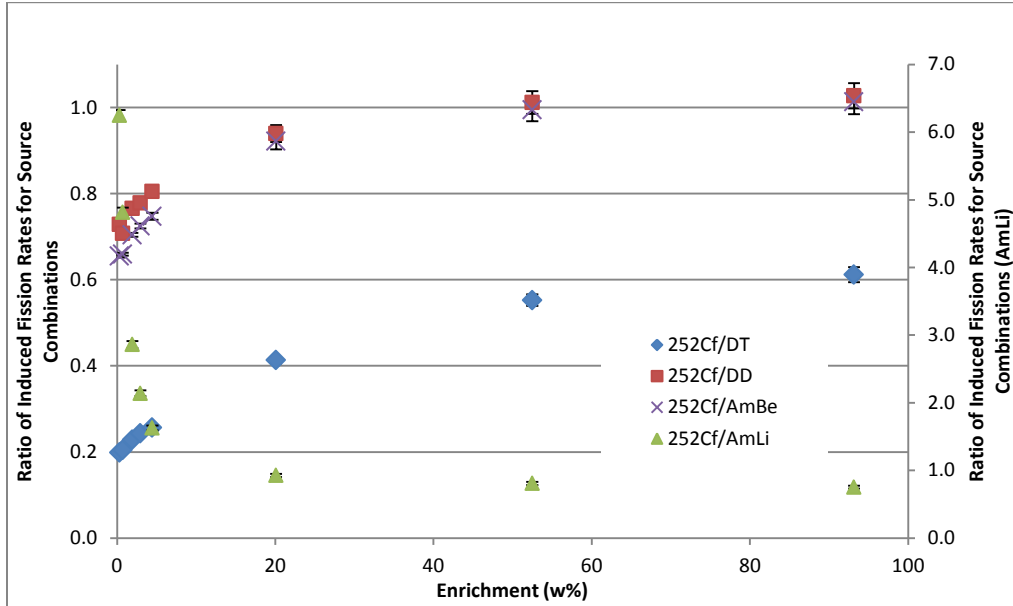


Figure 33. Ratio of ^{252}Cf -induced delayed neutrons to that of potential secondary neutron sources.

Strictly based on the simulated data, it appears that all of the evaluated neutron sources would work in the application being proposed in this dissertation. This assumption is based on the fact that there is a clear monotonically increasing (or decreasing in the case of the $^{252}\text{Cf}/\text{AmLi}$ ratio) relationship between the ratios and the uranium enrichment.

The AmLi ratio exhibited the largest and most pronounced difference as a function of enrichment (especially for LEU materials) implying it may be the best choice for the secondary neutron source; however, the difficulty of obtaining and the expense of AmLi sources deter its use. AmLi sources are also physically large (especially sources capable of generating the large neutron flux necessary for delayed neutron counting) and would

require a secondary source transfer mechanism to shuffle it in and out of the measurement chamber as is performed with the current ^{252}Cf .

The AmBe, D-D, and D-T ratios exhibit very similar relationships as evident by the similar shapes of the curves. The slope is largest for the $^{252}\text{Cf}/\text{D-T}$ ratio over the full range of enrichments, suggesting that D-T is the best choice of the three for the secondary source. While it appears that an AmBe source would work, the implementation of such source would require an additional source transfer mechanism which is prohibitive for this work. The D-D generator shows promising results as well; however, the D-T generator is preferred due to its larger neutron flux.

To summarize, the D-T neutron generated was selected as the secondary neutron source for four specific reasons:

- 1) The simulations indicate a monotonically increasing relationship between the delayed neutron ratios and the uranium enrichment,
- 2) The D-T neutron generator requires no additional source transfer mechanism or additional shielding and is relatively easy to install inside the ^{252}Cf shuffler,
- 3) It is capable of producing a large neutron flux, and
- 4) It is available for this work.

4.2 Optimal Positioning of the Secondary Source

Once selected, the installation of the D-T generator was considered. To increase measurement precision, the D-T generator was positioned such that the fission rates in the measurement item were maximized. This study was performed through MCNP6 simulation. Sixteen positions inside the shuffler measurement chamber were considered. Figure 34 shows the D-T positions evaluated. Note that the two concentric circles represent the measurement item and the small circle near the top of the cross-sectional diagram represents the ^{252}Cf location.

The stars represent the (x,y) coordinate positions. Note that while the shuffler appears to have left-right symmetry, there are slight differences (e.g., there is a gap in the Cd liner on the left side for the bare flux monitor). There were two heights evaluated for each (x,y) position: 12.5 cm and 36 cm. The measurement height of 12.5 cm represents the target location when the generator is sitting on the bottom or floor of the measurement chamber; whereas 36 cm corresponds to the target lined up directly centered on the nuclear material in the measurement item.

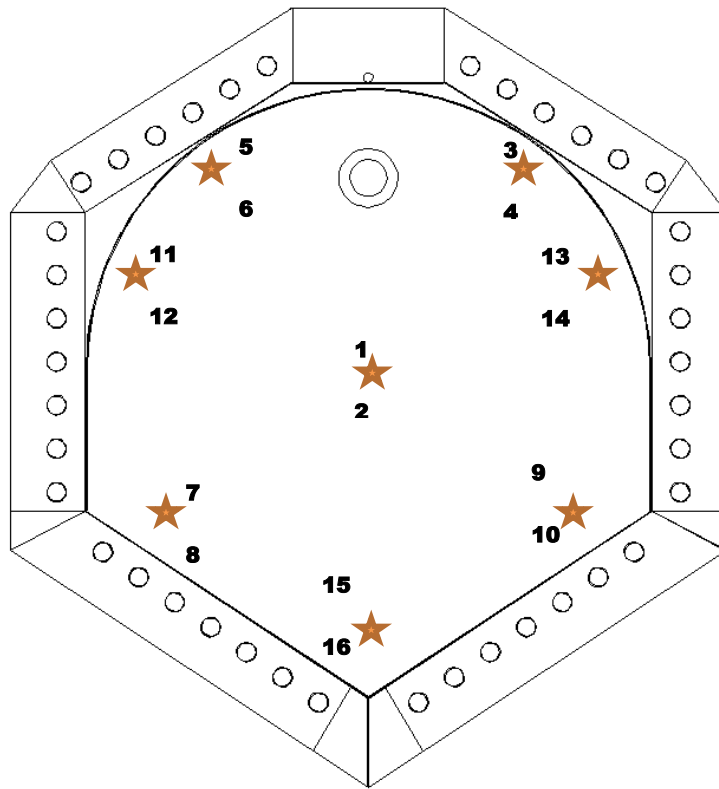


Figure 34. Cross-section (x,y) of the shuffler cavity showing the D-T generator positions evaluated.

In the MCNP6 simulations, the SDEF card was changed to include the 14.1 mono-energetic neutrons from the (D-T reaction) at each of the positions described above. Two CRM standards were included in this evaluation: natural uranium (NBS071) and HEU (NBL003). The resulting fission rates for each item were calculated and are provided in Table 7. A plot of the fission rates is provided in Figure 35.

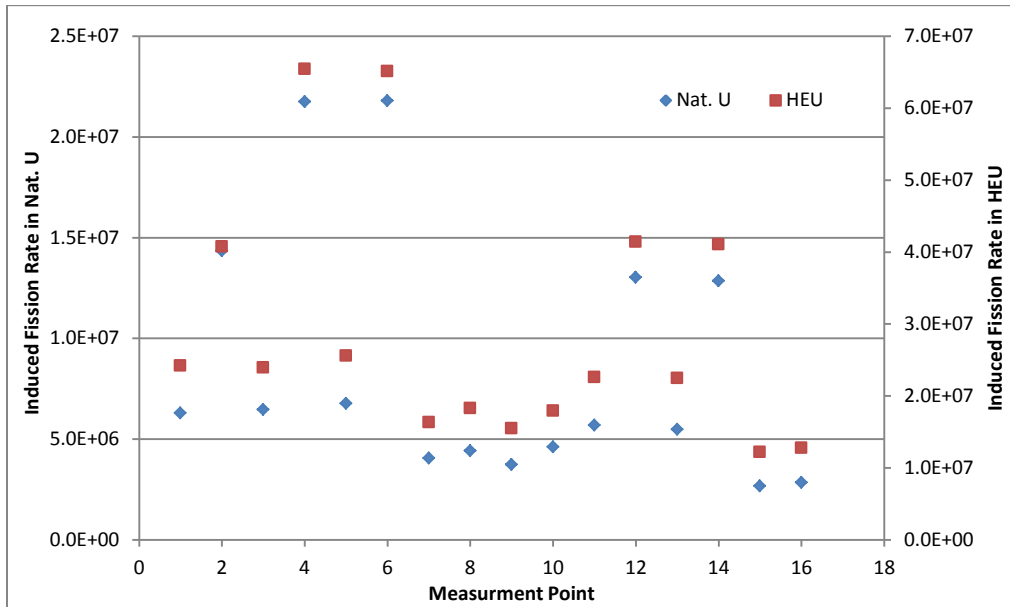


Figure 35. Induced fission rates for nat. U and HEU at various D-T positions.

For both sources, the fission rates were largest at position 4 (20, 20, 36) and position 6 (-20, 20, 36), which represent the vertical center of the nuclear material in the item. Although equivalent, position 6 is very close to the Cd gap in the chamber lining (which supports flux monitor calculations); therefore, position 4 was chosen for the installation of the D-T generator. Elevating the generator target line to the height of the uranium sample required suspending the generator in the air; however, it provided a two-fold

Table 7. Fission Rates per Source Particle for Various D-T Locations

Point Identification	x-	y-	z-	R _{IF} (Nat. U)	R _{IF} (HEU)
1	0	0	12.5	6.30E+06 ± 2.23E+04	2.42E+07 ± 4.83E+05
2	0	0	36	1.44E+07 ± 5.07E+04	4.08E+07 ± 8.07E+05
3	20	20	12.5	6.46E+06 ± 2.28E+04	2.40E+07 ± 4.76E+05
4	20	20	36	2.18E+07 ± 7.69E+04	6.54E+07 ± 1.30E+06
5	-20	20	12.5	6.77E+06 ± 2.39E+04	2.56E+07 ± 5.10E+05
6	-20	20	36	2.18E+07 ± 7.70E+04	6.51E+07 ± 1.29E+06
7	-25	-15	12.5	4.06E+06 ± 1.43E+04	1.63E+07 ± 3.27E+05
8	-25	-15	36	4.41E+06 ± 1.56E+04	1.83E+07 ± 3.65E+05
9	25	-15	12.5	3.73E+06 ± 1.32E+04	1.55E+07 ± 3.10E+05
10	25	-15	36	4.61E+06 ± 1.63E+04	1.79E+07 ± 3.55E+05
11	-25	15	12.5	5.69E+06 ± 2.01E+04	2.26E+07 ± 4.48E+05
12	-25	15	36	1.30E+07 ± 4.60E+04	4.14E+07 ± 8.21E+05
13	25	15	12.5	5.48E+06 ± 1.94E+04	2.25E+07 ± 4.45E+05
14	25	15	36	1.29E+07 ± 4.54E+04	4.11E+07 ± 8.14E+05
15	0	-35	12.5	2.67E+06 ± 9.42E+03	1.22E+07 ± 2.44E+05
16	0	-35	36	2.85E+06 ± 1.02E+04	1.28E+07 ± 2.55E+05

increase in the fission rate at that location. During installation, the D-T neutron generator was secured to the Cd liner inside the shuffler cavity to provide additional support for the generator. The final installation of the generator centers the target line at (23.5, 23.5, 36) just a few cm away from the proposed location.

The installed neutron generator is shown in Figure 36. For the development of this method, the can was positioned such that the ^{252}Cf flux was maximized. As a result, the measurement items were not placed in the center of the measurement cavity; instead, they were placed near the back of the measurement chamber, nearer to the ^{252}Cf source. Since the DEANI method uses both the ^{252}Cf and D-T signals, changes in the source-to-detector geometry would affect the results. In an ideal scenario, the item would be placed in the center of the cavity such that changes in geometry are coupled to both measurements equally. This would reduce position dependence and improve the measurement results when applied or extrapolated to the measurement of other geometries and sizes.



Figure 36. Installed D-T generator.

4.3 Selection of Spectrum Tailoring Materials

Because the difference in induced fission rates from various U_3O_8 cans when interrogated by a ^{252}Cf source or a D-T generator is explored, the neutron energies in the shuffler were examined. Figure 37 shows the traditional Watt fission spectrum for ^{252}Cf and a mono-energetic, 14.1 MeV source representing a D-T generator. Since the ^{252}Cf spectrum is said to be tailored to reduce fission in ^{238}U [65], simulations were performed to determine the neutron energies incident upon the measurement items inside the measurement chamber. These spectra are shown in Figure 38.

The results suggest that the average energy of the ^{252}Cf neutrons incident on the measurement item is reduced to approximately 1.6 MeV, which is expected since the goal of spectrum tailoring is to minimize fission in ^{238}U while maintaining the hardness of the spectrum to preserve penetrability. Similarly, the 14.1 MeV neutron source shows a slightly softened spectrum incident on the measurement item resulting in an average energy of approximately 7.3 MeV. The structure between 12 and 14 MeV is likely caused by those neutrons undergoing 1–2 scatters in the steel reflector before reaching the item. The key observation is that even though the lower energy regions are similar, simulations predict there to be a significant number of energetic 13–14 MeV neutrons incident on the measured item.

Because the goal of this work is to take advantage of the energy difference in the interrogation sources, it was decided to not include additional materials around the D-T generator. It is acknowledged, however, that further investigation on this topic should be pursued as follow-on work. It was also noted that moving the small CRM items directly in front of the D-T generator may have yielded better DEANI results since more 14.1 MeV neutrons would have been interrogating the samples as opposed to ~ 7 MeV neutrons (on average). While this was not addressed as part of this work, it has been identified as a topic of follow-on or future work.

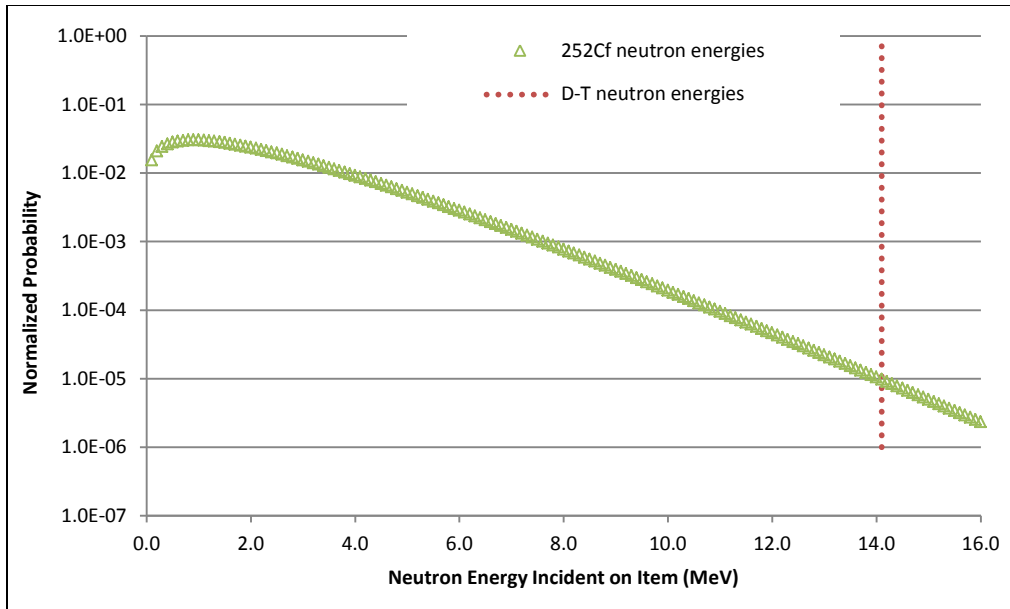


Figure 37. Neutron energy spectra for ^{252}Cf and D-T sources.

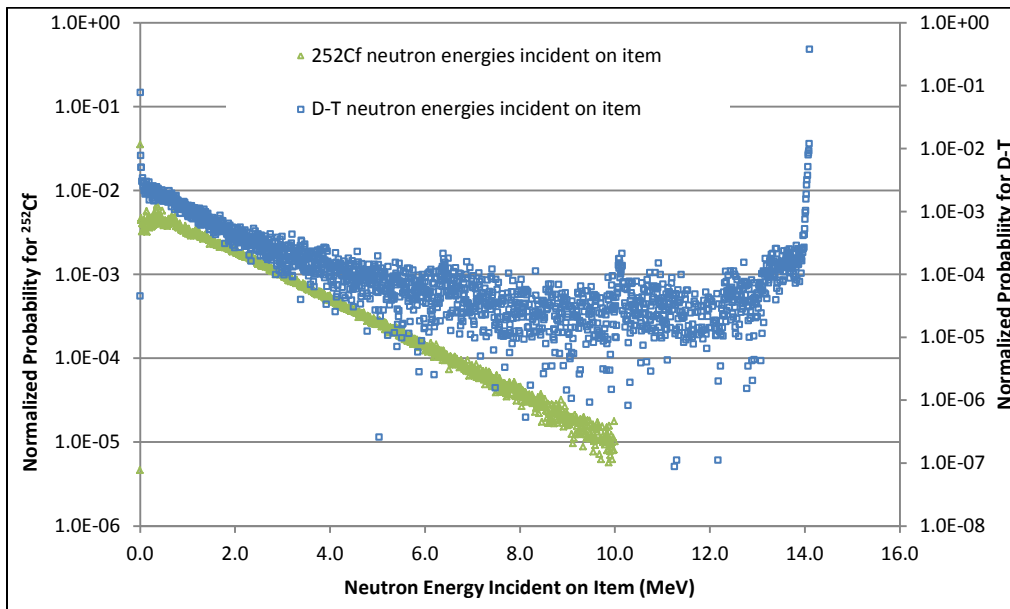


Figure 38. Neutron energy spectra incident on the measurement item for ^{252}Cf and D-T sources.

4.4 ^{252}Cf Shuffler Characterization

The INCC 5.12 software along with a JSR-15 was used for data acquisition during the characterization of the ^{252}Cf Shuffler. Details regarding the ^{252}Cf sources used for the high voltage plateau, efficiency measurements, die-away measurements, and dead-time measurements are provided in Appendix B. Note that ^{252}Cf -5685 was used for the efficiency mapping, ^{252}Cf -6081 was used for the overall efficiency measurement and die-away measurements, ^{252}Cf -5442 and ^{252}Cf -5870 were combined for the high voltage plateau, and ^{252}Cf -6081, ^{252}Cf -5442, and ^{252}Cf -5443 were all used in the dead-time determination.

4.4.1 *High Voltage Plateau*

The INCC 5.12 software is capable of generating a high voltage plateau (total counts as a function of operating high voltage) given the user supplies a minimum and maximum high voltage and the voltage increments for each step. Using this capability, the total counts were recorded for 20 V steps ranging from 1200 to 2000 V. The calculated singles rate over each 5 min. measurement period was also reported. The high voltage plateau is shown in Figure 39.

A linear regression was used to fit both the rising edge of the plateau and the more stable plateau region. The intersection of these fits occurs at 1600V. Since the goal of performing a high voltage plateau is to ensure stability of the counter over a long period of time, it is appropriate to increase the high voltage slightly to move away from the “knee” of the curve [95]. A good rule of thumb for optimal operating high voltage is this intersection plus 40 V. This suggests that 1640 V is the optimal operating high voltage. However, based on the manufacturer’s suggested parameters and the reasonable stability on that region of the plateau, 1670 V was chosen for this work.

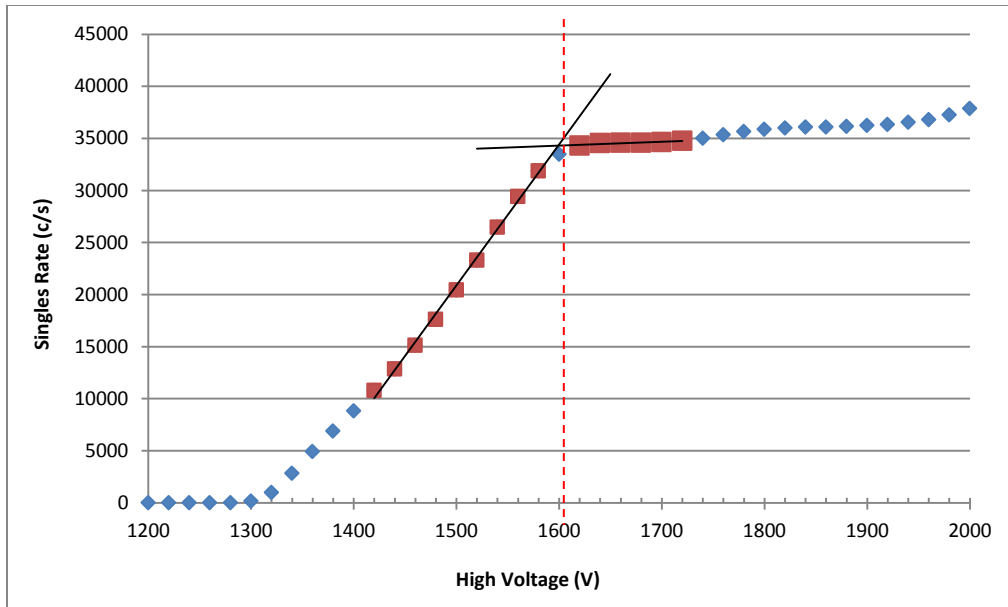


Figure 39. High Voltage Plateau for ^{252}Cf Shuffler

4.4.2 ^{252}Cf Efficiency

The absolute efficiency of the shuffler was measured apart from the efficiency mapping discussed above. A NIST-traceable ^{252}Cf source (6081) was placed at the center of the measurements chamber (0, 0, 57.5). The measurements were completed for the shuffler in its original configuration and with the DT generator installed inside the measurement cavity. The efficiency was measured to be $0.167 \pm 2.89\text{E-}05$ counts/n without the D-T generator inside the shuffler and $0.167 \pm 2.39\text{E-}05$ counts/n with the D-T generator inside the shuffler indicating no effect from the presence of the generator. Note that the uncertainties reported are statistical only. The emission rate of the source is only known to $\sim 1\%$ (quoted at 1σ).

4.4.3 *Delayed Neutron Efficiency*

While the ^{252}Cf efficiency is the most common method to determine the detection efficiency for most neutron instruments, it is not suitable for delayed neutron applications since delayed neutrons have much lower energies than prompt neutrons. Historically, delayed neutron data was needed for thermal reactor design and control and for these applications there was never significant motivation to improve the spectral data. Additionally, due to the difficulty in measuring a number of the short-lived precursors, the delayed neutron energy spectrum is considered the least well known parameter related to delayed neutron data [96]. The difference between the ^{252}Cf and delayed neutron efficiencies can be upwards of 5% [97]. There are two generally accepted techniques used to determine the shuffler efficiency for delayed neutron counting.

The first technique used to estimate the delayed neutron efficiency of the shuffler is to measure the efficiency using an AmLi source since its average neutron energy is quite like that of delayed neutrons. The difficulty in this method is knowing the emission rate of the AmLi to better than a few percent [97]. Because a reliable AmLi source was not available for measurement, an AmLi spectrum [9] was input into the MCNP6 model and the efficiency was calculated to be 22.4 % based on the captures in ^3He .

The second technique uses MCNP to calculate the efficiency using a delayed neutron spectrum on the SDEF card. Unfortunately, while many have measured the delayed neutron spectra for ^{235}U [28, 98-100], the aggregated delayed neutron energy spectra published to date are quite crude. Rinard and others' early work on the shuffler used the 9-bin energy spectra given in Table 8. The delayed neutron spectral data for the Hansen-Roach 16-group energy structure, also given in Table 8, was proposed along with the 8-group delayed neutron structure [63, 101]. It too was used to calculate a delayed neutron efficiency for the shuffler. These two delayed neutron spectra are shown in Figure 40.

Table 8. Reported Delayed Neutron Spectra

Rinard Spectrum		Hansen-Roach 16-group Energy Structure	
Energy Bin (MeV)	Probability	Energy Bin (MeV)	Probability
0 – 0.30	1.80	0.0001 – 0.00055	9.135e-5
0.30 – 0.40	1.65	0.00055 – 0.003	0.0014773
0.40 – 0.50	1.35	0.003 – 0.017	0.0154555
0.50 – 0.60	1.05	0.017 – 0.1	0.1152628
0.60 – 0.70	0.75	0.1 – 0.4	0.3974288
0.70 – 0.80	0.45	0.4 – 0.9	0.3525474
0.80 – 1.20	0.25	0.9 – 1.4	0.0930729
1.20 – 1.60	0.15	1.4 – 3	0.0279091
1.60 – 2.00	0.05	3- 17	0.001662

The average delayed neutron energies are quite similar at around 400 keV. Both spectra were used in MCNP6 to calculate a delayed neutron efficiency in the shuffler. The spectrum used by Rinard yielded an efficiency of 22.5%, while the Hansen-Roach spectrum yielded an efficiency of 22.3%. Since there is no significant difference in these efficiencies any of these values should suffice for these delayed neutron calculations. However, since Rinard was intimately involved in shuffler operations and developed the majority of the shuffler calculations, the simulated delayed neutron efficiency was taken to be 22.52%. Note that the source term was modeled as a point at the measurement item location (not the center of the measurement chamber).

Because the efficiency mapping discussed in Chapter 3 showed a ~4% difference in the measured and simulated efficiencies for ^{252}Cf at the measurement item location, the calculated efficiency for delayed neutrons was normalized by the ratio of the measured efficiency to the calculated efficiency of ^{252}Cf . Recall that the measured ^{252}Cf efficiency in the measurement location was 17.7 % while the simulated ^{252}Cf efficiency was 18.5 %. The normalized delayed neutron efficiency (used in the analytical calculations) was then calculated to be 21.3 %.

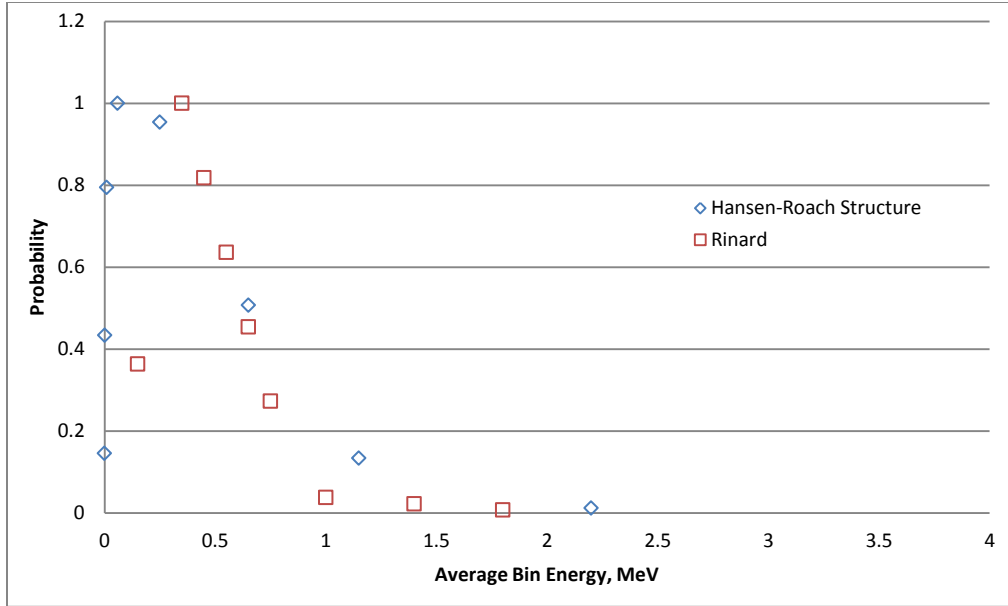


Figure 40. Delayed neutron energy spectra used to calculate efficiency in the shuffler.

4.4.4 Dead-time Measurements

Dead-time is defined as the minimum amount of time that is required between $^3\text{He}(n,p)$ events in order for them to be recorded as two separate events. Dead-time corrections are important for all radiation measurements since dead-time effects lead to reduced count rates. The dead-time, τ_{DT} , of the shuffler was measured using the non-paralyzable two-source method as described by Eq. 19 [95, 102]:

$$\tau_{DT} = \frac{M_1 + M_2 - M_{12} - B}{M_{12}^2 - M_1^2 - M_2^2}, \quad \text{Eq. 19}$$

where, M_i is the measured count rate for source 1, 2, or the combination of 1 and 2, and B is the background count rate. The equation for uncertainty is provided in Appendix C.

For these shuffler measurements, $^{252}\text{Cf-6081}$ represents source 1, $^{252}\text{Cf-5442}$ and $^{252}\text{Cf-5443}$ together represent source 2, and all three combined to represent source 12. INCC

was used to record the rates for 40-, 30 s cycles. The measured rates are presented in Table 9. The shuffler dead-time was then determined from the singles rate alone to be $5.85\text{E-}02 \mu\text{s} \pm 8.34\text{E-}03 \mu\text{s}$. For the measurement of delayed neutrons (where count rates are much lower than 2×10^4 c/s), the dead-time is negligible. Thus, formal dead-time corrections were not applied to the delayed neutron measurements.

Table 9. Dead-time Measurement Results

Source Configuration	Singles Rates	Doubles Rates
Source 1	52806.992 ± 8.876	8654.378 ± 17.589
Source 2	18071.281 ± 8.64	2757.75 ± 6.376
Source 12	70762.797 ± 9.618	11385.285 ± 24.129
Background	4.8 ± 0.08	0.41 ± 0.038

4.5 Measurement Setup

4.5.1 ^{252}Cf Measurement Setup

The measurement setup for the ^{252}Cf measurement is relatively straightforward since the measurement is being performed in the “traditional” sense and the system electronics and data acquisition system were already in place. The high voltage was supplied by an Ortec High Voltage Power Supply module. The +5V for the preamplifiers was provided by a Canberra DC Power Supply. The signal from each ^3He tube is daisy chained into a single signal output for each detector bank. Therefore, there were a total of 8 detector signals coming out of the shuffler directly into the 12 Channel Scalar utilized by the system. ^{252}Cf Shuffler Software v2.0 is used for data analysis. The signal from each detector bank is provided in the shuffler output files. The summed signal over all 8 banks is then used to determine the delayed neutron count rates for the established settings.

4.5.2 D-T Measurement Setup

The neutron generator used for this work was the Thermo Scientific P 211 D-T generator. This system is designed to produce no neutron background between pulses by using a pulsed accelerating voltage and ion source. The high voltage/current is provided to the source and the target using Sorenson DCS600-1.7E power supplies. It has a neutron output of 1.0×10^6 n/pulse and a pulse width of 10 μ s. It can be operated at 10, 50, or 100 Hz. For the measurements used in this work, 100 Hz was used.

Operation of the D-T generator required a tremendous amount of work. In addition to the work required to bring a D-T generator online at ORNL (e.g., nuclear material and accountability requirements for the ^3H , revisions to facility use agreements, radiological surveys, redundant safety interlocks, etc.), the measurement required installation and setup of an entirely new data acquisition system.

In order to extract the measurement signal from the shuffler detectors following the D-T irradiation, a Mirion Technologies (formerly Canberra Industries) Lynx was used. The Lynx is a multichannel analyzer that uses digital signal processing, which is used for many spectroscopy applications. The Lynx can be setup in multi-channel scalar mode where data is collected as a function of time. This MCS mode was used for the measurement of delayed neutrons following the D-T pulses.

The summed shuffler signal (from all 8 detector banks) was output from the 12 Channel Scalar into the MCS port on the LYNX. The pulse trigger was then output from the D-T generator Controller into the MCS SWEEP port on the LYNX. This allowed the counts (as a function of time) to be aggregated over the entire irradiation period providing a useful signal. Data acquisition was performed using Mirion Technologies Genie-2000 software.

In addition to the data acquisition system for the shuffler output, a flux monitor (a small ^3He tube wrapped in 1/8 in Cd) was placed at the bottom of the shuffler parallel to the

floor of the chamber to provide information related to the D-T generator emission rate. ^3He was a suitable choice for the flux monitor since only the intensity of the D-T flux was being normalized. A high voltage plateau was conducted and its operating voltage was set to 1720V. This was provided by an external high voltage power supply. The flux monitor signal was output to the MCS port on a second Lynx. The D-T generator trigger was also output to the Lynx MCS Sweep port on this Lynx such that the two Lynx systems were synced. The MCS bins were 1 μs wide for both the shuffler signal and the flux monitor signal, which is the shortest time allowed by the Genie software.

Post processing was performed on the time spectra to calculate the delayed neutron rates. The details of this analysis are discussed in later sections.

4.6 Optimization of Measurement Times

4.6.1 ^{252}Cf -based Measurements

The traditional ^{252}Cf Shuffler time structure is as follows: the source is shuffled into the measurement chamber (1.23 s), the source irradiates the measurement item for a given time, the source is removed from the shuffler measurement chamber (1.94 s), and finally delayed neutrons are counted during the prescribed counting window. The forward travel and reverse travel times for the source are fixed. The irradiation time and count time are adjustable; however, Rinard has shown that the number of counts during the measurement will be maximized when they are the same [58].

To obtain the optimal irradiation and count times, it is customary to either maximize the delayed neutron counts or minimize the relative precision of the measurement. The latter is often chosen as a measurement goal. Relative precision, described in Eq. 20 can be minimized by adjusting the number of shuffles, n , the irradiation time, t_i , the count time, t_c , or the background collection time, t_b via a parameter study.

$$\frac{\sigma_D}{D} = \frac{\sqrt{dT_C + bt_b \left(\frac{T_C}{t_b}\right) + bt_b \left(\frac{T_C}{t_b}\right)^2}}{dT_C} \quad \text{Eq. 20}$$

In this equation, d is the delayed neutron count rate, b is the background count rate, T_c is the total time for the assay, t_b is the total background count time. If the count rates d and b can be estimated, then the relative precision can be minimized by adjusting T_C and t_b . To begin, the following constraints were applied: 1) $t_i = t_c$, 2) $n = 85$, and 3) t_f and t_r are known and fixed. In addition, the background count time was fixed at 1000s. The number of cycles was increased to the maximum number of cycles (i.e., 85) allowed by the shuffler software since the ORNL ^{252}Cf source is old and weak with respect to a new shuffler source. Using the solver function in Microsoft ExcelTM, an optimum count time, t_{count} , was determined to be 6.72 s. For simplicity, this value was rounded up to 7 s. All “traditional” shuffler measurements for this work were performed with t_{irr} and t_{count} set to 7 s.

4.6.2 *D-T-based Measurements*

This timing structure for the D-T generator measurements is quite different for a couple of reasons. First, there is no transit time for the source moving in and out of the measurement chamber; it essentially turns on and off instantly (compared to the decay of the delayed neutrons). Second, the pulse rate is 100Hz so the count window must be extremely small to fit between the 10 μs wide pulses.

To determine an appropriate count window for this shortened time scheme, the MCS or time spectrometer was used to acquire the shuffler rates during D-T operation. The count rate window was then selected by analyzing the MCS data and choosing a window that maximized the signal-to-noise ratio for all seven CRM standards and the countable fraction. The counting window chosen for this analysis was 4000 μs – 9700 μs after the trigger. This counting window is highlighted in Figure 41.

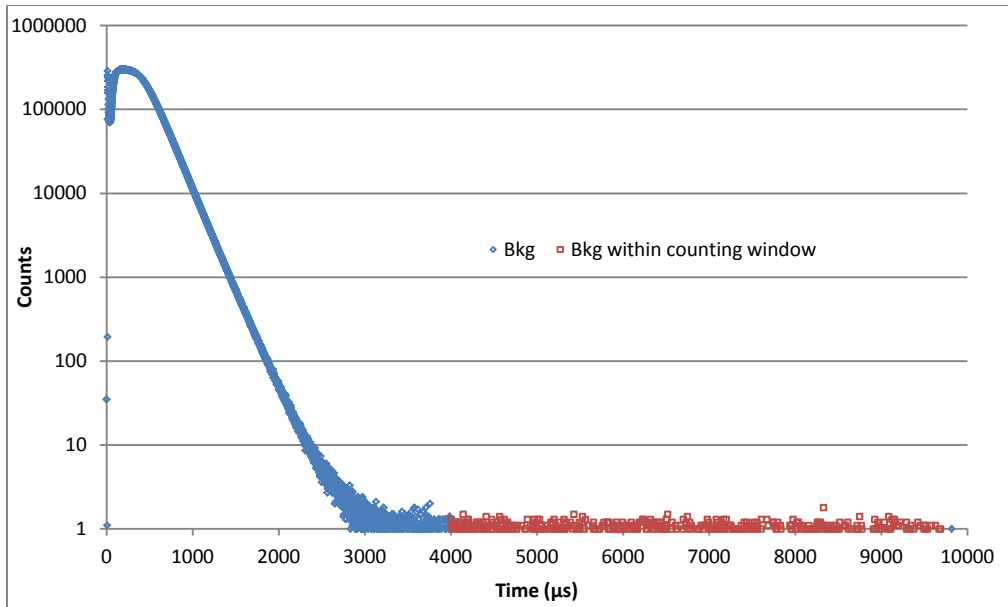


Figure 41. Shuffler counting window for the D-T measurements.

4.7 Measurement Method and Scenarios

The measurement methodology used to demonstrate that the DEANI method can determine the ^{235}U enrichment is outlined in this section. The uranium standards to be measured were placed on a small stand on top of a rotator inside the shuffler measurement cavity as shown in Figure 36. The center of the nuclear material was positioned near coordinates (0, 24.5, 36) cm unless otherwise noted. Recall that the center of origin is at the bottom of the measurement cavity (centered in the x- and y-position).

The DEANI method involves two separate measurements: one using ^{252}Cf for the interrogating flux and one using a D-T generator for the interrogating flux. The ^{252}Cf -induced measurements were performed with the ORNL ^{252}Cf Shuffler in the traditional manner except that the D-T generator was installed inside the measurement chamber. The ^{252}Cf Shuffler Software v2.0 was used to facilitate the measurements and to record the background corrected, delayed neutron rates. The key measurement parameters are

provided in Table 10. Due to the age of the ^{252}Cf source, eight measurements were completed for each uranium item.

Table 10. ^{252}Cf -based Shuffler Measurement Parameters

Shuffler Parameter	Value
Shuffler High Voltage (V)	1670
Source Transfer Distance (in)	82.15
Number of Cycles	85
Background Count Time (s)	1000
Nominal Count Time / Cycle (s)	7
Nominal Irradiation Time / Cycle (s)	7
Nominal Forward Time / Cycle (s)	2
Nominal Reverse Time / Cycle (s)	1.33

The data collection process for the D-T-based measurements was significantly different since there is no integrated software or course to extract the delayed neutron rates directly. The setup was discussed in a previous section. Recall that in addition to the shuffler measurement signal, the added flux monitor was used to provide normalization for the data.

Once both MCS acquisitions were started, the D-T generator was initiated. Each D-T measurement ran for 60000 pulses (at 100 Hz). The MCS data (for both the shuffler and the flux monitor) was summed over all pulses using the trigger. An example MCS output for the shuffler signal is shown in Figure 41 where the region of interest (in red) identifies the actual counting window between pulses. The counts in this window are the gross delayed neutron counts for all 60000 pulses. The complete analysis is outlined in the following chapter. Five measurements (60000 pulses each) were completed for each uranium item in order to check for consistency, improve precision, and enable statistical uncertainty to be checked from the scatter in the data.

The ratio of the ^{252}Cf -induced delayed neutron count rates to the D-T-induced delayed neutron count rates (referred to as the delayed neutron ratio hereafter) were then plotted to generate a calibration curve. This curve was then used to determine the ^{235}U enrichment of a few “unknown” standards and validate the DEANI method. In addition to the eight CRM standards, several other uranium items were measured to assess whether uranium mass, material type, or shape affected the delayed neutron ratio. These results are discussed in Chapter 5.

5 RESULTS AND ANALYSIS

Delayed neutron experiments were performed to study the newly proposed DEANI methodology and also to validate the MCNP6 model. These measurements were conducted on NBL CRM standards using both the traditional ^{252}Cf Shuffler and the added D-T generator capability. The analysis and results for these two-part measurements are discussed in this chapter, as are the results of the high-resolution gamma measurements performed on the same items. In addition, a sensitivity analysis for the 8-group delayed neutron structure (recently adopted by the IAEA) and the energy-dependent delayed neutron parameters are discussed. A comparison of die-away characteristics dependent on the interrogation source is also performed. Lastly, the results of a brief examination of the delayed neutron capabilities in MCNP6 are provided.

5.1 Expected Delayed Neutron Rates and DEANI Results

This section outlines the MCNP6-based calculations for the delayed neutron count rate ratios updated with optimized parameters discussed in Chapter 4. One hundred million histories were simulated for each scenario discussed.

5.1.1 *Simulated Induced Fission Rates*

To illustrate the concept of the DEANI method, the traditional ^{252}Cf source (represented by a Watt fission spectrum) and an isotropic, 14.1 MeV point source to represent a D-T generator were modeled in MCNP6. The weight gained from fission was extracted from the simulations and used to calculate the induced fission rates from each interrogating source for each CRM item as described by Eq. 17. The source strengths assumed for the ^{252}Cf and D-T sources were 3.2×10^7 n/s and 1×10^{11} n/s, respectively. These values were taken from the source certificates and the technical specifications for the D-T generator. Because the uncertainties on the emission rate are 10% for the ^{252}Cf and unknown for the D-T generator, they were not included in the error propagation. For these calculations,

contributions from the minor nuclides, ^{234}U and ^{236}U , have been ignored; thus, ^{235}U and ^{238}U were the only isotopes considered in the sample. Although ^{234}U and ^{236}U were included in the MCNP6 model, delayed neutron parameters are not currently available. The values of $\bar{\nu}_{U235}$ and $\bar{\nu}_{U238}$ used in these calculations were 2.47 ± 0.05 and 2.79 ± 0.10 , respectively. The MCNP6 output, G_I , and the predicted induced fission rates, R_I , for each item are presented in Table 11.

As expected, based on the fission cross-sections for ^{235}U and ^{238}U , G_I is larger for ^{235}U when interrogated by ^{252}Cf (more thermal fission) while G_I is larger for ^{238}U when interrogated by the D-T neutrons (fission by neutrons above the 1 MeV threshold). This is not directly obvious from the fission rates since the D-T source strength (used to calculate the fission rates) was much higher than the source strength of the ^{252}Cf source.

5.1.2 *Estimated Delayed Neutron Rates*

The induced fission rates were then used to analytically calculate the expected delayed neutron counts, D , contributed by each isotope as described in Eq. 9. The shuffler parameters used in these calculations are reported in Table 12, while group-specific delayed neutron parameters (i.e., the Keepin numbers) were previously listed in Table 3. The calculated delayed neutron counts over all groups are presented in Table 13. The results are given by individual *isotope* (showing the delayed neutron contribution from each isotope) and for each interrogation source (i.e., ^{252}Cf - or D-T-based measurements). The complex equations used to calculate uncertainties are provided in Appendix C.

As expected, the delayed neutron counts from ^{235}U decrease with decreasing enrichment, while the delayed neutron counts for ^{238}U increase with decreasing enrichment. This is true for both ^{252}Cf and D-T interrogation. The total delayed neutron counts expected from the *measurement items* are simply the sums of the total counts from each isotope. The expected delayed neutron count rates, R , were obtained by dividing the total counts for

Table 11. Calculated Induced Fission Rates for Various CRMs

Enrichment (w%)	Isotope	$G_I(^{252}\text{Cf})$	$G_I(\text{D-T})$	$R_{\text{IF}}(^{252}\text{Cf})$	$R_{\text{IF}}(\text{DT})$
93.17%	U-235	1.39E-03	8.803E-04	$3.02\text{E}+04 \pm 1.03\text{E}+03$	$5.99\text{E}+07 \pm 2.04\text{E}+06$
	U-238	1.35E-05	1.936E-05	$2.42\text{E}+02 \pm 1.35\text{E}+01$	$1.08\text{E}+06 \pm 6.04\text{E}+04$
52.49%	U-235	8.05E-04	5.124E-04	$1.75\text{E}+04 \pm 5.96\text{E}+02$	$3.49\text{E}+07 \pm 1.19\text{E}+06$
	U-238	1.04E-04	1.587E-04	$1.86\text{E}+03 \pm 1.04\text{E}+02$	$8.87\text{E}+06 \pm 4.95\text{E}+05$
20.11%	U-235	3.30E-04	2.076E-04	$7.17\text{E}+03 \pm 2.44\text{E}+02$	$1.41\text{E}+07 \pm 4.80\text{E}+05$
	U-238	1.72E-04	2.663E-04	$3.07\text{E}+03 \pm 1.71\text{E}+02$	$1.49\text{E}+07 \pm 8.31\text{E}+05$
4.49%	U-235	7.08E-05	4.286E-05	$1.54\text{E}+03 \pm 5.24\text{E}+01$	$2.92\text{E}+06 \pm 9.92\text{E}+04$
	U-238	1.83E-04	2.867E-04	$3.28\text{E}+03 \pm 1.83\text{E}+02$	$1.60\text{E}+07 \pm 8.95\text{E}+05$
2.95%	U-235	4.47E-05	2.559E-05	$9.72\text{E}+02 \pm 3.31\text{E}+01$	$1.74\text{E}+06 \pm 5.92\text{E}+04$
	U-238	1.81E-04	2.450E-04	$3.24\text{E}+03 \pm 1.81\text{E}+02$	$1.37\text{E}+07 \pm 7.65\text{E}+05$
1.94%	U-235	3.08E-05	1.792E-05	$6.71\text{E}+02 \pm 2.28\text{E}+01$	$1.22\text{E}+06 \pm 4.15\text{E}+04$
	U-238	1.83E-04	2.470E-04	$3.27\text{E}+03 \pm 1.83\text{E}+02$	$1.38\text{E}+07 \pm 7.71\text{E}+05$
0.71%	U-235	1.12E-05	6.610E-06	$2.44\text{E}+02 \pm 8.29\text{E}+00$	$4.50\text{E}+05 \pm 1.53\text{E}+04$
	U-238	1.88E-04	2.530E-04	$3.35\text{E}+03 \pm 1.87\text{E}+02$	$1.41\text{E}+07 \pm 7.90\text{E}+05$
0.31%	U-235	5.76E-06	3.500E-06	$1.25\text{E}+02 \pm 4.26\text{E}+00$	$2.38\text{E}+05 \pm 8.10\text{E}+03$
	U-238	1.86E-04	2.507E-04	$3.33\text{E}+03 \pm 1.86\text{E}+02$	$1.40\text{E}+07 \pm 7.83\text{E}+05$

Table 12. Fixed Parameters for Determining Delayed Neutron Counts

Parameter	²⁵² Cf	D-T
ε (cnt/n)	0.213	0.213
t_{for} (s)	1.94	0.0003
t_{irr} (s)	7.00	0.00001
t_{delay} (s)	1.23	0.00399
t_{count} (s)	7.00	0.0057
τ (s)	17.17	0.01
$\nu_{235\text{U}}$ (n/fiss)	2.47 ± 0.05	2.47 ± 0.05
$\nu_{238\text{U}}$ (n/fiss)	2.79 ± 0.10	2.79 ± 0.10
S (n/s)	$3.20\text{E}+07$	$1.00\text{E}+11$
n	85	60000

Table 13. Calculated Delayed Neutron Counts by Isotope

Enrichment (w%)	Isotope	D_{Cf} (counts)		D_{DT} (counts)	
93.17%	U-235	1.69E+04	± 7.52E+02	6.74E+04	± 2.48E+03
	U-238	2.63E+02	± 1.49E+01	3.20E+03	± 1.40E+02
52.49%	U-235	9.83E+03	± 4.36E+02	3.92E+04	± 1.45E+03
	U-238	2.03E+03	± 1.15E+02	2.62E+04	± 1.15E+03
20.11%	U-235	4.02E+03	± 1.78E+02	1.59E+04	± 5.86E+02
	U-238	3.33E+03	± 1.89E+02	4.40E+04	± 1.93E+03
4.49%	U-235	8.64E+02	± 3.83E+01	3.28E+03	± 1.21E+02
	U-238	3.56E+03	± 2.02E+02	4.74E+04	± 2.08E+03
2.95%	U-235	5.45E+02	± 2.42E+01	1.96E+03	± 7.22E+01
	U-238	3.52E+03	± 2.00E+02	4.05E+04	± 1.78E+03
1.94%	U-235	3.76E+02	± 1.67E+01	1.37E+03	± 5.06E+01
	U-238	3.55E+03	± 2.02E+02	4.08E+04	± 1.79E+03
0.71%	U-235	1.37E+02	± 6.06E+00	5.06E+02	± 1.87E+01
	U-238	3.65E+03	± 2.07E+02	4.18E+04	± 1.83E+03
0.31%	U-235	7.03E+01	± 3.12E+00	2.68E+02	± 9.88E+00
	U-238	3.62E+03	± 2.05E+02	4.14E+04	± 1.82E+03

the item, D , by the total count time ($n * t_{count}$). Table 14 lists the calculated values of R for each interrogation source. The delayed neutron ratios are also provided.

Table 14. The Expected Total Delayed Neutron Count Rates Over 34 Shuffles

Enrichment (w%)	R_{Cf} (c/s)	R_{D-T} (c/s)	Ratio ($^{252}Cf / D-T$)
93.17%	28.93 ± 1.26	206.37 ± 7.27	1.40E-01 ± 7.86E-03
52.49%	19.93 ± 0.76	191.38 ± 5.40	1.04E-01 ± 4.93E-03
20.11%	12.37 ± 0.44	175.15 ± 5.90	7.06E-02 ± 3.45E-03
4.49%	7.44 ± 0.35	148.15 ± 6.08	5.02E-02 ± 3.11E-03
2.95%	6.84 ± 0.34	124.14 ± 5.20	5.51E-02 ± 3.57E-03
1.94%	6.60 ± 0.34	123.40 ± 5.24	5.35E-02 ± 3.57E-03
0.71%	6.36 ± 0.35	123.76 ± 5.36	5.14E-02 ± 3.59E-03
0.31%	6.20 ± 0.34	121.96 ± 5.31	5.08E-02 ± 3.59E-03

The delayed neutron rates for ^{252}Cf interrogation and D-T interrogation are individually plotted in Figure 42. The difference in the shapes and slopes of these two curves provided confidence that the ratios could be used to determine the enrichment. The ratios are plotted in Figure 43 as a function of enrichment. The linear relationship is expected since the calibration standards are similar and delayed neutron ratios should not be susceptible to self-absorption. This simulated data suggests a monotonically increasing relationship between the ratio of delayed neutron rates from the dual-energy technique and the ^{235}U enrichment.

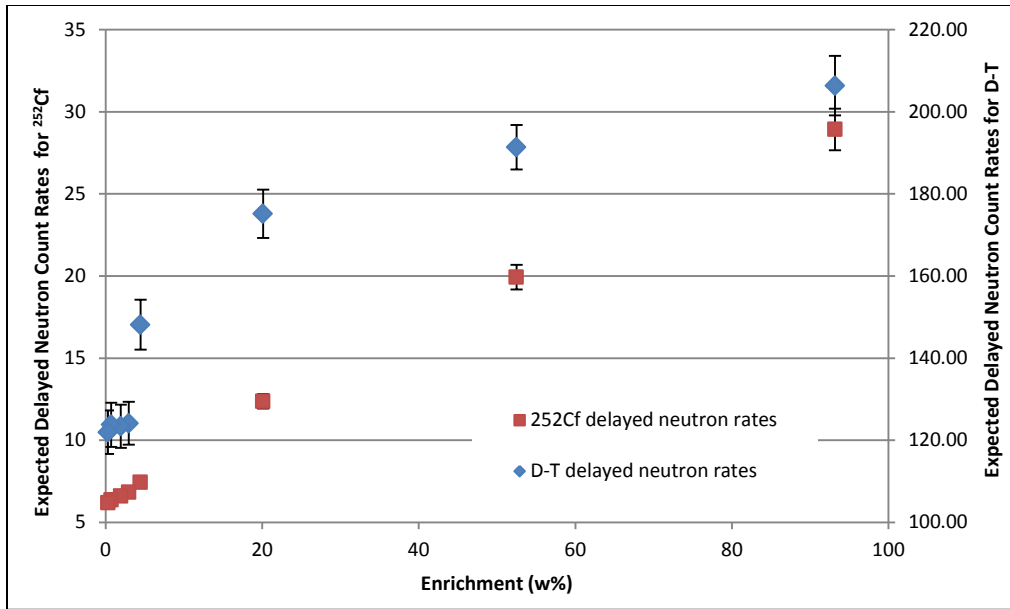


Figure 42. Expected delayed neutron rates from ^{252}Cf - and D-T- induced fissions.

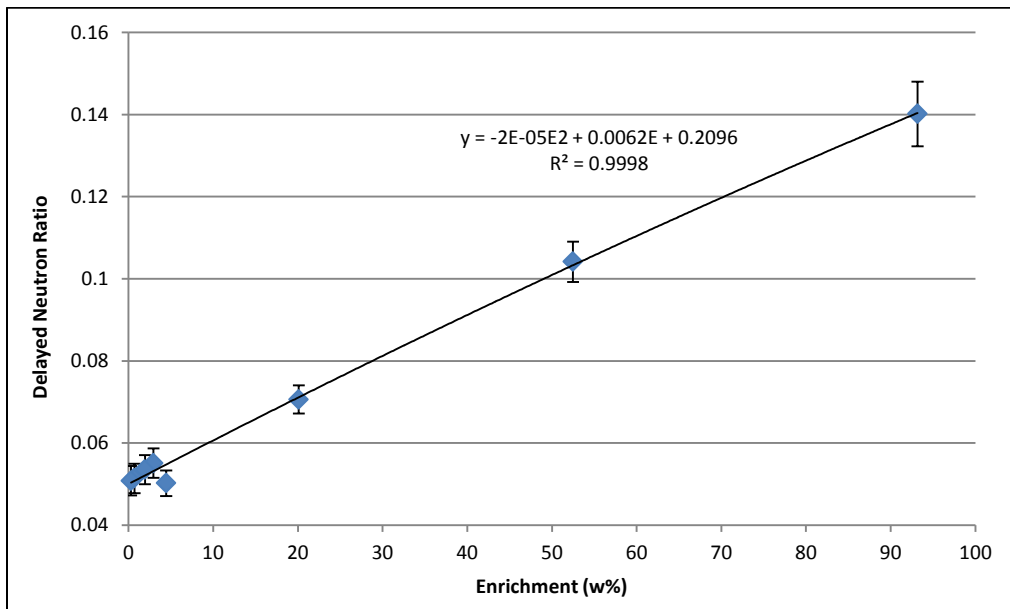


Figure 43. Ratio of delayed neutron count rates for ^{252}Cf and D-T interrogation vs. ^{235}U enrichment.

5.2 Measurement Data using DEANI method

The experimental results and the corresponding analyses are presented in this section.

5.2.1 Traditional ^{252}Cf Measurements

Recall that eight shuffler measurements were performed for each NBL CRM item to improve the measurement statistics. The items were not repositioned between measurements. In addition, the delayed neutrons were allowed to decay prior to the start of the next measurement. The delayed neutron rates, R_{Cf} were extracted from the shuffler software output. An example output file is provided in Appendix A. The delayed neutron count rates are corrected for background and decay of the ^{252}Cf source back to a common reference date. For the experimental measurements, the flux monitor corrections (from the shuffler flux monitors) were not applied since the NBL cans is small and similar in size, mass, and density. A cycle time correction (to account for differences in count times between cycles) was also omitted since the computer controlled shuffler mechanism keeps the system well timed (i.e., an assay is a fixed sequence controlled by the system Compumotor). The averaged delayed neutron count rates, R_{Cf} , and associated uncertainties for all eight measurements were calculated using Eq. 21 and Eq. 22, respectively. The statistical uncertainty for each shuffler measurement, $\sigma_{R_{Cf,i}}$, was obtained directly from the shuffler software.

$$R_{Cf} = \frac{\sum_1^8 R_{Cf,i}}{8} \quad \text{Eq. 21}$$

$$\sigma_{R_{Cf}} = \sqrt{\frac{\sum_1^8 (\sigma_{R_{Cf,i}})^2}{8}} \quad \text{Eq. 22}$$

The averaged measured values for R_{Cf} are given in Table 15. The measured rates are plotted in Figure 44 alongside the simulated rates.

Table 15. ²⁵²Cf-induced Delayed Neutron Rates

Enrichment (w%)	R _{Cf} (c/s)
93.17	25.26 ± 0.1785
52.49	17.60 ± 0.1582
20.11	10.68 ± 0.1427
4.46	5.859 ± 0.1301
2.95	5.808 ± 0.1293
1.94	5.729 ± 0.1316
0.71	5.580 ± 0.1319
0.31	5.270 ± 0.1315

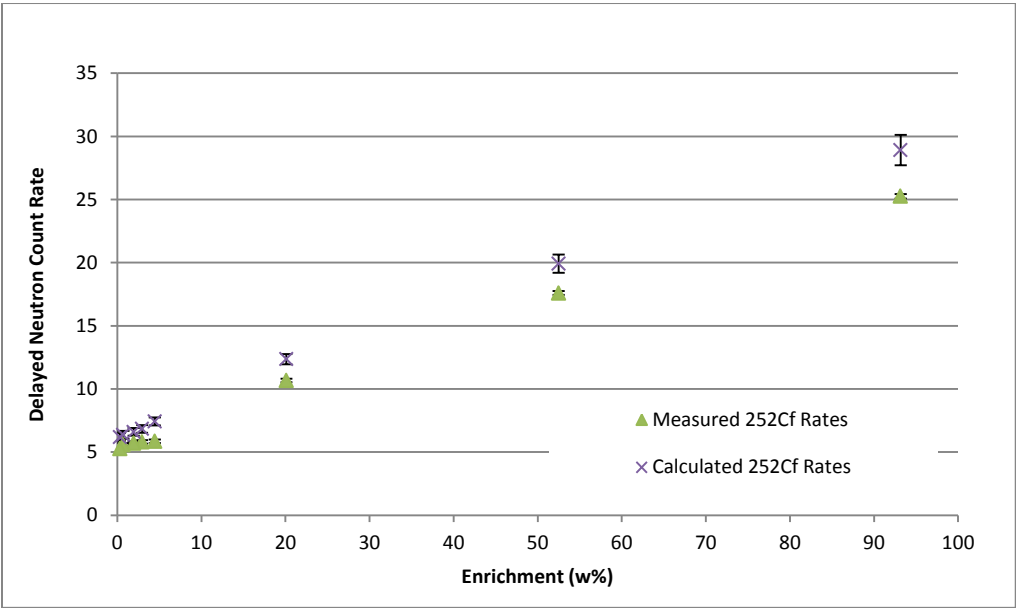


Figure 44. Comparison of measured and simulated delayed neutron rates from ²⁵²Cf interrogation.

The plots show agreement between the simulated and experimental data within $\sim 3\sigma$ and the two curves exhibit the same increasing trend as a function of enrichment. The difference between the simulated and measured rates is relatively constant for each sample at $\sim 13\%$. There are several possibilities as to why the simulated and experimental data do not agree better and why the data diverges as the enrichment increases. First, there are differences in the geometries of the model and the complex shuffler. For example, if there are differences in the materials surrounding the ^{252}Cf source, the MCNP6 model may predict a different distribution of neutron energies incident on the measurement item. Since the fission cross-section is dependent on the interrogation energy, a difference would affect the calculated delayed neutron rates. Second, the source strength of the ^{252}Cf source is only known to 10% and could result in a small scaling problem. Third, the MCNP6 model does not account for the dynamic nature of the shuffler measurement (i.e., the ^{252}Cf source oscillates 0.5 in vertically during the irradiation period).

5.2.2 D-T-based Measurements

Five-, 10 min measurements were performed for each of the CRM standards; Ten-, 10 min background measurements were performed. The D-T measurements required separate analyses to extract the measured delayed neutron rates. The shuffler response was evaluated using the MCS data as discussed in Chapter 4. The MCS output files were analyzed to determine the sum or total number of *gross* counts within the counting window, $C_{DT,G}$, as given by Eq 23. Recall the counting window was established in Chapter 4. In this summation, $c_{DT,i}$ is the number of counts in time bin i . The uncertainty, $\sigma_{C_{DT,G}}$, (assuming Poisson statistics) was calculated from the square root of the summed counts as shown in Eq. 24. A plot highlighting the count window was provided in Figure 41.

$$C_{DT,G} = \sum_{4\text{ ms}}^{9.7\text{ ms}} c_{DT,i} \quad \text{Eq. 23}$$

$$\sigma_{C_{DT,G}} \approx \sqrt{C_{DT,G}} \quad \text{Eq. 24}$$

This gross count was then normalized by the counts from the added flux monitor (for the same measurement) to account for fluctuations in the neutron output of the D-T generator from one run to the next (i.e., the ^3He flux monitor was used to normalize the intensity of the neutron generator). The response of the flux monitor was evaluated to determine whether the summed counts over all channels could be used to normalize the shuffler response. However, the dead-time of the flux monitor was too high at the beginning of the pulse during the irradiation period. Therefore, the summed counts in the flux monitor, C_{FM} , (after the tube recovered) from 80 μs to 250 μs were used for normalization, as shown in Eq. 25. In this summation, $c_{FM,i}$ is the number of counts in each time bin i . The uncertainty in the flux monitor counts, σ_{M_T} , is given by Eq. 26.

$$C_{FM} = \sum_{80 \mu\text{s}}^{250 \mu\text{s}} c_{FM,i} \quad \text{Eq. 25}$$

The *normalized* count is then described by Eq. 27, where $C_{DT,N}$ is the normalized, gross delayed neutron count and $\sigma_{C_{DT,N}}$ is the corresponding uncertainty calculated using Eq. 28. $C_{FM,0}$ is the averaged flux monitor counts over all ten background measurements (i.e., no measurement item was present in the measurement chamber). An example of the flux monitor signal used to normalize the shuffler counts is shown in Figure 45.

$$C_{DT,N} = \frac{C_{DT,G}}{C_{FM}} * C_{FM,0} \quad \text{Eq. 27}$$

$$\sigma_{C_{DT,N}} = C_{DT,N} \sqrt{\left(\frac{\sigma_{C_{DT,G}}}{C_{DT,G}}\right)^2 + \left(\frac{\sigma_{C_{FM}}}{C_{FM}}\right)^2 + \left(\frac{\sigma_{C_{FM,0}}}{C_{FM,0}}\right)^2} \quad \text{Eq. 28}$$

$$\sigma_{C_{FM}} \approx \sqrt{C_{FM}} \quad \text{Eq. 26}$$

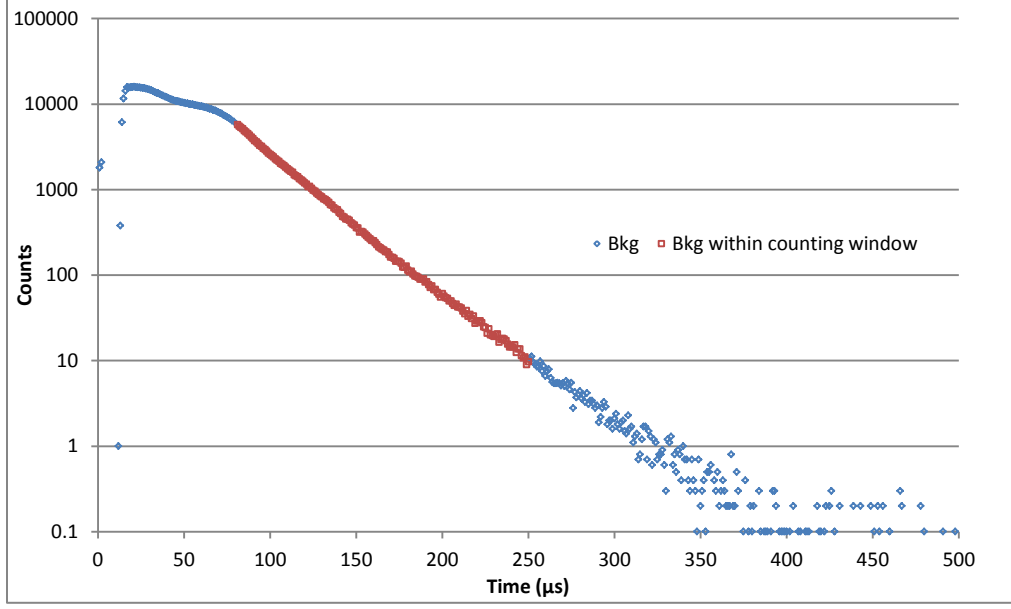


Figure 45. Flux monitor counting window for D-T measurements.

The *averaged* normalized counts, $\overline{C_{DT,N}}$, over the five D-T measurements were calculated as shown in Eq. 29, while the uncertainty, $\sigma_{\overline{C_{DT,N}}}$, was determined using Eq. 30.

$$\overline{C_{DT,N}} = \frac{\sum_1^5 C_{DT,N,i}}{5} \quad \text{Eq. 29}$$

$$\sigma_{\overline{C_{DT,N}}} = \sqrt{\frac{\sum_1^5 (\sigma_{C_{DT,N,i}})^2}{5}} \quad \text{Eq. 30}$$

To get the averaged, normalized, *net* counts, or delayed neutron counts, D_{DT} , the background was subtracted as shown in Eq. 31. The corresponding uncertainty, $\sigma_{D_{DT}}$, in the corrected counts is given by Eq. 32. In these equations, $\overline{C_B}$ is the averaged normalized *background* count in the counting window and $\sigma_{\overline{C_B}}$ is the uncertainty in those counts.

$$D_{DT} = \overline{C_{DT,N}} - \overline{C_B} \quad \text{Eq. 31}$$

$$\sigma_{D_{DT}} = \sqrt{(\sigma_{\overline{c_{DT,N}}})^2 + (\sigma_{\overline{c_B}})^2} \quad \text{Eq. 32}$$

To get the averaged, background-corrected delayed neutron count rate, R_{DT} , D_{DT} was divided by the count time and by the number cycles (i.e., number of generator pulses) as shown in Eq. 33. The uncertainty, $\sigma_{D_{DT}}$, is given in Eq. 34.

$$R_{DT} = \frac{D_{DT} * 10^6}{5700 * 60000} \quad \text{Eq. 33}$$

$$\sigma_{R_{DT}} = \frac{\sigma_{D_{DT}} * 10^6}{5700 * 60000} \quad \text{Eq. 34}$$

The measured values for R_{DT} are provided in Table 16 and plotted in Figure 46. The simulated values are also plotted for comparison.

Table 16. D-T-induced Delayed Neutron Rates

Enrichment (w%)	R_{DT} (c/s)
93.17	80.0 ± 0.304
52.49	67.4 ± 0.267
20.11	52.9 ± 0.222
4.46	42.0 ± 0.183
2.95	40.6 ± 0.179
1.94	41.2 ± 0.180
0.71	40.5 ± 0.177
0.31	41.4 ± 0.178

The data shows a large difference in magnitude between the expected count rates based on the MCNP6 simulations and the measured results (note that the expected rates are plotted on the secondary y-axis). However, the general increasing trends of the datasets agree. Again, there are several potential explanations for the differences in the data. In

addition to those reasons discussed in the previous section, the model of the D-T generator was simplified since the internal structure was not given by the manufacturer. This may affect the interrogating energies incident on the measurement item, thus changing the calculated induced fission rates. It is also worth emphasizing that the neutron emission rate from the D-T generator is not well known, therefore, the confidence in the magnitude of the expected data is low. Lastly, the delayed neutron data constants (i.e., the Keepin numbers) and their influence at various energies are not well understood. For the calculations discussed here, the thermal and fast parameters were used. A brief examination of the influence of these energy-dependent constants is discussed in a later section.

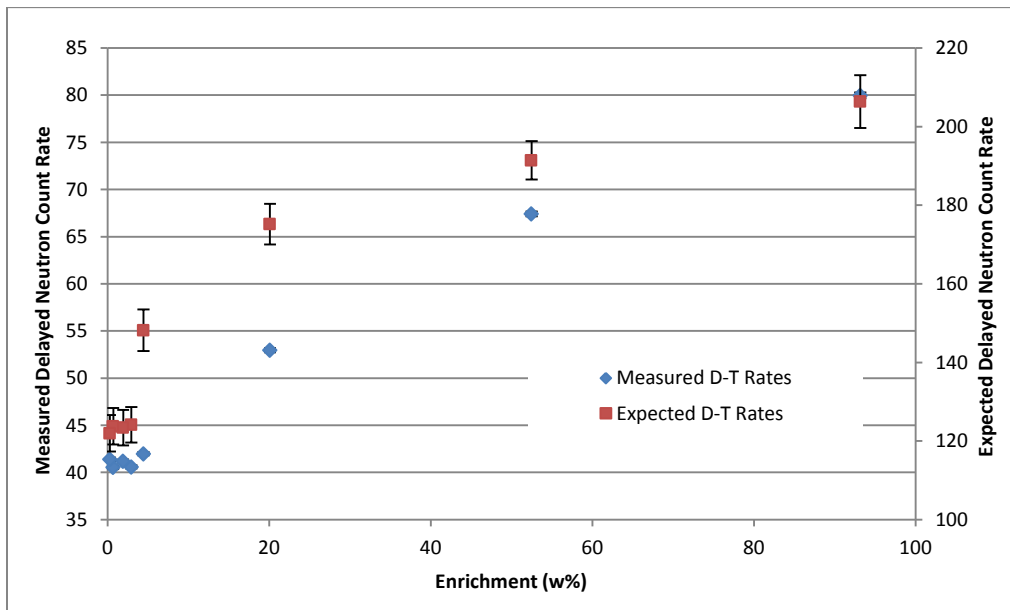


Figure 46. Comparison of measured and simulated delayed neutron rates from D-T interrogation.

5.2.3 Delayed Neutron Ratios

The approach of this work was to form a correlation between the delayed neutron ratios and the uranium enrichment. The delayed neutron ratio was computed for each measurement item as shown in Eq. 35. The uncertainty in the ratio, σ_{Ratio} , was calculated using Eq. 36.

$$Ratio = \frac{R_{Cf}}{R_{DT}} \quad \text{Eq. 35}$$

$$\sigma_{Ratio} = Ratio \sqrt{\left(\frac{\sigma_{R_{Cf}}}{R_{Cf}}\right)^2 + \left(\frac{\sigma_{R_{DT}}}{R_{DT}}\right)^2} \quad \text{Eq. 36}$$

The measured ratios are provided in Table 17. The simulation-based ratios are also provided. These ratios for the measured data are also plotted against ^{235}U enrichment in Figure 47. The simulated values are plotted for comparison. Both curves show a monotonically increasing relationship between the delayed neutron ratios and the enrichment; however, the difference in the magnitude of the data points is upwards of 90%.

Table 17. Delayed Neutron Ratios for CRM Items

Enrichment (w%)	Measured Ratio ($^{252}\text{Cf/D-T}$)	Simulated Ratio ($^{252}\text{Cf/D-T}$)
93.17	0.316 ± 0.00253	0.140 ± 0.00787
52.49	0.261 ± 0.00257	0.104 ± 0.00493
20.11	0.202 ± 0.00283	0.0706 ± 0.00345
4.46	0.140 ± 0.00316	0.0502 ± 0.00311
2.95	0.143 ± 0.00325	0.0551 ± 0.00357
1.94	0.139 ± 0.00325	0.0535 ± 0.00357
0.71	0.138 ± 0.00331	0.0514 ± 0.00359
0.31	0.127 ± 0.00322	0.0508 ± 0.00359

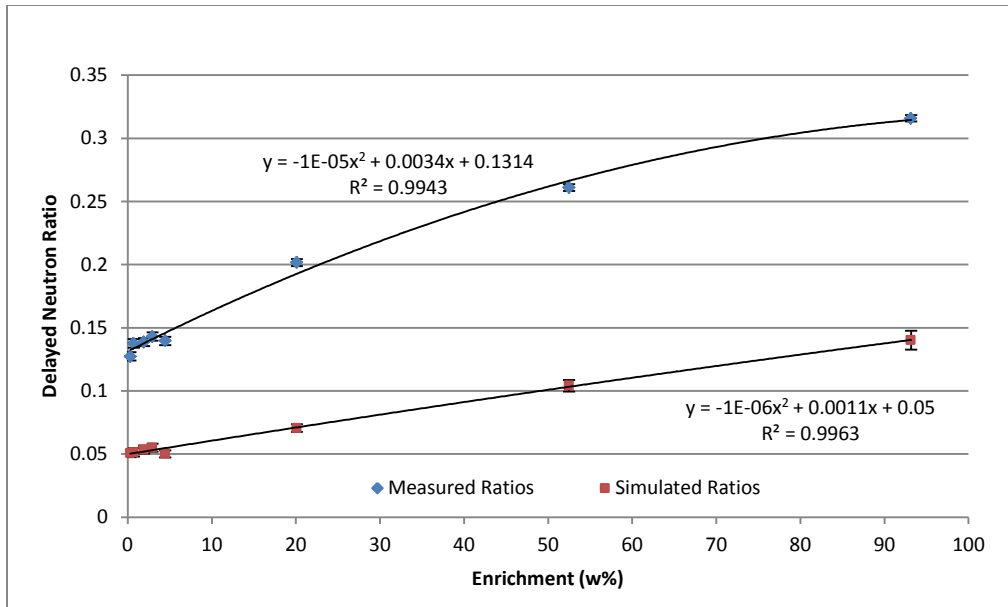


Figure 47. Comparison of measured and simulated ratios of delayed neutron rates.

Figure 48 shows the same data with the expected data on the secondary axis. This helps in the comparison of the behavior and trend of the two datasets. The differences in the calculated and measured data may be a result of the complicated measurement geometry. The shuffler itself is a complex measurement system. The model of the D-T generator was also crude and implementation of a more formal model of the generator may improve the results. The difference in induced fission rates with the simplified D-T generator model and without the added generator structure was 2% for the D-T rates and ~0.1% for the ^{252}Cf rates, with the exception of the 93.17% CRM where the rates differed by 0.7%. While this seems like a small change, it results in estimated enrichments that differ by tens of percent.

The delayed neutron data constants used in the calculations may also affect the calculated values and account for the differences in the two datasets. The fact that there are three discrete energy-dependent sets with no clear guidance as to when each dataset should be

used complicates the analysis. This was a potential cause of the differences between the expected and measured results and is further discussed in a later section.

Both the measured results and the calculated results show a functional dependence between the ratio of delayed neutron rates and the enrichment of the uranium item; however they do not appear to be the same functional dependence. Since the objective of establishing a representative model was primarily to extrapolate the technique to other material types, more work is needed to uncover the source of the disagreement.

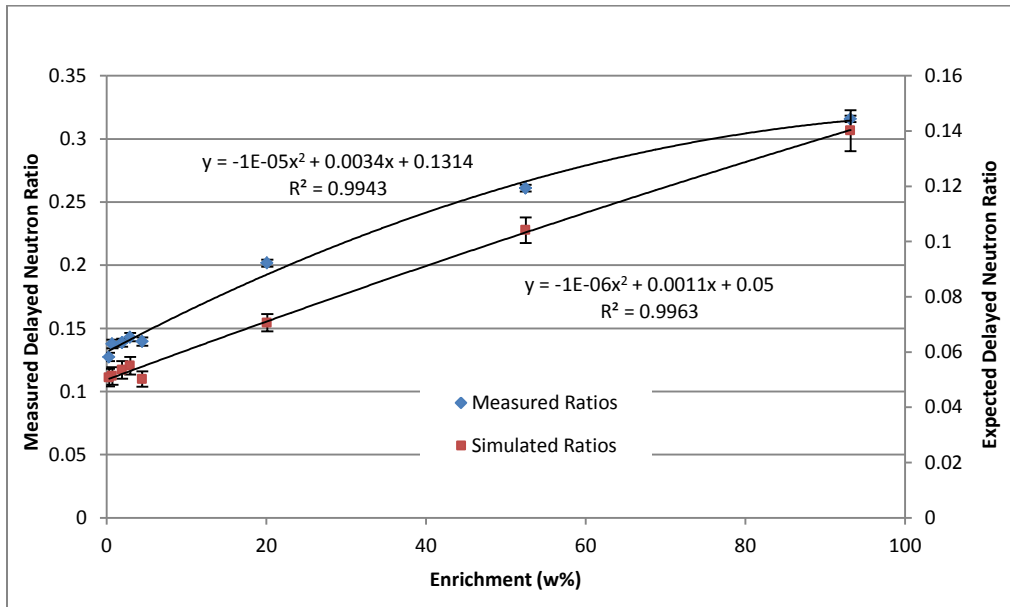


Figure 48. Delayed neutron ratios with scaling.

The CRM item with 4.46% enrichment is notably dissimilar from the rest of the LEU standards. This is evident in both the measured and calculated data. The fact that both the measured and calculated data show the anomaly at 4.46% suggests that the cause of the discrepancy is accounted for in the model. The cause of this discrepancy was investigated

using the MCNP6 model. The fill height of the 4.46% item is 15.8 mm, which is the same as the three HEU items; however, the total U gram quantity is 200 g, which is the same as the four LEU items. MCNP6 was used to estimate the delayed neutron rates from the 4.46% item using a fill height of 20.8 mm (the same as the other LEU items). The delayed neutron ratio changed from 0.0502 ± 0.00277 to 0.0572 ± 0.00354 , a 13% difference.

The fill height appears to significantly affect the expected delayed neutron rates. This is likely due to the poor source coupling of the system. Because of the position (and geometry) of the items with respect to each interrogation source (the item is nearer the ^{252}Cf source), changes in position or geometry do not affect the ^{252}Cf rates and the D-T rates proportionally (i.e., the source-to-sample coupling is poor). To illustrate, a measurement was performed in the center of the measurement cavity. The changes in the delayed neutron rates for the ^{252}Cf interrogation changes by a factor of ~ 3 while the rates from the D-T measurement only changed by a factor of ~ 0.5 . The internal structure (fill height) is currently being investigated using passive gamma-ray emission measurements.

Verification and validation of the measurement data is discussed in the next section. The curve for the measured data in Figure 47 will be used as the calibration curve for the verification of unknown samples.

5.3 Experimental Verification of the DEANI Measurement Technique

Several measurements on “unknown” items were performed to verify the DEANI methodology and determine its sensitivity to item characteristics such as mass, density, shape, and material type. The calibration curve (from the measured data discussed above) was inverted to obtain a traditional measurement relationship. The measured data was fit to a weighted quadratic function as shown in Eq. 37 using a reduced Chi-squared method. In this correlation, R is the delayed neutron ratio and E is the enrichment of the sample.

The coefficients a, b, and c were determined to be $-1.44 \times 10^{-5} \pm 1.54 \times 10^{-3}$, $3.31 \times 10^{-3} \pm 1.21 \times 10^{-4}$, and $0.132 \pm 1.31 \times 10^{-6}$ respectively.

$$R = aE^2 + bE + c \quad \text{Eq. 37}$$

The reduced Chi-squared value was 4.7 implying that the fit has not fully captured the data. This function was then inverted to obtain a traditional measurement curve where enrichment is estimated from the delayed neutron ratio. This measurement correlation is the inverse of the causal calibration plot.

$$E = \frac{(-b + \sqrt{b^2 - 4(c-R)a})}{2a} \quad \text{Eq. 38}$$

The leave-one-out method was used to determine how well the DEANI method estimated enrichment given the limited, but representative calibration points in the nearby regions. The results are presented in Table 18. The estimated values do not estimate the enrichments well. This is likely due to the very large gap in the fitted data between calibration points, particularly when using the leave-one-out method.

Table 18. Estimated Enrichments Using Leave-One-Out Method

“Unknown” Item ID	Declared Enrichment (w%)	DEANI Enrichment (w%)
NBS072	0.72	2.17 ± 1.09
NBS194	1.94	2.26 ± 1.09
NBS295	2.95	3.53 ± 1.08
NBS446	4.46	2.08 ± 1.08
NBL001	20.11	25.4 ± 1.27
NBL002	52.49	42.6 ± 1.95

Additional “unknown” measurements were performed to assess estimation performance and the sensitivity of the DEANI method to material type, mass, density, and geometry. It

should be noted that only a single DEANI measurement (one ^{252}Cf measurement and one D-T measurement) was performed for the following measurements, which explains why the uncertainties were much higher for these “unknown” measurements.

The NBL001 item was turned upside down and measured again to gage the spatial sensitivity. The delayed neutron ratio was measured to be 0.184 ± 0.0102 which correlates to an estimated enrichment of $17.06 \pm 3.64\%$, which implies the DEANI method is capable of estimating the enrichment of items with the same form.

To determine if the method is sensitive to material type, mass, and geometry, a 1 kg metal sphere of depleted uranium (called YST1B) was measured. The delayed neutron ratio was measured to be 0.129 ± 0.00262 . The enrichment based on this ratio was calculated to be $-0.749 + 0.926\%$. This negative enrichment was probably due to the declared enrichment of 0.21%, which is below the range of calibration. Even so, the result is within 1σ . This suggests that the ratio technique employed by the DEANI method may not be very sensitive to mass, material type, or density, but more data points are needed to verify. The spherical geometry was not expected to significantly affect the results since the material was centered at the same measurement plane as the CRM cans.

The effect of mass and geometry was examined by measuring an 8 kg depleted metal casting (called JAPO) in the shape of an annulus centered at the same measurement location as the calibration items. The delayed neutron ratio was measured as 0.143 ± 0.000846 . This leads to an over-estimated enrichment of $3.39 \pm 0.452\%$, which is well over the declared value of 0.31%. Several factors may have affected this result. First, the much larger mass may make a difference in measured enrichments, although YST1B did not exhibit the same overestimate of the enrichment. Second, the geometry (an annulus) was significantly different than the other items measured changing the source coupling. The annulus is approximately 9.25 cm tall with an inner diameter of 7.2 cm and outer diameter of 13.3 cm. The source was positioned on top of the source rotator like the

calibration sources instead of centering the nuclear material vertically. This also changes the source coupling. Both factors suggest that the DEANI technique has some spatial sensitivity. Multiplication was considered as well; however, because the ratio is being evaluated, multiplication is not expected to impact the results.

Next, two CRM standards were placed end-to-end in the shuffler cavity. The enrichment of the bottom item was 20.11% while the enrichment of the top item was 52.49 %. The measured delayed neutron ratio was 0.211 ± 0.00530 . This corresponds to an estimated enrichment of $27.1 \pm 2.13\%$. As expected, the estimated enrichment was between the enrichment values of the two standards. Since the geometry was affected by the scenario (i.e., the bottom item was upside down which raised the center of the nuclear material and the second item was elevated ever further), the results are not expected to agree exactly with the mean enrichment. On the other hand, this result indicates that the DEANI method should be capable of flagging anomalous items (e.g., shielded materials).

The effect of higher-Z materials on the measurement technique was also evaluated. The 52.49 % CRM was placed inside an aluminum can with ~0.5 mm thick walls. Additional steel and aluminum scrap filled the remaining container. The measured delayed neutron ratio was 0.265 ± 0.00851 which relates to an estimated enrichment of $51.8 \pm 4.74\%$. This implies that the DEANI method is not strongly affected by higher-z materials.

To understand the influence of a hydrogenous matrix, measurements on uranium items surrounded by nested HDPE shells were performed. Two shell thicknesses were used: 0.5 in and 1 in. NBL002 (with an enrichment of 52.49%) was measured in each configuration and NBL001 (with an enrichment of 20.11%) was measured in the 0.5 in configuration. The flux monitor corrections (using the two integrated shuffler flux monitors, not to be confused with the flux monitor used to normalize the D-T measurement data) applied to the NBL002 ratios were 1.28 for the 0.5 in shell and 1.69 for the 1 in shell. The correction for NBL001 in the 0.5 in shell was 1.29. These values account for the flux

monitor corrections that would have been applied to the calibration curve data had those corrections been initially applied. Recall that in the initial development of this methodology, the flux monitor corrections (from the shuffler) were ignored since the CRM standards have similar characteristics.

The delayed neutron ratio was computed and divided by the shuffler flux monitor correction. The corrected ratios for NBL002 were measured to be 0.359 ± 0.00310 for the 0.5 in case and 0.368 ± 0.00146 for the 1 in case. The corrected ratio for NBL001 was measured to be 0.329 ± 0.00366 for the 0.5 in case. These delayed neutron ratios are well outside the range of calibration and would suggest enrichments above 100%, thus are not estimated. Thus the DEANI technique grossly overestimates the enrichment when strong moderators are present. This is expected since the incident flux is thermalizing prior to reaching the fissionable material and are no longer markedly different. Additionally, the flux monitors are not well coupled to the source with respect to the D-T generator.

The results of the “unknown” measurements are plotted in Figure 49 along the fitted measurement curve. A summary of these results is provided in Table 19. Recall that only one DEANI measurement was performed for each verification scenario. The measurement uncertainties would be reduced by increasing the number of measurements.

Table 19. Summary of Verification Measurement Results

“Unknown” Item ID	Declared Enrichment (w%)	DEANI Enrichment (w%)
YST1B	0.207	-0.749 ± 0.926
JAPO	0.310	3.39 ± 0.452
NBL001 and NBL002 (stacked)	20.11 52.49	27.1 ± 2.13
NBL002 w/ 0.5in poly	52.49	--
NBL002 w/ 1.0in poly	52.49	--
NBL001 w/ 0.5in poly	20.11	--
NBL002 in Al can	52.49	51.8 ± 4.74
NBL001 upside down	20.11	17.1 ± 3.64

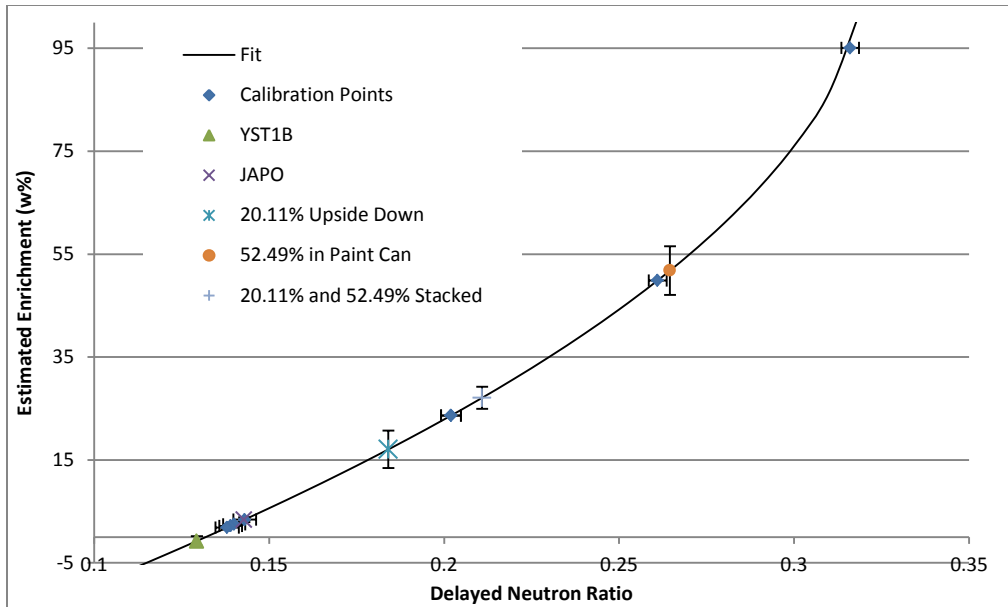


Figure 49. Verification measurements plotted along measurement curve.

5.4 Potential Replacements of the ^{252}Cf Source

During the development of the DEANI method, the MCNP6 model was used to identify an adequate secondary neutron interrogation source. As a result, the sources considered were also evaluated for their potential as a direct replacement for the ^{252}Cf source integral to shuffler applications. As discussed in Chapter 4, AmLi, AmBe, D-D, and D-T generators were considered. MCNP6 simulations were performed to support delayed neutron rate calculations. For this study, the parameters from Table 12 were used. The ^{252}Cf parameters were used for AmLi and AmBe calculations and the D-T parameters were used for the D-D calculations since optimized parameters were not determined for these additional sources. Using these parameters may affect the magnitude of the delayed neutron rates but is not expected to change the shapes or behaviors of the rate curves.

Figure 50 shows the calculated delayed neutron rates from each interrogation source normalized to unity. In general, the shapes of the datasets agree; they all show a

monotonically increasing relationship between the delayed neutron count rate and the enrichment of the item which can be described by a polynomial. This implies that any of these sources might be reasonable replacements with some adaptation. Experimental work would further support this theory.

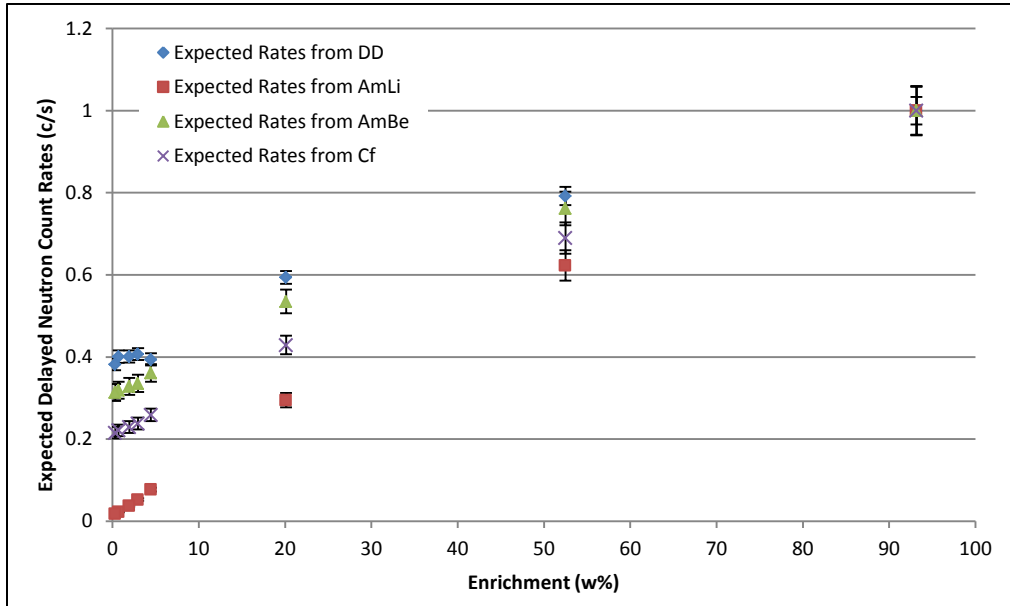


Figure 50. Comparison of delayed neutron rates from various interrogating neutron sources.

The AmLi source's main advantage over all other neutron sources considered in this study is its low average energy, which maximizes fissions in ^{235}U and reduces fissions in ^{238}U (this is evident in the data where the delayed neutron rates are near zero for low enrichments). This same property, however, can be a disadvantage in that it also means a lower penetrability of the interrogating flux (at thermal energies the mean free path of a neutron is on the order of a few centimeters; whereas, it can be as large as tens or hundreds of cm for high energies). Aside from these two major factors, AmLi sources are

difficult to characterize due their complex manufacturing process, expensive and difficult to obtain, and physically large. The size of an AmLi with a sufficient flux to provide good measurement precision would require a significant adaptation to the source transfer mechanism of the ^{252}Cf shuffler. It is therefore unlikely that AmLis will be pursued as a viable option for source replacement.

AmBe sources suffer many of the same disadvantages, the most significant being the size and mass of the source. However, the higher average neutron energy implies a more penetrating interrogation flux and the delayed neutron production follows closely with that of ^{252}Cf . Proper spectrum tailoring optimization may allow the AmBe to be used assuming the shuffling mechanism could be adapted.

LANL already conducted an extensive simulation based study to evaluate the potential of the D-T generator for replacement of the ^{252}Cf in the shuffler; therefore, D-T was not considered as a primary source in this study [86, 103]. D-D generators, however, were considered. With an average neutron energy similar to ^{252}Cf , a D-D neutron source would maintain the same penetrating power and sensitivity to ^{238}U as the ^{252}Cf . Thus, the D-D generator may be a suitable replacement for ^{252}Cf and is of particular interest for use in the DEANI method to reduce the footprint of the system.

Regarding the DEANI method, the ratio of delayed neutrons from interrogation by these alternative sources to that of D-T interrogation was examined. The results are plotted in Figure 51. The data implies that any of the alternative sources may work in place of the ^{252}Cf . The D-D/D-T delayed neutron ratio has the same behavior as the ^{252}Cf /D-T ratio and could be scaled by changing the interrogating source strengths. The AmLi/D-T ratio also follows the shape of the ^{252}Cf /D-T data. While the AmBe/D-T ratio is monotonically increasing, the slope is much smaller than the others. This is likely due to the increased fission rate in ^{238}U (AmBe has a higher average neutron energy than AmLi and D-D). It should be noted that spectrum tailoring may support improvements to these ratios.

Ultimately, these calculations support the potential replacement of ^{252}Cf with a D-D neutron generator, particularly with respect to DEANI methods. While neutron generators are generally cheaper than large ^{252}Cf sources, they do require more maintenance and offer less reliability. For D-D generators specifically, the major concern would be producing the neutron flux required for statistically sound measurements since, historically, D-D generators were limited to fluxes of $\sim 10^6$ n/s. Recent developments promise higher emission rates ($10^8 - 10^{10}$ n/s) and may allow D-D generators to be reconsidered for certain applications provided the physical size of the generator is acceptable. Still, the advantages of neutron generators include the speed at which the source can be turned off, the reduction in required shielding for the source (\sim reduction in $\frac{1}{2}$ weight and size in the case of the ^{252}Cf Shuffler), improved neutron penetration due to higher neutron energies, and no source decay requiring source replacement.

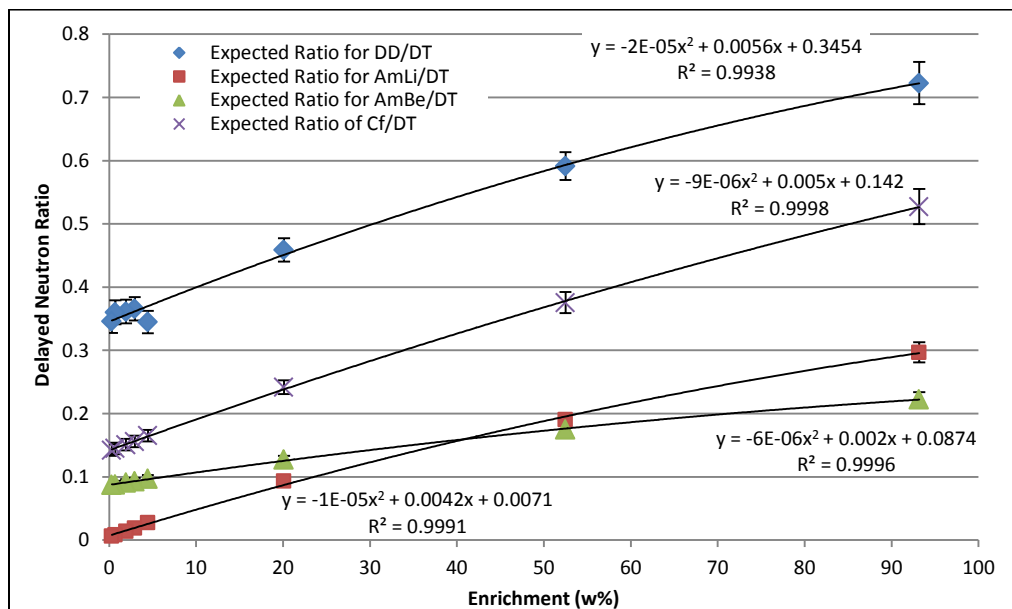


Figure 51. Delayed Neutron Ratios for interrogation by various alternatives to ^{252}Cf and D-T.

5.5 Die-away Measurements

In addition to using the die-away time constant to validate the MCNP6 model, the energy-dependence of the die-away time distribution was investigated. The behavior of the die-away on very short timescales was also examined. Specifically, the influence of neutron slowing down, thermalization and diffusion on the fission event-triggered capture time distribution of polyethylene moderated ^3He -based counters was studied. Slowing down and thermalization processes contribute to the initial rise or buildup in the fission event-triggered capture time distribution recorded from the instant of fission, but the detected/measured neutron-triggered coincidence die-away profiles do not exhibit this initial transient. Instead, the signal decreases smoothly, consistent with parasitic loss, detection, and leakage processes of the (essentially) thermal neutron population.

Figure 52 shows the capture time distribution for the ^{252}Cf source neutrons and the D-T source neutrons inside the shuffler. The general shapes are similar, especially after the initial 10 μs . Each curve was fit using a single exponential and a Chi-squared minimization was performed to obtain the estimated die-away time constants. The calculated die-away times were 61.3 μs using the D-T generator and 58.5 μs using the ^{252}Cf source. These values were obtained by fitting the data immediately after the buildup from ~ 0.7 μs out to 350 μs . Traditionally, neutron counters measuring time-correlated neutrons include a short pre-delay (e.g., 4.5 μs) in the timing structure. If the die-away is calculated using the data after this pre-delay (from 4.5 μs out to 350 μs) then the resulting time constants are 62.5 μs for D-T and for 59.6 μs for ^{252}Cf . This good agreement (<5% difference) implies that the die-away time of the counter is not strongly dependent of the interrogating neutron energy.

Figure 53 shows a zoomed in plot of the simulated fission event-triggered capture distribution. In this plot, the influence of the interrogating neutron energy can be seen. The ^{252}Cf neutrons with lower energies thermalize faster than the higher energy D-T neutrons. Because this temporal difference occurs during the pre-delay, it has no

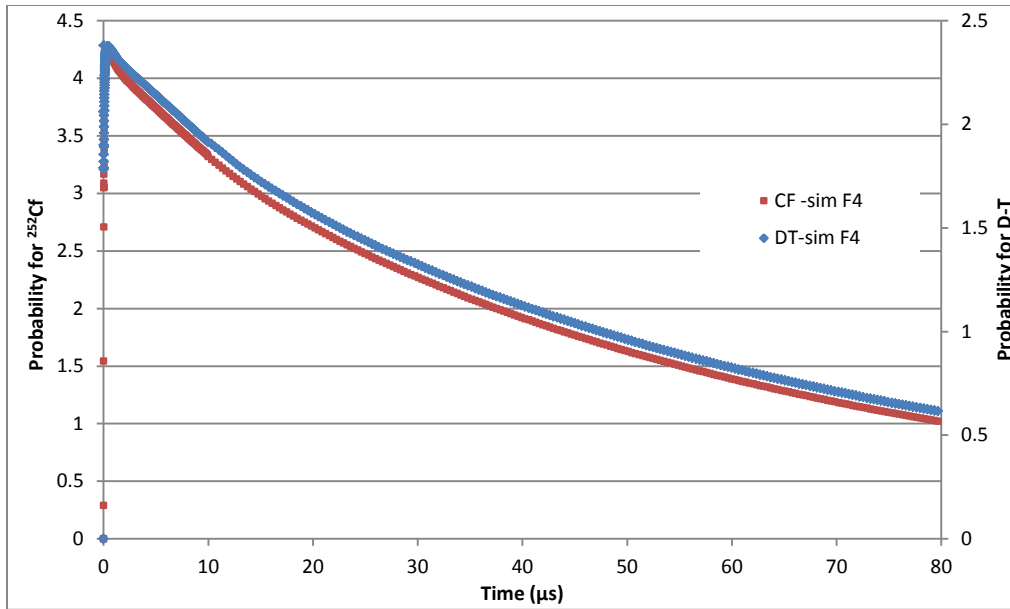


Figure 52. Simulated fission event-triggered capture distribution for ²⁵²Cf and D-T in the shuffler.

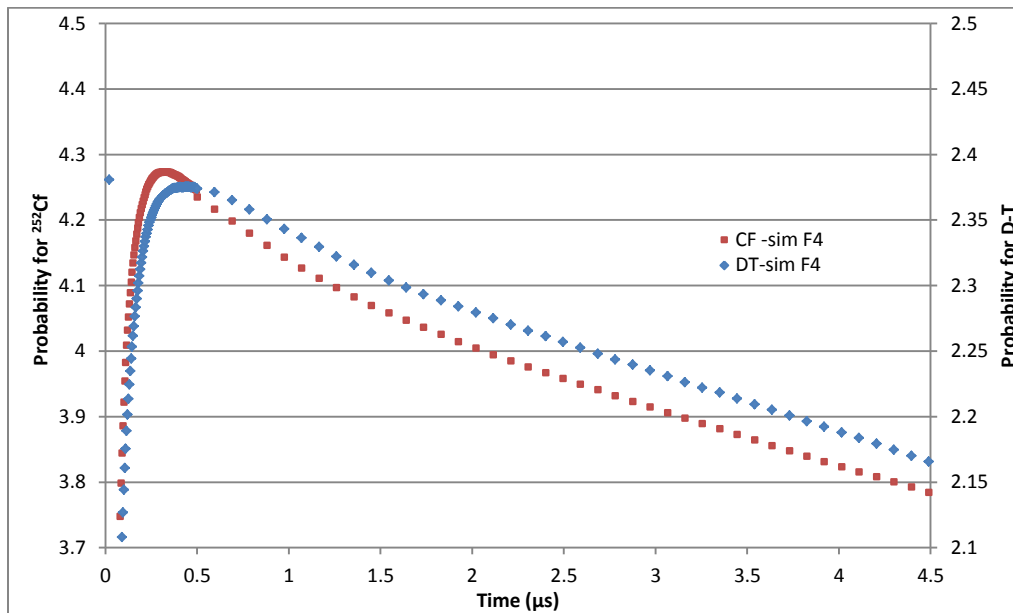


Figure 53. Fission event-triggered capture distribution showing buildup.

significant influence on time-correlated measurements. The temporal behavior of the neutrons during the thermalization process is an interesting topic that warrants further investigation. The spatial and spectral aspects should be visited as well.

The estimated time constant based on the F8 capture tally (discussed in Chapter 3) was 61.5 μs . Again, the values are in good agreement. The F8 capture tally utilized accounts for the pre-delay and gate width to simulate a neutron event-triggered capture distribution. A zoomed in plot of this neutron event-triggered distribution is provided in Figure 54 along with the equivalent fission event-triggered distribution. The key difference in data is the absence of the transient buildup in the neutron event-triggered simulation. This buildup from the time of fission gets removed and thus the neutron slowing-down and thermalization behavior gets overlooked.

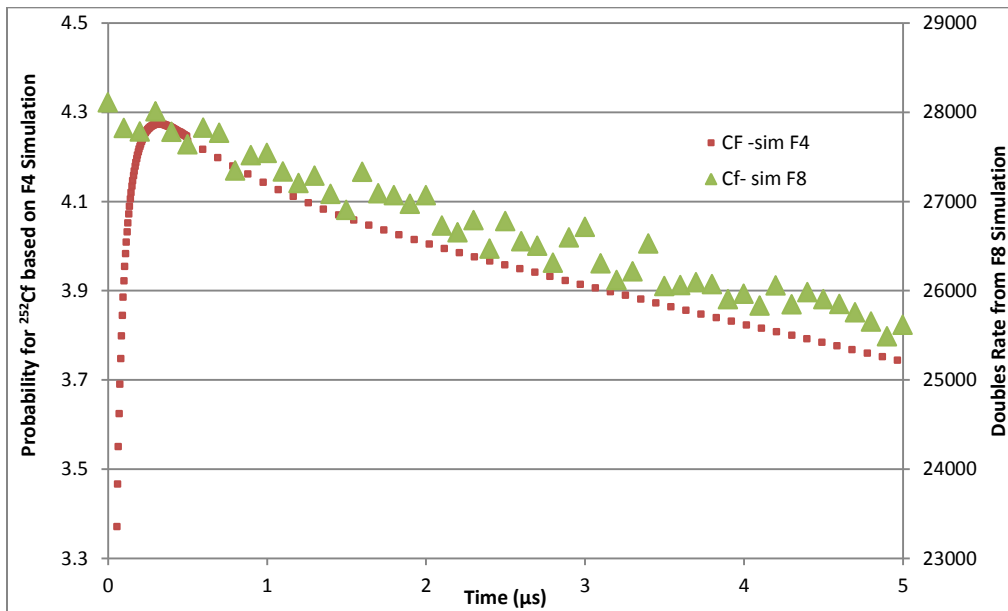


Figure 54. Comparison of fission event- and neutron event- triggered capture distributions.

5.6 Sensitivity to Energy-Dependent Delayed Neutron Group Constants

Since the DEANI method combines a traditional ^{252}Cf Shuffler measurement with a shuffler-like measurement using a D-T neutron generator for the first time, a brief analysis was performed on the influence of the delayed neutron data constants on the calculated delayed neutron rates. MCNP6 simulations were used to generate fission rates in various measurement items. To determine the estimated delayed neutron rates from those fission rates, the delayed neutron group constants are used. For traditional shuffler applications, it is common practice to use the thermal delayed neutron dataset for ^{235}U and the fast dataset for ^{238}U . However, the DEANI method uses both a ^{252}Cf fission source (with average energy of 2.14 MeV [7]) and a D-T neutron generator (a mono-energetic 14.1 MeV source was assumed in this study). This significant difference in interrogating energies warrants an investigation of the sensitivity of the technique to the different energy-dependent 6-group datasets. Thus, this sensitivity study highlights the energy dependence of these group constants and presents the results of a sensitivity analysis of the group constants as a function of the interrogating source used in the DEANI method.

Recall that in the mid- 1950s and 1960s, Keepin established a 6-group delayed neutron structure that is still widely used today. In addition to being isotope specific, these parameters are also dependent on the incident energy of the interrogating flux. Keepin reported delayed neutron constants for ^{235}U in the thermal energy range and in the fast (fission) energy range and in the fast energy range for ^{238}U [27]. East (and Keepin) later reported delayed neutron constants in the high energy range (~ 14 MeV) for both ^{235}U and ^{238}U [104]. Traditionally, delayed neutron systems are considered fast systems; however, the thermal datasets are often used for ^{235}U . Since the cross-section for ^{238}U is largely negligible at thermal energies, the fast datasets are often used. Since there is no clear guidance on the boundaries between the thermal, fast, and high energy regions, it has been recommended to use fast fission data for both ^{235}U and ^{238}U [62].

The total delayed neutron yields are provided in Table 20. Notice that the yield is almost a factor or two less at high interrogation energies than at fast interrogation energies. The nubar values used in the calculations are also listed. The values for the thermal and fast datasets are from Keepin, while the high-energy nubar values were taken from Zucker [105]. No uncertainties were reported. It should also be noted that these nubar values were for induced fission by 8 MeV neutrons. These values were selected since the average energy of the D-T flux incident on the measurement items was determined to be ~ 8 MeV.

Table 20. Total Delayed Neutron Yields

Energy	Energy-dependent Parameters		$\bar{\nu}(E)$	
	^{235}U	^{238}U	^{235}U	^{238}U
Thermal (<1 keV)	0.0158 ± 0.0005	--	2.47 ± 0.05	--
Fast (~ 1.45 MeV)	0.0165 ± 0.0005	0.0412 ± 0.0017	2.57 ± 0.04	2.79 ± 0.10
High (~ 14.7 MeV)	0.0095 ± 0.0008	0.0286 ± 0.0025	3.60	3.51

The energy dependent ^{235}U delayed neutron data evaluated in this sensitivity analysis are provided in Table 21. The data for ^{238}U are provided in Table 22. Although the Keepin 6-group delayed neutron constants are still widely used, alternative datasets exist for ^{235}U and ^{238}U (based on different precursors and measurement campaigns) [106]. For this sensitivity analysis, however, only the thermal- and fast-energy datasets from Keepin and the high-energy datasets from East and Keepin will be addressed.

Since the DEANI method examines the delayed neutron ratio, there is an opportunity to evaluate the use of more than one dataset within a single measurement result. For example, the traditional thermal constants for ^{235}U and fast constants for ^{238}U may be used for the ^{252}Cf -based measurement and for the D-T based measurement, or any combination of datasets may be used.

Table 21. Energy-dependent Delayed Neutron Group Constants for ^{235}U

THERMAL ^{235}U PARAMETERS - (Keepin 1965)						
Group	$T_{1/2}$ (s)	$\sigma(T_{1/2})$	λ_i (s^{-1})	$\sigma(\lambda_i)$	β_{iV}	$\sigma(\beta_{iV})$
1	55.72	1.28	0.01244	0.0003	0.00052	0.00005
2	22.72	0.71	0.03051	0.001	0.00346	0.00018
3	6.22	0.23	0.1114	0.004	0.0031	0.00036
4	2.3	0.09	0.3014	0.011	0.00624	0.00026
5	0.61	0.083	1.136	0.15	0.00182	0.00015
6	0.23	0.025	3.014	0.29	0.00066	0.00008
FAST ^{235}U PARAMETERS - (Keepin 1965)						
Group	$T_{1/2}$ (s)	$\sigma(T_{1/2})$	λ_i (s^{-1})	$\sigma(\lambda_i)$	β_{iV}	$\sigma(\beta_{iV})$
1	54.51	0.94	0.012716	0.0002	0.00063	0.0005
2	21.84	0.54	0.031738	0.0008	0.00351	0.00011
3	6	0.17	0.115525	0.003	0.0031	0.00028
4	2.23	0.06	0.310828	0.008	0.00672	0.00023
5	0.496	0.029	1.397474	0.081	0.00211	0.00015
6	0.179	0.017	3.872331	0.369	0.00043	0.00005
HIGH ^{235}U PARAMETERS - (East 1970)						
Group	$T_{1/2}$ (s)	$\sigma(T_{1/2})$	λ_i (s^{-1})	$\sigma(\lambda_i)$	β_{iV}	$\sigma(\beta_{iV})$
1	52.4	1.3	0.013228	0.53319	0.000124	1.41E-05
2	21.6	0.4	0.03209	1.732868	0.001302	0.000111
3	5	0.2	0.138629	3.465736	0.00152	0.000229
4	1.93	0.07	0.359144	9.902103	0.003705	0.000326
5	0.49	0.02	1.414586	34.65736	0.002185	0.000207
6	0.17	0.01	4.077336	69.31472	0.000713	7.65E-05

Table 22. Energy-dependent Delayed Neutron Group Constants for ^{238}U

FAST ^{238}U PARAMETERS - (Keepin 1965)						
Group	$T_{1/2}$ (s)	$\sigma(T_{1/2})$	λ_i (s^{-1})	$\sigma(\lambda_i)$	$\beta_{i\nu}$	$\sigma(\beta_{i\nu})$
1	52.38	1.29	0.0132	0.0003	0.00054	0.00005
2	21.58	0.39	0.0321	0.0006	0.00564	0.00025
3	5	0.19	0.139	0.005	0.00667	0.00087
4	1.93	0.07	0.358	0.014	0.01599	0.00081
5	0.49	0.023	1.41	0.067	0.00927	0.0006
6	0.172	0.009	4.02	0.214	0.00309	0.00024
HIGH ^{238}U PARAMETERS - (East 1970)						
Group	$T_{1/2}$ (s)	$\sigma(T_{1/2})$	λ_i (s^{-1})	$\sigma(\lambda_i)$	$\beta_{i\nu}$	$\sigma(\beta_{i\nu})$
1	53.6	5.1	0.012932	0.135911	0.000658	0.000144
2	21	0.8	0.033007	0.866434	0.004233	0.000146
3	5.1	0.5	0.135911	1.386294	0.004633	0.000868
4	2.2	0.2	0.315067	3.465736	0.010553	0.000695
5	0.61	0.07	1.136307	9.902103	0.005234	0.000373
6	0.21	0.02	3.300701	34.65736	0.003289	0.000523

Ultimately, there are four possibilities for each measurement: ^{235}U and ^{238}U datasets for the ^{252}Cf -based measurement and ^{235}U and ^{238}U datasets for the second D-T- based measurement. Table 23 summarizes the combinations of energy-dependent delayed neutron constants considered a given measurement. In this table, thermal-energy constants are represented by T, fast-energy constants are represented by F, and high-energy constants are represented by H.

Table 23. Summary of Delayed Neutron Datasets Considered

Energy-dependent Parameters	
^{235}U	^{238}U
T	F
T	H
F	F
F	H
H	H

Table 24 lists the combinations of delayed neutron parameters that were evaluated in this study. Not all combinations were considered since it would not make sense to use high energy parameters for ^{252}Cf interrogation but thermal or fast parameters for D-T interrogation. Notice the first five scenarios make use of the same datasets for both the Cf-based analysis and the DT-based analysis, while the rest take advantage of the ability to use different datasets in each of the two measurements.

Table 24. Combinations of Delayed Neutron Datasets Considered for Sensitivity Analysis

Scenario	^{252}Cf		DT	
	235	238	235	238
1	T	F	T	F
2	T	H	T	H
3	F	F	F	F
4	F	H	F	H
5	H	H	H	H
6	T	F	T	H
7	T	F	F	F
8	T	F	F	H
9	T	F	H	H
10	F	F	F	H
11	F	F	H	H
12	F	H	H	H

The delayed neutron ratios for each scenario in Table 24 are plotted in Figure 55. The delayed neutron rates were calculated in the same manner discussed in Section 5.1. Because the source strength is unknown (and there are other factors affecting the expected rates), only general conclusions can be drawn. The variability of the datasets indicates that the calculated delayed neutron ratios are dependent on the choice of 6-group delayed neutron parameters and choice of nubar.

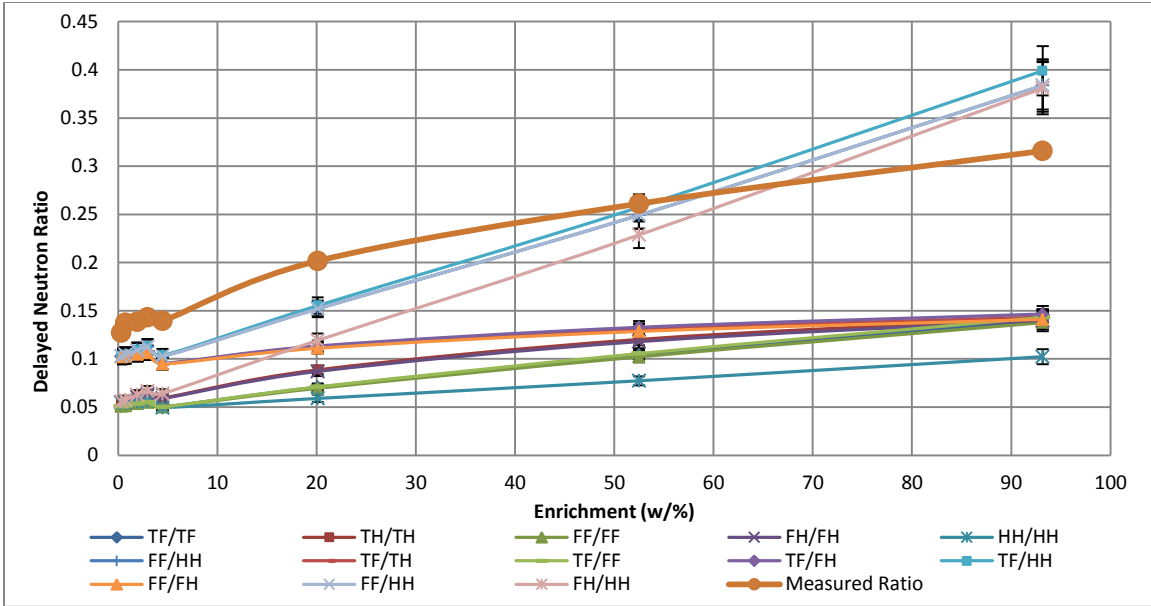


Figure 55. Analytically determined delayed neutron ratios using various combinations of delayed neutron group constants.

In comparing the general shapes of the curves, the following datasets appear to trend most like the measured data: TH/TH, and FH/FH. In fact, if some datasets that clearly do not behave in a similar manner are eliminated from the plot, the behavior of these datasets can be more clearly seen. This is shown in Figure 56. The plot suggests that these other datasets (dependent on both delayed neutron constants and nubar values) provide better predicted delayed neutron ratios and implies that the MCNP6-based calculations may be able to estimate the delayed neutron ratios (and related enrichment) after all.

Figure 57 and Figure 58 show the delayed neutron rates for ^{252}Cf and D-T calculations separately. The H/H energy parameters do not provide good agreement with the measured delayed neutron rates for either the ^{252}Cf or the D-T. The F/F parameters appear to have the same shape and trend as the measured data for ^{252}Cf , perhaps

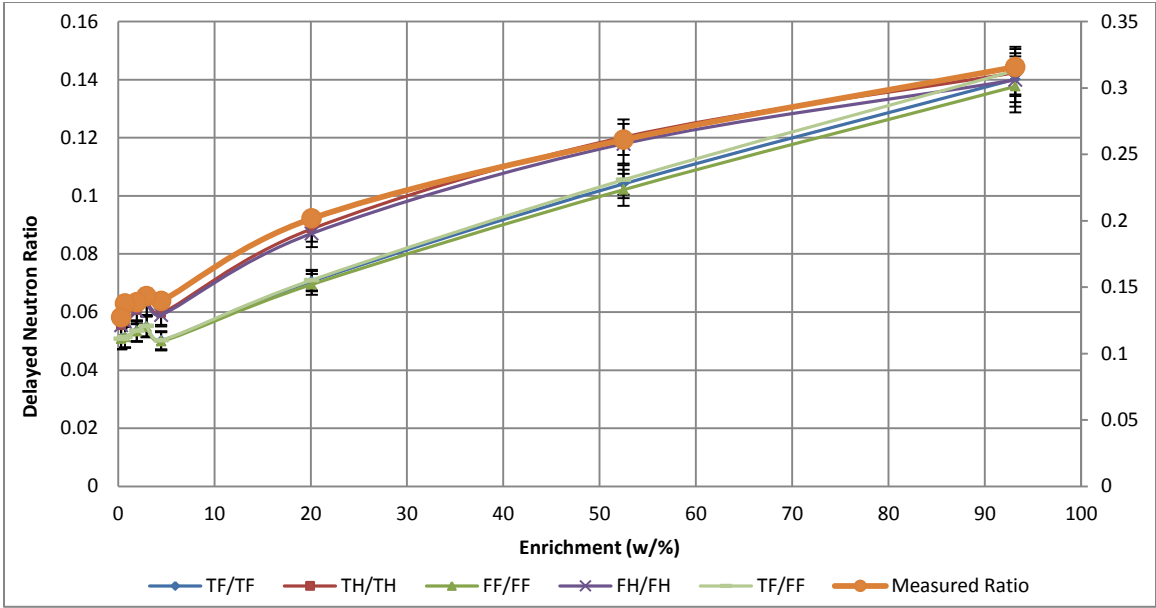


Figure 56. Energy-dependent delayed neutron data (reduced).

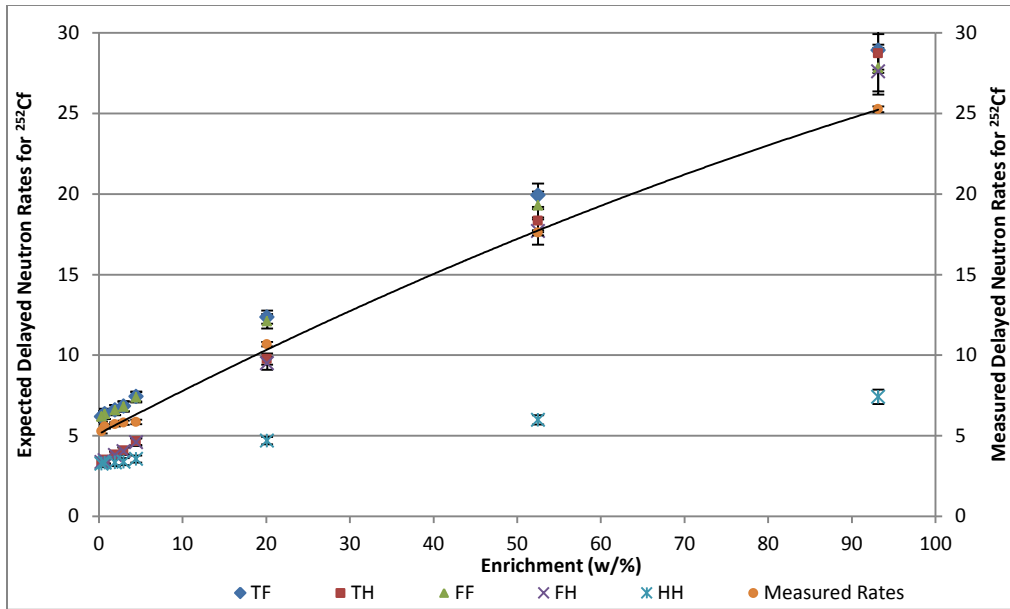


Figure 57. Delayed neutron rates from ^{252}Cf interrogation using various delayed neutron constants.

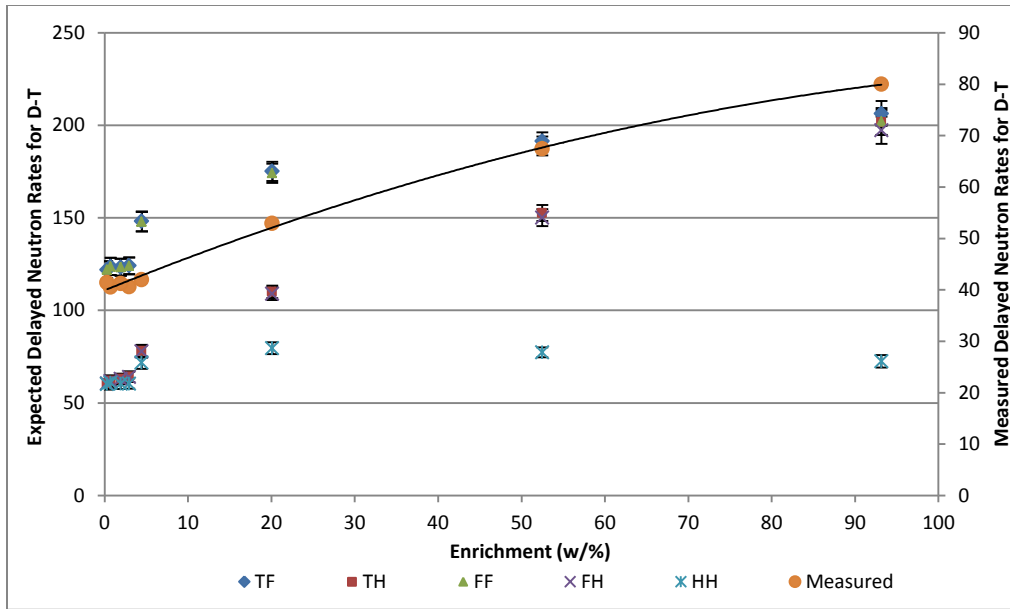


Figure 58. Delayed neutron rates from DT interrogation using various delayed neutron constants.

confirming Tuttle's belief that the fast datasets should be used. For the D-T rates, the T/H and F/H datasets trend closely to the measured data suggesting that either data set would provide better predictions than the T/F dataset.

To address one of the potential sources of the large bias between the calculated and measured delayed neutron rates, the D-T emission rate was estimated using the response of the added flux monitor. The averaged flux monitor response over ten D-T measurements (with no source in the measurement chamber) was 895333 counts. The efficiency of the added flux monitor was taken to be 1.79×10^{-5} based on MCNP6 simulations. The dead-time for the amplifier was estimated at 0.8 s, based on historical knowledge. Using an effective pulse width 30 μ s and a total of 60000 pulses, the source strength was estimated to be 4.15×10^{10} n/s. This implies that there may be a significant difference in the true emission rate and the quoted rate from the manufacturer. This may also account for a large portion of the systematic bias between the measured and calculated data. In fact, if this newly estimated source strength is applied to the calculations, the agreement between the data improves significantly. This is shown in Figure 59.

The agreement between the calculated and measured ratios can also be assessed using a bi-variate plot as shown in Figure 60. By plotting the expected/calculated ratio against the measured ratio, the correlation between the two can be observed. The data can be represented by a straight line indicating that there is a strong correlation between the datasets. In addition, the anomalous point (for the 4.46% item) is not apparent. This is because the model accurately represents the measurements, even for this anomalous point. This suggests that the model may be well suited for predicting delayed neutron ratios and for determining relative correction factors for future measurements.

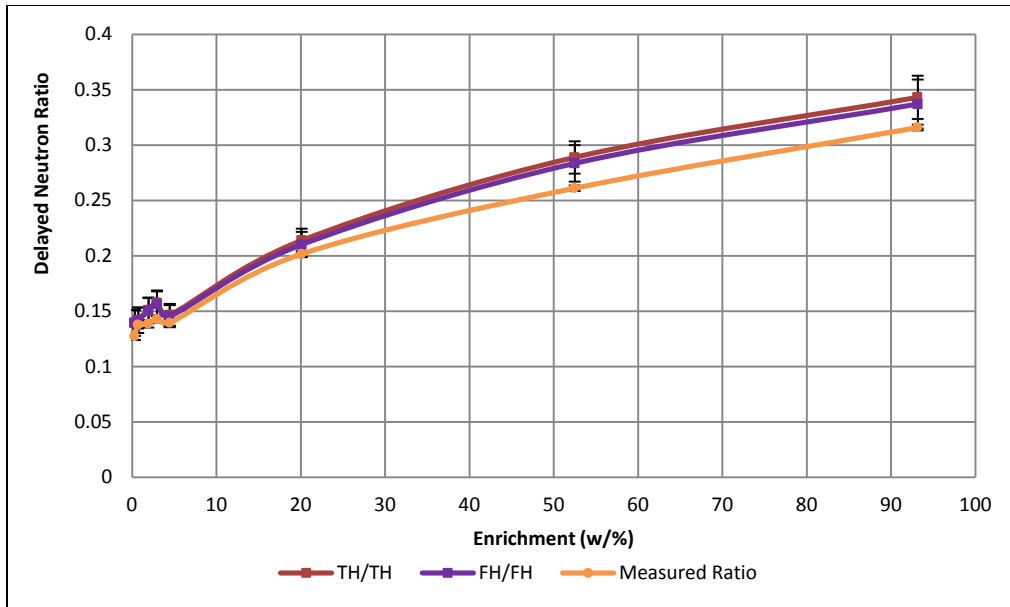


Figure 59. Measured and calculated ratios using estimated D-T emission rate.

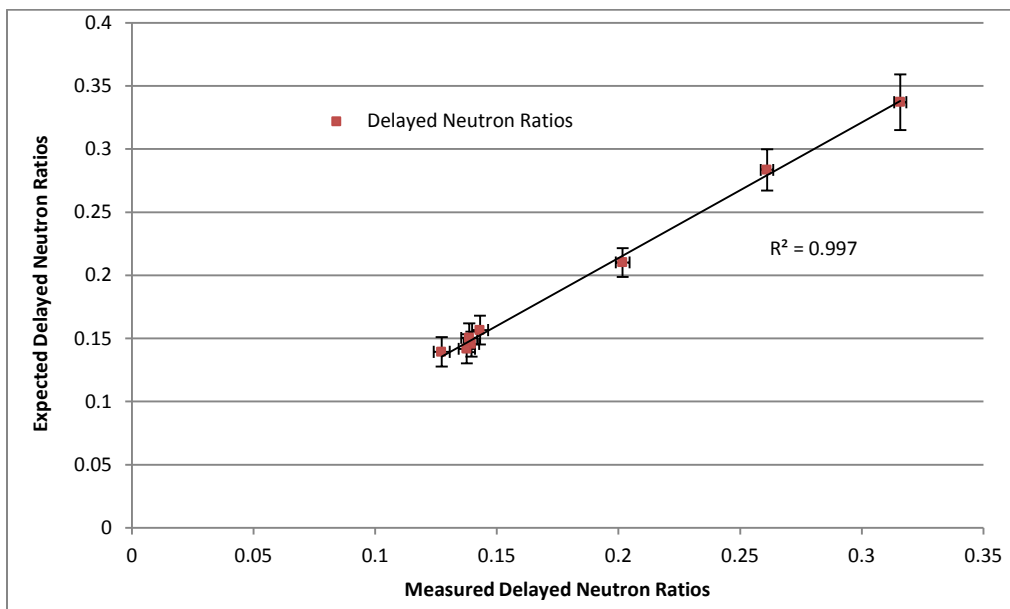


Figure 60. Bi-variate plot of calculated and measured delayed neutron ratios.

5.7 Influence of 8-Group Structure on Analytical Results

In 1957, Keepin concluded that the 6-group representation was satisfactory for reactor physics, a good compromise of simplicity and accuracy given data limitations. At the time, he used a least-squares method to iterate a linear superposition expression for various delayed neutron exponential decay periods. He determined that a 5 group representation did not converge well and resulted in large errors while a 7 group model ultimately yielded no advantage [61].

Since Keepin's original work, an 8-group model has been proposed by Los Alamos National Laboratory, in collaboration with IPPE Obninsk, to improve data associated with the three longest-lived, dominant delayed neutron precursors (^{87}Br , ^{127}I , and ^{88}Br) and to provide a single set of energy-independent decay constants that are applicable to all fissionable isotopes [63]. This international collaboration provided high quality data resulting from numerous fast critical assembly measurements. These 8-group parameters are listed in **Error! Reference source not found.**

Although an 8-group model has been proposed for over two decades, many computer models and codes still assume a 6-group representation. Many users have been complacent with the 6-group representation and have made no major efforts to adopt and integrate the 8-group model. Unlike measurements related to reactor kinetics (specifically related to strong negative reactivity insertions), no appreciable advantage in using the 8-group models was expected for delayed neutron measurement applications.

Figure 61 shows the calculated delayed neutron rates from ^{252}Cf and D-T-based scenarios. The overall shapes are similar to the 6-group data. The ratios of the ^{252}Cf to D-T rates are plotted in Figure 62. The agreement evident in the plots implies that the use of 8-group data does not significantly affect the calculations as related to the DEANI method.

Table 25. 8-group Delayed Neutron Constants

Delayed neutron parameters for ^{235}U						
Group	$T_{1/2}$ (s)	unc. $T_{1/2}$	λ_i (s^{-1})	λ_i unc.	$\beta_i v$	$\beta_i v$ unc.
1	55.6	--	0.012467	--	0.000531466	7E-05
2	24.5	--	0.028292	--	0.002493679	0.000134
3	16.3	--	0.042524	--	0.001474495	0.000153
4	5.21	--	0.133042	--	0.003192038	0.000385
5	2.37	--	0.292467	--	0.005360032	0.000197
6	1.04	--	0.666488	--	0.001461532	8.57E-05
7	0.424	--	1.634781	--	0.001315703	4.82E-05
8	0.195	--	3.554601	--	0.000371054	0.000154
Delayed neutron parameters for ^{238}U						
Group	$T_{1/2}$ (s)	unc. $T_{1/2}$	λ_i (s^{-1})	λ_i unc.	$\beta_i v$	$\beta_i v$ unc.
1	55.6	--	0.012467	--	0.0003906	6.37E-05
2	24.5	--	0.028292	--	0.004836	0.00027
3	16.3	--	0.042524	--	0.00174375	9.74E-05
4	5.21	--	0.133042	--	0.0063705	0.000986
5	2.37	--	0.292467	--	0.013671	0.0009
6	1.04	--	0.666488	--	0.009207	0.000487
7	0.424	--	1.634781	--	0.005952	0.000678
8	0.195	--	3.554601	--	0.00432915	0.000274

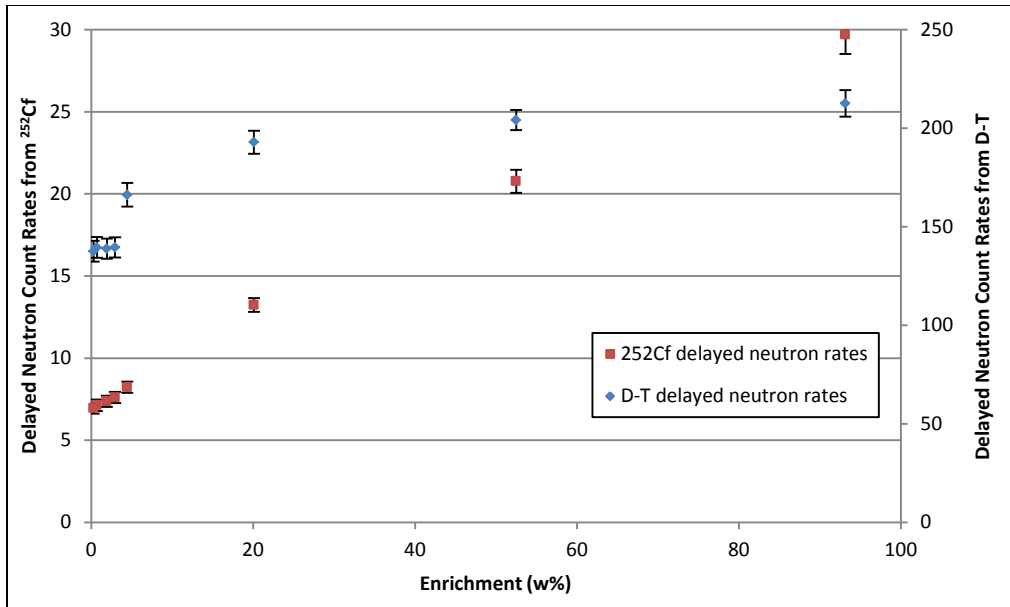


Figure 61. Expected delayed neutron rates using 8-group delayed neutron parameters.

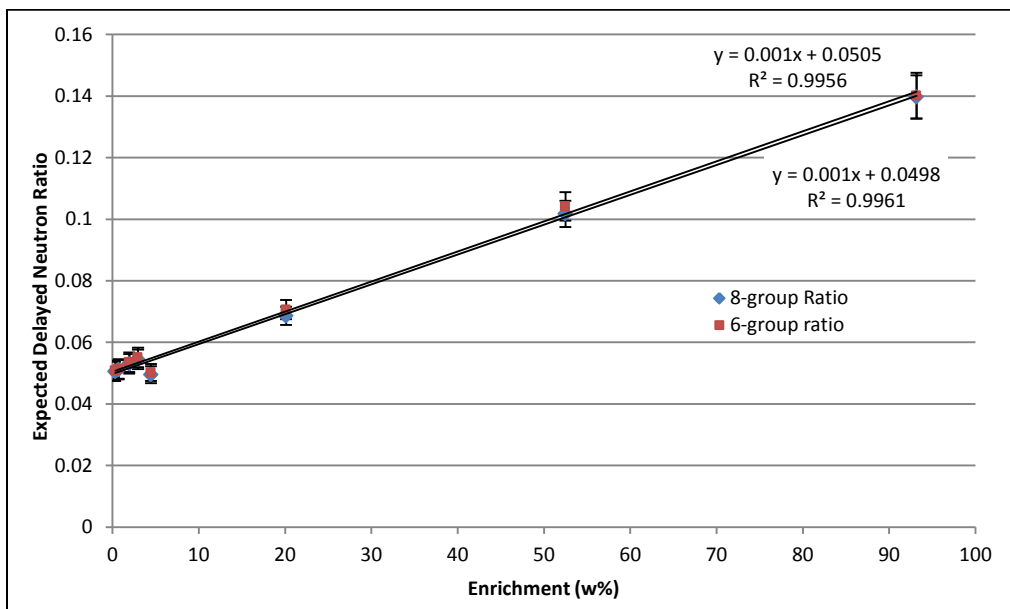


Figure 62. Calculated ratios using 6-group and 8-group parameters.

5.8 MCNP6 Delayed Neutron Data

Delayed particle (neutron and/or gamma) physics packages were first integrated into MCNPX and then transferred to MCNP6 in 2010. These delayed particle functions have been used for health physics, material assay, calibrations, radioanalytical chemistry, and other applications [83]. Thus, the delayed particle function is continuously undergoing improvements to support the user community.

Delayed neutron capabilities were briefly studied to determine if MCNP6 could be used to directly estimate the response of the ^{252}Cf shuffler (i.e., provide delayed neutron count rates). Currently, MCNP6 is used to estimate the fission rates in the uranium. Those fission rates are then used to analytically calculate the expected delayed neutron count rates. The analytical calculations rely on the 6-group structure to estimate the rates, however, MCNP6 can sample from the fission-yield distribution, thus eliminating the assumptions integrated into the group structure.

Delayed neutron emission can be implemented using either the library data, which used A Compact ENDF (ACE) data, or the physics model, which uses CINDER [CINDER-A one point]. The library data procedure involves the following steps: 1) calculating the source particle emission and interaction, 2) determining the identity of the fissioning nuclide, and 3) sampling the ACE data for the number, energy, time, and direction of each delayed neutron. The physics model procedure involves the following steps: 1) calculating the particle emission and interaction, 2) producing residuals for fission and activation reactions using either library or physics model techniques, 3) calculating atom densities for each residual and its decay products using CINDER, 4) calculating energies based on pre-calculated distributions and total delayed neutrons using atom densities, decay constants, and emission probabilities, and 5) sampling distributions for number of delayed neutrons, emission energy, time, and direction. MCNP6 distributions used for energy and emission time employ the trapezoidal rule such that the numerical evaluations of the integrals have errors. If the distributions are correct and the emission of delayed

neutrons is correct with respect to energy and time, calculating the expected delayed neutron count rates should be possible. While simulations and experimental measurements have been compared for the delayed gamma production, there is little in the literature to support the benchmarking of the improved delayed neutron capability.

To perform a brief examination of the delayed neutron capabilities, the shuffler model developed for this work was used. Delayed neutron production was enabled using the ACT card. Delayed neutrons were produced only from fissioning events using the FISSION=n entry. Both the library model and the physics model were used (the physics model when the library data did not exist) by setting the DN=BOTH entry. The traditional ^{252}Cf measurement was simulated. The SDEF card was modified using the TME entry with an even distribution between 0 and 7 sec to simulate an irradiation time of 7 sec. The time tallies were broken into 1 s bins.

One billion histories were run. Of those source particles, only ~9 percent caused fission in the measurement item resulting in the production of 16797 delayed neutrons. Based on the number of fission neutron produced (both prompt and delayed), $\bar{\nu}$ was calculated to be 2.567 n/fiss, which agrees with traditional values. Unfortunately, the statistical errors in the tallies were high; thus meaningful results were not obtained. It is unclear at this time whether the delayed neutron functions emit delayed neutrons properly with respect to time and/or energy.

5.9 Gamma Results

Enrichment measurements were performed on the same set of standards using both WinU235 and MGAU, both widely accepted gamma enrichment systems in nuclear safeguards. The results are discussed in the following subsections.

5.9.1 WinU235

The WINU235 algorithm is based on the absolute intensity of the characteristic 186 keV peak. The measurement was performed using a 1 in x 1 in EFC NaI detector with a 0.5 in thick lead collimator extending 1 in beyond the end of the detector face. The GBS Elektroniks MCA-166 was used for data collection. The settings used for the measurements are provided in Table 26.

Table 26. WINU235 Settings

PZC Value	2143 mV
HV	600 V
Coarse Gain	100
Fine Gain	1.21
Shaping Time	1 us
Input Polarity	POS
Pileup Rejection	ON
Stabilizer	ON
Mode	18 keV
Beginning ROI	230
Ending ROI	370
Centroid	300
Time	Live
Count time	300
Date	11/10/2016

WinU235 calculates and reports the area of the ROI, or the counts above the background within the designated ROI. This area is then used to determine the enrichment of the sample based on a two point calibration which was performed with the 93.17% item and the 0.31% item. The measured data are provided in Table 27.

Table 27. WINU235 Measurement Results

Declared Enrichment	²³⁵ U Enrichment (wt%)	Unc.
93.17	93.2702	1.8855
52.49	52.5060	1.0802
20.11	20.0217	0.4413
4.46	4.3377	0.1268
2.95	2.8452	0.0972
1.94	1.8730	0.0796
0.71	0.6273	0.0579
0.31	0.3351	0.0518

5.9.2 MGAU

MGAU uses various peak ratios to determine the enrichment of a given sample. Because high resolution is required to separate the low energy peaks of interest, a Mirion Technologies HPGe detector was used. An Inspector 2000 MCA was used to record the data. The count time was 900 s. The analysis software automatically calculates the enrichment of the sample based on internal calibration using a physical model of the relative efficiency. These results and the statistical uncertainties are summarized in Table 28. Note that no calibration measurements are required.

Table 28. MGAU Measurement Results

Declared Enrichment	²³⁵ U	Unc.	²³⁸ U	Unc.
93.17	93.827	1.659	5.461	1.681
52.49	52.811	0.354	46.907	0.358
20.11	19.772	0.153	80.12	0.155
4.46	4.457	0.048	95.52	0.049
2.95	3.063	0.039	96.916	0.039
1.94	1.949	0.033	98.04	0.033
0.71	0.797	0.033	99.202	0.034
0.31	0.279	0.043	99.721	0.044

6 CONCLUSIONS

Uranium enrichment measurements are mission critical components in comprehensive nuclear material safeguards and material accountancy. Enrichment is an attribute of interest in its own right for technical safeguards verification. It is also needed to interpret quantitative mass data. Gamma methods and passive neutron methods are not suitable for measuring inhomogeneous bulk uranium items, moderately shielded HEU, or uranium in large, dense matrices in most safeguards applications. To address this, a more penetrating active neutron technique using delayed neutrons was developed. The DEANI method is a dual-energy technique that takes advantage of the marked difference between the energy-dependence of the fission cross-sections of ^{235}U and ^{238}U . The two part measurement induces fission using interrogation sources of differing energies. The resulting delayed neutron count rates are obtained. The ratio of the two delayed neutron rates is then used to estimate the enrichment based on an established calibration curve.

This work was completed using the existing ^{252}Cf shuffler at ORNL, which was retrofitted with a pulsed, sealed D-T generator inside the counting chamber, together with a complete data acquisition system for multichannel scaling. The majority of the design was based on MCNP6 simulations and analytical calculations. Experimental measurements were performed to generate the initial calibration curve and to verify the proposed new assay methodology. The conclusions resulting from the development of this DEANI method are discussed below.

6.1 Discussion of Results and Research Outcomes

6.1.1 DEANI Methodology

The DEANI methodology was developed to provide the safeguards and nonproliferation community with a penetrating technique that can determine uranium enrichment in bulk uranium items. The combination of traditional delayed neutron counting and DEANI

provide both enrichment and mass determination without the need to rely on declared isotopes. The development of the method was achieved using a high-fidelity MCNP6 model of the adapted ORNL ^{252}Cf Shuffler. Separate simulations using interrogation sources of differing energies were conducted to estimate the fission rates in numerous CRM standards. These fission rates were used to analytically calculate an expected delayed neutron count rate for each item. These fission rates were used in the selection of the secondary neutron source (the ^{252}Cf source indigenous to the shuffler was used as the first interrogation source). It was determined that any of the secondary sources evaluated (AmLi, AmBe, D-D, or D-T) would likely work in the DEANI method. In short, ^{252}Cf provides a reasonably soft neutron spectrum that induces fission primarily in ^{235}U . Therefore the second interrogation source was chosen to have a harder spectrum in order to induce more fission in ^{238}U . The difference provides the discriminating power to assay enrichment. Practical considerations also play a major influence wherever a design for safeguards applications is being considered. The D-T generator was selected in part based on the relative ease of installation and integration into the shuffler system (AmLi and AmBe are heavy in comparison to ^{252}Cf and are not amenable to being quickly driven in and out of the system by the Teleflex cable) and because D-T is a far brighter source than D-D. It also offers a more distinct source spectrum relative to ^{252}Cf .

The induced fission rates from the simulations were also used to choose the placement of the D-T generator. The coordinates of the D-T generator were (23.5, 23.5, 36) cm which is in the back right of the measurement cavity. During this work, it was discovered that the D-T generator can transmit microphonic noise to the ^3He if on the same platform. The phenomenon was noted while measuring on the microsecond timescale structure. Thus, it is important that the installation and positioning of the D-T generator be done carefully.

The MCNP6 model was also used to estimate the efficiency of the shuffler with respect to delayed neutrons, since they have average energies much lower than ^{252}Cf (which is most often used to determine the efficiency of a neutron counter). Efficiencies were

calculated using the following source terms in MCNP6: 1) an AmLi spectrum (since average neutron energies are similar to that of delayed neutrons), 2) a 9-bin delayed neutron spectrum from Rinard, and 3) the Hansen-Roach 16-bin energy structure. While there was less than 1.1% difference between all the calculated efficiencies, 22.517% was used based on the data from Rinard. This evaluation of the delayed neutron efficiency also confirms that the use of an AmLi spectrum as a surrogate for a delayed neutron spectrum is a good approximation. The best estimate of the delayed neutron efficiency was made by scaling the measured efficiency using a certified ^{252}Cf source by the MCNP6 calculated ratio of the delayed neutron efficiency to ^{252}Cf efficiency.

To optimize the delayed neutron signal, the measurement timing structure was optimized. Recall that the shuffler repeatedly moves the ^{252}Cf into and out of the measurement cavity so the timing for the irradiation, source travel times, and count times must all be determined. This was performed by minimizing the relative precision of the measurements. The following criteria were applied: 1) the irradiation times and count times are equal, 2) the number of shuffler cycles was maximized at 85 cycles since the shuffler source is relatively weak, 3) the source transfer times are known and fixed by the shuffler system, and 4) the background count time was fixed at 1000 s. The optimized timing parameters (irradiation and count times) were determined to be 7 s. For the D-T generator, the timing structure was significantly different due to the speed at which the generator switches (i.e., pulse rate). A duty cycle of 100 Hz x 10 μs pulses was used to maximize yield and stability. Based on measurement analysis, the best counting window was between 4 ms and 9.7 ms relative to the start of the pulse, which allowed the counting window to be as long as possible (to capture the most delayed neutrons) without interferences from subsequent pulses. The countable fraction for the ^{252}Cf measurements was ~18% on average and was 47% on average for the D-T generator. The larger countable fraction is primarily due to the reduced delay time between the irradiation and

counting windows allowing more of the delayed neutrons from short-lived precursors to be measured.

Both simulation-based analytical calculations and measurements were performed for several CRM standards containing ~230 g of U_3O_8 spanning enrichments from DU to 93%. The simulations used a Watt distribution to represent the interrogation neutrons from ^{252}Cf and a mono-energetic 14.1 MeV point source to represent the D-T neutrons. The calculations used the thermal 6-group Keepin parameters for ^{235}U and the fast 6-group Keepin parameters for ^{238}U . The nubar values used in these calculations were also the values reported by Keepin. The experimental data was obtained using the original ^{252}Cf Shuffler software, which directly reported the background and decay corrected delayed neutron rates. The more complex D-T analysis was performed using multi-channel scalars (one for the shuffler measurement signal and one for the added flux monitor) and Genie 2000. Delayed neutron count rates were obtained through analyses of these time-spectra using code developed during the course of this work.

The experimental data was used to generate a calibration curve using the delayed neutron ratio as a function of enrichment. This dataset was inverted to obtain the measurement curve. This result shows in a direct way that the initial idea that motivated the present DEANI study has the potential to be used for determination of uranium enrichment. Verification measurements were performed to determine if the DEANI methodology could be used to determine the enrichment of unknown items. Based on the results of these measurements, the following conclusions were drawn:

- 1) The DEANI method is capable of estimating the enrichment of items for which the calibration data is representative. In other words, the CRM standards were used to generate the calibration curves and then verify the 20.11% CRM standard (which was left out of the calibration dataset). The DEANI method provided an enrichment value within $\sim 2\sigma$ of the declared value.

- 2) The DEANI method may not be significantly affected by material type (e.g., oxide or metal) or mass. A 1 kg depleted uranium (DU) metal sphere was measured resulting in an enrichment estimate within 1σ of the declared value, although the uncertainty was large. Additionally, simulations were used to estimate that a 10% increase in uranium density should change the estimated enrichment less than 0.1%. More measurements are needed to confirm.
- 3) The DEANI method is susceptible to spatial sensitivities. An 8 kg annular DU sample was measured. The estimated enrichment was $\sim 15\sigma$ above the declared value. The likely explanation for this large difference is the geometry of the sample. Because of its size and shape, the source-to-item coupling changed. In fact, simulations suggested that the delayed neutron rates from ^{252}Cf interrogation changes by a factor of ~ 3 while the rates from the D-T measurement only changed by a factor of ~ 0.5 . Had the ^{252}Cf source and D-T generator been co-located, the impact would have been less since the source-to-item coupling would have been improved. The spatial sensitivity may also be mitigated by calculating relative correction factors using the MCNP6 model. If the model is reliable, a correction factor could be obtained by simulating the original and new measurement location or sample geometries. The ratios of the calculated rates could then be used as a scaling factor that gets applied to the measurement results.
- 4) The DEANI method is capable of identifying discrepancies in at least some inhomogeneous samples. Two CRM standards (20.11% and 52.49%) were placed end-to-end in the measurement cavity. The DEANI was used to estimate an enrichment of $27.0 \pm 2.42\%$. Although the estimated value is over 2σ off from the mean ($\sim 36\%$), the geometry and positioning of the item affect the results. In fact, the items were flipped such that the 52.49% can was on bottom and the enrichment was estimated to be closer to 47%. Again, the geometry plays a strong role in the measured delayed neutron rates. In comparison, the gamma-based techniques used in many safeguards applications only “see” a few mm into a

- uranium item and/or require an infinitely thick geometry. Because the mean free path of 186 keV gamma-rays is only ~ 2 mm for the U_3O_8 in the CRMs, the measurement at one end would have reported an enrichment of $\sim 20\%$ from one end and 52% from the other, essentially blind to the other half of the sample. This is an example of how the DEANI method is a more penetrating technique and potentially useful in scenarios where gamma techniques would fail.
- 5) The presence of higher-Z shielding materials does not appear to adversely affect the DEANI results, or preclude its use. The 52.49% CRM was placed inside an aluminum can (~ 0.5 mm thickness). The can was also filled with various small steel and aluminum scraps. The DEANI measurement was able to estimate an enrichment of $56.0 \pm 5.31\%$, which is within $\sim 0.7\sigma$ of the declared values. While the upper limit of density and shielding was not explored, the result of this measurement has a very important implication: without knowing the density and materials making up the measurement item matrix, traditional gamma enrichment techniques could not be effectively applied, whereas the DEANI method could be applied to obtain reasonable estimates of the uranium enrichment.
 - 6) The DEANI method cannot, however, be sensibly applied to strongly moderating matrices, without further corrections or representative calibrations. CRM items were measured inside 0.5 in and 1 in HDPE shells. The results clearly indicate sensitivity to the moderating material. A flux monitor correction from the bare and Cd-covered flux monitors integrated into the shuffler was used in an effort to correct for the presence of the moderator, with no success. The physical reason is that inside the moderator, the interrogating spectra get thermalized and are no longer markedly differently.

Both the experimental and simulation-based results demonstrate that a clear relationship exists between the delayed neutron ratio from dual-energy interrogations and the ^{235}U enrichment. However, the initial curves from the simulated ratios and measured ratios

over the full range of enrichments did not agree well. After applying energy-appropriate delayed neutron constants and using a more appropriate value for $\bar{\nu}$ as described in Section 5.6, the calculated values agreed well with the measured data, in shape and in behavior. A significant source of uncertainty in the simulated results is the poorly known shuffler and D-T source emission rates. An estimated emission rate of 4.15×10^{10} was applied to the calculations and the systematic bias was considerably reduced. A systematic bias still remains, which means the model cannot be used to predict delayed neutron ratios directly.

On the other hand, the model could be used to calculate relative correction factors for differences in measurement geometry, material type, shape, density, etc. These relative correction factors could be determined using the ratios of simulated data to scale measured data appropriately.

There are several other possible reasons why the calculated and experimental ratios are not expected to agree perfectly.

- 1) There are differences in the modeled geometry and the physical geometry of the shuffler. Differences in the geometries could alter the neutron energies incident on the measurement item, affecting which materials and cross-sections are used (e.g., the HDPE density could vary between 0.912 and 0.962 g/cc which has been shown to produce 1-2% differences in the results [107]), and change the detector efficiency. In addition, the D-T generator was modeled as an isotropic, mono-energetic, 14.1 MeV point source (where some would argue that the neutrons are emitted slightly anisotropically [108]). Also, the MCNP6 model only simulates static measurements, whereas the ^{252}Cf is a dynamic measurement scanning over an entire item. Scanning of the item would likely reduce the spatial sensitivity observed and should be considered to mitigate the problem. Lastly, MCNP6 does not account for the pulse collection at or near the dead space of the ^3He tubes

where the electric field is weaker [107], which suggests MCNP6-based calculations may be biased high. This was observed even in the passive model validation measurements.

- 2) As discussed in Section 6.13, the delayed neutron group constants and neutron nubar values (used to calculate the induced fission rates) are energy-dependent; thus, the traditionally used thermal and fast Keepin numbers do not represent the measurement scenario (particularly for the D-T measurements).

6.1.2 Potential ^{252}Cf Source Replacement

Based on the results from the simulation-based source replacement study, many combinations of irradiation sources (given they have different interrogating energies) may be used in the DEANI method. D-D generators may be capable of replacing ^{252}Cf for applications such as the ^{252}Cf Shuffler. Advantages of such a replacement include a significant reduction in shielding and source storage, no source decay and replacement issues, and the ability to instantaneously turn on and off (i.e., no reverse or forward travel time for the source, which would provide the opportunity to glean more information related to short-lived isotopes). This work showed similar behavior of the delayed neutron rates as a function of enrichment of the two sources can be expected. It was also supports the expectation that the D-D/D-T delayed neutron ratio could be used in the DEANI method. Experimental validation of this assertion and optimization of such measurements is left for future work.

6.1.3 Sensitivity to Energy-Dependent Delayed Neutron Group Data

Because the D-T source emits neutrons with much higher average energies than the ^{252}Cf source, the effect on the calculated delayed neutron rates as a function of energy-dependent delayed neutron group constants (and energy dependent nubar values) was studied. Since the DEANI method is comprised of two separate measurements (^{252}Cf and D-T), there are four opportunities to select delayed neutron group constants: for the ^{252}Cf measurement there is one dataset for ^{235}U and one for ^{238}U and for the D-T measurement

there is one dataset for ^{235}U and one for ^{238}U . In addition, the induced fission multiplicities are dependent on the interrogating energies.

Analytical calculations were performed using various combinations of group constants and corresponding nu_{bar} values. The measured delayed neutron count rates from each interrogation source were compared to the calculated rates using various energy-dependent parameters. For the ^{252}Cf scenario, the F/F datasets with nu_{bar} of 2.57 and 2.79 n/fiss provided the best estimate of the measured rates. This supports Tuttle's recommendation to use F/F datasets. For the D-T scenario, the T/H and F/H parameters provided the best estimate of the delayed neutron rates.

The calculated delayed neutron ratios using the TH/TH dataset and nu_{bar} values of 2.47 and 3.51 n/fiss, for ^{235}U and ^{238}U respectively, exhibited behavior most like the measured ratios. The FH/FH dataset and nu_{bar} values of 2.57 and 3.51 n/fiss also displayed similar behavior. Interestingly, the FF/FF and TF/FF data trends very closely to the original TF/TF data used in early parts of this work. This suggests stronger sensitivity to the high-energy group constants and the nu_{bar} values used in those calculations rather than the differences between thermal and fast parameters.

Based on the results of this sensitivity study, MCNP6 simulations may be used to calculate an expected delayed neutron ratio if the proper energy-dependent delayed neutron group constants and nu_{bar} values are used.

6.1.4 Sensitivity Analysis for the 8- Group Delayed Neutron Data

Recall that the Keepin 6-group model defines a set of half-lives for different isotopes and is dependent on the incident energy of the neutron inducing the fission event. In current practice, it is common to use a fixed, representative half-life for each group for all fissioning systems; however, these approximate values degrade the agreement with expected delayed neutron data. While an 8-group delayed neutron structure has been proposed for many years, many delayed neutron applications continue to use Keepin's 6-

group structure. A brief analysis was conducted to determine the influence of the 8-group structure on the calculated delayed neutron rates, particularly for the DEANI method.

The delayed neutron ratios were computed using the 8-group structure and compared against those using the 6-group structure. No significant difference was observed between the two datasets for this application, suggesting no major benefit in adopting the 8-group structure.

6.2 Future Work

Future work on the following topics may provide a better understanding of or support improvements to the proposed DEANI method.

- 1) The emission rate of the D-T generator should be characterized to improve the MCNP6 model. This would likely reduce the difference between calculated and measured delayed neutron rates. This could be performed in free air using copper foils and basic NAA principles.
- 2) Originally, the measurement items were placed at the back of the shuffler cavity to improve the statistics for the ^{252}Cf -based measurement. The coupling of the ^{252}Cf source-to-measurement item was fixed to reduce the total assay time. The D-T generator was positioned in a location that minimized interference in the measurement chamber but also had a maximum flux incident on the measurement item. As such, the D-T-to-measurement item coupling was different than the ^{252}Cf coupling. However, since the CRM measurement items were similar in shape and size, the source-to-item geometry (with respect to both the ^{252}Cf and the D-T source) was consistent throughout the development of the technique. During verification measurements, this positioning of the original measurement items limited the types of materials, matrices, etc. that could be tested since larger items would change the source coupling. Thus, the extrapolation of this technique to large items (e.g., 55 gal waste drums or large UF_6 cylinders) was not conducted.

Better source coupling and spatial sensitivity of the method should be investigated. This work is proposed for future projects.

- 3) A more in depth look at the energy-dependent delayed neutron constants and nu_{bar} values should be performed. In fact, the average neutron energy incident on the measurement item was weighted by the induced fission cross-sections yielding average energies of 2.5 MeV for ²³⁵U and 5.7 MeV for ²³⁸U. Using the nu_{bar} values at these respective energies may produce a model that better represents the measured data.
- 4) Similarly, this technique was specifically developed for the analysis of delayed neutron measurements; however, the underlying principle (i.e., preferentially influencing the induced fission rates) should be applicable to other active neutron techniques such as delayed gamma measurements and even active gamma techniques. This is proposed as future work.
- 5) It was decided not to pursue additional spectrum tailoring in an effort to maximize the difference in neutron energies of the two interrogating fluxes. An investigation of the effects of tailoring the neutron energy spectrum would provide a stronger case for other secondary neutron sources and to complete the evaluation of a replacement source for the ²⁵²Cf.
- 6) A deeper study of the flux monitor corrections for highly moderating matrices would be hugely beneficial as it might allow low-Z items to be measured. Currently, the DEANI method does not support enrichment measurements of highly moderated materials.
- 7) The delayed neutron ratios for the 4.46% CRM standard do not behave as expected based on the delayed neutron rates from the other CRM items. This is true for both experimental and measured data, which implies that the anomaly is being accounted for in the MCNP6 model. Simulations suggest that the fill height significantly affects the DEANI results and indicate that the fill height may be erroneously recorded. A further look into the true fill height should be performed,

and a deeper understanding of the driving mechanism behind the anomaly should be obtained.

- 8) Further verification of the DEANI method should be conducted to determine limits of detection under various circumstances. This will require access to many more standards and matrix components. It would also require additional refinements (e.g., optimizing the source coupling by better positioning the D-T generator) and require a better understanding of the source emission rates.
- 9) Further benchmarking on the MCNP6 delayed neutron capabilities should be performed. In spite of an in-depth review of the available documentation and attempts to directly simulate the measurement of delayed neutrons, it was not directly obvious how to implement the simulated measurement of delayed neutrons. More work should be done to understand the capabilities and limitations of delayed neutrons applications of MCNP6.

6.3 Summary

Ultimately, the performance of an active interrogation method is dependent on numerous factors including the strength and energy of the interrogating source; the size, shape, and form of the nuclear material; the size, shape, density, etc. of the attenuating materials/matrix, the detector properties, and the measurement setup.

The DEANI method has been developed and used to experimentally demonstrate that uranium enrichment can be determined using the ratio of delayed neutron rates from interrogation sources of differing energies (in this case, ^{252}Cf and D-T). Limited verification measurements suggest it may not be strongly sensitive to mass, material type, or the presence of higher-Z materials. This technique is not appropriate for highly moderated items. Spatial variations may need to be addressed further before extrapolating to large items such as drums or cylinders.

Using the updated TH/TH (or FH/FH) delayed neutron constants and associated nuubar values drastically improved the agreement between the expected delayed neutron ratios based on MCNP6 simulations and the experimental data. If the source strength of the ^{252}Cf and D-T generator can be more exactly described, or through the use of a scaling factor, the simulation-based calculations can potentially provide estimated delayed neutron ratios and thus be used to estimate the enrichment of an item. This would allow for the technique to be more readily extrapolated to more complex materials and measurement systems through the use of relative correction factors.

This work has the potential to result in a practical comprehensive nondestructive assay (NDA) technique that leverages existing and commercially available equipment in such a way that a single measurement system could determine the individual masses of ^{235}U and ^{238}U without the need for prior knowledge of the isotopics. This may be especially useful if extended to systems that measure larger items, such as waste measurement or spent fuel measurement systems. Furthermore, and very importantly, active delayed neutron counting of the type exploited here might also be readily achieved using ^3He [helium-3]-free neutron detection systems (e.g., boron-coated straws) such that an instrument that is free of both high-purity germanium and ^3He may be imagined.

LIST OF REFERENCES

- [1] International Atomic Energy Agency, "Treaty on the Nonproliferation of Nuclear Weapons," INFCIRC/140, Vienna, Austria, 1970.
- [2] International Atomic Energy Agency. (2001). *IAEA Safeguards Glossary: 2001 Edition*. Available: https://www.iaea.org/sites/default/files/iaea_safeguards_glossary.pdf
- [3] M. D. Rosenthal, et.al., *Deterring Nuclear Proliferation: The Importance of IAEA Safeguards*. Brookhaven National Laboratory: National Nuclear Security Administration, 2013.
- [4] International Atomic Energy Agency, "The Structure and Content of Agreements between the Agency and States Required in Connection with the Treaty on the Nonproliferation of Nuclear Weapons," INFCIRC/153(corrected), Vienna, Austria, 1972.
- [5] International Atomic Energy Agency, "Nuclear Material Accounting Handbook," IAEA-SVS-15, International Atomic Energy Agency, Vienna, Handbook, May 2008.
- [6] P. M. J. Chard, S. Croft, "A Database of ^{240}Pu effective and ^{235}U effective Coefficients for Various Fertile and Fissile Isotopes," in *19th Annual ESARDA Symposium on Safeguards and Nuclear Material Management*, Montpellier, France, 1997, pp. 389-396.
- [7] D. Reilly, N. Ensslin, J. Smith, H. , and S. Kreiner, *Passive Nondestructive Assay of Nuclear Materials*. Washington, D.C., USA: US Nuclear Regulatory Commission, 1991.

- [8] B. Goddard, S. Croft, A. Lousteau, and P. Peerani, "Evaluation of AmLi neutron spectra data for active well type neutron multiplicity measurements of uranium," *Nuclear Instruments and Methods in Physics Research A*, vol. 830, pp. 256-264, May 2016.
- [9] P. M. Rinard, "Unpublished AmLi spectrum from IPPE, Obninsk, Russia," S. Croft, Ed., ed, 1999.
- [10] "Evaluated Nuclear Data File ENDF/B-VII," ed: (available and maintained by the National Nuclear Data Center at Brookhaven National Laboratory).
- [11] J. W. Boldeman, D. Culley, and R. J. Cawley, "Fission neutron spectrum from the spontaneous fission of ^{252}Cf ," *Transactions of the American Nuclear Society* vol. 32, pp. 733-735, 1979.
- [12] N. Ensslin, W. H. Geist, M. S. Krick, and M. M. Pickrell, "Active Neutron Multiplicity Counting: Addendum to Passive Nondestructive Assay of Nuclear Materials " LA-UR-07-1403, Los Alamos National Laboratory, Los Alamos, NM, 2007.
- [13] P. C. Durst, et.al., "Analysis of Advanced Safeguards Options for the National Enrichment Facility," ORNL/TM-2007/136, Oak Ridge National Laboratory, Oak Ridge, TN, Technical Manual, December 2007.
- [14] International Atomic Energy Agency, "Safeguards Techniques and Equipment: 2011 Edition," vol. International Nuclear Verification, p. 146, 2011.
- [15] Antech. (1996-2016, August 31). *B2102 Series, Fork Detectors (IAEA)* [Website]. Available: <http://antech-inc.com/products/b2102/>

- [16] M. Zendel, "IAEA Safeguards Equipment," presented at the Advanced Sensors for Safeguards, Santa Fe, NM, 2008.
- [17] N. Ensslin, W. C. Harker, M. S. Krick, D. G. Langner, M. M. Pickrell, and J. E. Stewart, "Application Guide to Neutron Multiplicity Counting," LA-13422-M, Los Alamos National Laboratory, Los Alamos, NM, 1998.
- [18] N. Pacilio, "Reactor Noise Analysis in the Time Domain," TID 24512, 1969.
- [19] K. A. Miller, H. O. Menlove, M. T. Swinhoe, and J. B. Marlow, "A New Technique for Uranium Cylinder Assay Using Passive Neutron Self-Interrogation," IAEA-CN-184/131, Los Alamos National Laboratory, Los Alamos, NM.
- [20] H. O. Menlove and D. H. Beddingfield, "Passive Neutron Reactivity Measurement Technique," LA-UR-97-2651, Los Alamos National Laboratory, 1997.
- [21] H. O. Menlove, "Description and Performance Characteristics for Neutron Coincidence Collar for the Verification of Reactor Fuel Assemblies," LA-8939-MS, Los Alamos National Laboratory, Los Alamos, NM, August 1981.
- [22] L. G. Evans, M. Swinhoe, H. O. Menlove, P. Schwalbach, P. De Baere, and M. C. Brown, "A New Fast Neutron Collar for Safeguards Inspection Measurements of Fresh Low Enriched Uranium Fuel Assemblies Containing Burnable Poison Rods," *Nuclear Instruments and Methods in Physics Research A*, vol. 729, pp. 740-746, August 2013.

- [23] J. T. Caldwell, R. D. Hastings, G. C. Herrera, W. E. Kunz, and E. R. Shunk, "Los Alamos second-generation system for passive and active neutron assays of drum-size containers," Los Alamos National Lab., NM (USA), 1986.
- [24] I. Pazsit, D. Chernikova, K. Axell, and M. Flaska, "The Cf-based Differential Die-Away Analysis Method," presented at the Institute of Nuclear Materials Management 55th Annual Meeting, Atlanta, GA, 2014.
- [25] M. Villani, L. C.-A. Bourva, S. Croft, and B. McElroy, "Optimal Differential Die-Away Early Gate Study for Difficult Assays," presented at the Waste Management 2006, Tucson, AZ 2004.
- [26] V. F. Batyaev, O. V. Bochkarev, and S. V. Sklyarov, "Fissile Materials Detection via Neutron Differential Die-Away Technique," *International Journal of Modern Physics: Conference Series*, vol. 27, p. 1460130, 2014.
- [27] G. R. Keepin, "Physics of Nuclear Kinetics," I. Addison-Wesley Publishing Company, Ed., ed. Reading, Massachusetts, 1965.
- [28] R. Batchelor and H. R. M. Hyder, "The energy of delayed neutrons from fission," *Journal of Nuclear Energy (1954)*, vol. 3, pp. 7-17, 1956/08/01 1956.
- [29] P. M. Rinard, "Application Guide to Shufflers," LA-13819-MS, Los Alamos National Laboratory, Los Alamos, New Mexico, 1991.
- [30] C. L. Hollas, D. A. Close, and C. E. Moss, "Analysis of fissionable material using delayed gamma rays from photofission," *Nuclear Instruments and Methods in Physics Research Section B: Beam Interactions with Materials and Atoms*, vol. 24, pp. 503-505, 1987.

- [31] D. H. Beddingfield and F. E. Cecil, "Identification of fissile materials from fission product gamma-ray spectra," *Nuclear Instruments and Methods in Physics Research Section A: Accelerators, Spectrometers, Detectors and Associated Equipment*, vol. 417, pp. 405-412, 11/11/ 1998.
- [32] R. E. Marrs, E. B. Norman, J. T. Burke, R. A. Macri, H. A. Shugart, E. Browne, *et al.*, "Fission-product gamma-ray line pairs sensitive to fissile material and neutron energy," *Nuclear Instruments and Methods in Physics Research Section A: Accelerators, Spectrometers, Detectors and Associated Equipment*, vol. 592, pp. 463-471, 7/21/ 2008.
- [33] T. Nicol, B. Pérot, C. Carasco, E. Brackx, A. Mariani, C. Passard, *et al.*, "Feasibility study of ^{235}U and ^{239}Pu characterization in radioactive waste drums using neutron-induced fission delayed gamma rays," *Nuclear Instruments and Methods in Physics Research Section A: Accelerators, Spectrometers, Detectors and Associated Equipment*, vol. 832, pp. 85-94, 10/1/ 2016.
- [34] A. Proctor, T. A. Gabriel, A. W. Hunt, J. Manges, and T. Handler, "Detecting fissionable materials in a variety of shielding matrices via delayed gamma and neutron photofission signatures—Part 2: Experimental results," *Nuclear Instruments and Methods in Physics Research Section A: Accelerators, Spectrometers, Detectors and Associated Equipment*, vol. 662, pp. 71-80, 1/11/ 2012.
- [35] H. Rennhofer, J. M. Crochemore, E. Roesgen, and B. Pedersen, "Detection of SNM by delayed gamma rays from induced fission," *Nuclear Instruments and Methods in Physics Research Section A: Accelerators, Spectrometers, Detectors and Associated Equipment*, vol. 652, pp. 140-142, 10/1/ 2011.

- [36] Q. Yahua, W. Jizong, Y. Yi, Z. Ming, and L. Shilong, "Determination of ^{235}U isotope abundance by measuring selected pairs of fission products," *Nuclear Instruments and Methods in Physics Research Section A: Accelerators, Spectrometers, Detectors and Associated Equipment*, vol. 665, pp. 70-73, 2/11/ 2011.
- [37] J. Csikai, *Handbook of Fast Neutron Generators*. Boca Raton, FL: CRC Press, Inc., 1989.
- [38] S. Andola, R. Niranjana, T. C. Kaushik, R. K. Rout, A. Kumar, D. B. Paranjape, *et al.*, "Use of delayed gamma rays for active non-destructive assay of ^{235}U irradiated by pulsed neutron source (plasma focus)," *Nuclear Instruments and Methods in Physics Research Section A: Accelerators, Spectrometers, Detectors and Associated Equipment*, vol. 753, pp. 138-142, 7/21/ 2014.
- [39] J. M. Hall, S. Asztalos, P. Bilot, J. Church, M. A. Descalle, T. Luu, *et al.*, "The Nuclear Car Wash: Neutron interrogation of cargo containers to detect hidden SNM," *Nuclear Instruments and Methods in Physics Research Section B: Beam Interactions with Materials and Atoms*, vol. 261, pp. 337-340, 2007/08/01/ 2007.
- [40] J. Knowles, S. Skutnik, D. Glasgow, and R. Kapsimalis, "A generalized method for characterization of ^{235}U and ^{239}Pu content using short-lived fission product gamma spectroscopy," *Nuclear Instruments and Methods in Physics Research Section A: Accelerators, Spectrometers, Detectors and Associated Equipment*, vol. 833, pp. 38-44, 10/11/ 2016.
- [41] H. Ottmar and H. Eberle, "The Hybrid K-Edge/ K-XRF Densitometer: Principles-Design-Performance," KfK 4590, Kernforschungszentrum Karlsruhe, Karlsruhe, February 1991.

- [42] ASTM International, "Standard Terminology of C26.10 Nondestructive Assay Methods," ed: ASTM International, 2010.
- [43] E. R. Martin, D. F. Jones, and J. L. Parker, "Gamma-ray measurements with the segmented gamma scan. [Maintenance manual],"; Los Alamos Scientific Lab., N.Mex. (USA), 1977.
- [44] Canberra Industries, Inc., "Standard Segmented Gamma Scanner," vol. C38548 - 04/11, ed, 2011.
- [45] Canberra Industries, Inc., "WM2900 TGS Tomographic Gamma Scanner," March 2010 ed, 2010.
- [46] W. Bertozzi, S. E. Korbly, R. J. Ledoux, and W. Park, "Nuclear resonance fluorescence and effective Z determination applied to detection and imaging of special nuclear material, explosives, toxic substances and contraband," *Nuclear Instruments and Methods in Physics Research Section B: Beam Interactions with Materials and Atoms*, vol. 261, pp. 331-336, 8// 2007.
- [47] M. T. Kinlaw and A. W. Hunt, "Time Dependence of Delayed Neutron Emission for Fissionable Isotope Identification," *Applied Physics Letter*, vol. 86, 2005.
- [48] R. C. Runkle, D. L. Chichester, and S. J. Thompson, "Rattling nucleons: New developments in active interrogation of special nuclear material," *Nuclear Instruments and Methods in Physics Research Section A: Accelerators, Spectrometers, Detectors and Associated Equipment*, vol. 663, pp. 75-95, 1/21/ 2012.

- [49] GBS Elektronik GmbH, "MCA166-USB User's Manual," GBS Elektroniks, Grosserkmannsdorf, Germany, Manual, 2007.
- [50] S. T. Hsue, J. E. Stewart, T. E. Sampson, G. Butler, C. R. Rudy, and P. M. Rinard, "Guide to Nondestructive Assay Standards: Preparation Criteria, Availability, and Practical Considerations," Los Alamos National Laboratory, Los Alamos, LA-13340-MS, 1997.
- [51] P. Matussek, "Accurate Determination of the ^{235}U Isotope Abundance by Gamma Spectrometry," Institut für Kernphysik, Karlsruhe, User Guide, 1985.
- [52] K. D. Ianakiev, et.al., "On-Line Enrichment Monitor for UF₆," LA-UR-11-02795, Los Alamos National Laboratory, Los Alamos, NM, 2011.
- [53] R. Gunnink, R. Arlt, and R. Berndt, "New Ge and NaI Analysis Methods for Measuring ^{235}U Enrichments," in *19th Annual Symposium on Safeguards and Nuclear Material Management*, Montpellier, France, 1997.
- [54] FLIR, "identiFINDER 2: Digital Handheld Gamma Spectrometer with Radionuclide Identification," identiFINDER 2/en/2.5(11773)/Jul2012, User Guide, July 2012 2012.
- [55] A. Bosko, S. Phillips, T. Gerent, and R. Gunnink, "MGAUV2.4: The Latest Evolution in the Multip-Group Analysis Code for Uranium," in *52nd Annual Meeting of the Institute of Nuclear Materials Management*, Palm Desert, 2011.
- [56] "Multi-Group Analysis for Uranium Specifications," Canberra, Inc., Specification Sheet, 2003.

- [57] T. E. Sampson, "Plutonium Isotopic Analysis Using PC/FRAM," LA-UR-03-4403, 2007.
- [58] P. M. Rinard, "Shuffler instruments for the nondestructive assay of fissile materials," 1991.
- [59] B. E. Watt, "Energy Spectrum of Neutrons from Thermal Fission of ^{235}U ," *Physical Review*, vol. 87, pp. 1037-1041, 1952.
- [60] R. B. Roberts, R. C. Mayer, and P. Wang, *Physics Review*, vol. 55, 1939.
- [61] G. R. Keepin, T. F. Wimett, and R. K. Zeigler, "Delayed neutrons from fissionable isotopes of uranium, plutonium and thorium," *Journal of Nuclear Energy (1954)*, vol. 6, pp. IN2-21, 1957/01/01 1957.
- [62] R. J. Tuttle, "Delayed-Neutron Data for Reactor-Physics Analysis," *Nuclear Science and Engineering*, vol. 56, pp. 37-71, 1975.
- [63] A. D'Angelo, G. Rudstam, P. Finck, and A. Filip, "Delayed Neutron Data for the Major Actinides," NEA/WPEC-6, Working Party on International Evaluation Cooperation of the NEA Nuclear Science Committee, Report, 2002 2002.
- [64] W. Myers, C. A. Goulding, C. L. Hollas, and C. Moss, "Photon and Neutron Active Interrogation of Highly Enriched Uranium," in *International Conference on Nuclear Data for Science and Technology*, 2005.
- [65] H. O. Menlove and T. W. Crane, "A ^{252}Cf Based Nondestructive Assay System for Fissile Materials," *Nuclear Instrumentation and Methods* vol. 152, pp. 549-557, 1978.

- [66] W. Myers, C. A. Goulding, and C. L. Hollas, "Determination of the ^{235}U Enrichment of Bulk Uranium Samples Using Delayed Neutrons," presented at the PHYSOR, Vancouver, BC, Canada, 2006.
- [67] M. T. Andrews and G. Bentoumi, et.al., " ^{235}U Determination Using an In-Beam Delayed Neutron Counting Technique at the NRU Reactor," LA-UR-15-24339, Los Alamos National Laboratory, Los Alamos, NM, 2015.
- [68] X. Li, R. Henkelmann, and F. Baumgartner, "Rapid Determination of Uranium and Plutonium Content in Mixtures Through Measurement of the Intensity-Time Curve of Delayed Neutrons " *Nuclear Instruments and Methods in Physics Research B*, vol. 215, pp. 246-251, 2004.
- [69] P. Blanc, S. J. Tobin, T. Lee, J. S. Hu, J. Hendricks, and S. Croft, *Delayed neutron detection with an integrated differential die-away and delayed neutron instrument*, 2010.
- [70] H. O. Menlove, R. H. Augustson, and D. B. Smith, "A Multi-Spectra Neutron Irradiation Technique for the Nondestructive Assay of Fissionable Materials," *Nuclear Technology*, vol. 10, pp. 366-379, 1971.
- [71] M. J. A. Armelin and M. B. A. Vasconcellos, "An Evaluation of the Delayed Neutron Counting Method for Simultaneous Analysis of Uranium and Thorium and For $^{235}\text{U}/^{238}\text{U}$ Isotopic Ratio Determination," *Journal of Radioanalytical and Nuclear Chemistry*, vol. 100, pp. 37-47, 1986.
- [72] J. L. Dolan, M. J. Marcath, M. Flaska, S. A. Pozzi, D. L. Chichester, A. Tomanin, et al., "Active-interrogation measurements of fast neutrons from induced fission in low-enriched uranium," *Nuclear Instruments and Methods in Physics Research*

- Section A: Accelerators, Spectrometers, Detectors and Associated Equipment*, vol. 738, pp. 99-105, 2014/02/21/ 2014.
- [73] W. Rosenstock, T. Koble, M. Risse, and W. Berky, "Detection of Concealed Fissionable Material by Delayed Neutron Counting," IAEA-SM/EN-09, Fraunhofer-INT, Euskirchen, Germany.
- [74] W. F. G. van Rooijen and D. Lathouwers, "Sensitivity analysis for delayed neutron data," *Annals of Nuclear Energy*, vol. 35, pp. 2186-2194, 2008/12/01/ 2008.
- [75] D. S. and J. Walker, "The Sensitivity of Fast Reactor Kinetic Behaviour to Variations in Delayed-Neutron Energy Spectra," in *Dealyed Neutron Properties, Proceedings of the Specialists' Meeting*, University of Birmingham, England, 1987, p. 275.
- [76] A. D'Angelo, "A Total Delayed Neutron Yields Adjustment Using "XPR" and "SNEAK" Beta Effective Integral Measurements," in *International Conference on the Physics of Reactors: Operation, Design and Computation*, Marseille, France, 1990, p. 111.
- [77] G. D. Spriggs, J. M. Campbell, and V. M. Piksaikin, "An 8-group delayed neutron model based on a consistent set of half-lives," *Progress in Nuclear Energy*, vol. 41, pp. 223-251, 2002/07/11/ 2002.
- [78] B. Geslot, C. Jammes, and B. Gall, "Influence of the delayed neutron group parameters on reactivity estimation by rod drop analysis," *Annals of Nuclear Energy*, vol. 34, pp. 652-660, 2007/08/01/ 2007.

- [79] V. M. Piksaikin, L. E. Kazakov, S. G. Isaev, M. Z. Tarasko, V. A. Roshchenko, R. G. Tertytchnyi, *et al.*, "Energy dependence of relative abundances and periods of delayed neutrons from neutron-induced fission of ^{235}U , ^{238}U , ^{239}Pu in 6- and 8-group model representation," *Progress in Nuclear Energy*, vol. 41, pp. 203-222, 2002/07/11 2002.
- [80] V. M. Piksaikin, V. A. Roshchenko, and G. G. Korolev, "Relative yield of delayed neutrons and half-life of their precursor nuclei from ^{238}U fission by 14.2–17.9 MeV neutrons," *Atomic Energy*, vol. 102, pp. 151-159, 2007.
- [81] J. T. Goorley, et.al., "Initial MCNP6 Release Overview - MCNP6 Version 1.0," LA-UR-13-22934, Los Alamos National Laboratory, Los Alamos, New Mexico, 2013.
- [82] G. W. McKinney, *MCNP6 enhancements of delayed-particle production*: American Nuclear Society - ANS; La Grange Park, IL (United States); American Nuclear Society, Inc., 555 N. Kensington Avenue, La Grange Park, Illinois 60526 (United States), 2012.
- [83] J. W. Durkee, et.al., "The MCNP6 Delayed-Particle Feature," LA-UR-12-00283, Los Alamos National Laboratory, Los Alamos, NM, 2012.
- [84] R. A. Weldon, M. L. Fensin, and G. W. McKinney, "Testing the Delayed Gamma Capability in MCNP6," *Nuclear Technology*, vol. 192, 2015.
- [85] M. Andrews, J. T. Goorley, E. C. Corcoran, and D. G. Kelly, "A Preliminary Comparison of MCNP6 Delayed Neutron Emission from ^{235}U and Experimental Measurements," *Transactions of the American Nuclear Society*, vol. 106, pp. 813-816, 2012.

- [86] S. J. Tobin, M. T. Swinhoe, and D. W. MacArthur, "Monte Carlo Study of Replacing Californium in a Shuffler with a Neutron Generator," presented at the Institute for Nuclear Materials Management Annual Meeting, Orlando, FL, 2004.
- [87] M. A. Schear and S. J. Tobin, "Replacing a ^{252}Cf source with a neutron generator in a shuffler - a conceptual design performed with MCNPX," p. Medium: ED, 2009.
- [88] "MATLAB " vol. R2016a, 9.0.0.341360 ed. Natick, Massachusetts: The Mathworks Inc., 2016.
- [89] Canberra Industries, Inc., "JSR-15 Handheld Multiplicity Register (HHMR)," in *www.canberra.com* vol. C40280, ed, 2014.
- [90] M. S. Krick, et.al., "The IAEA Neutron Coincidence Counting (INCC) and the Deming Least-Squares Fitting Program," LA-UR-98-2378, 1998.
- [91] R. D. McElroy, S. L. Cleveland, S. Croft, and A. Lousteau, "The D-D Neutron Generator as an Alternative to Isotropic Neutron Sources in International Safeguards," presented at the Institute for Nuclear Materials Management, Atlanta, GA, 2016.
- [92] L. Lebreton, A. Zimbal, and D. Thomas, "Experimental Comparison of ^{241}Am -Be Neutron Fluence Energy Distributions," *Radiation Protection Dosimetry*, vol. 126, pp. 3-7, 2007.
- [93] International Atomic Energy Agency, "Neutron Generators for Analytical Purposes," Vienna, Austria, 2012.

- [94] B. Palles, "Neutron Generators: Technology Review and Application to Concrete Printing," The Bredesen Center for Interdisciplinary Research and Graduate Education, University of Tennessee, Knoxville, TN, 2016.
- [95] G. F. Knoll, *Radiation Detection and Measurement*, 3rd ed. Hoboken, N.J.: John Wiley, 2010.
- [96] S. Das, "The importance of delayed neutrons in nuclear research—A review," *Progress in Nuclear Energy*, vol. 28, pp. 209-264, 1994/01/01 1994.
- [97] P. M. Rinard, "Calculating Shuffler Count Rates," LA-13815-MS, Los Alamos National Laboratory, Los Alamos, NM, 2001.
- [98] M. Burgy, L. A. Pardue, H. B. Willard, and E. O. Wollen, MDDC-16, U.S. Atomic Energy Commission Report, 1946.
- [99] D. Hughes, Cahn, and Hall, "Delayed Neutrons from Fission of ^{235}U ," *Physics Review*, vol. 73, 1948.
- [100] T. W. Bonner, S. J. Blame, and J. E. Evans, LADC 2083, U.S. Atomic Energy Commission Report, 1955.
- [101] J. M. Campbell and G. D. Spriggs, "Delayed Neutron Spectral Data for the Hansen-Roach Energy Group Structure," LANL 99-2988, Los Alamos National Laboratory, Los Alamos, NM, 1999.
- [102] A. E. Profio, *Experimental Reactor Physics*. New York: John Wiley and Sons, Inc., , 1976.

- [103] W. E. Koehler, S. J. Tobin, N. P. Sandoval, and M. L. Fensin, *Spectrum tailoring of the neutron energy spectrum in the context of delayed neutron detection*; Los Alamos National Laboratory (LANL), 2010.
- [104] L. V. East and G. R. Keepin, "Fundamental Fission Signatures and Their Applications to Nuclear Safeguards," *Physics and Chemistry of Fission*, pp. 647-666 1969.
- [105] M. S. Zucker and N. E. Holden, "Neutron Multiplicity for Neutron Induced Fission of ^{235}U , ^{238}U , and ^{239}Pu as a Function of Neutron Energy," BNL-38665, Brookhaven National Laboratory Upton, New York, Technical Report.
- [106] G. D. Spriggs and J. M. Campbell, "A summary of measured delayed neutron group parameters," *Progress in Nuclear Energy*, vol. 41, pp. 145-201, 2002/07/11 2002.
- [107] S. Croft, A. Favalli, M. T. Swinhoe, and C. D. Rael, "State of the Art Monte Carlo Modeling of Active Collar Measurements and Comparison with Experiment," in *Institute of Nuclear Materials Management*, 2011.
- [108] D. L. Chichester, J. D. Simpson, and M. Lemchak, "Advanced compact accelerator neutron generator technology for active neutron interrogation field work," *Journal of Radioanalytical and Nuclear Chemistry*, vol. 271, pp. 629-637, March 01 2007.

APPENDICES

Appendix A: Example Data Files

Example MCNP6 Input Deck

MCNP6 Updating the ORNL Shuffler

c

c GENERAL INFO

c

c This is the most complete version of the Shuffler and the base for

c all my dissertation work...I also reduced the universe to a smaller

c sphere in hopes of speeding things up.

c

c ***** Detector Banks *****

c

c Right side: 7 tubes, 39" active length, 4 atm

c Right Rear: 6 tubes, 39" active length, 4 atm

c Right door: 7 tubes, 39" active length, 4 atm

c Left side: 7 tubes, 39" active length, 4 atm

c Left rear: 6 tubes, 39" active length, 4 atm

c Left door: 7 tubes, 39" active length, 4 atm

c Top: 12 tubes, 26" active length, 4 atm

c Bottom: 12 tubes, 26" active length, 4 atm

c

c ***** All tubes: 1" outer diameter w/ 0.01" SS clad around *****

c *****

c

c

c

c *****

c *****

Cells

c *****

c *****

Cells are organized by bank

c

c

c

c

c

```

c ***** Right Side Bank *****
c
c ***** 7 He-3 tubes, 39" active length *****
c
c
c
c
c -----
c   He-3 tubes in RSB - active region
c *****
101 3 -0.00165  -101 11 -12  imp:n=1  $ 1st (bottom) tube
102 like 101 but *trcl=(0 5.92582  0)  $ 2nd tube up
103 like 101 but *trcl=(0 11.85164  0)  $ 3rd tube up
104 like 101 but *trcl=(0 17.77746  0)  $ 4th tube up
105 like 101 but *trcl=(0 23.70328  0)  $ 5th tube up
106 like 101 but *trcl=(0 29.6291  0)  $ 6th tube up
107 like 101 but *trcl=(0 35.55492  0)  $ 7th tube up
c
c -----
c   RSB: He-3 in bottom inactive region (0.82")
c *****
801 3 -0.00165  -101 811 -11  imp:n=1  $ 1st (bottom) tube
802 like 801 but *trcl=(0 5.92582  0)  $ 2nd tube up
803 like 801 but *trcl=(0 11.85164  0)  $ 3rd tube up
804 like 801 but *trcl=(0 17.77746  0)  $ 4th tube up
805 like 801 but *trcl=(0 23.70328  0)  $ 5th tube up
806 like 801 but *trcl=(0 29.6291  0)  $ 6th tube up
807 like 801 but *trcl=(0 35.55492  0)  $ 7th tube up
c
c -----
c   RSB: He-3 in top inactive region (1.24")
c *****
701 3 -0.00165  -101 -812 12  imp:n=1  $ 1st (bottom) tube
702 like 701 but *trcl=(0 5.92582  0)  $ 2nd tube up
703 like 701 but *trcl=(0 11.85164  0)  $ 3rd tube up
704 like 701 but *trcl=(0 17.77746  0)  $ 4th tube up
705 like 701 but *trcl=(0 23.70328  0)  $ 5th tube up
706 like 701 but *trcl=(0 29.6291  0)  $ 6th tube up
707 like 701 but *trcl=(0 35.55492  0)  $ 7th tube up
c
c -----
c   RSB: SS tubes/cladding (0.01")

```

```

c *****
401 16 -7.87 -102 13 -14 #101 #801 #701 imp:n=1      $ 1st (bottom) tube
402 like 401 but #102 #802 #702 *trcl=(0 5.92582 0) $ 2nd tube up
403 like 401 but #103 #803 #703 *trcl=(0 11.85164 0) $ 3rd tube up
404 like 401 but #104 #804 #704 *trcl=(0 17.77746 0) $ 4th tube up
405 like 401 but #105 #805 #705 *trcl=(0 23.70328 0) $ 5th tube up
406 like 401 but #106 #806 #706 *trcl=(0 29.6291 0) $ 6th tube up
407 like 401 but #107 #807 #707 *trcl=(0 35.55492 0) $ 7th tube up
c
c -----
c   RSB: Air gaps b/w detectors and poly
c *****
201 1 -0.00119 -201 391 -392 #101 #401 #801 #701 imp:n=1  $ 1st (bottom) tube
202 like 201 but #102 #402 #802 #702 *trcl=(0 5.92582 0) $ 2nd tube
203 like 201 but #103 #403 #803 #703 *trcl=(0 11.85164 0) $ 3rd tube
204 like 201 but #104 #404 #804 #704 *trcl=(0 17.77746 0) $ 4th tube
205 like 201 but #105 #405 #805 #705 *trcl=(0 23.70328 0) $ 5th tube
206 like 201 but #106 #406 #806 #706 *trcl=(0 29.6291 0) $ 6th tube
207 like 201 but #107 #407 #807 #707 *trcl=(0 35.55492 0) $ 7th tube
c
c -----
c   RSB: Poly Box(mod) (4" thick, 16" wide, 42.47" long)
c *****
301 4 -0.95 -301 302 303 -304 391 -392          $ Everything inside the poly
    #201 #202 #203 #204 #205 #206 #207          $ box except the active and
    #101 #102 #103 #104 #105 #106 #107          $ inactive tube regions, the
    #401 #402 #403 #404 #405 #406 #407          $ SS cladding, and the air gap
    #801 #802 #803 #804 #805 #806 #807
    #701 #702 #703 #704 #705 #706 #707 imp:n=1
c
c -----
c   RSB: Junction Box
c *****
3010 13 -2.702 -301 302 303 -304 -663 392 3010 imp:n=1  $ Outer junction box case
3011 1 -0.00119 -3010 imp:n=1          $ Air inside junction box
c
c -----
c   RSB: Cd in front of bank
c *****
601 9 -8.65 3610 -302 303 -304 1 -663 imp:n=1  $ Cd liner on RSB
c
c -----

```

c RSB: SS layer on bank
c *****
c 701 1 -0.00119 -361 799 303 -304 1 -663 imp:n=1 \$ changed to air, SS liner is part
of insert now

c
c -----
c RSB: Outer poly shielding

c *****
31 4 -0.95 31 301 -30 -32 -381 1 -45 imp:n=1 \$ Outer shielding

c
c
c
c

c

c ***** Right Rear Bank *****

c
c ***** 6 He-3 tubes, 39" active length *****

c

c
c
c -----

c He-3 tubes in RRB - active region

c *****
111 like 101 but *trcl=(-3.3122360 42.24824 0) \$ 1st tube (bottom, right)
112 like 101 but *trcl=(-8.3116240 45.42967 0) \$ 2nd tube up/left
113 like 101 but *trcl=(-13.311012 48.61110 0) \$ 3rd tube up/left
114 like 101 but *trcl=(-18.310397 51.79252 0) \$ 4th tube up/left
115 like 101 but *trcl=(-23.309784 54.97395 0) \$ 5th tube up/left
116 like 101 but *trcl=(-28.309170 58.15538 0) \$ 6th tube up/left

c
c -----

c RRB: He-3 in bottom inactive region (0.82")

c *****
811 like 801 but *trcl=(-3.3122360 42.24824 0) \$ 1st tube (bottom, right)
812 like 801 but *trcl=(-8.3116240 45.42967 0) \$ 2nd tube up/left
813 like 801 but *trcl=(-13.311012 48.61110 0) \$ 3rd tube up/left
814 like 801 but *trcl=(-18.310397 51.79252 0) \$ 4th tube up/left
815 like 801 but *trcl=(-23.309784 54.97395 0) \$ 5th tube up/left
816 like 801 but *trcl=(-28.309170 58.15538 0) \$ 6th tube up/left

```

c
c -----
c   RRB: He-3 in top inactive reigion (1.24")
c *****
711 like 701 but *trcl=(-3.3122360 42.24824 0) $ 1st tube (bottom, right)
712 like 701 but *trcl=(-8.3116240 45.42967 0) $ 2nd tube up/left
713 like 701 but *trcl=(-13.311012 48.61110 0) $ 3rd tube up/left
714 like 701 but *trcl=(-18.310397 51.79252 0) $ 4th tube up/left
715 like 701 but *trcl=(-23.309784 54.97395 0) $ 5th tube up/left
716 like 701 but *trcl=(-28.309170 58.15538 0) $ 6th tube up/left
c
c -----
c   RRB: SS tubes tubes/cladding (0.01")
c *****
411 like 401 but #111 #811 #711 *trcl=(-3.3122360 42.24824 0) $ 1st tube (bottom,
right)
412 like 401 but #112 #812 #712 *trcl=(-8.3116240 45.42967 0) $ 2nd tube up/left
413 like 401 but #113 #813 #713 *trcl=(-13.311012 48.61110 0) $ 3rd tube up/left
414 like 401 but #114 #814 #714 *trcl=(-18.310397 51.79252 0) $ 4th tube up/left
415 like 401 but #115 #815 #715 *trcl=(-23.309784 54.97395 0) $ 5th tube up/left
416 like 401 but #116 #816 #716 *trcl=(-28.309170 58.15538 0) $ 6th tube up/left
c
c -----
c   RRB: Air gaps b/w detectors and poly
c *****
211 like 201 but #111 #411 #811 #711 *trcl=(-3.3122360 42.24824 0) $ 1st
(bottom/right) tube
212 like 201 but #112 #412 #812 #712 *trcl=(-8.3116240 45.42967 0) $ 2nd tube
213 like 201 but #113 #413 #813 #713 *trcl=(-13.311012 48.61110 0) $ 3rd tube
214 like 201 but #114 #414 #814 #714 *trcl=(-18.310397 51.79252 0) $ 4th tube
215 like 201 but #115 #415 #815 #715 *trcl=(-23.309784 54.97395 0) $ 5th tube
216 like 201 but #116 #416 #816 #716 *trcl=(-28.309170 58.15538 0) $ 6th tube
c
c -----
c   RRB: Poly Box (4" thick, 16" wide, 42.47" long)
c *****
311 4 -0.95 -311 312 -313 314 -381 391 -392          $ Everything inside the poly
#211 #212 #213 #214 #215 #216          $ box except the active and
#111 #112 #113 #114 #115 #116          $ inactive tube regions, the
#411 #412 #413 #414 #415 #416          $ SS cladding, and the air gap
#711 #712 #713 #714 #715 #716
#811 #812 #813 #814 #815 #816 imp:n=1

```

c
c -----
c RRB: Junction Box
c *****
3110 13 -2.702 -311 312 -313 -315 -663 392 #3111 imp:n=1 \$ Outer junction box
3111 1 -0.00119 -3110 3111 -3112 -3113 3114 -3115 imp:n=1 \$ Air inside junction

c
c -----
c RRB: Cd in front of bank
c *****
611 9 -8.65 314 304 611 -312 1 -663 imp:n=1 \$ Cd on RR bank

c
c -----
c RRB: SS layer in front of bank
c *****
c 711 1 -0.00119 314 304 -611 711 1 -663 imp:n=1 \$ changed to air!!! SS on RR
bank

c
c
c

—
c

*
c ***** Right Door Bank *****

c
c ***** 7 He-3 tubes, 39" active length *****

c

*
c
c

c -----
c He-3 tubes in RDB

c *****
121 like 101 but *trcl=(-6.216533 -8.18 0) \$ 1st tube (top/right)
122 like 101 but *trcl=(-11.0572058 -11.59807 0) \$ 2nd tube down/left
123 like 101 but *trcl=(-15.8978794 -15.01615 0) \$ 3rd tube down/left
124 like 101 but *trcl=(-20.738553 -18.43422 0) \$ 4th tube down/left
125 like 101 but *trcl=(-25.5792266 -21.85229 0) \$ 5th tube down/left
126 like 101 but *trcl=(-30.4199 -25.27037 0) \$ 6th tube down/left

127 like 101 but *trcl=(-35.2605737 -28.68844 0) \$ 7th tube down/left

c

c -----

c RDB: He-3 in bottom inactive region (0.82")

c *****

- 821 like 801 but *trcl=(-6.216533 -8.18 0) \$ 1st tube (top/right)
- 822 like 801 but *trcl=(-11.0572058 -11.59807 0) \$ 2nd tube down/left
- 823 like 801 but *trcl=(-15.8978794 -15.01615 0) \$ 3rd tube down/left
- 824 like 801 but *trcl=(-20.738553 -18.43422 0) \$ 4th tube down/left
- 825 like 801 but *trcl=(-25.5792266 -21.85229 0) \$ 5th tube down/left
- 826 like 801 but *trcl=(-30.4199 -25.27037 0) \$ 6th tube down/left
- 827 like 801 but *trcl=(-35.2605737 -28.68844 0) \$ 7th tube down/left

c

c -----

c RDB: He-3 in top inactive region (1.24")

c *****

- 721 like 701 but *trcl=(-6.216533 -8.18 0) \$ 1st tube (top/right)
- 722 like 701 but *trcl=(-11.0572058 -11.59807 0) \$ 2nd tube down/left
- 723 like 701 but *trcl=(-15.8978794 -15.01615 0) \$ 3rd tube down/left
- 724 like 701 but *trcl=(-20.738553 -18.43422 0) \$ 4th tube down/left
- 725 like 701 but *trcl=(-25.5792266 -21.85229 0) \$ 5th tube down/left
- 726 like 701 but *trcl=(-30.4199 -25.27037 0) \$ 6th tube down/left
- 727 like 701 but *trcl=(-35.2605737 -28.68844 0) \$ 7th tube down/left

c

c -----

c RDB: SS tubes tubes/cladding (0.01")

c *****

- 421 like 401 but #121 #821 #721 *trcl=(-6.216533 -8.18 0) \$ 1st tube (top/right)
- 422 like 401 but #122 #822 #722 *trcl=(-11.0572058 -11.59807 0) \$ 2nd tube down/left
- 423 like 401 but #123 #823 #723 *trcl=(-15.8978794 -15.01615 0) \$ 3rd tube down/left
- 424 like 401 but #124 #824 #724 *trcl=(-20.738553 -18.43422 0) \$ 4th tube down/left
- 425 like 401 but #125 #825 #725 *trcl=(-25.5792266 -21.85229 0) \$ 5th tube down/left
- 426 like 401 but #126 #826 #726 *trcl=(-30.4199 -25.27037 0) \$ 6th tube down/left
- 427 like 401 but #127 #827 #727 *trcl=(-35.2605737 -28.68844 0) \$ 7th tube down/left

c

c -----

c RDB: Air gaps b/w detectors and poly

c *****

- 221 like 201 but #121 #421 #821 #721 *trcl=(-6.216533 -8.18 0) \$ 1st (top/right)
- 222 like 201 but #122 #422 #822 #722 *trcl=(-11.0572058 -11.59807 0) \$ 2nd tube
- 223 like 201 but #123 #423 #823 #723 *trcl=(-15.8978794 -15.01615 0) \$ 3rd tube

224 like 201 but #124 #424 #824 #724 *trcl=(-20.738553 -18.43422 0) \$ 4th tube
 225 like 201 but #125 #425 #825 #725 *trcl=(-25.5792266 -21.85229 0) \$ 5th tube
 226 like 201 but #126 #426 #826 #726 *trcl=(-30.4199 -25.27037 0) \$ 6th tube
 227 like 201 but #127 #427 #827 #727 *trcl=(-35.2605737 -28.68844 0) \$ 7th tube

c

c -----

c RDB: Poly Box (4" thick, 16" wide, 42.47" long)

c *****

321 4 -0.95 -321 322 623 -324 391 -392 \$ Everything inside the poly
 #221 #222 #223 #224 #225 #226 #227 \$ box except the active and
 #121 #122 #123 #124 #125 #126 #127 \$ inactive tube regions, the
 #421 #422 #423 #424 #425 #426 #427 \$ SS cladding, and the air gap
 #721 #722 #723 #724 #725 #726 #727
 #821 #822 #823 #824 #825 #826 #827 imp:n=1

c

c RDB: Junction Box

c *****

3210 13 -2.702 -321 322 -325 -324 -663 392 #3211 imp:n=1 \$ Outer junction box
 case
 3211 1 -0.00119 -3210 3211 -3212 -3213 3114 -3115 imp:n=1 \$ Air inside
 junction box

c

c -----

c RDB: Cd in front bank

c *****

621 9 -8.65 -303 37 -322 621 1 -663 imp:n=1 \$ Cd on LD bank
 622 9 -8.65 -622 37 -321 322 1 -663 imp:n=1 \$ Cd on side of door
 623 9 -8.65 -321 322 -323 -623 -301 1 -663 imp:n=1 \$ Cd on inner side

c

c -----

c RDB: SS layer in front of bank

c *****

1721 16 -7.87 -303 37 721 -621 1 -663 imp:n=1 \$ SS on LD bank

c

c -----

c RDB: Outer poly shielding behind RDB

c *****

32 4 -0.95 -31 -30 -38 36 37 321 1 -663 imp:n=1 \$ Outer shielding
 3232 4 -0.95 663 -45 -31 -30 361 321 -38 imp:n=1 \$ Outer shielding extending up
 (part 1)
 3233 4 -0.95 663 -45 -684 -361 37 36 321 -38 imp:n=1 \$ Outer shielding extending up
 (part 2)

c
 42 4 -0.95 -301 -381 (311:383) 1 -663 imp:n=1 \$ Poly wedge behing RRB
 4242 4 -0.95 663 -45 361 -381 (311:383) -301 imp:n=1 \$ Poly wedge extending up
 (part 1)
 4243 4 -0.95 663 -45 -361 364 -381 311 imp:n=1 \$ Poly wedge extending up (part
 2) !!!
 c
 52 4 -0.95 324 322 622 -321 1 -663 imp:n=1 \$ Poly triangle at RD opening
 c
 c
 c

c

 c ***** Left Side Bank *****
 c
 c ***** 7 He-3 tubes, 39" active length *****
 c

 c
 c

c -----
 c He-3 tubes in LSB
 c *****
 131 like 101 but *trcl=(-83.9724 0 0) \$ 1st tube (bottom)
 132 like 101 but *trcl=(-83.9724 5.92582 0) \$ 2nd tube up
 133 like 101 but *trcl=(-83.9724 11.85164 0) \$ 3rd tube up
 134 like 101 but *trcl=(-83.9724 17.77746 0) \$ 4th tube up
 135 like 101 but *trcl=(-83.9724 23.70328 0) \$ 5th tube up
 136 like 101 but *trcl=(-83.9724 29.6291 0) \$ 6th tube up
 137 like 101 but *trcl=(-83.9724 35.55492 0) \$ 7th tube up
 c

c -----
 c LSB: He-3 in bottom inactive region (0.82")
 c *****
 831 like 801 but *trcl=(-83.9724 0 0) \$ 1st tube (bottom)
 832 like 801 but *trcl=(-83.9724 5.92582 0) \$ 2nd tube up
 833 like 801 but *trcl=(-83.9724 11.85164 0) \$ 3rd tube up
 834 like 801 but *trcl=(-83.9724 17.77746 0) \$ 4th tube up
 835 like 801 but *trcl=(-83.9724 23.70328 0) \$ 5th tube up
 836 like 801 but *trcl=(-83.9724 29.6291 0) \$ 6th tube up
 837 like 801 but *trcl=(-83.9724 35.55492 0) \$ 7th tube up

```

c
c -----
c   LSB: He-3 in top inactive region (1.24")
c *****
731 like 701 but *trcl=(-83.9724 0 0) $ 1st tube (bottom)
732 like 701 but *trcl=(-83.9724 5.92582 0) $ 2nd tube up
733 like 701 but *trcl=(-83.9724 11.85164 0) $ 3rd tube up
734 like 701 but *trcl=(-83.9724 17.77746 0) $ 4th tube up
735 like 701 but *trcl=(-83.9724 23.70328 0) $ 5th tube up
736 like 701 but *trcl=(-83.9724 29.6291 0) $ 6th tube up
737 like 701 but *trcl=(-83.9724 35.55492 0) $ 7th tube up
c
c -----
c   LSB: SS tubes tubes/cladding (0.01")
c *****
431 like 401 but #131 #831 #731 *trcl=(-83.9724 0 0) $ 1st tube (bottom)
432 like 401 but #132 #832 #732 *trcl=(-83.9724 5.92582 0) $ 2nd tube up
433 like 401 but #133 #833 #733 *trcl=(-83.9724 11.85164 0) $ 3rd tube up
434 like 401 but #134 #834 #734 *trcl=(-83.9724 17.77746 0) $ 4th tube up
435 like 401 but #135 #835 #735 *trcl=(-83.9724 23.70328 0) $ 5th tube up
436 like 401 but #136 #836 #736 *trcl=(-83.9724 29.6291 0) $ 6th tube up
437 like 401 but #137 #837 #737 *trcl=(-83.9724 35.55492 0) $ 7th tube up
c
c -----
c   LSB: Air gaps b/w detectors and poly
c *****
231 like 201 but #131 #431 #831 #731 *trcl=(-83.9724 0 0) $ 1st (bottom) tube
232 like 201 but #132 #432 #832 #732 *trcl=(-83.9724 5.92582 0) $ 2nd tube
233 like 201 but #133 #433 #833 #733 *trcl=(-83.9724 11.85164 0) $ 3rd tube
234 like 201 but #134 #434 #834 #734 *trcl=(-83.9724 17.77746 0) $ 4th tube
235 like 201 but #135 #435 #835 #735 *trcl=(-83.9724 23.70328 0) $ 5th tube
236 like 201 but #136 #436 #836 #736 *trcl=(-83.9724 29.6291 0) $ 6th tube
237 like 201 but #137 #437 #837 #737 *trcl=(-83.9724 35.55492 0) $ 7th tube
c
c -----
c   LSB: Poly Box (4" thick, 16" wide, 42.47" long)
c *****
331 4 -0.95 331 -332 303 -304 391 -392          $ Everything inside the poly
    #231 #232 #233 #234 #235 #236 #237          $ box except the active and
    #131 #132 #133 #134 #135 #136 #137          $ inactive tube regions, the
    #431 #432 #433 #434 #435 #436 #437          $ SS cladding, and the air gap
    #831 #832 #833 #834 #835 #836 #837

```

```

#731 #732 #733 #734 #735 #736 #737 imp:n=1
c
c -----
c   LSB: Junction Box
c *****
3310 13 -2.702 331 -332 303 -304 -663 392 3310 imp:n=1 $ Outer junction box case
3311 1 -0.00119 -3310 imp:n=1 $ Air inside junction box
c
c -----
c   LSB: Cd in front of bank
c *****
631 9 -8.65 332 -3620 303 -304 1 -663 imp:n=1 $ Cd on RS bank
c
c -----
c   LSB: SS layer on bank
c *****
c 731 1 -0.00119 -731 362 303 -304 1 -663 imp:n=1 $ changed to air!!! SS on RS
bank
c
c -----
c   LSB: Outer poly shielding
c *****
33 4 -0.95 31 -331 33 -34 -381 1 -45 imp:n=1
c
c
c

```

```

c
*****
c ***** Left Rear Bank *****
c
c ***** 6 He-3 tubes, 39" active length *****
c
*****
c
c
c -----
c   He-3 tubes in LRB
c *****
141 like 101 but *trcl=(-80.660164 42.24824 0) $ 1st tube (bottom/left)
142 like 101 but *trcl=(-75.660776 45.42967 0) $ 2nd tube (up/right)
143 like 101 but *trcl=(-70.661388 48.61110 0) $ 3rd tube (up/right)

```

144 like 101 but *trcl=(-65.662003 51.79252 0) \$ 4th tube (up/right)
145 like 101 but *trcl=(-60.662616 54.97395 0) \$ 5th tube (up/right)
146 like 101 but *trcl=(-55.663230 58.15538 0) \$ 6th tube (up/right)

c

c -----

c LRB: He-3 in bottom inactive region (0.82")

c *****

841 like 801 but *trcl=(-80.660164 42.24824 0) \$ 1st tube (bottom/left)
842 like 801 but *trcl=(-75.660776 45.42967 0) \$ 2nd tube (up/right)
843 like 801 but *trcl=(-70.661388 48.61110 0) \$ 3rd tube (up/right)
844 like 801 but *trcl=(-65.662003 51.79252 0) \$ 4th tube (up/right)
845 like 801 but *trcl=(-60.662616 54.97395 0) \$ 5th tube (up/right)
846 like 801 but *trcl=(-55.663230 58.15538 0) \$ 6th tube (up/right)

c

c -----

c LRB: He-3 in top inactive region (1.24")

c *****

741 like 701 but *trcl=(-80.660164 42.24824 0) \$ 1st tube (bottom/left)
742 like 701 but *trcl=(-75.660776 45.42967 0) \$ 2nd tube (up/right)
743 like 701 but *trcl=(-70.661388 48.61110 0) \$ 3rd tube (up/right)
744 like 701 but *trcl=(-65.662003 51.79252 0) \$ 4th tube (up/right)
745 like 701 but *trcl=(-60.662616 54.97395 0) \$ 5th tube (up/right)
746 like 701 but *trcl=(-55.663230 58.15538 0) \$ 6th tube (up/right)

c

c -----

c LRB: SS tubes tubes/cladding (0.01")

c *****

441 like 401 but #141 #841 #741 *trcl=(-80.660164 42.24824 0) \$ 1st tube
(bottom/left)
442 like 401 but #142 #842 #742 *trcl=(-75.660776 45.42967 0) \$ 2nd tube (up/right)
443 like 401 but #143 #843 #743 *trcl=(-70.661388 48.61110 0) \$ 3rd tube (up/right)
444 like 401 but #144 #844 #744 *trcl=(-65.662003 51.79252 0) \$ 4th tube (up/right)
445 like 401 but #145 #845 #745 *trcl=(-60.662616 54.97395 0) \$ 5th tube (up/right)
446 like 401 but #146 #846 #746 *trcl=(-55.663230 58.15538 0) \$ 6th tube (up/right)

c

c -----

c LRB: Air gaps b/w detectors and poly

c *****

241 like 201 but #141 #441 #841 #741 *trcl=(-80.660164 42.24824 0) \$ 1st
(bottom/left) tube
242 like 201 but #142 #442 #842 #742 *trcl=(-75.660776 45.42967 0) \$ 2nd tube
243 like 201 but #143 #443 #843 #743 *trcl=(-70.661388 48.61110 0) \$ 3rd tube

244 like 201 but #144 #444 #844 #744 *trcl=(-65.662003 51.79252 0) \$ 4th tube
245 like 201 but #145 #445 #845 #745 *trcl=(-60.662616 54.97395 0) \$ 5th tube
246 like 201 but #146 #446 #846 #746 *trcl=(-55.663230 58.15538 0) \$ 6th tube

c

c -----

c LRB: Poly Box (4" thick, 16" wide, 42.47" long)

c *****

341 4 -0.95 -341 342 -343 -344 -381 391 -392 \$ Everything inside the poly
#241 #242 #243 #244 #245 #246 \$ box except the active and
#141 #142 #143 #144 #145 #146 \$ inactive tube regions, the
#441 #442 #443 #444 #445 #446 \$ SS cladding, and the air gap
#841 #842 #843 #844 #845 #846
#741 #742 #743 #744 #745 #746 imp:n=1

c

c -----

c LRB: Junction Box

c *****

3410 13 -2.702 -341 342 -344 -345 -663 392 #3411 imp:n=1 \$ Outer junction box
case
3411 1 -0.00119 -3410 3411 -3412 -3413 3114 -3115 imp:n=1 \$ Air inside
junction box

c

c -----

c LRB: Cd in front of bank

c *****

641 9 -8.65 304 -343 -342 641 1 -663 imp:n=1 \$ Cd on LR bank

c

c -----

c LRB: SS layer on bank

c *****

c 741 1 -0.00119 304 -343 741 -641 1 -663 imp:n=1 \$ changed to air!!! SS on LR
bank

c

c -----

c LRB: Outer poly shielding behind LRB and RRD

c *****

34 4 -0.95 -35 -34 -32 381 1 -45 imp:n=1

c

c

c

```

c
*****
c ***** Left Door Bank *****
c
c ***** 7 He-3 tubes, 39" active length *****
c
*****
c
c
c -----
c   He-3 tubes in LDB
c *****
151 like 101 but *trcl=(-77.755867 -8.18 0) $ 1st tube (top/left)
152 like 101 but *trcl=(-72.9151942 -11.59807 0) $ 2nd tube (down/right)
153 like 101 but *trcl=(-68.0745206 -15.01615 0) $ 3rd tube (down/right)
154 like 101 but *trcl=(-63.233847 -18.43422 0) $ 4th tube (down/right)
155 like 101 but *trcl=(-58.3931734 -21.85229 0) $ 5th tube (down/right)
156 like 101 but *trcl=(-53.5525 -25.27037 0) $ 6th tube (down/right)
157 like 101 but *trcl=(-48.7118263 -28.68844 0) $ 7th tube (down/right)
c
c -----
c   LDB: He-3 in bottom inactive region (0.82")
c *****
851 like 801 but *trcl=(-77.755867 -8.18 0) $ 1st tube (top/left)
852 like 801 but *trcl=(-72.9151942 -11.59807 0) $ 2nd tube (down/right)
853 like 801 but *trcl=(-68.0745206 -15.01615 0) $ 3rd tube (down/right)
854 like 801 but *trcl=(-63.233847 -18.43422 0) $ 4th tube (down/right)
855 like 801 but *trcl=(-58.3931734 -21.85229 0) $ 5th tube (down/right)
856 like 801 but *trcl=(-53.5525 -25.27037 0) $ 6th tube (down/right)
857 like 801 but *trcl=(-48.7118263 -28.68844 0) $ 7th tube (down/right)
c
c -----
c   LDB: He-3 in top inactive region (1.24")
c *****
751 like 701 but *trcl=(-77.755867 -8.18 0) $ 1st tube (top/left)
752 like 701 but *trcl=(-72.9151942 -11.59807 0) $ 2nd tube (down/right)
753 like 701 but *trcl=(-68.0745206 -15.01615 0) $ 3rd tube (down/right)
754 like 701 but *trcl=(-63.233847 -18.43422 0) $ 4th tube (down/right)
755 like 701 but *trcl=(-58.3931734 -21.85229 0) $ 5th tube (down/right)
756 like 701 but *trcl=(-53.5525 -25.27037 0) $ 6th tube (down/right)
757 like 701 but *trcl=(-48.7118263 -28.68844 0) $ 7th tube (down/right)
c

```

```

c -----
c   LDB: SS tubes tubes/cladding (0.01")
c *****
451 like 401 but #151 #851 #751 *trcl=(-77.755867 -8.18 0) $ 1st tube (top/left)
452 like 401 but #152 #852 #752 *trcl=(-72.9151942 -11.59807 0) $ 2nd tube
(down/right)
453 like 401 but #153 #853 #753 *trcl=(-68.0745206 -15.01615 0) $ 3rd tube
(down/right)
454 like 401 but #154 #854 #754 *trcl=(-63.233847 -18.43422 0) $ 4th tube
(down/right)
455 like 401 but #155 #855 #755 *trcl=(-58.3931734 -21.85229 0) $ 5th tube
(down/right)
456 like 401 but #156 #856 #756 *trcl=(-53.5525 -25.27037 0) $ 6th tube
(down/right)
457 like 401 but #157 #857 #757 *trcl=(-48.7118263 -28.68844 0) $ 7th tube
(down/right)

```

```

c -----
c   LDB: Air gaps b/w detectors and poly
c *****
251 like 201 but #151 #451 #851 #751 *trcl=(-77.755867 -8.18 0) $ 1st (top/left)
tube
252 like 201 but #152 #452 #852 #752 *trcl=(-72.9151942 -11.59807 0) $ 2nd tube
253 like 201 but #153 #453 #853 #753 *trcl=(-68.0745206 -15.01615 0) $ 3rd tube
254 like 201 but #154 #454 #854 #754 *trcl=(-63.233847 -18.43422 0) $ 4th tube
255 like 201 but #155 #455 #855 #755 *trcl=(-58.3931734 -21.85229 0) $ 5th tube
256 like 201 but #156 #456 #856 #756 *trcl=(-53.5525 -25.27037 0) $ 6th tube
257 like 201 but #157 #457 #857 #757 *trcl=(-48.7118263 -28.68844 0) $ 7th tube

```

```

c -----
c   LDB: Poly Box (4" thick, 16" wide, 42.47" long)
c *****
351 4 -0.95 -351 352 -353 653 391 -392          $ Everything inside the poly
    #251 #252 #253 #254 #255 #256 #257          $ box except the active and
    #151 #152 #153 #154 #155 #156 #157          $ inactive tube regions, the
    #451 #452 #453 #454 #455 #456 #457          $ SS cladding, and the air gap
    #851 #852 #853 #854 #855 #856 #857
    #751 #752 #753 #754 #755 #756 #757 imp:n=1

```

```

c -----
c   LDB: Junction Box
c *****

```

```

3510 13 -2.702 -351 352 -355 -353 -663 392 #3511 imp:n=1 $ Outer junction box
case
3511 1 -0.00119 -3510 3511 -3512 -3513 3114 -3115 imp:n=1 $ Air inside
junction box
c
c -----
c LDB: Cd in front of bank
c *****
651 9 -8.65 -303 -37 -352 651 1 -663 imp:n=1 $ Cd on LD bank
652 9 -8.65 652 -37 -351 352 1 -663 imp:n=1 $ Cd on side of door
653 9 -8.65 -351 352 -653 -354 1 -663 331 imp:n=1 $ Cd on inner side of door
c
c -----
c LDB: SS layer on bank
c *****
1751 16 -7.87 -303 -37 751 -651 1 -663 imp:n=1 $ SS on LD bank
c
c -----
c LDB: Outer poly shielding
c *****
35 4 -0.95 -31 351 -37 36 -39 33 1 -663 imp:n=1 $ Outer shielding
3535 4 -0.95 663 -45 -31 33 -362 -39 351 imp:n=1 $ Outer shielding extending up
(part 1)
3536 4 -0.95 663 -45 -684 36 -37 362 -39 351 imp:n=1 $ Outer shielding extending up
(part 2)
c
45 4 -0.95 331 -381 (341:384) 1 -663 imp:n=1 $ Poly wedge behing LRB
4545 4 -0.95 663 -45 331 -362 -381 (341:384) imp:n=1 $ Poly wedge extending up
(part 1)
4546 4 -0.95 663 -45 362 364 -381 341 imp:n=1 $ Poly wedge extending up (part
1) !!!!
c
55 4 -0.95 353 352 -351 -652 1 -663 imp:n=1 $ Poly triangle at LD opening
c
c
c
c

```

```

c
*****
**

```

```

c ***** Top Bank
*****
c
c ***** 12 He-3 tubes, 26" active length *****
c
*****
**
c
c
c -----
c   He-3 tubes in top bank
c *****
161 3 -0.00165  -161 61 -62  imp:n=1  $ 1st (left) tube
162 like 161 but *trcl=( 6.005288 0 0) $ 2nd tube
163 like 161 but *trcl=(12.010576 0 0) $ 3rd tube
164 like 161 but *trcl=(18.015864 0 0) $ 4th tube
165 like 161 but *trcl=(24.021152 0 0) $ 5th tube
166 like 161 but *trcl=(30.026440 0 0) $ 6th tube
167 like 161 but *trcl=(36.031728 0 0) $ 7th tube
168 like 161 but *trcl=(42.037016 0 0) $ 8th tube
169 like 161 but *trcl=(48.042304 0 0) $ 9th tube
170 like 161 but *trcl=(54.047592 0 0) $ 10th tube
171 like 161 but *trcl=(60.052880 0 0) $ 11th tube
172 like 161 but *trcl=(66.058168 0 0) $ 12th tube
c
c -----
c   Top: He-3 in bottom inactive region (0.82")
c *****
861 3 -0.00165  -161 -864 62  imp:n=1  $ 1st (left) tube
862 like 861 but *trcl=( 6.005288 0 0) $ 2nd tube
863 like 861 but *trcl=(12.010576 0 0) $ 3rd tube
864 like 861 but *trcl=(18.015864 0 0) $ 4th tube
865 like 861 but *trcl=(24.021152 0 0) $ 5th tube
866 like 861 but *trcl=(30.026440 0 0) $ 6th tube
867 like 861 but *trcl=(36.031728 0 0) $ 7th tube
868 like 861 but *trcl=(42.037016 0 0) $ 8th tube
869 like 861 but *trcl=(48.042304 0 0) $ 9th tube
870 like 861 but *trcl=(54.047592 0 0) $ 10th tube
871 like 861 but *trcl=(60.052880 0 0) $ 11th tube
872 like 861 but *trcl=(66.058168 0 0) $ 12th tube
c
c -----

```

c Top: He-3 in top inactive region (1.24")

c *****

761 3 -0.00165 -161 -61 863 imp:n=1 \$ 1st (left) tube
762 like 761 but *trcl=(6.005288 0 0) \$ 2nd tube
763 like 761 but *trcl=(12.010576 0 0) \$ 3rd tube
764 like 761 but *trcl=(18.015864 0 0) \$ 4th tube
765 like 761 but *trcl=(24.021152 0 0) \$ 5th tube
766 like 761 but *trcl=(30.026440 0 0) \$ 6th tube
767 like 761 but *trcl=(36.031728 0 0) \$ 7th tube
768 like 761 but *trcl=(42.037016 0 0) \$ 8th tube
769 like 761 but *trcl=(48.042304 0 0) \$ 9th tube
770 like 761 but *trcl=(54.047592 0 0) \$ 10th tube
771 like 761 but *trcl=(60.052880 0 0) \$ 11th tube
772 like 761 but *trcl=(66.058168 0 0) \$ 12th tube

c

c -----

c Top: SS tubes/cladding (0.01")

c *****

461 16 -7.87 -162 63 -64 #161 #861 #761 imp:n=1 \$ 1st (left) tube
462 like 461 but #162 #862 #762 *trcl=(6.005288 0 0) \$ 2nd tube
463 like 461 but #163 #863 #763 *trcl=(12.010576 0 0) \$ 3rd tube
464 like 461 but #164 #864 #764 *trcl=(18.015864 0 0) \$ 4th tube
465 like 461 but #165 #865 #765 *trcl=(24.021152 0 0) \$ 5th tube
466 like 461 but #166 #866 #766 *trcl=(30.026440 0 0) \$ 6th tube
467 like 461 but #167 #867 #767 *trcl=(36.031728 0 0) \$ 7th tube
468 like 461 but #168 #868 #768 *trcl=(42.037016 0 0) \$ 8th tube
469 like 461 but #169 #869 #769 *trcl=(48.042304 0 0) \$ 9th tube
470 like 461 but #170 #870 #770 *trcl=(54.047592 0 0) \$ 10th tube
471 like 461 but #171 #871 #771 *trcl=(60.052880 0 0) \$ 11th tube
472 like 461 but #172 #872 #772 *trcl=(66.058168 0 0) \$ 12th tube

c

c -----

c Top: Air gaps b/w detectors and poly

c *****

261 1 -0.00119 -261 363 -364 #161 #461 #861 #761 imp:n=1 \$ 1st (left) tube
262 like 261 but #162 #462 #862 #762 *trcl=(6.005288 0 0) \$ 2nd tube
263 like 261 but #163 #463 #863 #763 *trcl=(12.010576 0 0) \$ 3rd tube
264 like 261 but #164 #464 #864 #764 *trcl=(18.015864 0 0) \$ 4th tube
265 like 261 but #165 #465 #865 #765 *trcl=(24.021152 0 0) \$ 5th tube
266 like 261 but #166 #466 #866 #766 *trcl=(30.026440 0 0) \$ 6th tube
267 like 261 but #167 #467 #867 #767 *trcl=(36.031728 0 0) \$ 7th tube
268 like 261 but #168 #468 #868 #768 *trcl=(42.037016 0 0) \$ 8th tube

269 like 261 but #169 #469 #869 #769 *trcl=(48.042304 0 0) \$ 9th tube
 270 like 261 but #170 #470 #870 #770 *trcl=(54.047592 0 0) \$ 10th tube
 271 like 261 but #171 #471 #871 #771 *trcl=(60.052880 0 0) \$ 11th tube
 272 like 261 but #172 #472 #872 #772 *trcl=(66.058168 0 0) \$ 12th tube
 c
 c -----
 c Top: Poly box/moderator (4" thick, 28" wide, " long)
 c *****
 361 4 -0.95 -361 362 363 -364 365 -366 \$ Everything inside the
 poly
 #261 #262 #263 #264 #265 #266 #267 #268 #269 #270 #271 #272 \$ box except
 the active and
 #161 #162 #163 #164 #165 #166 #167 #168 #169 #170 #171 #172 \$ inactive
 tube regions, the
 #461 #462 #463 #464 #465 #466 #467 #468 #469 #470 #471 #472 \$ SS
 cladding, and the air gap
 #861 #862 #863 #864 #865 #866 #867 #868 #869 #870 #871 #872
 #761 #762 #763 #764 #765 #766 #767 #768 #769 #770 #771 #772 imp:n=1
 c
 c Top: Junction Box
 c *****
 3610 13 -2.702 -361 362 -363 684 365 -366 #3612 imp:n=1 \$ Outer junction box
 case
 3612 1 -0.00119 -3616 3611 -3612 3613 3614 -3615 imp:n=1 \$ Air inside junction
 box
 c
 c
 3611 4 -0.95 662 -45 362 363 -361 -364 imp:n=1 \$ Poly above bank
 c
 c -----
 c Top: Cd around top bank
 c *****
 661 9 -8.65 -361 362 684 -364 -365 661 imp:n=1 \$ Cd on top of top bank
 662 9 -8.65 -361 362 363 -364 366 -662 imp:n=1 \$ Cd on bottom of top bank
 c
 c -----
 c Top: SS top bank holder
 c *****
 663 16 -7.87 -361 362 363 -364 -661 663 imp:n=1 \$ SS bank holder
 c
 c

c

—

c

*

c ***** Bottom Bank *****

c

c ***** 12 He-3 tubes, 26" active length *****

c

*

c

c

c -----

c He-3 tubes in bottom bank

c *****

- 181 like 161 but *trcl=(0 0 -131.158) \$ 1st (left) tube
- 182 like 161 but *trcl=(6.005288 0 -131.158) \$ 2nd tube
- 183 like 161 but *trcl=(12.010576 0 -131.158) \$ 3rd tube
- 184 like 161 but *trcl=(18.015864 0 -131.158) \$ 4th tube
- 185 like 161 but *trcl=(24.021152 0 -131.158) \$ 5th tube
- 186 like 161 but *trcl=(30.026440 0 -131.158) \$ 6th tube
- 187 like 161 but *trcl=(36.031728 0 -131.158) \$ 7th tube
- 188 like 161 but *trcl=(42.037016 0 -131.158) \$ 8th tube
- 189 like 161 but *trcl=(48.042304 0 -131.158) \$ 9th tube
- 190 like 161 but *trcl=(54.047592 0 -131.158) \$ 10th tube
- 191 like 161 but *trcl=(60.052880 0 -131.158) \$ 11th tube
- 192 like 161 but *trcl=(66.058168 0 -131.158) \$ 12th tube

c

c -----

c Bottom: He-3 in bottom inactive region (0.82")

c *****

- 881 like 861 but *trcl=(0 0 -131.158) \$ 1st (left) tube
- 882 like 861 but *trcl=(6.005288 0 -131.158) \$ 2nd tube
- 883 like 861 but *trcl=(12.010576 0 -131.158) \$ 3rd tube
- 884 like 861 but *trcl=(18.015864 0 -131.158) \$ 4th tube
- 885 like 861 but *trcl=(24.021152 0 -131.158) \$ 5th tube
- 886 like 861 but *trcl=(30.026440 0 -131.158) \$ 6th tube
- 887 like 861 but *trcl=(36.031728 0 -131.158) \$ 7th tube
- 888 like 861 but *trcl=(42.037016 0 -131.158) \$ 8th tube
- 889 like 861 but *trcl=(48.042304 0 -131.158) \$ 9th tube

890 like 861 but *trcl=(54.047592 0 -131.158) \$ 10th tube
891 like 861 but *trcl=(60.052880 0 -131.158) \$ 11th tube
892 like 861 but *trcl=(66.058168 0 -131.158) \$ 12th tube

c

c -----

c Bottom: He-3 in top inactive region (1.24")

c *****

781 like 761 but *trcl=(0 0 -131.158) \$ 1st (left) tube
782 like 761 but *trcl=(6.005288 0 -131.158) \$ 2nd tube
783 like 761 but *trcl=(12.010576 0 -131.158) \$ 3rd tube
784 like 761 but *trcl=(18.015864 0 -131.158) \$ 4th tube
785 like 761 but *trcl=(24.021152 0 -131.158) \$ 5th tube
786 like 761 but *trcl=(30.026440 0 -131.158) \$ 6th tube
787 like 761 but *trcl=(36.031728 0 -131.158) \$ 7th tube
788 like 761 but *trcl=(42.037016 0 -131.158) \$ 8th tube
789 like 761 but *trcl=(48.042304 0 -131.158) \$ 9th tube
790 like 761 but *trcl=(54.047592 0 -131.158) \$ 10th tube
791 like 761 but *trcl=(60.052880 0 -131.158) \$ 11th tube
792 like 761 but *trcl=(66.058168 0 -131.158) \$ 12th tube

c

c -----

c Bottom: SS tubes/cladding (0.01")

c *****

481 like 461 but #181 #881 #781 *trcl=(0 0 -131.158) \$ 1st (left) tube
482 like 461 but #182 #882 #782 *trcl=(6.005288 0 -131.158) \$ 2nd tube
483 like 461 but #183 #883 #783 *trcl=(12.010576 0 -131.158) \$ 3rd tube
484 like 461 but #184 #884 #784 *trcl=(18.015864 0 -131.158) \$ 4th tube
485 like 461 but #185 #885 #785 *trcl=(24.021152 0 -131.158) \$ 5th tube
486 like 461 but #186 #886 #786 *trcl=(30.026440 0 -131.158) \$ 6th tube
487 like 461 but #187 #887 #787 *trcl=(36.031728 0 -131.158) \$ 7th tube
488 like 461 but #188 #888 #788 *trcl=(42.037016 0 -131.158) \$ 8th tube
489 like 461 but #189 #889 #789 *trcl=(48.042304 0 -131.158) \$ 9th tube
490 like 461 but #190 #890 #790 *trcl=(54.047592 0 -131.158) \$ 10th tube
491 like 461 but #191 #891 #791 *trcl=(60.052880 0 -131.158) \$ 11th tube
492 like 461 but #192 #892 #792 *trcl=(66.058168 0 -131.158) \$ 12th tube

c

c -----

c Bottom: Air gaps b/w detectors and poly

c *****

281 like 261 but #181 #481 #881 #781 *trcl=(0 0 -131.158) \$ 1st (left) tube
282 like 261 but #182 #482 #882 #782 *trcl=(6.005288 0 -131.158) \$ 2nd tube
283 like 261 but #183 #483 #883 #783 *trcl=(12.010576 0 -131.158) \$ 3rd tube

284 like 261 but #184 #484 #884 #784 *trcl=(18.015864 0 -131.158) \$ 4th tube
 285 like 261 but #185 #485 #885 #785 *trcl=(24.021152 0 -131.158) \$ 5th tube
 286 like 261 but #186 #486 #886 #786 *trcl=(30.026440 0 -131.158) \$ 6th tube
 287 like 261 but #187 #487 #887 #787 *trcl=(36.031728 0 -131.158) \$ 7th tube
 288 like 261 but #188 #488 #888 #788 *trcl=(42.037016 0 -131.158) \$ 8th tube
 289 like 261 but #189 #489 #889 #789 *trcl=(48.042304 0 -131.158) \$ 9th tube
 290 like 261 but #190 #490 #890 #790 *trcl=(54.047592 0 -131.158) \$ 10th tube
 291 like 261 but #191 #491 #891 #791 *trcl=(60.052880 0 -131.158) \$ 11th tube
 292 like 261 but #192 #492 #892 #792 *trcl=(66.058168 0 -131.158) \$ 12th tube

c

c -----

c Bottom: Poly box/moderator (4" thick, 28" wide, " long)

c *****

381 4 -0.95 -361 362 363 -364 -385 386 \$ Everything inside the poly
 #281 #282 #283 #284 #285 #286 #287 #288 #289 #290 #291 #292 \$ box except
 the active and
 #181 #182 #183 #184 #185 #186 #187 #188 #189 #190 #191 #192 \$ inactive tube
 regions, the
 #481 #482 #483 #484 #485 #486 #487 #488 #489 #490 #491 #492 \$ SS cladding,
 and the air gap
 #881 #882 #883 #884 #885 #886 #887 #888 #889 #890 #891 #892
 #781 #782 #783 #784 #785 #786 #787 #788 #789 #790 #791 #792 imp:n=1

c

c Bottom: Junction Box

c *****

3810 13 -2.702 -361 362 -363 684 386 -385 #3811 imp:n=1 \$ Outer junction box
 case
 3811 1 -0.00119 -3616 3611 -3612 3613 3814 -3815 imp:n=1 \$ Air inside junction
 box

c

c -----

c Bottom: Cd Around Bank

c *****

681 9 -8.65 -361 362 684 -364 385 -681 imp:n=1 \$ Cd on top of bottom bank
 682 9 -8.65 -361 362 363 -364 -386 682 imp:n=1 \$ Cd on bottom of bottom bank

c

c

c

—

c

—

c

c

c -----

c Other cells in counting chamber

c *****

20 16 -7.87 20 -21 92 -23 -1 683 imp:n=1 \$ Stainless steel turntable plate
 2020 16 -5.85 20 -21 22 -23 -683 681 imp:n=1 \$ Stainless steel turntable plate
 21 16 -7.87 382 -381 343 -314 1 -663 901 imp:n=1 \$ SS reflector around Cf guide
 tube
 22 9 -8.65 343 -314 3644 -382 1 -663 imp:n=1 \$ Cd in front of SS reflector
 23 9 -8.65 -24 25 26 1 -663 imp:n=1 \$ Cd liner around counting chamber
 24 16 -7.87 -25 27 26 1 -663 imp:n=1 \$ SS liner around counting chamber
 25 9 -8.65 -26 303 28 -29 1 -663 imp:n=1 \$ Cd liner extension on left
 26 16 -7.87 -26 303 29 -19 1 -663 imp:n=1 \$ SS liner extension on left
 27 16 -7.87 -26 303 16 -17 1 -663 imp:n=1 \$ SS liner extension on left
 28 9 -8.65 -26 303 17 -18 1 -663 imp:n=1 \$ Cd liner extension on right
 1761 16 -7.87 343 -314 -3644 761 1 -663 imp:n=1 \$ SS layer in front of reflector

c

c

c

c -----

c Concrete supports and surroundings

c *****

90 14 -2.32 (-90 93 94 -95 5 -1):(-90 93 96 -97 5 -1):
 (-90 91 94 -97 5 -1):(-92 93 94 -97 5 -1) imp:n=1 \$ Shuffler base/stand

c

c

c

c

c *****

c ***** Sources *****

c

c ***** Cell 900 is Cf in the center of the assay chamber *****

c *****

c

c

900 1 -0.00119 -900 imp:n=1 \$ Cf-252 source replaced with air

901 1 -0.00119 -901 1 -661 imp:n=1 \$ Cf-252 guide tube

902 4 -0.95 -40 41 44 -43 -42 45 imp:n=1 \$ Source storage housing (poly)

c

940 16 -7.87 1 -941 -948 947 -949 950 imp:n=1 \$ Bottom stand plate

941 16 -7.87 942 -943 -948 947 -949 950 imp:n=1 \$ Bottom stand plate

942 16 -7.87 -951 -944 943 imp:n=1 \$ Motor

943 16 -7.87 -952 -945 944 imp:n=1 \$ Axle

944 16 -7.87 -953 -946 945 imp:n=1

c

10011 13 -2.72 -10001 10002 10004 imp:n=1 \$ Al can

10012 94 -2.5 -10002 imp:n=1 \$ SNM- U3O8

10014 1 -0.00119 -10004 imp:n=1 \$ Air space

c

10020 16 -7.87 -10021 10020 imp:n=1 \$ SS shell of tube

10021 29 -10.48 -10022 imp:n=1 \$ copper heat sink

10022 17 -0.00617 -10020 #10021 imp:n=1 \$SF6 gas

c

10030 3 -0.00165 -10031 imp:n=1

10031 13 -2.72 10031 -10030 imp:n=1

10032 9 -8.65 10030 -10032 imp:n=1

c

c

c ***** Outside universe *****

c

c

c

c

c

1 1 -0.00119 -9000 900 #10011 #10012 #10014 #10020 #10021 #10022

(301:-302:-303:304:-391:392)

(311:-312:313:-314:-391:392)

(321:-322:323:324:-391:392)

(-331:332:-303:304:-391:392)

(341:-342:343:344:-391:392)

(351:-352:353:354:-391:392)

(361:-362:-363:364:-365:366)

(361:-362:-363:364:385:-386)

#20 #681 #682 #5 #661 #662 #663

#31 #33 #34 #32 #35 #42 #45 #2020


```

19 px -37.8      $ Left side SS liner
18 px 38        $ Right side Cd liner
17 px 37.9      $ Right side liner interface
16 px 37.8      $ Right side SS liner
c
8999 box -150 -200 -30.48 300 0 0 0 300 0 0 0 -15.24 $ Concrete floor
9000 sph 0 0 0 400 $ Outside universe
c
c
c

```

```

c
*****

```

```

c
c           Side banks
c
c *** A single tube is explicitly modeled with surfaces including the ***
c He-3, SS cladding, and air gaps. All other tubes in the side
c banks are modeled as cell transformations of the first tube.
c
*****

```

```

c
*****

```

```

c
c
c -----

```

```

c 1st (Bottom) He-3 tube in right side bank
c *****
101 c/z 41.9862 -17.77746 1.2446 $ 1st tube, radius = OD of He-3
11 pz 3.54 $ Bottom of active He-3 region (39" active length)
12 pz 102.6 $ Top of active He-3 region
c
811 pz 1.4572 $ Bottom of inactive region
812 pz 105.75 $ Top of inactive region
c

```

```

c -----

```

```

c SS cladding for 1st (bottom) He-3 tube
c *****
102 c/z 41.9862 -17.77746 1.27 $ 1st tube, radius = OD of SS
13 pz 1.4318 $ Bottom of SS Clad
14 pz 105.775 $ Top of SS clad
c

```

```

c -----
c   Air Gap for 1st (Bottom) He-3 Tube
c *****
201 c/z 41.9862 -17.77746 1.3462   $ 1st tube, radius = OD of air gap
c
c
c

```

```

c
c *****
*
c           Bank surfaces
c
c *****
*
c
c *****
*
c
c
c -----

```

```

c   RSB surfaces
c *****
301 px 48.26           $ Outer wall of right side bank
302 px 38.2143        $ Inner wall of right side bank
303 py -20.32         $ Bottom wall of right side bank
304 py 20.32          $ Top wall of right side bank
c                   $ Bottom wall = Surface 391
c                   $ Top wall  = Surface 392
c
3010 box 38.85 19.69 109.1438 8.78 0 0 0 -39.37 0 0 0 7.3212 $ Inner junction box
c
3610 px 38.1143       $ Cd wall layer
799 px 38.0238        $ Outer plane for SS layer
c

```

```

c -----
c   RRB surfaces
c *****
311 p 54.08022 20.32 0 54.08022 20.32 10 10.16 48.3343 0   $ Outer RRB
312 p 38.2143 20.32 0 38.2143 20.32 10 10.16 38.2143 0   $ Inner RRB
313 p 38.2143 20.32 0 38.2143 20.32 10 43.65647 28.85212 0 $ Right RRB

```



```

c
c
c -----
c   1st (Left) He-3 Tube in top bank
c *****
161 c/y -33.029084 121.134 1.2446 $ 1st tube, radius = OD of He-3
61  py -32.825          $ Bottom of active He-3 region
62  py  32.215          $ Top of active He-3 region
c
863 py -35.9746
864 py  35.2978
c
c -----
c   1st (Left) SS clad for top bank tube
c *****
162 c/y -33.029084 121.134 1.27   $ 1st tube, radius = OD of SS
63  py -36              $ Bottom of SS Clad
64  py  35.3232         $ Top of SS clad
c
c -----
c   1st (Left) Air Gap in Top Bank
c *****
261 c/y -33.029084 121.134 1.3462 $ 1st tube, radius = OD of air gap
c
c
c -----
c ***** Top bank surfaces ***** moved up
c *****
361 px  35.56          $ Right side of top bank
362 px -35.56          $ Left side of top bank
363 py -38.1           $ Bottom side of top bank
364 py  37.46          $ Upper side of top bank
3644 py  38.1          $ Upper side of top bank (old) but used for other stuff
365 pz 117.4           $ Bottom of top bank
366 pz 127.408         $ Top of top bank
c
661 pz 117.3           $ Cd bottom on top bank/top assay chamber
662 pz 127.508         $ Cd top on top bank
663 pz 117.1           $ SS bank holder slot thing
c

```


383 p 48.26 20.32 0 48.26 20.32 10 42.81 27.51 0 \$ Outer right air pocket
 384 p -48.26 20.32 0 -48.26 20.32 10 -42.81 27.51 0 \$ Outer left air pocket
 391 pz 0 \$ Bottom of poly/det banks
 392 pz 107.8738 \$ Top of poly/det banks
 393 pz 150 \$ Top of outer shields
 c
 30 px 76.2 \$ Right side shield
 31 py -25.7833 \$ Right side shield
 32 p 38.1 76.2 0 38.1 76.2 10 66.04 48.26 -10 \$ Top R RS shield
 33 px -76.2 \$ Left side shield
 34 p -38.1 76.2 0 -38.1 76.2 10 -66.04 48.26 -10 \$ Top R plane LS shield
 35 py 76.2 \$ Back of rear shield
 36 py -85.5452 \$ Right door shield
 37 px 0 \$ Centerline in x
 38 p 18.034 -85.5452 0 18.034 -85.5452 10 76.2 -44.4988 0 \$ Right door outer shield
 39 p -18.034 -85.5452 0 -18.034 -85.5452 10 -76.2 -44.4988 0 \$ Left door outer shield
 c
 40 py 46.99 \$ Source Storage upper side
 41 py -46.99 \$ Source Storage lower side
 42 pz 263.82 \$ Source storage top
 45 pz 144.508 \$ Source storage bottom
 43 px 46.99 \$ Source storage right
 44 px -46.99 \$ Source storage left
 c
 90 py 78.74 \$ Back plane of concrete base
 91 py 38.1 \$ Back plane of concrete hole
 92 py -124.46 \$ Front plane of concrete hole
 93 py -170.18 \$ Front plane of concrete base
 94 px -91.44 \$ Left plane of concrete base
 95 px -40.64 \$ Left plane of concrete hole
 96 px 40.64 \$ Right plane of concrete hole
 97 px 91.44 \$ Right plane of concrete base

761 py 38.0238 \$ Outer plane for SS liner in front of back wall

c
 c _____
 c *****
 c ***** Sources *****
 c
 c ***** Cell 900 is Cf in the center of the assay chamber *****
 c *****

```

c
900 s 20 20 36.04 0.1    $ Cf point source
901 c/z 0 38.8113 0.635 $ Cf guide tube
c
c -----
c ***** Source Stand *****
c *****
941 pz 0.5      $ Top of bottom stand plate
942 pz 27.0     $ Bottom of top stand plate
943 pz 27.5     $ Top of top stand plate
944 pz 32.5     $ Top of motor
945 pz 34.5     $ Bottom of holder plate
946 pz 34.7     $ Top of holder plate
947 px -10.0    $ Left side of stand plate
948 px 10.0     $ Right side of stand plate
949 py 35.1     $ Back of stand plate
950 py 15.1     $ Front (towards door) of stand plate
951 c/z 0 25.1 5.25 $ Motor
952 c/z 0 25.1 1.75 $ Axle
953 c/z 0 25.1 6.5 $ Holder plate
c
10001 rcc 0 25.1 34.8 0 0 9.0 4.0      $ container
10002 rcc 0 25.1 35.0 0 0 2.08 3.5     $ uranium volume
10004 rcc 0 25.1 39.74 0 0 4.0 2.5     $ air volume
c
10020 rcc 21.5 22 24 0 0 30 6.1 $ inner tube
10021 rcc 21.5 22 23.5 0 0 31 6.3 $ outer tube
10022 rcc 21.5 22 36.01 0 0 2.5 6 $ copper heat sink
c
10030 rcc -23.75 -17.95 2.2 0 36.8 0 1.27 $ Flux monitor tube
10031 rcc -23.75 -9.06 2.2 0 20.32 0 1.07 $ Flux monitor tube inner
10032 rcc -23.75 -17.95 2.2 0 36.8 0 1.5875 $Cd

```

```

c
c

```

```

c
*****
***
c *****
c *****
c *****
c *****

```

Data Cards

```

c
*****
***
c
mode n
print
prdmp 3j 4
c
c
c *****
c ***** Sources *****
c *****
c
sdef erg=D1 pos=0 38.8113 35.79    $ Cf source centered in counting chamber
sp1 -3 1.025 2.926
c si3 0.11
c sdef erg=14.1 pos=20 20 36.04    $ D-T at 20 20 36.04
c
c
c
c
c *****
c ***** Materials *****
c *****
c
c
c -----
c   Air 0.00119 g/cc
c *****
m1 7014.80c -0.79    $ N
   8016.80c -0.21    $ O
c
c -----
c   He-3 0.00165 g/cc
c *****
m3 2003.80c 0.4301    $ He
   18000.59c 0.03225    $ Ar
   6000.80c 0.10752    $ C
   1001.80c 0.4301    $ H
c
c -----
c   HDPE 0.95 g/cc

```

```

c *****
m4 6000.80c 1      $ C
    1001.80c 2      $ H
mt4 poly.60t
c
c -----
c 8% Borated Poly 0.95 g/cc
c *****
m5 6000.80c -0.78780 $ C
    1001.80c -0.13220 $ H
    5010.80c -0.01474 $ B
    5011.80c -0.06526 $ B
c
c -----
c Graphite 2.25 g/cc
c *****
m6 6000.80c 1      $ C
c
c -----
c Cadmium 8.65 g/cc
c *****
m9 48000.50c 1     $ Cd
c
c -----
c Al 2.702 g/cc
c *****
m13 13027.80c 1    $ Al
c
c -----
c Concrete 2.32 g/cc
c *****
m14 6000.80c 0.23232 $ Concrete
    14000.60c 0.12121
    8016.80c 0.40404
    1001.80c 0.10101
    12000.62c 0.0202
    20000.62c 0.12121
c
c -----
c SS 7.87 g/cc
c *****
m16 6000.80c 0.0036 $ Stainless Steel

```

14000.60c 0.0195
24000.50c 0.1899
25055.80c 0.0199
28000.50c 0.0933
41093.80c 0.0047
26000.55c 0.6688

c

c -----

c SF6

c *****

m17 16000.66c 1 \$ S

9019.80c 6

c

c -----

c Fe 7.86 g/cc

c *****

m26 26000.55c 1 \$ Fe

c

c -----

c Cu 10.48 g/cc

c *****

m29 29000.50c 1 \$ Cu

c

c -----

c W 19 g/cc

c *****

m74 74000.80c 1 \$ W

c

c -----

c Lead 11.35 g/cc

c *****

m82 82000.80c 1 \$ Pb

c

c -----

c U-235/ Al alloy 3.35792 g/cc

c *****

m92 92235.80c 0.0372 \$ U-235

92238.80c 0.0028 \$ U-238

13027.80c 0.96 \$ Al

c

c -----

c Depleted U 19.1 g/cc

c *****
m93 92235.80c 0.002 \$ U-235
92238.80c 0.998 \$ U-235

c
c -----
c NBS071 0.72% can 3.4 g/cc
c *****
m94 8016.80c 0.152
92235.80c 0.006 \$ U-235
92238.80c 0.842 \$ U-238

c
c -----
c Californium g/cc
c *****
m98 98252.80c -1 \$ Cf-252

c
c
c
c
c -----
c *****
c ***** Tallies *****
c *****

c
c
c -----
c Flux tally
c
c Tracklength estimate of cell flux
c based on (n,p) reaction in He-3
c
c The time cards can be use to
c generate a die-away curve
c *****

F4:n (101 5i 107)
(111 4i 116)
(121 5i 127)
(131 5i 137)
(141 4i 146)
(151 5i 157)
(161 10i 172)
(181 10i 192) T

FM4 -1 3 103 \$ -1=> 1 X He density, 4=> m4, 103+>He(n,p)D reaction

total over all cells by nuclide	total collisions	collisions * weight	wgt. lost to capture	wgt. gain by fission	wgt. gain by (n,xn)	photons produced	photon wgt produced	avg photon energy
1001.80c	974537601	9.7454E+01	4.9197E-01	0.0000E+00	0.0000E+00	0	0.0000E+00	0.0000E+00
2003.80c	1615680	1.6157E-01	1.6117E-01	0.0000E+00	0.0000E+00	0	0.0000E+00	0.0000E+00
6000.80c	66956147	6.6956E+00	3.2039E-03	0.0000E+00	0.0000E+00	0	0.0000E+00	0.0000E+00
7014.80c	119132	1.1913E-02	3.9650E-04	0.0000E+00	0.0000E+00	0	0.0000E+00	0.0000E+00
8016.60c	3671	3.6710E-04	6.0000E-07	0.0000E+00	0.0000E+00	0	0.0000E+00	0.0000E+00
8016.80c	3809206	3.8092E-01	8.1500E-05	0.0000E+00	0.0000E+00	0	0.0000E+00	0.0000E+00
9019.80c	5353	5.3530E-04	1.3000E-06	0.0000E+00	0.0000E+00	0	0.0000E+00	0.0000E+00
12000.62c	199420	1.9942E-02	1.2270E-04	0.0000E+00	0.0000E+00	0	0.0000E+00	0.0000E+00
13027.80c	853582	8.5358E-02	6.0310E-04	0.0000E+00	1.0000E-07	0	0.0000E+00	0.0000E+00
14000.60c	1623196	1.6232E-01	2.1133E-03	0.0000E+00	3.0000E-07	0	0.0000E+00	0.0000E+00
16000.66c	524	5.2400E-05	1.5000E-06	0.0000E+00	0.0000E+00	0	0.0000E+00	0.0000E+00
18000.59c	149	1.4900E-05	1.9000E-06	0.0000E+00	0.0000E+00	0	0.0000E+00	0.0000E+00
20000.62c	879685	8.7968E-02	5.3731E-03	0.0000E+00	0.0000E+00	0	0.0000E+00	0.0000E+00
24000.50c	10751639	1.0752E+00	1.9003E-02	0.0000E+00	3.5200E-05	0	0.0000E+00	0.0000E+00
25055.80c	2201323	2.2013E-01	8.3017E-03	0.0000E+00	3.7000E-06	0	0.0000E+00	0.0000E+00
26000.55c	38033978	3.8034E+00	5.2928E-02	0.0000E+00	4.6400E-05	0	0.0000E+00	0.0000E+00
28000.50c	8207188	8.2072E-01	1.6662E-02	0.0000E+00	2.4000E-06	0	0.0000E+00	0.0000E+00
29000.50c	258242	2.5824E-02	2.1650E-04	0.0000E+00	8.0000E-07	0	0.0000E+00	0.0000E+00
41093.80c	465833	4.6583E-02	1.0240E-03	0.0000E+00	5.7000E-06	0	0.0000E+00	0.0000E+00
48000.50c	3972986	3.9730E-01	1.8740E-01	0.0000E+00	3.6400E-05	0	0.0000E+00	0.0000E+00
92234.60c	585	5.8500E-05	5.4000E-06	8.1000E-06	0.0000E+00	0	0.0000E+00	0.0000E+00
92235.60c	48860	4.8860E-03	1.6240E-04	1.3576E-03	4.7000E-06	0	0.0000E+00	0.0000E+00
92236.60c	131	1.3100E-05	1.1000E-06	7.0000E-07	0.0000E+00	0	0.0000E+00	0.0000E+00
92238.60c	3044	3.0440E-04	1.0700E-05	1.5800E-05	6.0000E-07	0	0.0000E+00	0.0000E+00

Table A. 1 Excerpt from MCNP6 Output File

Example Shuffler Software v2.0 Output File

Transfer to assay position

Distance (inches): 73.50
Acceleration (steps/sec-sec): 500000
Velocity (steps/sec): 50000
Number of shuffles per assay: 85
Nominal number of shuffles: 34
Nominal count time (sec): 7.000
Nominal irradiate time (sec): 7.000
Nominal forward time (sec): 1.850
Nominal reverse time (sec): 1.230

Source Scan

Distance (inches): 9.00
Acceleration (steps/sec): 100000.
Velocity (steps/sec): 5700.
Scans per shuffle (one way): 6
Pause at top (sec): 0.1
Pause at bottom (sec): 0.1
Background count time in seconds: 1000.0
Rotate table: ON

Assay Diagnostic Parameters

Expected DN Ratio: 0.0000 +/- % 0.000 Using Banks 0 and 0
Expected DN Ratio: 0.0000 +/- % 0.000 Using Banks 0 and 0
Expected DN Ratio: 0.0000 +/- % 0.000 Using Banks 0 and 0

Reject item Parameter: 0.0000

Reference transmission rate: 0.0000e+0005

Minimum transmission fraction: 0.000000

Use flux monitors: ON

Allowed percent dev. of cycle correction factor: 0.0000

Flux monitor dead time (micro sec): 0.000000

Calibration Parameters

Enrichment Value 100.000

$$f(x) = a_3x^3 + a_2x^2 + a_1x + a_0$$

a0: 0.000000

a1: 20.000000

a2: 0.000000

a3: 0.000000

a0, a0 0.0000e+0005

a0, a1 1.0000e-0015

a0, a2 0.0000e+0005

a0, a3 0.0000e+0005

a1, a1 0.0000e+0005

a1, a2 0.0000e+0005

a1, a3 0.0000e+0005

a2, a2 0.0000e+0005

a2, a3 0.0000e+0005

a3, a3 0.0000e+0005

Bias Correction Parameters

$$f(x) = a_2x^2 + a_1x + a_0$$

a0: 0.000000

a1: 1.000000

a2: 0.000000

a0 a1 a2

a0, a0 0.0000e+0005
 a0, a1 0.0000e+0005
 a0, a2 0.0000e+0005
 a1, a1 0.0000e+0005
 a1, a2 0.0000e+0005
 a1, a3 0.0000e+0005

Normalization Parameters

Normalization factors: 1.000
 Uncertainty in normalization factor: 0.000

CALIBRATION OpID: cms Item ID: DU5359 Cal1 JANY 03-Jun-2016 17:35:21
 Type: U233_scan Wt: 0.0 Cycle: 1 of 1 Status: 1051
 Corrected Count Rate: 342.87538

BACKGROUND RAW DATA
 Background count time = 1000.016600
 Background flux monitor 1 Counts = 56
 Background flux monitor 2 Counts = 51
 Background delayed neutron 1 Counts = 5981
 Background delayed neutron 2 Counts = 6684
 Background delayed neutron 3 Counts = 9614
 Background delayed neutron 4 Counts = 9884
 Background delayed neutron 5 Counts = 6506
 Background delayed neutron 6 Counts = 6055
 Background delayed neutron 7 Counts = 4342
 Background delayed neutron 8 Counts = 5319
 Total Background delayed neutron counts = 54385

RAW DATA FOR EACH OF 85 SHUFFLES

Shuffle	----- Times (s) -----			Count
	Forward	Irradiate	Reverse	
1	1.236600	7.036600	1.250400	6.991900
2	1.938600	7.066600	1.231200	7.001600
3	1.823500	7.055000	1.245600	6.989200
4	1.929500	7.067800	1.249400	6.990900
5	1.934000	7.070000	1.250500	6.999000
6	1.932800	7.060800	1.232700	6.996200

7	1.818700	7.056100	1.232600	6.981700
8	1.782800	7.054000	1.234800	6.994800
9	1.793500	7.060000	1.237200	6.991500
10	1.957700	7.053900	1.238600	7.003800
11	1.928400	7.039400	1.233100	6.990200
12	1.798200	7.056000	1.236100	6.991700
13	1.936100	7.043600	1.237300	6.989600
14	1.806800	7.075200	1.233100	6.998300
15	1.810700	7.051200	1.236900	6.999100
16	1.977800	7.056400	1.252500	6.998300
17	1.833900	7.068500	1.236100	6.990200
18	1.793800	7.059500	1.236900	6.991600
19	1.925000	7.039100	1.234100	6.980400
20	1.820800	7.066100	1.234000	6.992300
21	1.815000	7.075300	1.250600	7.003800
22	1.808000	7.063700	1.240200	7.001000
23	1.839800	7.039300	1.250400	6.999300
24	1.800100	7.062800	1.238000	6.996800
25	1.783200	7.038200	1.238400	6.990900
26	1.810400	7.058200	1.233800	6.995200
27	1.799500	7.068100	1.229600	7.000200
28	1.832500	7.047000	1.242600	6.991300
29	1.800500	7.059100	1.232700	6.989700
30	1.799200	7.063000	1.233500	7.002100
31	1.798400	7.070400	1.233500	6.995000
32	1.826000	7.055100	1.237500	6.994600
33	1.813200	7.063600	1.247500	7.004400
34	1.788900	7.055200	1.231000	6.991300
35	1.787900	7.050400	1.234900	6.993400
36	1.810600	7.067200	1.233000	7.002300
37	1.806900	7.045700	1.233400	6.995900
38	1.801100	7.062900	1.238000	6.995800
39	1.803500	7.036200	1.250200	6.992000
40	1.804400	7.059400	1.232000	7.002100
41	1.778300	7.051500	1.234600	7.001600
42	1.818000	7.050200	1.237700	6.991700
43	1.801800	7.054300	1.233700	6.991900
44	1.816100	7.041500	1.238700	7.001100
45	1.814800	7.047000	1.233800	7.002000
46	1.790100	7.047900	1.237600	6.990800
47	1.806800	7.040600	1.251600	6.998600
48	1.809200	7.066100	1.233500	6.989100

49	1.838900	7.038900	1.251100	7.000200
50	1.820400	7.059300	1.232800	7.001100
51	1.795600	7.067200	1.233900	7.001200
52	1.814700	7.060000	1.229000	6.994200
53	1.813500	7.060400	1.229800	6.994000
54	1.806400	7.067300	1.236900	7.002400
55	1.828100	7.048300	1.245700	6.991000
56	1.817700	7.062700	1.233600	6.999100
57	1.803700	7.060200	1.250300	6.998900
58	1.821000	7.063500	1.233100	6.995500
59	1.807200	7.060400	1.249400	6.996300
60	1.812600	7.063200	1.236900	7.000600
61	1.792300	7.034000	1.249700	6.990200
62	1.799000	7.063300	1.232600	7.002800
63	1.937000	7.052200	1.232800	7.000400
64	1.816500	7.043200	1.236800	7.001000
65	1.803500	7.035500	1.233300	6.994300
66	1.814800	7.039100	1.236800	6.991400
67	1.796900	7.055100	1.238400	6.991900
68	1.815600	7.043200	1.241600	6.997300
69	1.780400	7.045400	1.246600	6.993900
70	1.802800	7.042200	1.237700	6.999400
71	1.800100	7.043400	1.237500	7.000900
72	1.798700	7.035900	1.241800	6.990000
73	1.806500	7.046600	1.239100	6.989600
74	1.805300	7.042900	1.233300	7.000400
75	1.788700	7.043100	1.233400	7.001100
76	1.927000	7.043600	1.241800	6.994600
77	1.801300	7.064600	1.231600	7.000200
78	1.788400	7.063300	1.233100	6.997100
79	1.799700	7.026000	1.239100	7.001600
80	1.814500	7.059700	1.232900	6.990500
81	1.825600	7.043100	1.253700	6.991000
82	1.821600	7.059100	1.232600	6.999800
83	1.811800	7.063600	1.229800	6.992500
84	1.809000	7.062300	1.237300	6.989000
85	1.823000	7.061000	1.232600	6.996500

----- Delayed Neutron Counts -----
Shuffle DN1 DN2 DN3 DN4

1	139	137	215	212
---	-----	-----	-----	-----

2	153	156	254	256
3	148	154	226	249
4	162	179	237	284
5	191	181	233	281
6	175	163	257	299
7	177	181	241	278
8	164	181	258	310
9	189	188	256	263
10	171	201	239	284
11	162	192	251	310
12	170	193	233	267
13	196	180	230	291
14	163	183	238	289
15	171	200	242	298
16	150	171	225	298
17	173	150	250	262
18	162	175	224	266
19	159	208	265	301
20	149	179	247	313
21	187	196	267	249
22	163	187	246	276
23	164	167	238	263
24	188	180	268	303
25	173	173	233	263
26	176	194	248	303
27	163	179	252	284
28	168	175	242	274
29	155	177	265	298
30	161	182	243	286
31	166	167	250	278
32	184	195	222	290
33	164	165	282	288
34	142	192	255	282
35	186	177	220	274
36	149	189	265	284
37	173	199	232	294
38	171	170	249	266
39	175	163	254	292
40	173	182	233	303
41	144	171	232	289
42	143	195	226	275
43	188	184	256	302

44	172	222	240	258
45	147	175	240	281
46	175	178	240	278
47	169	175	239	301
48	166	177	253	263
49	149	192	231	296
50	150	180	250	283
51	158	136	250	289
52	195	181	254	288
53	180	211	248	264
54	184	175	260	317
55	156	178	239	276
56	159	196	254	267
57	179	171	246	289
58	157	186	244	290
59	167	159	259	290
60	158	204	245	287
61	198	153	234	279
62	160	157	232	275
63	161	177	259	304
64	175	188	242	285
65	168	179	244	278
66	182	179	274	269
67	170	145	209	310
68	183	179	236	272
69	179	160	264	259
70	125	160	273	296
71	187	172	264	291
72	179	186	234	260
73	167	193	238	282
74	155	174	240	293
75	163	170	249	298
76	147	180	230	269
77	158	193	239	290
78	188	162	254	250
79	170	164	223	296
80	178	176	237	272
81	175	176	251	252
82	179	171	243	301
83	160	175	247	274
84	173	167	261	272
85	163	178	231	267

Shuffle	DN5	DN6	DN7
1	183	147	96
2	194	162	119
3	170	144	128
4	178	176	104
5	197	177	148
6	192	173	128
7	206	170	128
8	185	162	113
9	201	151	126
10	189	188	115
11	223	155	137
12	191	207	137
13	213	194	125
14	191	162	123
15	199	174	113
16	198	172	104
17	183	192	100
18	179	169	128
19	195	195	112
20	203	166	121
21	193	185	110
22	203	183	124
23	204	183	134
24	192	194	141
25	176	185	127
26	185	185	142
27	186	168	120
28	204	188	101
29	192	181	149
30	216	171	116
31	207	186	140
32	195	175	116
33	193	198	128
34	193	172	124
35	208	167	120
36	193	175	133
37	184	177	143
38	183	169	117
39	204	191	107

40	183	159	110
41	179	168	119
42	203	186	130
43	222	180	138
44	204	186	130
45	174	177	126
46	181	192	126
47	176	180	135
48	159	178	127
49	199	157	117
50	218	158	125
51	207	167	138
52	193	193	130
53	202	163	114
54	186	197	111
55	171	188	114
56	183	187	148
57	178	164	111
58	191	191	131
59	220	174	119
60	202	154	115
61	175	160	105
62	169	179	123
63	214	179	121
64	193	156	135
65	176	164	116
66	205	165	132
67	178	183	116
68	178	161	111
69	184	185	117
70	176	154	111
71	181	151	112
72	200	186	124
73	187	150	115
74	190	176	144
75	179	192	111
76	166	175	139
77	189	160	136
78	198	189	124
79	190	182	121
80	173	169	109
81	195	146	127

82	196	184	134
83	184	178	118
84	187	152	137
85	182	179	119

----- Irradiation Counts -----
 Shuffle FM1 FM2 FM3 FM4 Transmission

SUMMED DATA FOR 85 SHUFFLES

Forward Time (s) = 154.503200 Irradiation Time (s) = 599.598500
 Reverse Time (s) = 105.233500 Count Time (s) = 594.638100
 Flux Monitor 1 Counts = 1040784
 Flux Monitor 2 Counts = 954945
 Transmission Monitor Counts = 5995985
 Delayed Neutron 1 Counts = 14244
 Delayed Neutron 2 Counts = 15121
 Delayed Neutron 3 Counts = 20799
 Delayed Neutron 4 Counts = 23938
 Delayed Neutron 5 Counts = 16257
 Delayed Neutron 6 Counts = 14823
 Delayed Neutron 7 Counts = 10468
 Delayed Neutron 8 Counts = 9734
 Total Delayed Neutron Counts = 125384
 Flux Monitor Ratio(1:2) = 1.089889
 Delayed Neutron Ratio(0:0) = 1.000000
 Delayed Neutron Rate (cps) = 210.858 +/- 0.595
 Transmission Rate: 1.0000e+004
 Corrected transmission rate: 0.0000e+000
 Transmission value: 0.0000e+000

RESPONSE CORRECTIONS

BACKGROUND and Cf-252 DECAY

Delayed Neutron Background Rate (cps) = 54.384 +/- 0.233
 Background Corrected Delayed Neutron Rate (cps) = 156.474 +/- 0.640

Reference Date = 05/30/2013 Current Date = 03-Jun-2016 17:35:21
 Number of Days Since Reference Date = 1100.72

Decay Constant (1/d) = 0.0007127
Decay Correction Factor = 2.191267
Cf Decay Corrected Delayed Neutron Rate (cps) = 342.875 +/- 1.401

FLUX MONITOR

Flux Monitor Correction Factor = 1.000
Flux Monitor Corrected Delayed Neutron Rate (cps) = 342.875 +/- 1.401

CYCLE CORRECTION

Nominal Number of Shuffles per Assay = 34
Nom. Fwd. Time (s) = 1.850000 Nom. Irrad. Time (s) = 7.000000
Nom. Rev. Time (s) = 1.230000 Nom. Count Time (s) = 7.000000
Dsum(nominal) = 30.07730
Dsum = 30.17150
Correction Factor = 0.99688
Cycle Corrected Delayed Neutron Count Rate (cps) = 342.8754 +/- 1.3970

NORMALIZATION

Normalization factor = 1.00000 +/- 0.00000
Normalization corrected delayed neutron count rate = 342.87538 +/- 1.39698

Appendix B: Source Information

Table B. 1. Source Activities

Source ID	Activity	Date
²⁵² Cf-5865	7.2E-06 Ci	2/29/2008
²⁵² Cf-5442	161.37 uCi	6/7/2005
²⁵² Cf-5870	94.9 uCi	7/11/2011
²⁵² Cf-6081	270.3 uCi	5/9/2014
²⁵² Cf-5895	302 mCi	4/8/1999

Table B. 2. NBL CRM Source Specifications

ID	Enrichment	H (mm)	h (mm)	D (mm)	d (mm)	t (mm)	U3O8 Density (g/cm ³)
NBS031	0.31	100	20.8	80	70	2	2.5
NBS072	0.72	100	20.8	80	70	2	2.5
NBS194	1.94	100	20.8	80	70	2	2.5
NBS295	2.95	100	20.8	80	70	2	2.5
NBS446	4.46	100	15.8	80	70	2	3.4
NBL001	20.11	100	15.8	80	70	2	3.78
NBL002	52.49	100	15.8	80	70	2	3.78
NBL003	93.17	100	15.8	80	70	2	3.78

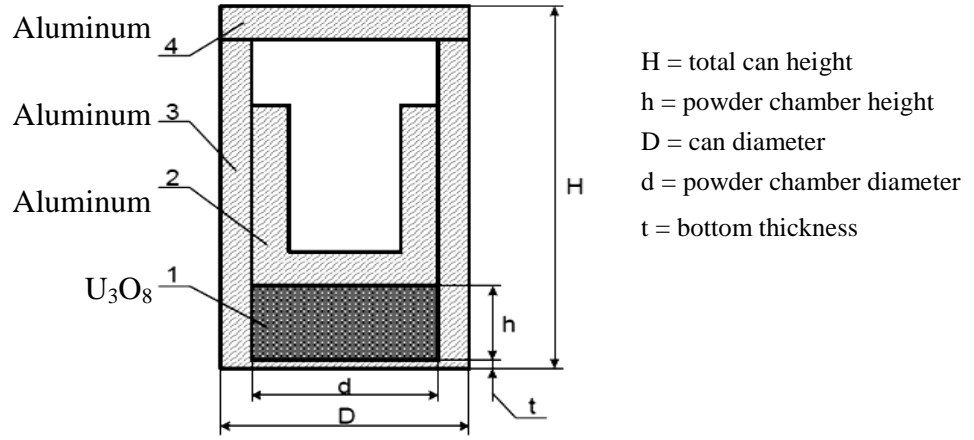


Figure B. 1. Diagram of the CRM containers.

AmLi Energy Distribution

```

si1 h 0 0.025 0.05 0.075 0.1 0.15 0.2 0.25
    0.3 0.35 0.4 0.45 0.5 0.55 0.6 0.65
    0.7 0.75 0.8 0.85 0.9 0.95 1 1.05
    1.1 1.15 1.2 1.25 1.3 1.35 1.4 1.45
    1.5 1.75 2 2.25 2.5 3 3.5
sp1 d 0 0.048 0.065 0.084 0.1 0.129 0.178 0.203
    0.212 0.189 0.155 0.106 0.09 0.085 0.08
    0.07 0.06 0.054 0.05 0.046 0.038 0.031
    0.028 0.022 0.017 0.012 0.009 0.005 0.004
    0.004 0.004 0.003 0.004 0.025 0.04 0.03
    0.025 0.01 0.007
  
```

AmBe Energy Distribution

si1 l 0

7.14E-02	1.41E-01	2.11E-01	2.80E-01	3.50E-01	4.19E-01	4.89E-01
5.59E-01	6.28E-01	6.98E-01	7.67E-01	8.37E-01	9.07E-01	9.76E-01
1.05E+00	1.12E+00	1.19E+00	1.26E+00	1.32E+00	1.39E+00	1.46E+00
1.53E+00	1.60E+00	1.67E+00	1.74E+00	1.81E+00	1.88E+00	1.95E+00
2.02E+00	2.09E+00	2.16E+00	2.23E+00	2.30E+00	2.37E+00	2.44E+00
2.51E+00	2.58E+00	2.65E+00	2.72E+00	2.79E+00	2.86E+00	2.93E+00
3.00E+00	3.06E+00	3.13E+00	3.20E+00	3.27E+00	3.34E+00	3.41E+00
3.48E+00	3.55E+00	3.62E+00	3.69E+00	3.76E+00	3.83E+00	3.90E+00
3.97E+00	4.04E+00	4.11E+00	4.18E+00	4.25E+00	4.32E+00	4.39E+00
4.46E+00	4.53E+00	4.60E+00	4.67E+00	4.74E+00	4.80E+00	4.87E+00
4.94E+00	5.01E+00	5.08E+00	5.15E+00	5.22E+00	5.29E+00	5.36E+00
5.43E+00	5.50E+00	5.57E+00	5.64E+00	5.71E+00	5.78E+00	5.85E+00
5.92E+00	5.99E+00	6.06E+00	6.13E+00	6.20E+00	6.27E+00	6.34E+00
6.41E+00	6.48E+00	6.54E+00	6.61E+00	6.68E+00	6.75E+00	6.82E+00
6.89E+00	6.96E+00	7.03E+00	7.10E+00	7.17E+00	7.24E+00	7.31E+00
7.38E+00	7.45E+00	7.52E+00	7.59E+00	7.66E+00	7.73E+00	7.80E+00
7.87E+00	7.94E+00	8.01E+00	8.08E+00	8.15E+00	8.22E+00	8.28E+00
8.35E+00	8.42E+00	8.49E+00	8.56E+00	8.63E+00	8.70E+00	8.77E+00
8.84E+00	8.91E+00	8.98E+00	9.05E+00	9.12E+00	9.19E+00	9.26E+00
9.33E+00	9.40E+00	9.47E+00	9.54E+00	9.61E+00	9.68E+00	9.75E+00
9.82E+00	9.89E+00	9.96E+00	1.00E+01	1.01E+01	1.02E+01	1.02E+01
1.03E+01	1.04E+01	1.04E+01	1.05E+01	1.06E+01	1.07E+01	1.07E+01
1.08E+01	1.09E+01					

sp1 d 0

6.99E-03	4.42E-03	7.18E-03	9.46E-03	9.16E-03	8.36E-03	9.35E-03
8.62E-03	7.95E-03	9.08E-03	8.09E-03	7.84E-03	5.63E-03	6.96E-03
6.66E-03	6.51E-03	6.35E-03	5.73E-03	6.69E-03	5.87E-03	6.61E-03
6.78E-03	5.76E-03	5.86E-03	4.59E-03	6.01E-03	6.45E-03	8.44E-03
6.37E-03	6.82E-03	8.36E-03	8.67E-03	7.61E-03	7.03E-03	8.78E-03
6.70E-03	9.25E-03	7.43E-03	8.12E-03	1.09E-02	1.07E-02	1.24E-02
1.33E-02	1.42E-02	1.40E-02	1.42E-02	1.15E-02	1.30E-02	1.06E-02
1.10E-02	1.16E-02	1.03E-02	1.02E-02	1.01E-02	9.53E-03	1.03E-02
1.04E-02	1.06E-02	8.62E-03	8.98E-03	1.03E-02	1.09E-02	8.03E-03
9.01E-03	9.82E-03	9.95E-03	1.01E-02	1.13E-02	1.00E-02	1.19E-02
1.19E-02	1.22E-02	1.06E-02	9.06E-03	9.82E-03	9.37E-03	8.02E-03
1.08E-02	7.87E-03	6.89E-03	7.84E-03	7.66E-03	7.28E-03	7.33E-03
4.45E-03	4.68E-03	5.49E-03	5.80E-03	7.12E-03	7.36E-03	5.85E-03
6.98E-03	6.64E-03	6.06E-03	5.43E-03	6.34E-03	5.77E-03	5.24E-03
5.18E-03	4.77E-03	5.44E-03	3.36E-03	6.57E-03	5.71E-03	5.54E-03
6.65E-03	6.17E-03	5.57E-03	6.40E-03	6.06E-03	6.39E-03	7.68E-03
4.37E-03	6.29E-03	5.64E-03	4.09E-03	3.59E-03	3.64E-03	4.06E-03
3.45E-03	3.38E-03	2.25E-03	1.78E-03	1.51E-03	1.93E-03	1.76E-03
1.47E-03	9.41E-04	1.19E-03	1.09E-03	1.22E-03	1.46E-03	5.67E-04
1.15E-03	2.21E-03	1.53E-03	1.79E-03	1.93E-03	2.94E-03	1.61E-03
2.88E-03	1.90E-03	2.18E-03	2.34E-03	1.84E-03	2.12E-03	1.21E-03
8.14E-04	1.78E-03	5.54E-04	4.20E-04	1.13E-03	4.28E-04	1.44E-04
2.91E-04	0.00E+00					

Appendix C: Uncertainty Analyses and Equations

For simple error propagation, the uncertainty equations are provided in the main text.

The uncertainty equation used for calculating dead-time is provided in Eq. C.1.

$$\sigma_{\tau_{DT}} = \tau_{DT} \sqrt{\left(\frac{1}{(M_1+M_2-M_{12}-B)} + \frac{2M_1}{M_{12}^2-M_1^2-M_2^2}\right)^2 \sigma_{M_1}^2 + \left(\frac{1}{(M_1+M_2-M_{12}-B)} + \frac{2M_2}{M_{12}^2-M_1^2-M_2^2}\right)^2 \sigma_{M_2}^2 + \left(\frac{1}{(M_1+M_2-M_{12}-B)} + \frac{2M_3}{M_{12}^2-M_1^2-M_2^2}\right)^2 \sigma_{M_3}^2 + \left(\frac{\sigma_B}{M_1+M_2-M_{12}-B}\right)^2}$$

Eq. C.1

The uncertainty calculation for the analytical calculation of delayed neutron counts is outlined here. Eq. 9 provided the calculation for the estimated delayed neutron counts for all groups. For the uncertainty calculations, each group is first considered separately such that Eq. C.2 represents the calculation of the delayed neutron counts from a single group, D_i :

$$D_i = \frac{\varepsilon R_{IF} \bar{\nu} \beta_i}{\lambda_i} [1 - \exp(-\lambda_i t_i)] [\exp(-\lambda_i t_d)] [1 - \exp(-\lambda_i t_c)] * \left\{ \frac{n - (n+1) \exp(-\lambda_i \tau) + \exp(-(n+1)\lambda_i \tau)}{(1 - \exp(-\lambda_i \tau))^2} \right\},$$

Eq. C.2

where ε is the detector efficiency, R_{IF} is the induced fission rate, $\beta \bar{\nu}$ is the delayed neutron yield, λ is the group-dependent decay constant, t_i is the irradiation time, t_d is the delay time due to source removal, t_c is the count time, τ is the total time of each shuffle, and n is the number of shufflers per assay.

The following parameters were considered to have no (or negligible) uncertainty: ε , t_i , t_d , t_c , τ , and n . The uncertainty in the efficiency is easy to propagate as it is a simple scaling factor and it is common to all groups. Therefore, the uncertainty in the delayed neutron counts can be described by Eq. C.3 where $\beta_i \bar{\nu}$ is treated as a single entity and we assume it and λ_i are uncorrelated.

$$\sigma_{D_i} = \sqrt{\left(\frac{\partial D_i}{\partial R_{IF}}\right)^2 \sigma_{R_{IF}}^2 + \left(\frac{\partial D_i}{\partial \beta_i \bar{\nu}}\right)^2 \sigma_{\beta_i \bar{\nu}}^2 + \left(\frac{\partial D_i}{\partial \lambda_i}\right)^2 \sigma_{\lambda_i}^2}$$

Eq. C.3

The terms are defined in the following equations.

$$\frac{\partial D_i}{\partial R_{IF}} = \frac{D_i}{R_{IF}} \quad \text{Eq. C.4}$$

$$\sigma_{R_{IF}} = R_{IF} \frac{\sigma_v}{v-1} \quad \text{Eq. C.5}$$

$$\frac{\partial D_i}{\partial \beta_{i\nu}} = \frac{D_i}{\beta_{i\nu}} \quad \text{Eq. C.6}$$

The uncertainty in the yield, $\sigma_{\beta_{i\nu}}$, is reported for each group and isotope in Table 3.

The partial derivative with respect to λ is more complicated. The derivation is provided below.

Let:

$$D(\lambda) = \varepsilon R_{IF} \bar{v}_I \beta_i \frac{g(\lambda)}{h(\lambda)}, \quad \text{Eq. C.7}$$

such that $g(\lambda)$ and $h(\lambda)$ can be defined using Eqs. C.7 and C.8, respectively.

$$\begin{aligned} g(\lambda) = & n \cdot \exp(-t_d \lambda) - (n+1) \exp(-(t_d + \tau) \lambda) + \exp(-(t_d + (n+1)\tau) \lambda) - n \cdot \exp(-(t_d + t_c) \lambda) \\ & + (n+1) \exp(-(t_d + t_c + \tau) \lambda) - \exp(-(t_d + t_c + (n+1)\tau) \lambda) - n \cdot \exp(-(t_i + t_d) \lambda) \\ & + (n+1) \exp(-(t_i + t_d + \tau) \lambda) - \exp(-(t_i + t_d + (n+1)\tau) \lambda) + n \cdot \exp(-(t_i + t_d + t_c) \lambda) \\ & - (n+1) \exp(-(t_i + t_d + t_c + \tau) \lambda) + \exp(-(t_i + t_d + t_c + (n+1)\tau) \lambda) \end{aligned} \quad \text{Eq. C.8}$$

$$h(\lambda) = \lambda[1 - \exp(-\tau\lambda)]^2 \quad \text{Eq. C.9}$$

Then the partial derivative of D with respect to λ is given by Eq. C.9:

$$D'(\lambda) = \frac{g'(\lambda)h(\lambda) - g(\lambda)h'(\lambda)}{h(\lambda)^2}, \quad \text{Eq. C.10}$$

The derivatives are then given by Eqs. C.10 and C.11.

$$\begin{aligned} g'(\lambda) = & -nt_d \cdot \exp(-t_d\lambda) + (n+1)(t_d + \tau) \exp(-(t_d + \tau)\lambda) \\ & - (t_d + (n+1)\tau) \exp(-(t_d + (n+1)\tau)\lambda) + n(t_d + t_c) \cdot \exp(-(t_d + t_c)\lambda) \\ & - (n+1)(t_d + t_c + \tau) \exp(-(t_d + t_c + \tau)\lambda) + (t_d + t_c + (n+1)\tau) \exp(-(t_d + t_c + (n+1)\tau)\lambda) \\ & + n(t_i + t_d) \cdot \exp(-(t_i + t_d)\lambda) - (n+1)(t_i + t_d + \tau) \exp(-(t_i + t_d + \tau)\lambda) \\ & + (t_i + t_d + (n+1)\tau) \exp(-(t_i + t_d + (n+1)\tau)\lambda) - n(t_i + t_d + t_c) \cdot \exp(-(t_i + t_d + t_c)\lambda) \\ & + (n+1)(t_i + t_d + t_c + \tau) \exp(-(t_i + t_d + t_c + \tau)\lambda) \\ & - (t_i + t_d + t_c + (n+1)\tau) \exp(-(t_i + t_d + t_c + (n+1)\tau)\lambda) \end{aligned} \quad \text{Eq. C.11}$$

$$h'(\lambda) = 1 - 2 \exp(-\tau\lambda) + 2\tau\lambda \exp(-\tau\lambda) - 2\lambda\tau \exp(-2\tau\lambda) + \exp(-2\tau\lambda), \quad \text{Eq. C.12}$$

The uncertainty in the decay constants, σ_{λ_i} , are given in Table 3.

VITA

Angela Lynn Lousteau was born March 12, 1982 in Houston, TX. She earned a B.S. and M.S. in Nuclear Engineering from Texas A&M University in 2005 and 2007, respectively. Angie began her career in international safeguards and nuclear nonproliferation as an intern in the Department of Safeguards at the International Atomic Energy Agency. She completed additional internships at Los Alamos National Laboratory and Lawrence Livermore National Laboratory before accepting a staff position at Oak Ridge National Laboratory. Over the past 9 years, Angie has become an integral part of the Nondestructive Assay Team in the Safeguards and Security Technology Group, supporting both international and domestic safeguards projects through various research and development efforts, international engagement, and training activities.

As a graduate student, she was nominated to join the Honor Society of Phi Kappa Phi, the Golden Key International Honour Society, and Alpha Sigma Nu, the Nuclear Engineering Honorary Society. She enrolled in the Nuclear Engineering Ph.D. program at the University of Tennessee in 2013.